Chemical Partitioning of Emerging Indoor Organic Pollutants

by

Shuang Wu

A thesis submitted in partial fulfillment of the requirements for the degree of

Doctor of Philosophy

Department of Chemistry
University of Alberta

Abstract

Given that modern humans spend the majority of their time indoors, the indoor environment plays an essential role in chemical exposure. Emerging indoor organic pollutants have direct impacts on air quality and human health. For example, microbial volatile organic compounds (MVOCs) emitted by molds and fungi are responsible for malodors and can cause certain health issues. Long-term exposure to these compounds may be harmful even at low concentrations. Similarly, the flavoring agents added in e-cigarettes and their adducts formed in e-liquids may pose health risks through thirdhand exposure. This term refers to the residual chemicals or toxins left on indoor surfaces, which can affect occupants long after the initial use. The phase distributions for these chemicals determine the pathways of human exposure, including inhalation, ingestion, and dermal permeation. The recent discovery of a large volume of indoor reservoirs signifies the importance of indoor partitioning, which is governed by partitioning coefficients. However, current data are insufficient to predict the environmental behaviors of indoor volatile organic compounds (VOCs). Consequently, the indoor chemical partitioning and phase distribution for these harmful VOCs are poorly understood.

This work focuses on utilizing a chemical two-dimensional (2D) partitioning model framework to visualize the phase distributions of emerging indoor organic pollutants. Target species were assumed to achieve equilibrium in a triphasic indoor system (air, polar, and weakly-polar reservoirs) according to their water-air partitioning coefficient (K_{WA}) and octanol-air partitioning coefficient (K_{OA}). The aim is to provide more experimental constraints to Henry's Law constant (H), equivalent to K_{WA},

which is subject to the influence of other factors, such as hydration and liquid-phase reactions. Partitioning coefficients were determined with the inert gas-stripping (IGS) method and variable phase ratio headspace (VPR-HS) technique. The hydration process and liquid-phase reactions were monitored by proton nuclear magnetic resonance (^{1}H NMR) spectroscopy. For the chemicals not amenable to these methods, the EAS-E Suite and polyparameter linear free energy relationships (pp-LFERs) were used to predict the partitioning coefficients. The obtained values were input into the model to display indoor phase distribution and assess the pathways of human exposure to target indoor VOCs. This study reports novel findings indicating that many VOCs are likely distributed between indoor air and weakly polar (e.g., organic-rich) reservoirs. The fraction in each phase is highly dependent on environmental conditions such as temperature and reservoir size. Furthermore, the hydration process significantly affects laboratory measurements of H, emphasizing the necessity of correctly applying this constant under varying conditions. Additionally, the work demonstrates that flavoring adducts formed in e-cigarette liquids exhibit different chemical and toxicological properties compared to the original compounds, which further influence indoor partitioning behavior and human exposure. These insights contribute to the field by highlighting the dynamic nature of indoor phase distributions and the importance of accurate measurements and modeling in assessing indoor air quality and exposure risks.

Preface

Chapter 1

Introduction

Contributions: The introduction was written by Shuang Wu with review and feedback by Dr. Ran Zhao.

Chapter 2

Henry's Law Constants and Indoor Partitioning of Microbial Volatile Organic Compounds

Wu, S., Hayati, S. K., Kim, E., de la Mata, A. P., Harynuk, J. J., Wang, C., & Zhao, R. (2022). Henry's law constants and indoor partitioning of microbial volatile organic compounds. *Environmental Science & Technology*, 56(11), 7143-7152.

Contributions: This study was led by Shuang Wu. The research ideas were developed collaboratively by Shuang Wu and Dr. Ran Zhao. Shuang Wu was responsible for experiment design and method development. The experimental work was conducted by Shuang Wu, with assistance from Siti K. Hayati and Erica Kim. Data analysis was performed by Shuang Wu. Training in gas chromatography was provided by Dr. Harynuk J. James and Dr. de la Mata A. Paulina. The manuscript was written by Shuang Wu and reviewed by Dr. Ran Zhao.

Chapter 3

Indoor partitioning and potential thirdhand exposure to carbonyl flavoring agents added in e-cigarettes and hookah tobacco

Wu, S., Kim, E., Vethanayagam, D., & Zhao, R. (2022). Indoor partitioning and potential thirdhand exposure to carbonyl flavoring agents added in e-cigarettes and hookah tobacco. *Environmental Science: Processes & Impacts*, 24(12), 2294-2309.

Contributions: This study was led by Shuang Wu. The research ideas were developed collaboratively by Shuang Wu, Dr. Ran Zhao and Dr. Dilini Vethanayagam. Shuang Wu was responsible for experiment design and method development. The experimental work was conducted by Shuang Wu, with assistance from Erica Kim. Data analysis was performed by Shuang Wu. The manuscript was written by Shuang Wu and reviewed by Dr. Ran Zhao.

Chapter 4

Acetal Formation of Flavoring Agents with Propylene Glycol in E-Cigarettes: Impacts on Indoor Partitioning and Thirdhand Exposure

Wu, S., Kim, E., & Zhao, R. (2023). Acetal Formation of Flavoring Agents with Propylene Glycol in E-Cigarettes: Impacts on Indoor Partitioning and Thirdhand Exposure. *Environmental Science & Technology*, 57(50), 21284-21294.

Contributions: This study was led by Shuang Wu. The research ideas were developed collaboratively by Shuang Wu and Dr. Ran Zhao. Shuang Wu was responsible for experiment design and method development. The experimental work was conducted by Shuang Wu, with assistance from Erica Kim. Data analysis was performed by Shuang Wu. The manuscript was written by Shuang Wu and reviewed by Dr. Ran Zhao.

Chapter 5

Conclusions and Future Work

The conclusion was written by Shuang Wu with review and feedback by Dr. Ran Zhao.

Acknowledgements

I would like to extend my heartfelt gratitude to everyone who has supported and guided me throughout my PhD journey.

First and foremost, I am profoundly grateful to my supervisor, Dr. Ran Zhao, for his invaluable guidance, unwavering support, and encouragement. His mentorship has been crucial in navigating this research.

My sincere thanks also go to my committee members, Dr. Wolfgang Jäger and Dr. Lingzi Sang, as well as Dr. Shira Joudan, for their insightful feedback and shared knowledge, which have greatly enriched my work.

I am particularly thankful to Dr. Frank Wania for his stimulating discussions and critical research ideas that have significantly shaped this study. I also wish to acknowledge Dr. Chen Wang for her pivotal contributions to the modeling aspect of this research; her work has been an essential resource.

I am grateful to both past and present members of the Zhao Group for their constant support and camaraderie. Special thanks to undergraduate research assistants Siti K. Hayati and Erica Kim for their invaluable help with the experiments.

To my partner, family, and friends—your unwavering support, understanding, and encouragement have been my source of strength throughout this challenging yet rewarding journey. Your belief in me has kept me motivated and focused.

Finally, I want to thank everyone who contributed, directly or indirectly, to this work. Your support has been indispensable, and I deeply appreciate all your efforts.

Thank you.

Table of Contents

List of Tables

List of Figures

Abbreviations

F_{acetal} Fraction of PG acetal formation.

F_g Fraction in the gas phase.

F_o Fraction in the organic phase.

F_p Fraction in the PG aerosol phase.

F_w Fraction in the water phase.

H Henry's law constant.

H^{cp}_s Intrinsic Henry's law constant, 's' denotes Henry's law solubility (i.e., aqueous over gas phase), while 'cp' represents the ratio between concentration and partial pressure.

$H^{cp}_{s,eff}$ Effective Henry's law constant, 's' denotes Henry's law solubility (i.e., aqueous over gas phase), while 'cp' represents the ratio between concentration and partial pressure.

H_{eff} Effective Henry's law constant.

K_{hyd} Hydration equilibrium constant.

K_{oa} Octanol–air partitioning coefficient.

K_{ow} Octanol-water partitioning coefficient.

K_{pa} PG aerosol and air partitioning coefficient.

K_{wa} Water–air partitioning coefficient.

^{1}H NMR Proton nuclear magnetic resonance.

2D Two-dimensional.

DMSO Dimethyl sulfoxide.

Electronic cigarettes E-cigarettes.

EV Enhanced ventilation.

FID Flame ionization detector.

GC Gas chromatography.

GC-MS Gas chromatography-mass spectrometry.

HPLC High Performance Liquid chromatography.

IGS Inert gas-stripping.

MS Mass spectrometry.

MVOCs Microbial volatile organic compounds.

NMR Nuclear magnetic resonance.

PG Propylene glycol.

PM Particulate matter.

ppLFERs Poly-parameter linear free energy relationships.

QSPR Quantitative structure-property relationship.

S/V Surface-to-volume.

sccm Standard cubic centimeters per minute.

SOA Secondary organic aerosol.

TCA 2,4,6-Trichloroanisole.

TVOC Total volatile organic compound.

UV Ultraviolet.

VG Vegetable glycerin.

VOCs Volatile organic compounds.

VPR-HS Variable phase ratio headspace.

Chapter 1

Introduction

Contributions: The introduction was written by Shuang Wu with review and feedback by Dr. Ran Zhao.

1.1 The Atmosphere in Indoor Environments

The atmosphere in indoor environments plays a crucial role in determining the comfort, health, and productivity of occupants. Factors such as air quality, temperature, and humidity critically influence this indoor atmosphere. In today's world, people increasingly spend their time indoors, including in residences, offices, enclosed vehicles, and other indoor spaces. According to the National Human Activity Pattern Survey (NHAPS) conducted by the U.S. Environmental Protection Agency, individuals spend 86.9% of their time indoors and 5.5% in enclosed vehicles each day, as illustrated in Figure 1.1. Consequently, the quality of indoor air and the overall atmosphere significantly impacts public health and well-being. As such, it is imperative to understand the composition and sources of indoor air pollutants, and to discover effective mitigation strategies.

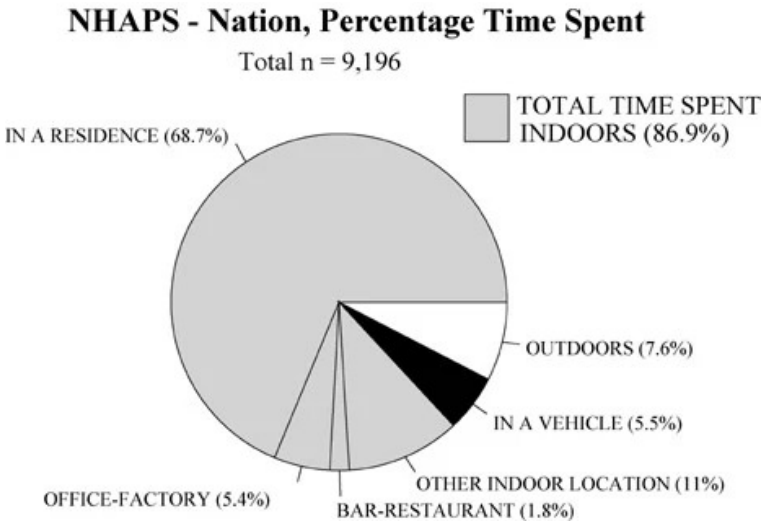

Figure 1.1: Pie chart showing the mean percentage of time the NHAPS respondents spent in six different locations on the diary data (weighted). Time spent indoors (composed of time in a residence, in an office or factory, in a bar or restaurant, or in some other indoor location) is represented by lightly shaded slices. The percentages in the figure are the mean percentages taken over individual percentages for people in the NHAPS sample. Individual percentages were calculated from the time spent in each location over the total amount of time spent, which was equal to 24 h (1440 min) for each individual. From Klepeis *et al.* "The National Human Activity Pattern Survey (NHAPS): a resource for assessing exposure to environmental pollutants" *Journal of exposure science & environmental epidemiology* 11.3 (2001): 231-252.[1] Reprinted with permission from Springer Nature.

Indoor air pollutants are introduced by a range of sources, from the infiltration of outdoor pollutants to emissions from indoor activities, such as cooking, cleaning, smoking, and the use of consumer products. Modern building designs, aimed at enhancing energy efficiency, often result in more airtight structures that reduce natural ventilation, thereby allowing pollutants to accumulate. Poor air quality, often due to inadequate ventilation and the presence of pollution sources, can lead to health issues such as allergies, respiratory problems, and fatigue.[2] A notable example is Sick Building Syndrome, a phenomenon where building occupants experience complex health issues due to poor air quality resulting from inadequate ventilation, chemical contaminants, and biological pollutants like mold.[3] These symptoms often improve after leaving the building, underscoring the impact of indoor air quality on health. Proper temperature and humidity control are essential not only for comfort but also to prevent issues like mold growth and dehydration. Additionally, indoor chemical reactions can generate secondary pollutants, further degrading air quality.[4]

Research on atmospheric conditions has traditionally concentrated on the outdoor environment, examining issues such as air pollution and climate change. While the research has deepened our understanding of outdoor air quality, there has been less focus on indoor air composition and its associated chemistry. The Clean Air Act, established in the United States in 1970, provides comprehensive regulations for outdoor air quality, yet there are no equivalent standards for indoor air quality.[5] This began to change in the 1990s when attention shifted towards the indoor atmosphere due to its complexity and the fact that people spend the majority of their time indoors.[6] Indoor air quality presents unique challenges. The variability of indoor environments, influenced by individual activities and building characteristics, requires fast-response instruments and high coverage to accurately monitor and assess air quality. The complexity of indoor air chemistry has been recognized only recently. Advanced instrumentation has revealed that indoor environments undergo significant chemical changes, with the concentrations of indoor pollutants varying with the time of day, seasons, and geographic locations. Surface chemistry, involving interactions with skin, hair, clothing, and building materials, often has a larger impact on indoor air quality than gas-phase chemistry.[7] Despite these advancements, much remains to be learned about indoor air quality. As our understanding of indoor chemistry grows,

it becomes increasingly clear that understanding dynamic multiphase chemistry that occurs indoors is essential to mitigate health risks and ensure safe and comfortable indoor spaces.

1.1.1 Characteristics of the Indoor Environment

Indoor spaces offer a unique environment compared to the outdoors. Despite differences in layouts, uses, and occupancy patterns, indoor spaces share common characteristics from the perspectives of indoor air quality and indoor chemistry.

First, indoor spaces are enclosed by physical boundaries such as walls, floors, and ceilings. This enclosure creates a controlled environment that is distinct from outdoor conditions. Ventilation, which refers to the exchange of indoor air with outdoor air or air from other rooms, is a crucial aspect of maintaining indoor air quality. Indoor spaces can use natural ventilation methods, such as windows and doors, mechanical systems like heating, ventilation, and air conditioning, or a combination of both. Proper ventilation serves several essential functions: (i) regulating indoor humidity and temperature, (ii) introducing fresh air and maintaining oxygen levels, and (iii) removing indoor air pollutants and reducing the concentration of airborne contaminants.[8] In contrast, poor ventilation can lead to the accumulation of indoor air pollutants, adversely affecting occupant comfort and health. The ventilation rate, often measured in air changes per hour, should be appropriate for the room's size, occupancy, and intended use. According to a United States survey, the median residential air exchange rate is reported to be 0.5 h^{-1}, with a standard deviation of 0.9 h^{-1}, meaning the air is replaced every one to two hours.[9] In commercial buildings, the air is replaced more frequently due to higher ventilation rates.[10]

The second feature of indoor spaces is the high surface-to-volume (S/V) ratio compared to outdoor settings. According to a recent study, the average S/V ratio in indoor spaces, accounting for contents, is about 3.2 ± 1.2 m^{-1}. Without contents, this ratio is approximately 1.8 ± 0.3 m^{-1}.[11] The large surface area indoors provides more opportunities for chemical reactions, sorption, and desorption. Specifically, heterogeneous reactions between gas phases and surfaces play a significant role, particularly under certain environmental conditions. The sorption and desorption processes of gases and particles on surfaces significantly influence their concentrations

in indoor air. Some surface materials, such as paintings and furniture, have sufficiently high porosity, allowing molecules to diffuse into them.[12] In a comprehensive study measuring more than 20 typical rooms in indoor environments, including bedrooms, kitchens, and offices, it was found, as illustrated in Figure 1.2, that painted surfaces are the predominant materials indoors, accounting for 42 ± 14% of the total surface area on average. Wood surfaces are the second most prevalent, comprising 22 ± 12% of the total surface area.[11] These surface reservoirs can drive both non-reactive partitioning processes and reactive chemistry, potentially leading to changes in pollutant concentrations. Additionally, surfaces can act as both sinks and sources for indoor gas-phase compounds, influencing long-term indoor air quality.

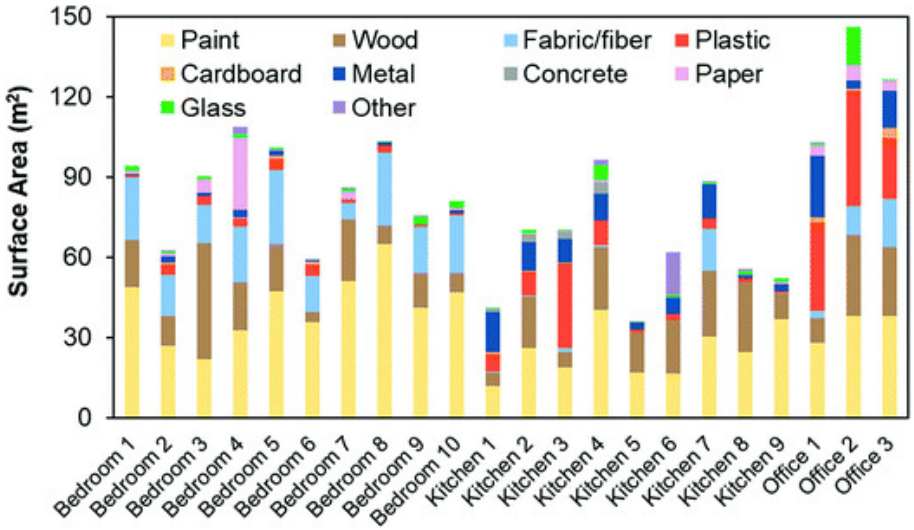

Figure 1.2: Surface area by material of all contents in each room. Paint refers to paint-covered surfaces, and Wood refers to stained wood. From Manuja *et al.* "Total surface area in indoor environments" *Environmental Science: Processes & Impacts* 21.8 (2019): 1384-1392.[11] Reprinted with permission from Royal Society of Chemistry.

Thirdly, indoor spaces generally have low photon fluxes, especially ultraviolet (UV) radiation. Most UV radiation is filtered by windows, and indoor lighting sources generally do not emit UV radiation.[13] With reduced UV light, indoor environments typically have lower levels of major oxidants like ozone and hydroxyl radicals. However, these oxidants still play a key role in indoor oxidation processes, resulting in differences from outdoor environments.[14] Certain pollutants that are quickly oxi-

dized outdoors may persist longer indoors.

Finally, human activities and the specific products used indoors differentiate the indoor environment from outdoor settings in terms of air quality and pollution sources. Activities such as smoking, cooking, cleaning, and personal care product use are significant contributors to indoor air pollutants.[15] Additionally, human behavior impacts indoor air quality through ventilation practices, heating and air conditioning system maintenance, and the introduction of outdoor pollutants. Furthermore, multiphase chemistry occurring on clothing and skin also influences indoor air quality.[16]

1.1.2 Sources of Indoor Chemicals

Indoor environments contain a complex mixture of chemicals originating from both indoor and outdoor sources, present in the form of particulate matter (PM), inorganic gas and volatile organic compounds(VOCs).

Indoor PM originates from both primary and secondary sources. Primary PM is directly emitted from activities such as cooking, heating, tobacco smoking, and cleaning. Cooking, particularly high-temperature methods like frying, releases substantial amounts of ultrafine and fine particles.[17] Biomass fuels, such as coal and wood, used for cooking and heating, also give rise to high concentrations of PM.[18] Tobacco smoke, from cigarettes and e-cigarettes, is another major source of indoor PM, with concentrations of PM and toxic trace elements being notably higher during smoking.[19, 20] Incense burning significantly adds to indoor PM levels, often producing higher concentrations compared to cigarettes.[21] Secondary sources of indoor PM are formed through chemical reactions that occur within the indoor environment.[22] These reactions can involve indoor pollutants reacting with each other or with outdoor pollutants that have infiltrated the indoor space through ventilation systems. Outdoor pollutants include those from vehicle emissions, industrial activities, and natural events like wildfire smoke.[23, 24]

Indoor inorganic gases can originate from both indoor and outdoor sources. Carbon dioxide is a major indoor pollutant, mainly produced from occupant respiration.[25] It can also arise from combustion processes, such as burning candles.[26] High carbon dioxide concentrations often indicate poor ventilation, which can lead to the accumulation of other pollutants and potentially increase the risk of airborne diseases.[27]

Nitrogen oxides and carbon monoxide are also common indoor pollutants. They can originate from outdoor sources, such as traffic, as well as from indoor combustion activities like heating and cooking.[28] Ozone, though less frequently found indoors, primarily enters buildings via ventilation and infiltration from outdoor sources. It can also be emitted by office equipment, such as laser printers and electrostatic air cleaners.[29]

Indoor VOCs are a large and diverse group of chemicals that easily evaporate at room temperature. The next section will summarize the sources of indoor VOCs and their environmental behaviors.

1.2 Indoor Volatile Organic Compounds

Organic compounds are chemicals that generally contain carbon atoms bonded to hydrogen, oxygen, nitrogen, or other elements. These compounds can be further classified into several categories based on their boiling points: very volatile organic compounds, volatile organic compounds, semi-volatile organic compounds, and non-volatile organic compounds. Specifically, VOCs are organic compounds with boiling point ranges between 50 °C and 260 °C.[30] VOCs typically have low boiling points, high vapor pressures, and low molecular weights, allowing them to easily transition from liquid or solid form to gas at room temperature. VOCs are commonly found in indoor air and are among the most prevalent and studied indoor air pollutants due to their widespread sources and potential health impacts.[31]

1.2.1 Sources of Indoor VOCs

Indoor VOCs are often found at significantly higher concentrations compared to outdoor levels.[32] This elevated presence is primarily due to a variety of sources within indoor environments. Understanding these sources is crucial for managing indoor air quality and mitigating potential health risks associated with VOC exposure. This section provides an overview of the primary sources of indoor VOCs, including specific chemicals emitted from each source.

Construction materials and furnishings are significant contributors to indoor VOC levels, especially when new. Modern synthetic materials, chosen for their properties

such as economy, preservation, and desirable performance (including water, fire, and mold resistance), often contain VOCs found in paints, fabrics, and furniture. Building materials like carpets, paints, and pressed wood products can emit formaldehyde, terpenes, and other VOCs.[33–35] Flooring and furniture are also sources to various VOCs including acetaldehyde, phenol, benzene and toluene.[36]

Cleaning agents, air fresheners, and personal care products are also major sources.[37–39] For example, cleaning agents and air fresheners commonly emit terpenes, sodium hypochlorite, ammonia, and acetic acid.[40] Perfumes and hairsprays are common sources of compounds, such as α-pinene, limonene, ethanol, and methanol.[41] Combustion sources like gas stoves and smoking emit smoke containing a complex mixture of chemicals, including benzene, formaldehyde, and toluene.[42, 43] Consumer electronics, particularly when new or heated during operation, can emit VOCs. A recent study reported that liquid crystal displays, commonly used in smartphones, computer monitors, laptops, and televisions, can emit more than 30 VOCs indoors.[44] The rising popularity of vaping has introduced a new source of indoor VOCs, with e-cigarette aerosols containing a complex mixture of compounds, including nicotine, flavoring compounds, benzaldehyde, and formaldehyde.[45]

Certain human activities, such as cooking (especially frying and grilling), can release VOCs.[46] Additionally, human metabolism contributes to indoor VOC levels, with isoprene being emitted in human breath.[47] A recent study found that human occupants can contribute up to 40% of indoor VOC concentrations.[48] Microbial activities, such as those from bacteria and fungi, represent a significant and often overlooked source of indoor VOCs.[49] For example, mold growth in damp areas and dust mites in carpets and bedding emit microbial volatile organic compounds (MVOCs), including 2-methyl-1-propanol, 3-methyl-1-butanol, and 2-pentanol, which often contribute to the musty odor associated with mold growth.[50]

While the focus is on indoor sources, it is important to note that outdoor VOCs can infiltrate indoor spaces. Vehicle exhaust, industrial emissions, and pesticides used in landscaping can all contribute to indoor VOC levels. Moreover, certain emerging sources of indoor VOCs have been identified in recent studies. For instance, 3D printers, increasingly common in homes and offices, have been found to emit more than 200 VOCs and ultrafine particles during operation.[51] Additionally, the growing

use of essential oils and diffusers for aromatherapy purposes introduces a new source of terpenes and other VOCs into indoor environments.[52]

1.2.2 Emission and Behavior of Indoor VOCs

The emission of VOCs from indoor sources can be both persistent and intermittent, creating a complex mixture of compounds in the air. Persistent emissions, such as those from building materials and furniture, occur through off-gassing, which can last for months or years, leading to prolonged exposure.[53] Intermittent sources, like smoking, cooking, and painting, release VOCs in bursts, contributing to variable indoor air quality.[54–56] Emission rates of VOCs can vary based on environmental factors. For instance, a rising temperature can accelerate VOC emissions from materials. A study found that VOC emissions from flooring materials rose notably when the temperature increased from 23 °C to 50 °C.[57] This variability complicates the management of indoor VOC levels, potentially leading to high peak concentrations.

Indoor VOCs are not only primary pollutants but also precursors to secondary pollutants through chemical reactions. One critical concern is the formation of Secondary Organic Aerosols (SOAs). VOCs can undergo multiphase chemistry, reacting with other indoor pollutants to form more harmful compounds, such as formaldehyde, a known carcinogen.[58] Exposure to indoor VOCs poses significant health risks. Short-term exposure can cause symptoms like eye and respiratory tract irritation, headaches, and dizziness.[59] Long-term exposure is even more concerning, with potential damage to the liver, kidneys, and central nervous system.[60]

Recent advancements in indoor air quality research have highlighted the role of indoor chemical partitioning. This process involves the interaction between VOCs and indoor surfaces, influencing the fate and transport of these compounds. Understanding these interactions is crucial for developing more effective strategies to manage indoor air quality.

1.2.3 Analysis of Indoor VOCs

In real-world measurements of indoor environments, the term "total volatile organic compounds" (TVOCs) is used to describe the total concentration of multiple VOCs present in indoor air. These measurements capture the combined effect of multiple

VOCs, which can be more representative of overall air quality than focusing on a single compound.[61] TVOC levels serve as a useful indicator of general indoor air quality and potential sources of pollution. However, the negative health impact of air pollution is dictated by specific chemical species rather than TVOC. Often, these specific species are unknown. As such, efforts have been made in the past decades to obtain more detailed information about the VOCs in the air.

Sampling methods for indoor VOCs can be broadly categorized into off-line and on-line techniques. Off-line methods typically involve collecting air samples on sorbent materials for later analysis, while on-line techniques provide real-time measurements.[62] One of the most widely used offline techniques for VOC analysis is active sampling using sorbent tubes. In this method, a known volume of air is pumped through a tube containing an adsorbent material, which traps the VOCs. The trapped compounds are subsequently thermally desorbed and analyzed using gas chromatography-mass spectrometry (GC-MS).[63, 64] Gas chromatography (GC) coupled with various detectors remains a cornerstone technique for VOC analysis. GC-MS is particularly powerful due to its ability to separate and identify a wide range of compounds. However, this method has limitations, particularly its low time resolution, making it challenging to capture changes in indoor VOC concentrations that occur over short timescales, such as within seconds or minutes. Online techniques offer the advantage of real-time measurements, which are essential for understanding the dynamics of indoor VOC concentrations. Proton transfer reaction-mass spectrometry and chemical ionization mass spectrometry are powerful online techniques that allow for high-sensitivity, real-time detection of VOCs.[65, 66] These methods provide high time resolution (seconds to minutes) and enable non-targeted measurements of indoor VOCs.

As research in this field progresses, emerging techniques such as comprehensive two-dimensional gas chromatography are expanding the capabilities for indoor VOC analysis.[67] Concurrently, advances in sensor technology have led to the development of low-cost, portable VOC sensors.[68] Although these devices often lack the specificity and sensitivity of laboratory-grade instruments, they offer significant potential for widespread deployment and continuous monitoring. Many studies now employ a combination of these techniques to provide a comprehensive assessment of indoor

VOCs.

1.3 Indoor Chemical Partitioning

1.3.1 The Presence and Dynamics of Chemical Partitioning in Indoor Environments

In indoor environments, chemicals are constantly changing, which leads to the dynamic transfer of chemicals between various phases. Partitioning refers to the distribution of chemicals among these phases under equilibrium within a system, while the partitioning process refers to the transfer of chemicals among phases before the system reaches equilibrium. The phase distribution of chemicals further influences the pathways and duration of human exposure to indoor pollutants, as well as the effectiveness of removal strategies.

The distinctive "new car smell" has long been recognized as a result of VOC emissions from interior materials in vehicles.[69] This phenomenon provided early indications of how materials used in enclosed spaces can release chemicals into the air over time. Similarly, the concept of thirdhand smoke, which refers to the residual contamination released into the air again from tobacco smoke left on surfaces and in dust after smoking events, highlights the persistence of chemical compounds in indoor environments.[70] These early observations indicated interactions between VOCs and indoor surfaces, but the full complexity of these interactions has only been shown recently.

A recent study conducted by Chen Wang et al., represents a significant advancement in the understanding of indoor chemical partitioning.[71] Their research provided a detailed examination of the dynamic partitioning behavior of VOCs with indoor surfaces. Figure 1.3 presents data collected during a field campaign at the experimental house. This figure illustrates the indoor mixing ratios of several acids during repetitive Enhanced Ventilation (EV) experiments.[71] In this context, EV refers to a scenario with a higher ventilation rate, achieved by opening windows and doors, as opposed to normal ventilation where the house remains closed.

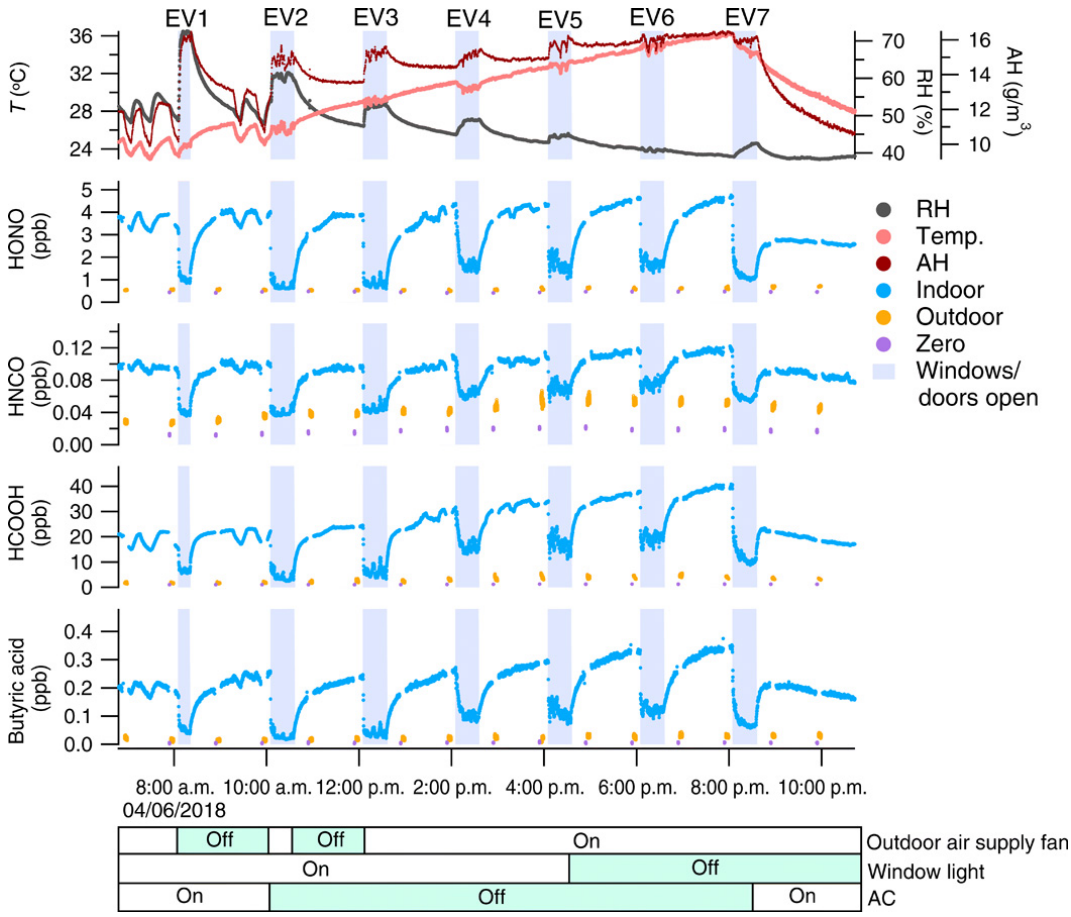

Figure 1.3: Indoor mixing ratios of several acids during EV experiments. The top panel shows the measured house temperature (T; left axis), relative humidity (RH; right axis), and absolute humidity (AH; second right axis). The shaded areas indicate when doors and windows were open to increase the ventilation rate of the house. The hourly 2-min background measurement (measuring zero air) is shown with purple dots, followed by a 5-min outdoor measurement (orange dots). The color bars at the bottom of the plot show the state of outdoor air supply fan (on/off), window light (with/without), and air conditioning (AC) (on/off) during the experiment, with the green shaded periods showing when the fan, window light, and AC were off. From Wang *et al.* "Surface reservoirs dominate dynamic gas-surface partitioning of many indoor air constituents" *Science advances* 6.8 (2020): eaay8973.[71] Reprinted with permission from AAAS.

The EV experiments revealed that indoor mixing ratios of acids exhibited a sharp initial decrease at the beginning of each EV period. This was followed by a rapid rebound during each period of normal ventilation. Specifically, the response time for the small acids measured ranged between 700 and 1000 seconds. These observations provide compelling evidence that indoor surfaces function as both sinks and sources of

VOCs, highlighting the presence of dynamic partitioning between the air and indoor surfaces. Moreover, the repetitive nature of these observations across multiple EV experiments suggested the existence of substantial indoor reservoirs. This is evidenced by the indoor mixing ratios consistently returning to similar levels after each EV period, despite repeated cycles of EV.

1.3.2 Reservoirs in Indoor Environment

As previously discussed, the recent discovery of highly active chemical partitioning of indoor VOCs underscores the importance of understanding the properties of indoor reservoirs. Indoor reservoirs are defined as the surfaces and volumes within indoor environments where chemicals can be partition into. Specifically, these reservoirs include surfaces, surface films, deposited particles, internal voids, and permeable materials, as illustrated in Figure 1.4.[72] These reservoirs can be either solid or liquid, with the partitioning process occurring between the air and any type of reservoir.

Surface materials like carpets and fabrics are permeable, allowing gas-phase chemicals to slowly partition into them over time, thereby acting as long-term reservoirs.[73, 74] In contrast, impermeable materials, such as metal, stone, and window glass, do not allow mass transfer into their interiors over relevant timescales. Instead, these surfaces permit molecules and deposited particles to accumulate as films with thicknesses ranging from nanometers to micrometers, growing at a rate of approximately 0.05 nm/day.[75–77] Through this process, the formed films serve as new and continuously-changing surfaces, which contributes to the complexity of indoor reservoirs.

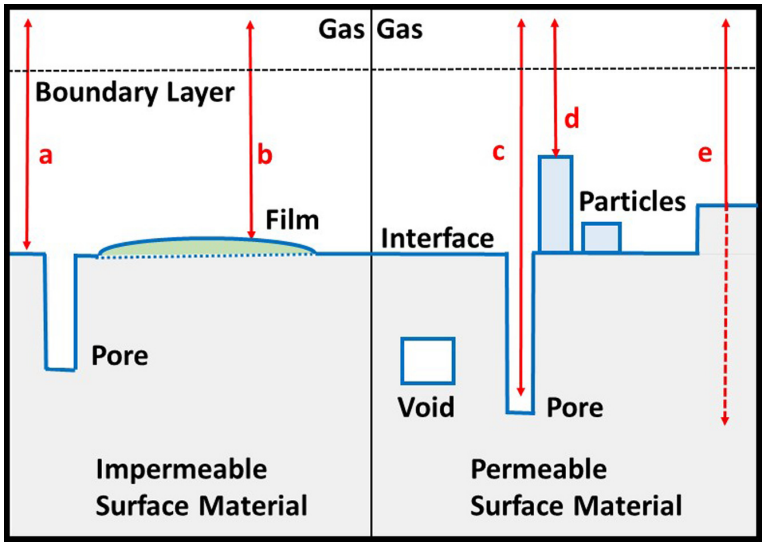

Figure 1.4: Indoor surface reservoirs, including interfaces with the gas phase (solid blue lines), films, deposited particles, internal voids, and permeable bulk materials. Via mass transfer processes (red arrows), gaseous molecules can adsorb to interfaces (a), create surface films (b), partition to deposited particles (d), and move into surface materials by diffusion within pores (c) or within the condensed-phase material (e). Multiphase reactions can occur within any surface reservoir. The red arrows are two-headed, indicating mass transfer both to and from surface reservoirs. Mass transfer in the gas phase is depicted with a solid red arrow, whereas a dashed red arrow is used for (slower) diffusion in the condensed phase. Gas-phase mass transfer occurs via diffusion through a few mm-thick boundary layer adjacent to the interface. Internal voids may or may not interact with the gas phase depending on condensed-phase mass transfer rates. From Abbatt *et al.* "How should we define an indoor surface?" *Indoor Air* 32(1) (2022).[20] Reprinted with permission from John Wiley and Sons.

Different types of reservoirs may lead to different partitioning processes over varying timescales. The timescales for gas-phase molecules partitioning into surface films are typically rapid, occurring within microseconds.[12, 78] In contrast, partitioning into materials can take significantly longer. For example, partitioning into a dried painting with a thickness of 50 μm can take hours, while partitioning into building materials like concrete can take years.[58, 79]

In addition to indoor reservoirs, another important phase in the indoor chemical partitioning process is aerosol particles. Although the residence time of aerosol particles can only be as long as the ventilation timescale, the concentration of aerosol particles can be extremely high under specific conditions, such as during cooking and smoking, especially under poorly ventilated conditions.[80] Importantly, chem-

icals partitioned to particles from the air can be inhaled by humans, thus making it crucial to consider aerosols in indoor chemical partitioning and the interactions between the gas phase, indoor reservoirs, and the aerosol phase. An exemplary case is thirdhand smoke. During smoking events, released compounds can undergo gas-reservoir partitioning or gas-particle-reservoir partitioning. After the smoking events, the residual compounds in the reservoirs can be re-emitted into the indoor air, leading to reservoir-gas-particle interactions.[81, 82]

1.3.3 Partitioning Coefficients

When a compound is introduced into the environment, it tends to migrate between phases to establish equilibrium. For example, nicotine from smoking tends to transfer to indoor surfaces after being released into the air.[83] Similarly, persistent organic pollutants tend to be found in indoor dust.[84] In essence, the equilibrium between gas and condensed phases is a result of the need to balance the chemical potentials and the influence of intermolecular forces. Even highly volatile compounds cannot be 100% in the gas phase because equilibrium requires that some fraction remains in the condensed phases to balance the overall distribution and maintain stability. These processes are primarily governed by partitioning coefficients between two phases, such as the water-air partitioning coefficient (K_{wa}), octanol-air partitioning coefficient (K_{oa}) and octanol-water partitioning coefficient (K_{ow}), which quantify the compound's tendency to move between phases. Notably, 1-octanol has long been used as a surrogate for various organic phases in phase distribution studies.[85]

Partitioning coefficients describe how a compound distributes between different phases, such as air, water, and organic matter, at equilibrium. These coefficients are dependent on environmental conditions such as temperature and are essential for elucidating the environmental dynamics of organic compounds. In fact, they have been employed widely by environmental chemists to illustrate the fate, distribution, and exposure pathways of organic pollutants in outdoor environments.[85] The application of these partitioning coefficients to indoor environments has garnered attention in recent years.[86] However, in real environments, non-ideal conditions arise because pure water or organic phases rarely exist. While partitioning coefficients offer valuable insights into distribution trends, they must be interpreted considering these complex-

ities for a more accurate depiction of compound behavior.

K_{wa}, K_{oa}, and K_{ow} are defined by the following equations, where c_{w}, c_{a}, c_{o} represent the equilibrium concentrations of a compound in the aqueous, gas, and octanol phases, respectively:

$$K_{\mathrm{wa}} = c_{\mathrm{w}}/c_{\mathrm{a}} \tag{1.1}$$

$$K_{\mathrm{oa}} = c_{\mathrm{o}}/c_{\mathrm{a}} \tag{1.2}$$

$$K_{\mathrm{ow}} = c_{\mathrm{o}}/c_{\mathrm{w}} \tag{1.3}$$

They are often presented as unitless or in logarithmic form due to their wide range of values. If two of these three partitioning coefficients are known, the third can be determined using the following equation:

$$K_{\mathrm{ow}} = K_{\mathrm{oa}}/K_{\mathrm{wa}} \tag{1.4}$$

Compounds with low K_{wa} are likely to evaporate easily from the water phase, resulting in higher concentrations in the air. By contrast, compounds with high K_{oa} tend to partition into organic phases, such as the organic films in indoor environments, further affecting human exposure to pollutants and bioaccumulation potential.[87]

1.3.4 Measurement and Prediction of Partitioning Coefficients

Accurate measurement of partitioning coefficients is crucial for reliable predictions of the transport and fate of organic compounds. The determination of K_{wa} can be achieved through various experimental methods, which will be introduced in the following section. The measurement methods for the K_{oa} and the K_{ow} are introduced here.

The measurement of K_{oa} involves various experimental techniques categorized into static, dynamic, and indirect methods. Static methods include headspace techniques, where solutes are allowed to equilibrate between a stationary octanol phase and the headspace in a closed container.[88] The equilibrium concentration of the solute in

the headspace is then measured, often using GC. Dynamic techniques such as the generator column method pass a stream of air through a column containing a stationary octanol phase, allowing for the partitioning of solutes between the air and octanol.[89] Inert gas stripping (IGS) method involves passing a stream of air over a stationary phase of octanol, removing the solutes and measuring their concentrations.[90] Indirect techniques, such as GC retention time methods, allow analytes to pass through the GC column, simulating the octanol phase. The K_{oa} is determined by comparing the retention times of the analytes to those of reference compounds with known K_{oa} values.[91] Each technique has specific applicability ranges and temperature conditions, with headspace techniques suited for volatile compounds and gas stripping and generator column methods better for less volatile solutes. The selection of an appropriate method depends on the solute's volatility, concentration, and the desired temperature range for the measurement.[92]

Common methods for measuring K_{ow} include the shake-flask method and high-performance liquid chromatography (HPLC). The shake-flask method involves equilibrating the compound between octanol and water phases and analyzing the concentrations in each phase to determine K_{ow}.[93] Although this method is straightforward and widely used, it can be time-consuming and requires substantial amounts of sample and solvents. In contrast, HPLC provides a faster and more automated approach. In this method, compounds are separated and quantified on a chromatographic column, and K_{ow} is determined by comparing the retention times or peak areas of the compound in an octanol-like stationary phase versus a water phase, using calibration standards with known K_{ow} values.[94]

Modeling techniques have been developed to predict partitioning coefficients when experimental data is unavailable, as measuring these coefficients for all compounds and reservoirs experimentally is challenging. Advanced tools and databases, such as the EAS-E Suite, have been created to aid in predicting partitioning coefficients and provide estimated values for various chemicals.[95] These tools often incorporate poly-parameter linear free energy relationships (ppLFERs) to estimate partitioning coefficients. This method considers multiple descriptors, such as polarity of the molecule and H-bonding interactions, to account for various types of interactions between chemicals and environmental phases based on molecular structure and prop-

erties.[96] The uncertainty and bias of the ppLFERs model come from several sources. First, predictions for chemicals outside the domain of the model exhibit higher uncertainty due to extrapolation beyond the training data, which can significantly affect accuracy. Errors also arise from the variability in experimental data and the inherent challenges in measuring partitioning coefficients. Typically, the root mean squared error of prediction for partitioning coefficients ranges from 0.7 to 1.4.[97]

1.3.5 Indoor Chemical Partitioning Model

Indoor chemical partitioning models are essential tools for understanding the distribution and behavior of chemicals in indoor environments. These models help predict how various compounds interact with different phases, ultimately affecting indoor air quality and human exposure.

A key component in indoor chemical partitioning models is the Chemical Two-Dimensional (2D) Partitioning Space Plot. This tool, initially utilized to illustrate the phase distribution of organic compounds in the atmosphere, has subsequently been adapted for indoor environments. In this model, the three phases include the gas phase (air), the polar phase (represented by water), and the weakly polar phase (represented by 1-octanol), which are widely accepted terms.[98, 99] The plot typically uses two axes representing different partition coefficients, K_{wa} and K_{oa}. By combining partition coefficients with the sizes of reservoirs, the model can determine the amount of a chemical in each phase under equilibrium. This visualization technique provides a comprehensive view of how chemicals distribute among different phases in an indoor environment under equilibrium. Plotting chemicals on this 2D space helps to quickly visualize and compare the partitioning behavior of different compounds. This approach aids in the preliminary screening of chemicals that are likely to be important in specific phases of interest.

An illustrative application of this model framework is shown in Figure 1.5, which depicts the phase distribution of common atmospheric molecules in both outdoor and indoor environments.[100] This plot demonstrates that, in indoor settings, the majority of chemical constituents tend to partition into surface reservoirs. The larger the volume of these reservoirs, the greater the proportion of chemicals that remain in them. Consequently, many VOCs that are entirely volatile in outdoor environments

may exhibit SVOC behavior indoors due to the increased partitioning capacity of indoor surfaces.

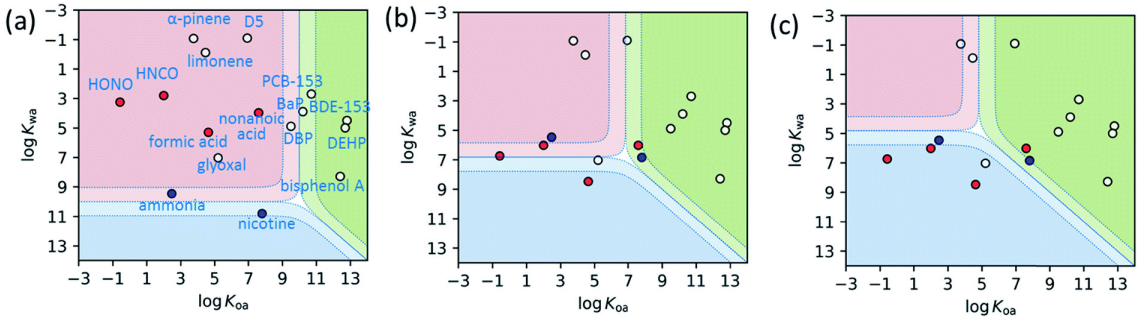

Figure 1.5: Two-dimensional phase partitioning plots for common atmospheric molecules. Species in the red region reside largely in the gas phase, whereas those in the blue and green regions are predicted to reside in the polar and weakly-polar reservoirs, respectively. The solid boundaries and dotted boundaries represent 50:50 and 90:10 partitioning, respectively. Acidbase effects are considered in the polar reservoir as they would occur in water. Non-dissociating molecules are indicated by white circles, acids by red circles and bases by blue circles. (a) is for outdoor polluted conditions, with the equivalent of 100 $\mu g\,m^{-3}$ of both polar (pH 3) and weakly-polar aerosol mass loading. (b) represents conditions for 50 nm-thick water (i.e. polar, assumed pH 7) and organic (i.e. weakly polar) films in an indoor space of $S/V = 3\ m^{-1}$. (c) represents conditions for 100 larger surface reservoir volumes than those in (b), to model partitioning into building materials and furnishings. Chemical names are labeled in (a), with HONO, HNCO, D5, BaP, DBP, DEHP representing nitrous acid, isocyanic acid, decamethylcyclopentasiloxane, benzo[a]pyrene, dibutyl phthalate, and bis(2-ethylhexyl)phthalate, respectively. From Abbatt and Wang "The atmospheric chemistry of indoor environments" *Environmental Science: Processes & Impacts* 22.1 (2020): 25-48.[100] Reprinted with permission from Royal Society of Chemistry.

The human exposure model based on K_{oa} and K_{wa} is an extension of this concept, focusing on how these partitioning behaviors affect potential human exposure routes.[101, 102] A recent study employed the PROTEX model to predict human exposure to indoor organic compounds via inhalation, dermal contact, and dietary and non-dietary ingestion.[103] For instance, compounds with high K_{oa} values are more likely to partition into organic materials and may lead to increased dermal exposure or ingestion through dust. Chemicals with low K_{wa} values might volatilize from the aqueous phase into indoor air, potentially leading to increased inhalation exposure.

These models are especially valuable for understanding the behavior of VOCs in

indoor environments. Accurate determination of partitioning coefficients is crucial for predicting the behavior of these chemicals in indoor settings.

1.4 Henry's Law Constant

This section provides a detailed introduction to Henry's law constant (H), as its measurement is a central focus of this thesis. Henry's law is named after the English chemist William Henry, who first described the experimental observation that the amount of dissolved gas is proportional to its partial pressure in the gas phase in the early 19th century.[104] H is defined as the proportional ratio between the aqueous-phase concentration in an infinitely diluted solution and the partial pressure in the gas phase under equilibrium. The water-air partitioning coefficient, K_{wa}, is equivalent to H after accounting for the gas constant and temperature. The conversion can be obtained via the ideal gas law using the following equation:

$$K_{\mathrm{wa}} = H \times RT \tag{1.5}$$

where R is the ideal gas constant 8.314 $\mathrm{Pa{\cdot}m^3{\cdot}mol^{-1}{\cdot}K^{-1}}$ and T is the absolute temperature in K, H is typically in units of $\mathrm{mol{\cdot}m^{-3}{\cdot}Pa^{-1}}$.

It should be noted that Henry's law constants are highly temperature-dependent, following the van 't Hoff equation:[105]

$$\mathrm{d}\ln H/\mathrm{d}(1/T) = -\Delta_{\mathrm{sol}}H/R \tag{1.6}$$

where $\Delta_{\mathrm{sol}}H$ is the molar enthalpy of dissolution ($\mathrm{kJ{\cdot}mol^{-1}}$). This equation is typically valid for temperatures close to the reference temperature of 298.15 K (25 °C). It is applicable within a specific temperature range where $\Delta_{\mathrm{sol}}H$ does not vary significantly with temperature. For many environmental applications, such as indoor air quality studies, the approximation provided by the van 't Hoff equation should be reasonably accurate.

In atmospheric chemistry, H enables scientists to assess how pollutants partition between air and liquid cloud droplets or aerosol particles, influencing their persistence and distribution in the environment.[106] From a climate science perspective, Henry's law explains the dissolution of atmospheric gases in water bodies such as

oceans and lakes. This understanding is crucial for studying gas exchange between the atmosphere and oceans.[107]

1.4.1 Laboratory Approach to Study Henry's Law Constant

Various laboratory methods have been employed to determine H values for different compounds. Theoretically, three primary approaches can be used to obtain these values: Firstly, H values can be determined by independently measuring the solubility and vapor pressure of the compound of interest. Secondly, H values can be obtained by measuring the solubility and vapor pressure of the compound in a system at equilibrium. Techniques such as headspace analysis are used, where the compound's concentration in both the air and liquid phases is measured once equilibrium is reached. Lastly, H values can be measured during an equilibrium air-water exchange process, such as the IGS method.

Headspace analysis is a widely used technique to determine H values.[108] This method involves equilibrating a liquid sample containing the compound of interest with its vapor phase in a sealed container. After reaching equilibrium, a gas phase sample is collected from the vial's headspace using a syringe or automated sampler and analyzed to determine the gas-phase concentration. By comparing this with the initial concentration in the aqueous phase, H values can be calculated as the ratio of these concentrations. This approach facilitates the determination of H values over a range of temperatures, offering insights into the temperature dependence of these constants.

IGS method was initially developed by Leroi et al.[90] This method involves measuring the relative change in the gas phase during an equilibrium air-water exchange process. In this setup, an inert gas stream is bubbled through a liquid column containing the dissolved compound of interest. The contact time between bubbles and the liquid should be long enough to ensure gas-liquid equilibria. By continuously monitoring the gas-phase concentration using suitable detection techniques, the H values can be derived from the rate of concentration decline:

$$\ln(c_t/c_0) = -Gt/HVRT = St \tag{1.7}$$

$$H = -G/SVRT \tag{1.8}$$

where c_t and c_0 represent the gas-phase concentrations at time t and 0, G is the gas flow rate in units of $m^3 \cdot min^{-1}$, t is time in units of min, V is the volume of solution in m^3, R is the ideal gas constant (8.314 $Pa \cdot m^3 \cdot mol^{-1} \cdot K^{-1}$), T is the absolute temperature in K, S is the constant slope as the logarithm of the concentration c_t, normalized to the initial concentration c_0, decreases linearly over time. H here is in units of $mol \cdot m^{-3} \cdot Pa^{-1}$. Additionally, the gas flow rate, liquid volume, and temperature are required for accurate results. This method is advantageous due to its simplicity and the direct measurement of equilibrium states.

Both headspace analysis and IGS setups can be connected to a Gas Chromatography-Flame Ionization Detector (GC-FID) system to analyze the gas phase concentration of the compound, as shown in Figure 1.6.[109] The process begins with injecting the gas-phase sample into the GC, where it is carried by an inert gas (such as helium) through a heated column. This column contains a stationary phase that interacts with the sample components, causing them to separate based on their chemical properties. Once the separated components exit the column, they enter the FID. In the FID, the sample is mixed with hydrogen and an oxidant (typically air) and burned in a hydrogen flame. This combustion ionizes the carbon-containing compounds, generating positive ions and electrons. These ions are attracted to a negatively charged collector plate, creating an electric current proportional to the number of carbon atoms burned. This current is measured and recorded, producing a chromatogram that displays the concentration of each component in the sample based on the peak areas. GC-FID is widely used in environmental research due to its sensitivity and ability to detect a broad range of VOCs, especially in indoor environments.[110]

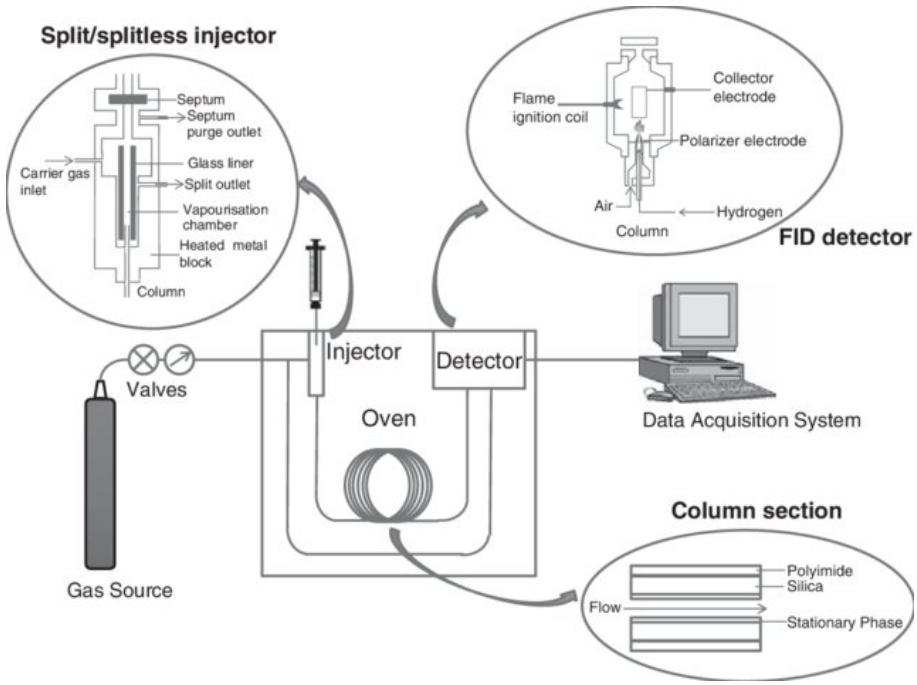

Figure 1.6: Scheme of a GC-FID equipment. From Soria *et al.* "Gas chromatographic analysis of food bioactive oligosaccharides" *Food Oligosaccharides: Production, Analysis and Bioactivity* 21.8 (2014): 370-398. [109] Reprinted with permission from Wiley Books.

1.4.2 Effective Henry's Law constant

The Henry's law constant discussed so far does not consider any chemical equilibria in the aqueous phase. When H refers to the same species in both the aqueous and gas phases, it is called the intrinsic or physical Henry's law constant. In contrast, the H that accounts for additional equilibria occurring to the species in the aqueous phase is called the effective Henry's law constant (H_{eff}).

Figure 1.7 illustrates the impact of the hydration process on the indoor partitioning of VOCs. On the left side, a partitioning equilibrium is shown between the gas phase and surface films, governed by partitioning coefficients such as H. On the right side, the figure demonstrates that when a VOC undergoes hydration in a water-rich surface film, it converts to its hydrated form, thereby affecting the equilibrium between the gas phase and the aqueous phase. This process "pulls" more VOC into the water-rich film, resulting in an increased concentration of VOC in the aqueous phase to achieve equilibrium. H_{eff} represents the ratio of the VOC concentration, including

both unhydrated and hydrated forms, in the aqueous phase to its concentration in the gas phase. Similarly, acid-base chemistry also affects the H value due to dissociation in the aqueous phase.[111]

H_{eff} is a dynamic and multifaceted parameter that extends the classical understanding of gas solubility to accommodate real-world complexities. By considering factors such as hydration, pH, salinity, and the presence of other solutes, H_{eff} provides a more accurate and practical understanding of gas-aqueous interactions occurring in the environment.[112]

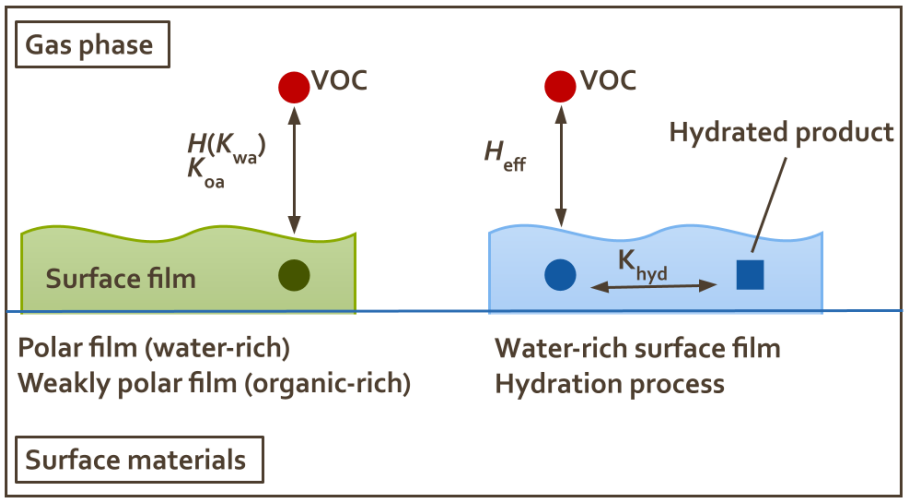

Figure 1.7: Indoor chemical partitioning processes of VOCs between the gas phase and surface films.

Aqueous reactions, such as the hydration process, can be effectively observed and quantified using nuclear magnetic resonance (NMR) spectroscopy.[113] NMR spectroscopy relies on the magnetic properties of certain atomic nuclei, such as hydrogen and carbon-13. As depicted in Figure 1.8, samples are typically placed in a strong external magnetic field.[114] Within this field, these nuclei act like tiny magnets, with their spins aligning either with or against the direction of the field, resulting in different energy levels. By applying a radiofrequency pulse at a specific resonance frequency, nuclei are excited from a lower energy state to a higher energy state. When the pulse is removed, the nuclei undergo a relaxation process, releasing energy in the process. This released energy is detected and recorded as an NMR

signal. The frequency of this energy release, known as the chemical shift, depends on the chemical environment of the nuclei and is measured in parts per million. In the context of compound hydration, analyzing the chemical shifts and the resulting splitting patterns provides crucial insights into the progress of the hydration reaction. This analysis helps to characterize both the original compound and the hydrated product.

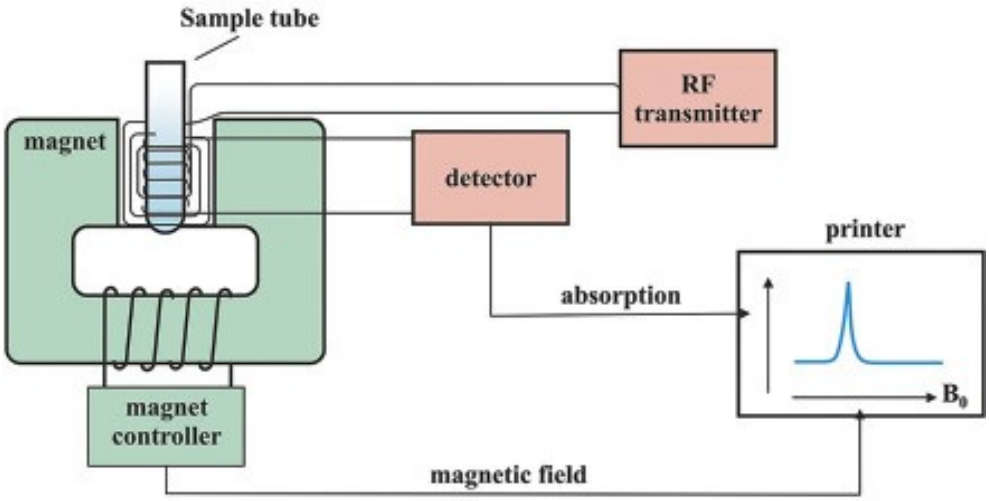

Figure 1.8: Schematic presentation of a typical nuclear magnetic resonance spectrometer showing the relationship of various components (magnet, magnetic field, and detector). From Zia *et al.* "Nuclear magnetic resonance spectroscopy for medical and dental applications: a comprehensive review" *European journal of dentistry* 13.01 (2019): 124-128. [114] Reprinted with permission from Georg Thieme Verlag KG.

1.5 Motivation

The indoor environment is a critical factor in human exposure to organic pollutants, with potential exposure routes including inhalation, ingestion of dust, and skin absorption. Compared to outdoor environments, indoor settings are more complex due to the diverse sources of pollutants, particularly those associated with human activities. As individuals spend a significant amount of their time indoors, prolonged exposure to even low concentrations of pollutants can result in considerable adverse health effects. Indoor environments can also contain unexpectedly large reservoirs that function as both sources and sinks for indoor organic contaminants. These reser-

voirs facilitate persistent exposure by allowing VOCs that would have no interactions with surfaces outdoors to act as semi-volatile organic compounds indoors. Consequently, VOCs can accumulate in these reservoirs and later re-emit into the indoor air, contributing to involuntary and enduring forms of exposure. Chemical partitioning processes are governed by partitioning coefficients; however, the available data for these coefficients concerning key indoor VOCs remains insufficient. Therefore, it is essential to experimentally determine accurate partitioning coefficients to advance our understanding of chemical partitioning dynamics. Additionally, employing advanced partitioning models to predict the indoor phase distribution of VOCs will offer deeper insights into their behavior and potential exposure pathways. The primary motivation of this study is to understand the complex dynamics of indoor air quality. By advancing our understanding of indoor chemical partitioning and exposure mechanisms, this research aims to enhance indoor air quality and mitigate associated health risks.

1.6 Thesis Objectives

The overall aim of this thesis is to investigate the chemical partitioning and human exposure pathways of indoor organic pollutants, such as MVOCs and e-cigarette emissions. Specifically, the objectives are:

- To establish reliable laboratory methods for measuring partitioning coefficients of VOCs.
- To monitor aqueous reactions that may affect the measurement of partitioning coefficients for VOCs and quantify the resulting products.
- To visualize the indoor phase partitioning of target VOCs using laboratory measurement inputs and estimate the pathways of human exposure.

1.7 Thesis Outline

This thesis consists of five chapters. Chapter 1 provides an overview of the atmosphere in indoor environments, common sources of indoor VOCs, and the theory of indoor chemical partitioning. It discusses a chemical 2D partitioning model framework to

visualize phase distribution for compounds, and laboratory and model techniques for obtaining reliable partitioning coefficients. Chapter 2 explores the phase distribution and potential pathways of human exposure to air pollutants originating from microbes in indoor environments. This investigation is conducted under varying temperatures and different indoor settings by combining laboratory-measured partitioning coefficients with a chemical 2D partitioning model framework. Chapter 3 examines indoor chemical partitioning and potential thirdhand exposure to flavoring agents added to e-cigarettes and hookah tobacco. This involves obtaining H_{eff} using ^{1}H NMR and GC-FID, and comparing them with intrinsic H values. Chapter 4 builds on the work from Chapter 3 by further investigating the formation of acetals between flavoring agents and propylene glycol in e-cigarettes using NMR. It explores the impacts on chemical partitioning and thirdhand exposure, with the partitioning model framework also incorporating bioaccumulation considerations. Chapter 5 presents a summary of the thesis, including the key findings, challenges encountered, and proposed directions for future research.

References

[1] N. E. Klepeis *et al.*, "The national human activity pattern survey (NHAPS): A resource for assessing exposure to environmental pollutants," *Journal of Exposure Science & Environmental Epidemiology*, vol. 11, no. 3, pp. 231–252, 2001.

[2] A. Cincinelli and T. Martellini, "Indoor air quality and health," *International Journal of Environmental Research and Public Health*, vol. 14, no. 11, p. 1286, 2017.

[3] C. A. Redlich, J. Sparer, and M. R. Cullen, "Sick-building syndrome," *The Lancet*, vol. 349, no. 9057, pp. 1013–1016, 1997.

[4] T. Wainman, J. Zhang, C. J. Weschler, and P. J. Lioy, "Ozone and limonene in indoor air: A source of submicron particle exposure.," *Environmental Health Perspectives*, vol. 108, no. 12, pp. 1139–1145, 2000.

[5] A. P. Jones, "Indoor air quality and health," *Atmospheric Environment*, vol. 33, no. 28, pp. 4535–4564, 1999.

[6] C. Weschler, "Chemistry in indoor environments: 20 years of research," *Indoor Air*, vol. 21, no. 3, pp. 205–218, 2011.

[7] G. Morrison, *Interfacial chemistry in indoor environments*, 2008.

[8] I. Turiel, C. Hollowell, R. Miksch, J. Rudy, R. Young, and M. Coye, "The effects of reduced ventilation on indoor air quality in an office building," *Atmospheric Environment (1967)*, vol. 17, no. 1, pp. 51–64, 1983.

[9] D. M. Murray and D. E. Burmaster, "Residential air exchange rates in the United States: Empirical and estimated parametric distributions by season and climatic region," *Risk Analysis*, vol. 15, no. 4, pp. 459–465, 1995.

[10] A. K. Persily, "Field measurement of ventilation rates," *Indoor Air*, vol. 26, no. 1, pp. 97–111, 2016.

[11] A. Manuja *et al.*, "Total surface area in indoor environments," *Environmental Science: Processes & Impacts*, vol. 21, no. 8, pp. 1384–1392, 2019.

[12] L. B. Algrim, D. Pagonis, J. A. de Gouw, J. L. Jimenez, and P. J. Ziemann, "Measurements and modeling of absorptive partitioning of volatile organic compounds to painted surfaces," *Indoor Air*, vol. 30, no. 4, pp. 745–756, 2020.

[13] M. Blocquet *et al.*, "Impact of the spectral and spatial properties of natural light on indoor gas-phase chemistry: Experimental and modeling study," *Indoor Air*, vol. 28, no. 3, pp. 426–440, 2018.

[14] C. J. Young, S. Zhou, J. A. Siegel, and T. F. Kahan, "Illuminating the dark side of indoor oxidants," *Environmental Science: Processes & Impacts*, vol. 21, no. 8, pp. 1229–1239, 2019.

[15] C. J. Weschler, "Roles of the human occupant in indoor chemistry," *Indoor Air*, vol. 26, no. 1, pp. 6–24, 2016.

[16] L. S. Pandrangi and G. C. Morrison, "Ozone interactions with human hair: Ozone uptake rates and product formation," *Atmospheric Environment*, vol. 42, no. 20, pp. 5079–5089, 2008.

[17] K. L. Abdullahi, J. M. Delgado-Saborit, and R. M. Harrison, "Emissions and indoor concentrations of particulate matter and its specific chemical components from cooking: A review," *Atmospheric Environment*, vol. 71, pp. 260–294, 2013.

[18] T. Li *et al.*, "Household concentrations and personal exposure of $PM_{2.5}$ among urban residents using different cooking fuels," *Science of the Total Environment*, vol. 548, pp. 6–12, 2016.

[19] E. K. Soule, S. F. Maloney, T. R. Spindle, A. K. Rudy, M. M. Hiler, and C. O. Cobb, "Electronic cigarette use and indoor air quality in a natural setting," *Tobacco Control*, vol. 26, no. 1, pp. 109–112, 2017.

[20] G. Drago *et al.*, "Relationship between domestic smoking and metals and rare earth elements concentration in indoor $PM_{2.5}$," *Environmental Research*, vol. 165, pp. 71–80, 2018.

[21] T.-C. Lin, G. Krishnaswamy, and D. S. Chi, "Incense smoke: Clinical, structural and molecular effects on airway disease," *Clinical and Molecular Allergy*, vol. 6, pp. 1–9, 2008.

[22] W. Ji and B. Zhao, "Contribution of outdoor-originating particles, indoor-emitted particles and indoor secondary organic aerosol (SOA) to residential indoor $PM_{2.5}$ concentration: A model-based estimation," *Building and Environment*, vol. 90, pp. 196–205, 2015.

[23] I. Rivas *et al.*, "Outdoor infiltration and indoor contribution of UFP and BC, OC, secondary inorganic ions and metals in $PM_{2.5}$ in schools," *Atmospheric Environment*, vol. 106, pp. 129–138, 2015.

[24] Y. Liang, D. Sengupta, M. J. Campmier, D. M. Lunderberg, J. S. Apte, and A. H. Goldstein, "Wildfire smoke impacts on indoor air quality assessed using crowdsourced data in California," *Proceedings of the National Academy of Sciences*, vol. 118, no. 36, e2106478118, 2021.

[25] A. Persily and L. de Jonge, "Carbon dioxide generation rates for building occupants," *Indoor Air*, vol. 27, no. 5, pp. 868–879, 2017.

[26] A. Klosterköther, R. Kurtenbach, P. Wiesen, and J. Kleffmann, "Determination of the emission indices for NO, NO_2, HONO, HCHO, CO, and particles emitted from candles," *Indoor Air*, vol. 31, no. 1, pp. 116–127, 2021.

[27] Z. Peng and J. L. Jimenez, "Exhaled CO_2 as a COVID-19 infection risk proxy for different indoor environments and activities," *Environmental Science & Technology Letters*, vol. 8, no. 5, pp. 392–397, 2021.

[28] W. M. Alberts, "Indoor air pollution: NO, NO_2, CO, and CO_2," *Journal of Allergy and Clinical Immunology*, vol. 94, no. 2, pp. 289–295, 1994.

[29] W. W. Nazaroff and C. J. Weschler, "Indoor ozone: Concentrations and influencing factors," *Indoor Air*, vol. 32, no. 1, e12942, 2022.

[30] M. Maroni, B. Seifert, and T. Lindvall, *Indoor air quality: a comprehensive reference book*. Elsevier, 1995.

[31] S. K. Brown, M. R. Sim, M. J. Abramson, and C. N. Gray, "Concentrations of volatile organic compounds in indoor air-A review," *Indoor Air*, vol. 4, no. 2, pp. 123–134, 1994.

[32] J. L. Adgate *et al.*, "Outdoor, indoor, and personal exposure to VOCs in children," *Environmental Health Perspectives*, vol. 112, no. 14, pp. 1386–1392, 2004.

[33] C.-C. Lin and R. Corsi, "Texanol® ester alcohol emissions from latex paints: Temporal variations and multi-component recoveries," *Atmospheric Environment*, vol. 41, no. 15, pp. 3225–3234, 2007.

[34] T. Salthammer, S. Mentese, and R. Marutzky, "Formaldehyde in the indoor environment," *Chemical Reviews*, vol. 110, no. 4, pp. 2536–2572, 2010.

[35] C. Yu and D. Crump, "A review of the emission of VOCs from polymeric materials used in buildings," *Building and Environment*, vol. 33, no. 6, pp. 357–374, 1998.

[36] J.-Y. Chin *et al.*, "Levels and sources of volatile organic compounds in homes of children with asthma," *Indoor Air*, vol. 24, no. 4, pp. 403–415, 2014.

[37] M. Odabasi, "Halogenated volatile organic compounds from the use of chlorine-bleach-containing household products," *Environmental Science & Technology*, vol. 42, no. 5, pp. 1445–1451, 2008.

[38] D. A. Olson and R. L. Corsi, "In-home formation and emissions of trihalomethanes: The role of residential dishwashers," *Journal of Exposure Science & Environmental Epidemiology*, vol. 14, no. 2, pp. 109–119, 2004.

[39] J. Wong, N Carslaw, R Zhao, S Zhou, and J. Abbatt, "Observations and impacts of bleach washing on indoor chlorine chemistry," *Indoor Air*, vol. 27, no. 6, pp. 1082–1090, 2017.

[40] W. W. Nazaroff and C. J. Weschler, "Cleaning products and air fresheners: Exposure to primary and secondary air pollutants," *Atmospheric Environment*, vol. 38, no. 18, pp. 2841–2865, 2004.

[41] C. Arata *et al.*, "Volatile organic compound emissions during HOMEChem," *Indoor Air*, vol. 31, no. 6, pp. 2099–2117, 2021.

[42] R. J. Shaughnessy, T. McDaniels, and C. J. Weschler, "Indoor chemistry: Ozone and volatile organic compounds found in tobacco smoke," *Environmental Science & Technology*, vol. 35, no. 13, pp. 2758–2764, 2001.

[43] G. Pandit, P. Srivastava, and A. M. Rao, "Monitoring of indoor volatile organic compounds and polycyclic aromatic hydrocarbons arising from kerosene cooking fuel," *Science of the Total Environment*, vol. 279, no. 1-3, pp. 159–165, 2001.

[44] Q. Liu and J. P. Abbatt, "Liquid crystal display screens as a source for indoor volatile organic compounds," *Proceedings of the National Academy of Sciences*, vol. 118, no. 23, e2105067118, 2021.

[45] B. G. Ooi, D. Dutta, K. Kazipeta, and N. S. Chong, "Influence of the e-cigarette emission profile by the ratio of glycerol to propylene glycol in e-liquid composition," *ACS Omega*, vol. 4, no. 8, pp. 13 338–13 348, 2019.

[46] Y. Huang, S. S. H. Ho, K. F. Ho, S. C. Lee, J. Z. Yu, and P. K. Louie, "Characteristics and health impacts of VOCs and carbonyls associated with residential cooking activities in Hong Kong," *Journal of Hazardous Materials*, vol. 186, no. 1, pp. 344–351, 2011.

[47] R. Hyšpler, Š. Crhová, J. Gasparič, Z. Zadák, M. Čížková, and V. Balasová, "Determination of isoprene in human expired breath using solid-phase microextraction and gas chromatography–mass spectrometry," *Journal of Chromatography B: Biomedical Sciences and Applications*, vol. 739, no. 1, pp. 183–190, 2000.

[48] S Liu *et al.*, "Contribution of human-related sources to indoor volatile organic compounds in a university classroom," *Indoor Air*, vol. 26, no. 6, pp. 925–938, 2016.

[49] P. K. Misztal *et al.*, "Emission factors of microbial volatile organic compounds from environmental bacteria and fungi," *Environmental Science & Technology*, vol. 52, no. 15, pp. 8272–8282, 2018.

[50] A. Korpi, J. Järnberg, and A.-L. Pasanen, "Microbial volatile organic compounds," *Critical Reviews in Toxicology*, vol. 39, no. 2, pp. 139–193, 2009.

[51] A. Y. Davis, Q. Zhang, J. P. Wong, R. J. Weber, and M. S. Black, "Characterization of volatile organic compound emissions from consumer level material extrusion 3D printers," *Building and Environment*, vol. 160, p. 106 209, 2019.

[52] H. Schwartz-Narbonne, B. Du, and J. A. Siegel, "Volatile organic compound and particulate matter emissions from an ultrasonic essential oil diffuser," *Indoor Air*, vol. 31, no. 6, pp. 1982–1992, 2021.

[53] D. A. Missia, E. Demetriou, N Michael, E. Tolis, and J. G. Bartzis, "Indoor exposure from building materials: A field study," *Atmospheric Environment*, vol. 44, no. 35, pp. 4388–4395, 2010.

[54] C. H. Halios, V. D. Assimakopoulos, C. G. Helmis, and H. A. Flocas, "Investigating cigarette-smoke indoor pollution in a controlled environment," *Science of the Total Environment*, vol. 337, no. 1-3, pp. 183–190, 2005.

[55] F. Klein, U. Baltensperger, A. S. Prévôt, and I. El Haddad, "Quantification of the impact of cooking processes on indoor concentrations of volatile organic species and primary and secondary organic aerosols," *Indoor Air*, vol. 29, no. 6, pp. 926–942, 2019.

[56] L. Wallace *et al.*, "The Los Angeles TEAM Study: Personal exposures, indoor-outdoor air concentrations, and breath concentrations of 25 volatile organic compounds.," *Journal of Exposure Analysis and Environmental Epidemiology*, vol. 1, no. 2, pp. 157–192, 1991.

[57] R. Wiglusz, E. Sitko, G. Nikel, I. Jarnuszkiewicz, and B. Igielska, "The effect of temperature on the emission of formaldehyde and volatile organic compounds (VOCs) from laminate flooring—case study," *Building and Environment*, vol. 37, no. 1, pp. 41–44, 2002.

[58] C. J. Weschler, "Ozone's impact on public health: Contributions from indoor exposures to ozone and products of ozone-initiated chemistry," *Environmental Health Perspectives*, vol. 114, no. 10, pp. 1489–1496, 2006.

[59] C.-Y. Lu, J.-M. Lin, Y.-Y. Chen, and Y.-C. Chen, "Building-related symptoms among office employees associated with indoor carbon dioxide and total volatile organic compounds," *International Journal of Environmental Research and Public Health*, vol. 12, no. 6, pp. 5833–5845, 2015.

[60] A. J. Li, V. K. Pal, and K. Kannan, "A review of environmental occurrence, toxicity, biotransformation and biomonitoring of volatile organic compounds," *Environmental Chemistry and Ecotoxicology*, vol. 3, pp. 91–116, 2021.

[61] L Mølhave *et al.*, "Total volatile organic compounds (TVOC) in indoor air quality investigations," *Indoor Air*, vol. 7, no. 4, pp. 225–240, 1997.

[62] T. Vera, F Villanueva, L Wimmerová, and E. Tolis, "An overview of methodologies for the determination of volatile organic compounds in indoor air," *Applied Spectroscopy Reviews*, vol. 57, no. 8, pp. 625–674, 2022.

[63] C. P. Weisel, S. Alimokhtari, and P. F. Sanders, "Indoor air VOC concentrations in suburban and rural New Jersey," *Environmental Science & Technology*, vol. 42, no. 22, pp. 8231–8238, 2008.

[64] B. Son, P. Breysse, and W. Yang, "Volatile organic compounds concentrations in residential indoor and outdoor and its personal exposure in Korea," *Environment International*, vol. 29, no. 1, pp. 79–85, 2003.

[65] D. K. Farmer *et al.*, "Overview of HOMEChem: House observations of microbial and environmental chemistry," *Environmental Science: Processes & Impacts*, vol. 21, no. 8, pp. 1280–1300, 2019.

[66] Y. Liu *et al.*, "Characterizing sources and emissions of volatile organic compounds in a northern California residence using space-and time-resolved measurements," *Indoor Air*, vol. 29, no. 4, pp. 630–644, 2019.

[67] C. Veenaas, M. Ripszam, and P. Haglund, "Analysis of volatile organic compounds in indoor environments using thermal desorption with comprehensive two-dimensional gas chromatography and high-resolution time-of-flight mass spectrometry," *Journal of Separation Science*, vol. 43, no. 8, pp. 1489–1498, 2020.

[68] J. P. Sá, M. C. M. Alvim-Ferraz, F. G. Martins, and S. I. Sousa, "Application of the low-cost sensing technology for indoor air quality monitoring: A review," *Environmental Technology & Innovation*, vol. 28, p. 102 551, 2022.

[69] S. Yang, X. Yang, and D. Licina, "Emissions of volatile organic compounds from interior materials of vehicles," *Building and Environment*, vol. 170, p. 106 599, 2020.

[70] K. Yeh, L. Li, F. Wania, and J. P. Abbatt, "Thirdhand smoke from tobacco, e-cigarettes, cannabis, methamphetamine and cocaine: Partitioning, reactive fate, and human exposure in indoor environments," *Environment International*, vol. 160, p. 107 063, 2022.

[71] C. Wang *et al.*, "Surface reservoirs dominate dynamic gas-surface partitioning of many indoor air constituents," *Science Advances*, vol. 6, no. 8, eaay8973, 2020.

[72] J. P. Abbatt, G. C. Morrison, V. H. Grassian, M. Shiraiwa, C. J. Weschler, and P. J. Ziemann, "How should we define an indoor surface?" *Indoor air*, vol. 32, no. 1, e12955, 2022.

[73] A Saini, J. Okeme, J Mark Parnis, R. McQueen, and M. Diamond, "From air to clothing: Characterizing the accumulation of semi-volatile organic compounds to fabrics in indoor environments," *Indoor Air*, vol. 27, no. 3, pp. 631–641, 2017.

[74] D. Won, R. L. Corsi, and M. Rynes, "New indoor carpet as an adsorptive reservoir for volatile organic compounds," *Environmental Science & Technology*, vol. 34, no. 19, pp. 4193–4198, 2000.

[75] Q.-T. Liu, R. Chen, B. E. McCarry, M. L. Diamond, and B. Bahavar, "Characterization of polar organic compounds in the organic film on indoor and outdoor glass windows," *Environmental Science & Technology*, vol. 37, no. 11, pp. 2340–2349, 2003.

[76] C. J. Weschler and W. W. Nazaroff, "Growth of organic films on indoor surfaces," *Indoor Air*, vol. 27, no. 6, pp. 1101–1112, 2017.

[77] C. Y. Lim and J. P. Abbatt, "Chemical composition, spatial homogeneity, and growth of indoor surface films," *Environmental Science & Technology*, vol. 54, no. 22, pp. 14 372–14 379, 2020.

[78] Y. Fang *et al.*, "A molecular picture of surface interactions of organic compounds on prevalent indoor surfaces: Limonene adsorption on SiO_2," *Chemical Science*, vol. 10, no. 10, pp. 2906–2914, 2019.

[79] C. Liu, B. Kolarik, L. Gunnarsen, and Y. Zhang, "C-depth method to determine diffusion coefficient and partition coefficient of PCB in building materials," *Environmental Science & Technology*, vol. 49, no. 20, pp. 12 112–12 119, 2015.

[80] G. Löfroth, C. Stensman, and M. Brandhorst-Satzkorn, "Indoor sources of mutagenic aerosol particulate matter: Smoking, cooking and incense burning," *Mutation Research/Genetic Toxicology*, vol. 261, no. 1, pp. 21–28, 1991.

[81] A. Matsunaga and P. J. Ziemann, "Gas-wall partitioning of organic compounds in a Teflon film chamber and potential effects on reaction product and aerosol yield measurements," *Aerosol Science and Technology*, vol. 44, no. 10, pp. 881–892, 2010.

[82] P. F. DeCarlo, A. M. Avery, and M. S. Waring, "Thirdhand smoke uptake to aerosol particles in the indoor environment," *Science Advances*, vol. 4, no. 5, eaap8368, 2018.

[83] G. E. Matt *et al.*, "Thirdhand tobacco smoke: Emerging evidence and arguments for a multidisciplinary research agenda," *Environmental Health Perspectives*, vol. 119, no. 9, pp. 1218–1226, 2011.

[84] G. Meng, Z. Nie, Y. Feng, X. Wu, Y. Yin, and Y. Wang, "Typical halogenated persistent organic pollutants in indoor dust and the associations with childhood asthma in Shanghai, China," *Environmental Pollution*, vol. 211, pp. 389–398, 2016.

[85] S. Baskaran and F. Wania, "Applications of the octanol-air partitioning ratio: A critical review," *Environmental Science: Atmospheres*, vol. 3, no. 7, pp. 1045–1065, 2023.

[86] C. J. Weschler and W. W. Nazaroff, "Semivolatile organic compounds in indoor environments," *Atmospheric Environment*, vol. 42, no. 40, pp. 9018–9040, 2008.

[87] F. A. Gobas, B. C. Kelly, and J. A. Arnot, "Quantitative structure activity relationships for predicting the bioaccumulation of pops in terrestrial foodwebs," *QSAR & Combinatorial Science*, vol. 22, no. 3, pp. 329–336, 2003.

[88] C. B. Castells, P. W. Carr, D. I. Eikens, D. Bush, and C. A. Eckert, "Comparative study of semitheoretical models for predicting infinite dilution activity coefficients of alkanes in organic solvents," *Industrial & Engineering Chemistry Research*, vol. 38, no. 10, pp. 4104–4109, 1999.

[89] T. Harner and D. Mackay, "Measurement of octanol-air partition coefficients for chlorobenzenes, PCBs, and DDT," *Environmental Science & Technology*, vol. 29, no. 6, pp. 1599–1606, 1995.

[90] J.-C. Lerol, J.-C. Masson, H. Renon, J.-F. Fabries, and H. Sannier, "Accurate measurement of activity coefficient at infinite dilution by inert gas stripping and gas chromatography," *Industrial & Engineering Chemistry Process Design and Development*, vol. 16, no. 1, pp. 139–144, 1977.

[91] X. Zhang *et al.*, "A method to estimate the octanol-air partition coefficient of semivolatile organic compounds," *Analytical Chemistry*, vol. 71, no. 17, pp. 3834–3838, 1999.

[92] S. Baskaran, Y. D. Lei, and F. Wania, "A database of experimentally derived and estimated octanol–air partition ratios (K_{oa})," *Journal of Physical and Chemical Reference Data*, vol. 50, no. 4, 2021.

[93] M. Zhu, H. Su, Y. Bao, J. Li, and G. Su, "Experimental determination of octanol-water partition coefficient (K_{ow}) of 39 liquid crystal monomers (LCMs) by use of the shake-flask method," *Chemosphere*, vol. 287, p. 132 407, 2022.

[94] B. McDuffie, "Estimation of octanol/water partition coefficients for organic pollutants using reverse-phase HPLC," *Chemosphere*, vol. 10, no. 1, pp. 73–83, 1981.

[95] S. Endo and K.-U. Goss, "Applications of polyparameter linear free energy relationships in environmental chemistry," *Environmental Science & Technology*, vol. 48, no. 21, pp. 12 477–12 491, 2014.

[96] T. N. Brown, "Empirical regressions between system parameters and solute descriptors of polyparameter linear free energy relationships (PPLFERs) for predicting solvent-air partitioning," *Fluid Phase Equilibria*, vol. 540, p. 113 035, 2021.

[97] T. N. Brown, A. Sangion, and J. A. Arnot, "Identifying uncertainty in physical–chemical property estimation with IFSQSAR," *Journal of Cheminformatics*, vol. 16, no. 1, p. 65, 2024.

[98] F Wania, Y. Lei, C Wang, J. Abbatt, and K.-U. Goss, "Using the chemical equilibrium partitioning space to explore factors influencing the phase distribution of compounds involved in secondary organic aerosol formation," *Atmospheric Chemistry and Physics*, vol. 15, no. 6, pp. 3395–3412, 2015.

[99] C. Wang *et al.*, "Uncertain Henry's law constants compromise equilibrium partitioning calculations of atmospheric oxidation products," *Atmospheric Chemistry and Physics*, vol. 17, no. 12, pp. 7529–7540, 2017.

[100] J. P. Abbatt and C. Wang, "The atmospheric chemistry of indoor environments," *Environmental Science: Processes & Impacts*, vol. 22, no. 1, pp. 25–48, 2020.

[101] X. Zhang, J. A. Arnot, and F. Wania, "Model for screening-level assessment of near-field human exposure to neutral organic chemicals released indoors," *Environmental Science & Technology*, vol. 48, no. 20, pp. 12 312–12 319, 2014.

[102] A. Askari, F. Wania, and A. W. Chan, "Modeling the fate and involuntary exposure to tetrahydrocannabinol emitted from indoor cannabis smoking," *Environmental Science: Atmospheres*, vol. 3, no. 4, pp. 760–772, 2023.

[103] L. Li, J. A. Arnot, and F. Wania, "How are humans exposed to organic chemicals released to indoor air?" *Environmental Science & Technology*, vol. 53, no. 19, pp. 11 276–11 284, 2019.

[104] W. Henry, "Experiments on the quantity of gases absorbed by water, at different temperatures, and under different pressures," in *Abstracts of the Papers Printed in the Philosophical Transactions of the Royal Society of London*, The Royal Society London, 1832, pp. 103–104.

[105] E. Atlas, R. Foster, and C. Giam, "Air-sea exchange of high-molecular weight organic pollutants: Laboratory studies," *Environmental Science & Technology*, vol. 16, no. 5, pp. 283–286, 1982.

[106] R. Sander, "Modeling atmospheric chemistry: Interactions between gas-phase species and liquid cloud/aerosol particles," *Surveys in Geophysics*, vol. 20, pp. 1–31, 1999.

[107] R. Weiss, "Carbon dioxide in water and seawater: The solubility of a non-ideal gas," *Marine chemistry*, vol. 2, no. 3, pp. 203–215, 1974.

[108] L. Ettre, C Welter, and B Kolb, "Determination of gas-liquid partition coefficients by automatic equilibrium headspace-gas chromatography utilizing the phase ratio variation method," *Chromatographia*, vol. 35, pp. 73–84, 1993.

[109] A. C. Soria, S. Rodríguez-Sánchez, J. Sanz, and I. Martínez-Castro, "Gas chromatographic analysis of food bioactive oligosaccharides," *Food Oligosaccharides: Production, Analysis and Bioactivity*, pp. 370–398, 2014.

[110] K. Badjagbo, S. Sauvé, and S. Moore, "Real-time continuous monitoring methods for airborne VOCs," *TrAC Trends in Analytical Chemistry*, vol. 26, no. 9, pp. 931–940, 2007.

[111] W. Winiwarter *et al.*, "Henry's law and the behavior of weak acids and bases in fog and cloud," *Journal of Atmospheric Chemistry*, vol. 19, pp. 173–188, 1994.

[112] R. Sander, "Compilation of Henry's law constants (version 4.0) for water as solvent," *Atmospheric Chemistry and Physics*, vol. 15, no. 8, pp. 4399–4981, 2015.

[113] M. Rivlin, U. Eliav, and G. Navon, "NMR studies of the equilibria and reaction rates in aqueous solutions of formaldehyde," *The Journal of Physical Chemistry B*, vol. 119, no. 12, pp. 4479–4487, 2015.

[114] K. Zia, T. Siddiqui, S. Ali, I. Farooq, M. S. Zafar, and Z. Khurshid, "Nuclear magnetic resonance spectroscopy for medical and dental applications: A comprehensive review," *European journal of dentistry*, vol. 13, no. 01, pp. 124–128, 2019.

Chapter 2

Henry's Law Constants and Indoor Partitioning of Microbial Volatile Organic Compounds

2.1 Chapter Overview

Microbial volatile organic compounds (MVOCs) play an essential role in many environmental fields, such as indoor air quality. Long-term exposure to odorous and toxic MVOCs can negatively affect the health of occupants. Recently, the involvement of surface reservoirs in indoor chemistry has been realized, which signifies the importance of the phase partitioning of volatile organic pollutants. However, reliable partition coefficients of many MVOCs are currently lacking. Equilibrium partition coefficients, such as Henrys law constant, H, are crucial for understanding the environmental behavior of chemicals. This study aims to experimentally determine H values and their temperature dependence for key MVOCs under temperature relevant to the indoor environment. The H values were determined with the inert gas-stripping (IGS) method and variable phase ratio headspace (VPR-HS) technique. A two-dimensional partitioning model was applied to predict the indoor phase distribution of MVOCs and potential exposure pathways to the residences. The findings show that the MVOCs are likely distributed between the gas and weakly-polar (e.g., organic-rich) reservoirs indoors. Temperature and the volume of reservoirs can sensitively affect indoor partitioning. Our results give a more comprehensive view of indoor chemical partitioning and exposure.

2.2 Introduction

Microbial volatile organic compounds (MVOCs) are metabolites of various microorganisms ranging from fungi to bacteria. MVOCs play an important role in numerous chemical processes occurring in both natural and built environments.[116] In the ecosystem, a large variety of MVOCs are emitted from the soil into the atmosphere, leading to a broad impact on atmospheric chemistry and soil microbial processes.[117–119] Meanwhile, the use of MVOCs as tracers of microorganisms has a wide range of applications in food safety, water quality and indoor air problem.[120–122] The most recent MVOCs database archives over 2000 compounds emitted from over 1000 microbial species.[123] While the top emitted species are generic VOCs that are not specific to microbial sources, those unique to microbial sources are emitted in trace amounts, and their chemical properties are less understood.[49]

MVOCs in indoor environments have gained attention in the past years as a class of important pollutants closely related to human activities. On one aspect, modern humans spend the majority of their time ($\sim$ 90%) indoors;[1, 124] in parallel, as indoor spaces offer a unique environment with restrained ventilation, pollutants from indoor sources can accumulate to a problematic level.[71, 125, 126] This applies to MVOCs as well. Mold odour is generally considered as a sign of microbial growth in buildings.[127, 128] According to a review article published by Korpi *et al.*,[50] literature focusing on indoor air studies has reported approximately 200 MVOCs, with 15 of them listed as the most often detected species in living environments.

Besides malodors, certain indoor MVOCs have been linked with adverse health effects. The unpleasant smell produced by chloroanisole formation occurring in buildings can induce health symptoms correlated with stress.[129] A number of studies have found that exposure to 1-octen-3-ol can cause irritations and neurotoxic effects.[130, 131] Clearly, long-term exposure to odorous and toxic MVOCs, even at low concentrations, can significantly affect the quality of life and health of occupants.[132] It's critical to know more about the MVOCs' behavior and related influence on indoor air chemistry.[133]

The fate of organic compounds can be implied by their chemical partitioning under equilibrium in a given environment. Indoor chemical partitioning also dictates the

pathways of human exposure.[103] Partition coefficients describe the distribution of a chemical between two phases at equilibrium. Water-air partition coefficient (K_{wa}) and octanol-air partition coefficient (K_{oa}) are commonly used to evaluate properties and partitioning of organic pollutants. The unitless K_{wa} and K_{oa} can be expressed by eq 2.1 and eq 2.2:

$$K_{\mathrm{wa}} = c_{\mathrm{w}}/c_{\mathrm{a}} \tag{2.1}$$

$$K_{\mathrm{oa}} = c_{\mathrm{o}}/c_{\mathrm{a}} \tag{2.2}$$

where the c_{w}, c_{a} and c_{o} are equilibrium concentrations of a certain species in aqueous, gas and octanol phases, respectively, in units of $\mathrm{mol{\cdot}m^{-3}}$.

Henry's law constant (H) is equivalent to K_{wa} but is presented in units of $\mathrm{mol{\cdot}m^{-3}{\cdot}Pa^{-1}}$ or $\mathrm{M{\cdot}atm^{-1}}$, which is defined as the equilibrium ratio between the aqueous-phase concentration and partial pressure in the gas phase (eq 2.3). Conversion of K_{wa} to H can be obtained *via* ideal gas law using eq 2.4:

$$H = c_{\mathrm{w}}/P \tag{2.3}$$

$$K_{\mathrm{wa}} = H \times RT \tag{2.4}$$

where R is the ideal gas constant 8.314 $\mathrm{Pa{\cdot}m^3{\cdot}mol^{-1}{\cdot}K^{-1}}$ and T is the absolute temperature in K. While a variety of units are used to describe H values in the literature, all the H values are herein reported as $\mathrm{mol{\cdot}m^{-3}{\cdot}Pa^{-1}}$, and equations are also arranged to correspond to this unit.

The H value of a given compound is highly temperature-dependent, the relationship can be described by the van't Hoff equation:[112]

$$\mathrm{d}\ln H/\mathrm{d}(1/T) = -\Delta_{\mathrm{sol}}H/R \tag{2.5}$$

where $\Delta_{\mathrm{sol}}H$ is the molar enthalpy of dissolution ($\mathrm{J{\cdot}mol^{-1}}$).

Recent studies have identified a few types of indoor reservoirs that allow chemical partitioning and reactions to occur; for example, periodically wet areas tend to have high MVOCs concentrations from active microbial activities.[134, 135] Moreover, residential settings have a large surface area that can sustain temporary reservoirs for MVOCs. [11, 76, 86] In particular, a recent paper has demonstrated an unexpectedly

large volume of polar and weakly polar reservoirs in indoor environments. The partitioning between surface reservoirs and the gas phase occurs at a time scale faster than that of air exchange.[71] Despite the evidence of these indoor reservoirs, partitioning coefficients of many indoor VOCs have not been carefully determined. Currently, H and K_{oa} values also their temperature-dependent data of many typical indoor MVOCs have not been reported yet. For those H values that have been studied, there are large variations among the reported values either predicted *via* the quantitative structure-property relationship (QSPR) or calculated using vapor pressure of the pure substance divided by aqueous solubility.[112] More experimental constraints to these values are needed for a reliable prediction of MVOCs' indoor partitioning and distribution.

The overall goal of this work is to deepen our understanding of chemical partitioning and potential exposure pathways of indoor MVOCs. Specifically, we aim to provide reliable H values of key MVOC species through carefully designed laboratory experiments. For many of these MVOCs, this study is the first to report their temperature dependence. In addition to indoor air, our measurements can be of great benefit for many other research areas, such as environmental soil chemistry, agriculture and food chemistry, and volatilomics. We further discuss the implications to the indoor environment with the assistance of a two-dimensional chemical partitioning model. This study is the first of its kind to focus on the partitioning of indoor MVOCs, with a combination of measurement and modeling.

2.3 Methods

2.3.1 Choice of MVOCs

The target MVOC compounds investigated in this work are shown in Supplementary Information (SI) Section A.1.1. These MVOC species are emitted specifically from microbes and frequently analysed in buildings with moisture and microbial damage.[50, 136] 1-Octen-3-ol, 3-octanol, 2-ethyl-1-hexanol and 3-octanone are long-chain alcohols and ketones, which represent major groups of indoor MVOCs. The surface-active nature of these species makes the accurate determination of H values challenging,[137] which has resulted in inconsistent literature values.[112] 2,4,6-trichloroanisole (TCA)

is a highly odorous and harmful MVOC that has also been detected indoors.[129] While there are other species listed as most frequently detected indoor MVOCs, a few of them have already been studied thoroughly in the literature, while some others are not available commercially. These species were also considered in the partitioning model discussed later in this work. Chemicals were purchased from Sigma-Aldrich (CA) without further purification: butan-1-ol (1-butanol) (≥99 %), octan-1-ol (1-octanol) (≥99%), oct-1-en-3-ol (1-octen-3-ol) (98%), octan-3-ol (3-octanol) (99%), 3-octanone (>98%), 2,4,6-trichloroanisole (TCA) (99%) and 2-ethylhexan-1-ol (2-ethyl-1-hexanol) (≥99%).

2.3.2 Inert Gas-Stripping (IGS) Method

The IGS method has been widely used to determine H values since 1977. [90, 138–143] The main part of the IGS method is a bubbler setup, in which the inert gas is used to sparge the target compound away from the solution. If the equilibrium between air and water has been established, the rate of the disappearance of chemical concentration from either the gas or aqueous phase over time can be used to estimate H values by eq 2.6:[144]

$$\ln(c_t/c_0) = -Gt/HV_tRT = St \tag{2.6}$$

$$H = -G/SV_tRT \tag{2.7}$$

where c_0 and c_t are concentrations at time 0 and t in min, G is the gas flow rate in $m^3 \cdot min^{-1}$, and V_t is the volume of solution in m^3 at time t. c_t and c_0 can be replaced by the signals of any given instruments at time 0 and t, respectively. If we assume that the evaporation of the solution over time is negligible (V_t remains constant), then the logarithm of the concentration c_t, normalized to the initial concentration c_0 decreases linearly over time and gives a constant slope, S (eq 2.6). The H value can then be calculated from the slope using eq 2.7. The IGS method has two main advantages: (i) Only the concentration of target compounds in one phase needs to be measured. (ii) Quantification of concentration is unnecessary, as the calculation only depends on signal decay over time.[145]

The IGS experiments were conducted in triplicates for target MVOCs at 15, 25, 35 and 50 °C. Stock solutions containing individual target compounds were prepared

at 0.1 g·L^{-1} and kept refrigerated. Before being transferred to the bubbler setup, the solution was diluted to 0.001 g·L^{-1}. The bubbler setup consists of two glass parts, which is similar to the one used by Mackay *et al.*[144] The bottom part was a cylinder container (25 cm high, 2 cm I.D.), holding the aqueous solution of a single target compound (35 mL). The upper glass tube ($\frac{1}{4}$ inch I.D.) introduced inert gas N_2 (high purity 4.8, Praxair, CA) to the bottom of the container and created bubbles to sparge the compound from the aqueous phase. Upon exiting the bubbler, the N_2 gas flow containing the target compound was introduced to the analytical instrument. The temperature of the bottom container was controlled by a Fisher Isotemp 1006S Refrigerated Chiller Heated Water Bath. The investigated temperature range of 15 to 35 °C represents the typical range in indoor environments, while 50 °C allows us to better derive the temperature dependence of H.

The chemical concentration of the bubbler headspace was monitored by a Thermo Scientific TRACE 1310 gas chromatograph (GC) with an RTX-5 capillary column (7 m, 0.32 mm I.D., 0.25 μm film thickness, Thermo Scientific, CA) and flame ionization detector (FID) set at 250 °C. The inlet port has a gas sampling valve, which allows the sample to be injected automatically. The time interval between each injection relied on the duration of method. The injection port temperature was at 100°C, and the flow of carrier gas, He (ultra high purity 5.0, Praxair, CA), was set at 3 ml·min^{-1}. The default oven setting for most of the MVOC species was splitless injection, with the temperature held at 50 °C for 1 min, then ramped with 125 °C·min^{-1} to a final temperature of 175 °C (no hold). Slight adjustments for optimization were made for certain species, e.g., ramping up to a final temperature of 200 °C (no hold) for TCA and using the split method (5:1 ratio) for 1-butanol.

2.3.3 Quality Control Considerations for IGS

Although the IGS method is a rapid and simple way to determine H values, several considerations must be made to ensure its accuracy.

2.3.3.1 Bubble Size

Previous studies have documented potential bias in the IGS method due to chemical substances adsorbing on the surface of the bubbles.[146] The relationship expressed

by eq 2.6 above only considers mass transfer from the aqueous phase to the gas phase. A surface-bound chemical substance can also be transferred to the gas phase when the bubbles burst, resulting in more chemical loss and underestimating the H values.[137] To avoid the potential error of H measurement caused by bubble size, there is a need to use two different bubble sizes for the MVOCs, depending on their adsorption coefficient K_{ia}, in units of m, expressed as the partition coefficient between the water-air interface (on the bubble surface) and the gas phase (inside the bubble).[147] A detailed discussion on the estimation of K_{ia}, the impact of bubble size on H determination, and the optimization of bubble size can be found in Section A.1.2.

2.3.3.2 Flow Rate of N_2

The flow rate of N_2 passing through the solution must be slow enough to ensure a water-air equilibrium. However, slow flow rates make the experiment long and add instability to the system. In this study, most experiments were performed with the flow rate of 200 standard cubic centimeters per minute (sccm) using a mass flow controller, but some experiments were performed with a lower flow rate of 50 or 100 sccm. A reasonable agreement between different flow rates informs that the equilibrium has been established. The details of flow rate adjustment can be found in Section A.1.3.

2.3.3.3 Ideality of Solutions

Henry's law applies only to ideal solutions, in which the interaction between target molecules in the aqueous phase can be neglected. In other words, the solution concentration must be sufficiently low. To ensure the MVOC concentration of chemical substance used in this work was appropriate, we examined the response of GC-FID to the aqueous-phase concentration of 1-octanol. Overall, we observed that the GC-FID response was linear to the concentration up to 0.02 $\mathrm{g{\cdot}L^{-1}}$. The linearity indicates two important aspects of our method: (i) Henry's law is obeyed at this concentration range, which means the gas-phase mixing ratio in the bubbler directly reflects the aqueous-phase concentration. (ii) The signal falls within the linear range of our GC-FID detection. Considering the limit of detection of GC-FID, the optimal concentrations used for the IGS method and VPR-HS technique (please see below) were

0.001 g·L^{-1} and 0.01 g·L^{-1}, respectively.

2.3.3.4 Comparison with Literature and Variable Phase Ratio Headspace (VPR-HS) Technique

To confirm that the optimized IGS method described above resulted in accurate and reproducible H values, we performed additional experiments using 1-butanol and 1-octanol as testing chemicals. The choice of testing compounds is due to (i) plenty of literature data for these two compounds, including the temperature dependence of H values. (ii) The difference in carbon chain length makes them good representatives for compounds with small and large K_{ia} values, respectively. For selected species, we further determined the H value using a different technique, VPR-HS. Previous studies considered the VPR-HS technique a more accurate method due to less interference from the bubble surface and water evaporation.[145]

2.3.4 Variable Phase Ratio Headspace Technique (VPR-HS)

The VPR-HS technique was performed to selected compounds and temperatures to ensure the accuracy of H values determined using the IGS method. In the VPR-HS technique, the solution with individual target compounds is transferred to several closed vials with variable volumes and phase ratios (gas phase volume/water volume, $V_{\mathrm{a}}/V_{\mathrm{w}}$), quantification of the gaseous concentration at equilibrium allows the calculation of H.[108]

The reciprocal of the gaseous concentration (or peak area, A) in the vial has a linear relationship with the phase ratio (eq 2.8):[145]

$$1/A = 1/c_0 \cdot K_{\mathrm{wa}} + 1/c_0 \cdot (V_{\mathrm{a}}/V_{\mathrm{w}}) \tag{2.8}$$

where c_0 is the initial solution concentration in units of mol·m^{-3}. Based on eq 2.8, the K_{wa} value can be described by the ratio of the intercept and slope of the linear regression line (i.e., as intercept/slope).

The VPR-HS technique was carried out for 1-octanol, 1-octen-3-ol and TCA. Individual solutions of target compounds were prepared at 0.01 g·L^{-1}. A variety of volumes, 0.1, 0.3, 0.5, 1 and 2 mL, were transferred into 20 mL headspace vials, corresponding to phase ratios of 199, 66, 39, 19 and 9, respectively. The vials were

immersed in a temperature-controlled water bath at 25 or 50 °C for 1 hour to reach equilibrium. A 500 μL gas sample was injected manually into the GC-FID by using a 1000 μL gas-tight syringe (Hamilton, USA) each time. The injection was repeated four or five times for the smallest and the largest ratios due to their pronounced impact on slope and intercept; triplicate experiments were performed for other phase ratios.

In theory, K_{oa} values can be derived in a similar way, by using 1-octanol as the liquid phase and replacing the V_{W} with V_{O} (volume of 1-octanol) in eq 2.8. However, the VPR-HS technique only works reliably for a limited range according to Lei *et al.*[148], and all of our target MVOCs have K_{oa} values that are out of the range. For this reason, we used the modelling approach to obtain the K_{oa} values (Section A.1.4).

For the VPR-HS technique, the headspace was monitored by an Agilent 6890 GC with an RTX-5 capillary column (30 m, 0.25 mm I.D., 0.25 μm film thickness, Restek, CA) and the FID at 250 °C. The injection port was at 100°C, and the flow rate of carrier gas He was 3 ml·min^{-1} with a split method (ratio 5:1). The oven was held at 50 °C for 2 mins, then ramped with 25 °C·min^{-1} to a final temperature of 225 °C (no hold).

2.3.5 Chemical Two-Dimensional (2D) Partitioning Model

To better understand the behaviors of MVOCs in an indoor environment, a simple modeling approach, the 2D-partitioning model was applied. This approach has been used for organic compounds in ambient atmosphere previously,[98, 99] and then developed to estimate indoor chemical species phase distribution.[100] Briefly, indoor MVOCs are assumed to be in equilibrium among gas phase, polar (e.g., water-rich) and weakly polar (e.g., organic-rich) reservoir. The fraction of a target MVOC at equilibrium can be predicted based on their dimensionless partition coefficients K_{wa} and K_{oa}. The 2D-partitioning space plots provide us with an intuitive visualization for the equilibrium distribution of MVOCs in three phases under different scenarios. A detailed description of the 2D-partitioning model can be found in Sections S5.

2.4 Results and Discussion

2.4.1 Determination of H values using the IGS method

Figure 2.1 shows the GC chromatograms of 3-octanone during an example IGS experiment. A gradual decrease of the 3-octanone signal was observed over time. Decrease of the signal follows the first-order decay profile and expresses the rate at which the inert gas carries aqueous-phase 3-octanone away. The decline of $\ln(C_t/C_0)$ against time at four different temperatures (15, 25, 35 and 50°C) is also presented in Figure 2.1. As discussed in the method section before, the H values of MVOC are obtained according to eq 2.7. Excellent linearity was obtained under all temperatures. While only 3-octanone is presented here as an example, all the other MVOCs exhibit the same trends, and their first-order decay plots have been included in Section A.1.6.

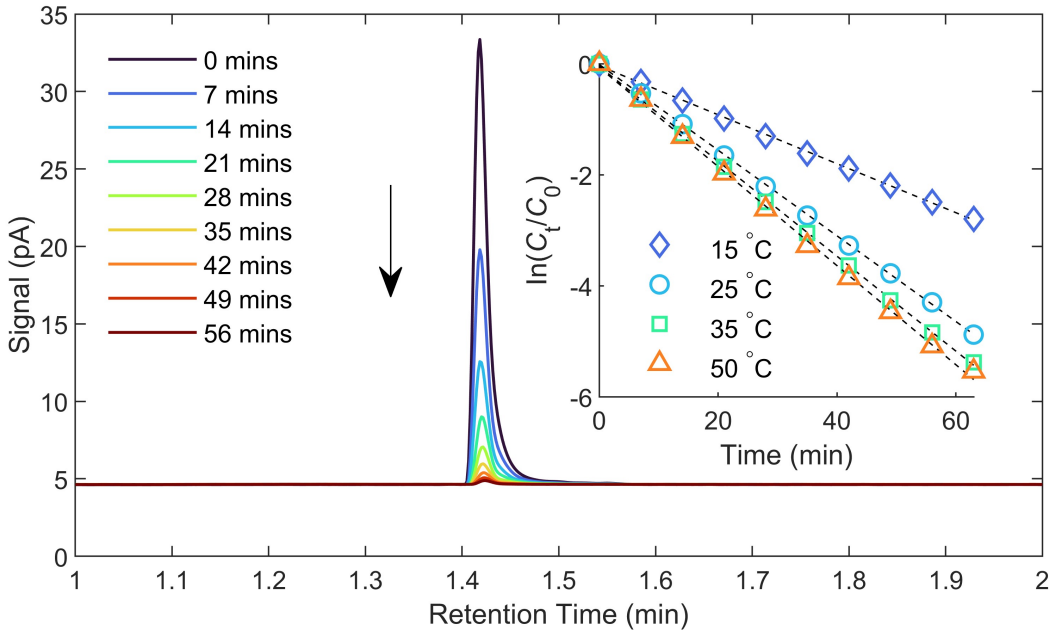

Figure 2.1: First-order decline of 3-octanone signal during an example IGS experiment. The main figure shows the graduate decrease of its GC-FID peak over time at 25 °C. The inset presents plots of $\ln(C_t/C_0)$ *vs.* time at 15, 25, 35 and 50 °C.

Figure 2.2 presents the temperature dependence of H values in the format of the van't Hoff plot. The markers and error bars represent the average values and standard deviations. The figure also includes linear regressions of the measured data points and shows excellent linearity, with most r^2 values being 0.99 or higher.

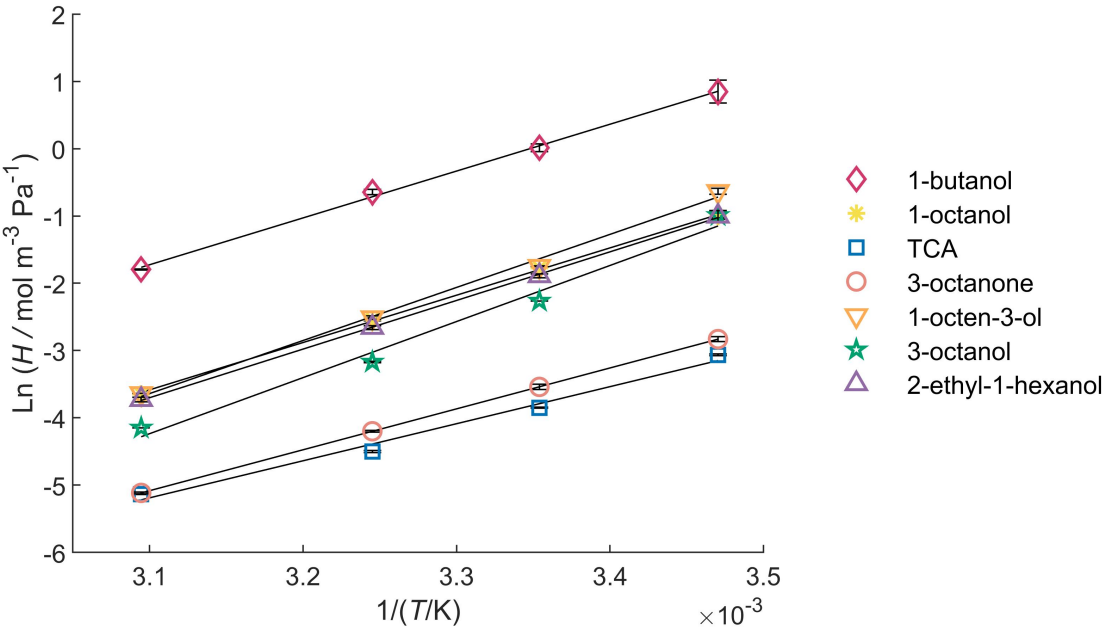

Figure 2.2: The van't Hoff plots obtained by the IGS method for the target MVOCs between 15 °C and 50 °C. The lines are linear regressions of the measured data points.

A major limitation of the IGS method is that it works reliably for compounds with a specific range of H values. MVOCs with small H values leave the water quickly and the signal reaches the detection limit before obtaining a reliable decay profile. MVOCs with larger H values take a longer time to show the decay. It should be noted that water evaporation is no longer negligible in prolonged IGS experiments. In this study, decay profiles during only the first hour of experiments were analyzed to obtain H values, except for 1-butanol under 15 °C (3 hours detection due to the slower decay). With our current setup, a compound with a H value smaller than 3.0×10^{-3} mol·m^{-3}· Pa^{-1} would be challenging to measure because its signal reaches the limit of detection within three chromatographic runs. On the other hand, the H value of 1-butanol at 15 °C (H = 2.3 mol·m^{-3}· Pa^{-1}) is close to the largest H value we can detect, as the experiment took three hours, and the fluctuation of signals was significant (Figure A.3(a)). For the MVOC species and the temperature range we chose in this work, all of the H values fell within this reliable range for the IGS method.

While we only investigated the impact of temperature on H values in this work, H values are subject to the influence of other factors, such as hydration,[149, 150]

acid-base chemistry,[151] and salinity.[152, 153] Acid-base chemistry does not affect the target MVOCs in this work, as none of them is acidic. Certain carbonyl compounds can undergo hydration in the aqueous phase , affecting their effective Henry's law constants.[154] This is applicable only to 3-octanone in this work, but the model-estimated hydration constant from SPARC for 3-octanone is 5.8×10^{-3}, which is too small to affect our results. Salinity is a factor we did not investigate in the current work because the concentrations of salts dissolved in indoor polar and weakly polar reservoirs are unknown. Previous studies[155, 156] have shown that common salts, if present at high concentrations in the environment, can cause the salting-out effect to 2-octanone and 1-hexanol, which are structurally similar to MVOCs investigated in this work. The magnitude of salting-out must be investigated should a high concentration of salts be detected in indoor reservoirs in future studies.

2.4.2 Comparison between IGS and the Literature

The H values at 25 °C, their temperature dependence and the molar enthalpy of dissolution of MVOCs derived by the IGS method are listed in Table 2.1 to be compared with previous literature. Particularly important comparisons are those of our testing compounds, 1-butanol and 1-octanol. Significant variations exist in previously published H values:[112] a factor of ten for 1-butanol and three for 1-octanol. This discrepancy expresses the challenges of obtaining accurate H values experimentally. The agreement between our results and the literature data for 1-butanol and 1-octanol indicates the robustness of our IGS setup for compounds with a wide range of K_{ia} values. For target MVOCs, their H values at 25 °C have only been reported by a few studies. Our results were generally consistent with previous data, but a difference up to a factor of five is observed for TCA (Table 2.1). A comparison between the IGS and VPR-HS methods is addressed in the next section to verify our results. The current work is the first to provide the temperature dependence of H values for 1-octen-3-ol, 3-octanol, 3-octanone and 2-ethyl-1-hexanol.

Table 2.1: Comparison of H values and temperature dependence for MVOCs measured by the IGS method with literature values.

	H at 25 °C ($mol \cdot m^{-3} \cdot Pa^{-1}$)			$d \ln H / d \ln(1/T)$ (K)		$\Delta_{sol}H$ ($kJ \cdot mol^{-1}$)
	this study	lit. data	ref.[b]	this study	lit. data[b]	this study
1-butanol[a]	1.01 ± 0.06	(1.4∼18)×10^{-1}		7000	5600∼7500	58
1-octanol[a]	(1.70 ± 0.05)×10^{-1}	(1.9∼6.5)×10^{-1}		7000	6000∼8900	58
TCA	(2.13 ± 0.02)×10^{-2}	(4.4∼4.6)×10^{-3}		5500	640[157]	46
3-octanone	(2.88 ± 0.12)×10^{-2}	7.6×10^{-2}	[158]	6000	-	50
1-octen-3-ol	(1.74 ± 0.05)×10^{-1}	1.3×10^{-1}	[159]	7900	-	66
3-octanol	(1.03 ± 0.02)×10^{-1}	3.1×10^{-1}	[160]	8300	-	69
2-ethyl-1-hexanol	(1.51 ± 0.04)×10^{-1}	(3.1∼4.3)×10^{-1}		7200	-	60

[a]Testing compounds. [b]Previous published data summarized by Sander[112] unless otherwise noted.

2.4.3 Comparison between IGS and VPR-HS

Applying the VPR-HS technique, we aim to confirm the H values of 1-octanol, 1-octen-3-ol, and TCA at 25°C and 50°C from the IGS method. The relationships between reciprocal peak area ($1/A$) and the phase ratio (V_A/V_W) of 1-octen-3-ol under these two temperatures, obtained by the VPR-HS technique, are shown in Figure 2.3. Plots for other MVOCs and more details are provided in Section A.1.7. All regression analyses show reasonably linear data, with most r^2 values higher than 0.9 (Table A.6).

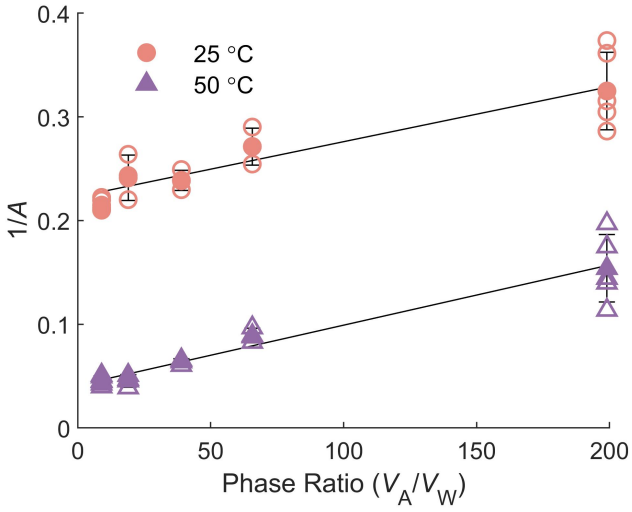

Figure 2.3: Linear relationships between the reciprocal of the chemical concentration (peak area, A) in the gas phase over phase ratio (V_A/V_W) of 1-octen-3-ol at 25 °C and 50 °C.

The solid markers in Figure 2.3 are the averages of all the replicates performed at a certain phase ratio, while the hollow markers represent the results of each individual measurement. The error bar around the regression line is derived by propagating the standard deviations of the slope and intercept from the regression analysis. The standard uncertainty presents a steady increase with the phase ratio, which can be explained by high phase ratio with a small solution volume in the capped vial, leading to low signal response and poor repeatability.

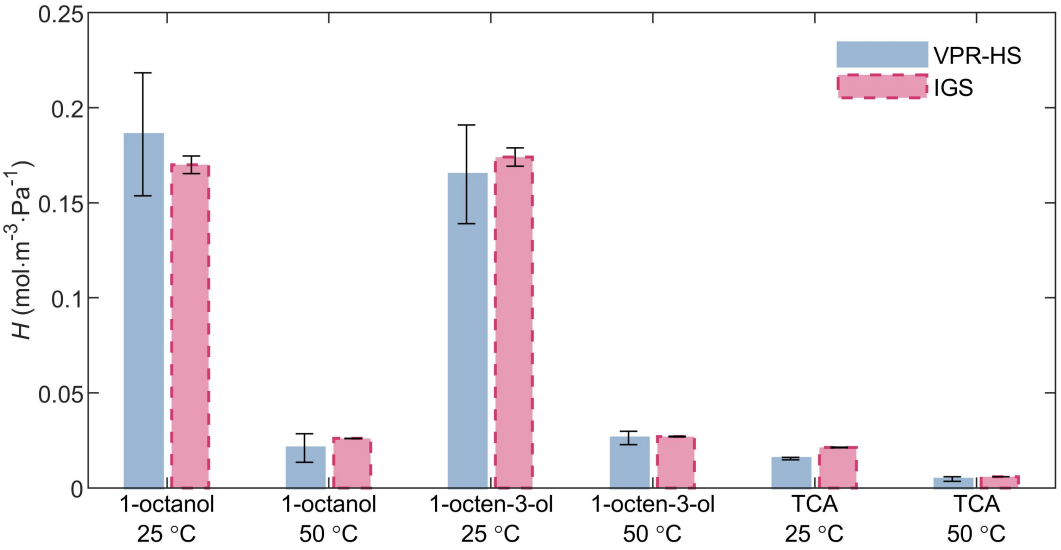

Figure 2.4: Comparison of H values obtained by the VPR-HS technique and the IGS method.

Figure 2.4 compares the H values determined by the VPR-HS technique and the IGS method for 1-octanol, 1-octen-3-ol and TCA at 25 °C and 50 °C. Good consistency was observed between the two methods, with a difference within 25%. This magnitude of difference is much smaller than the variation reported in the literature,[112] as well as the difference between our IGS results and a few available literature values. Thus, we conclude that our results are reproducible, as confirmed by an excellent agreement between two independent methods. Particularly for TCA, the VPR-HS results confirmed the temperature dependence obtained with IGS. We note that the values obtained by the VPR-HS technique always have a relatively large error than that of the IGS method, which is attributed to two factors. First, the injections were completed manually due to the absence of the headspace autosampler. Second, small chromatographic peaks are associated with larger relative standard deviations, especially applicable to vials with large phase ratios, the lower temperature condition (25 °C) and more water-soluble compounds. The VPR-HS technique has been generally applied at temperatures higher than 50 °C in previous studies.[145, 148] We have pushed the limit of the VPR-HS method to 25 °C to represent temperatures relevant to the indoor environment.

2.4.4 Chemical 2D-Partitioning Space Plots and Implications to Indoor Air

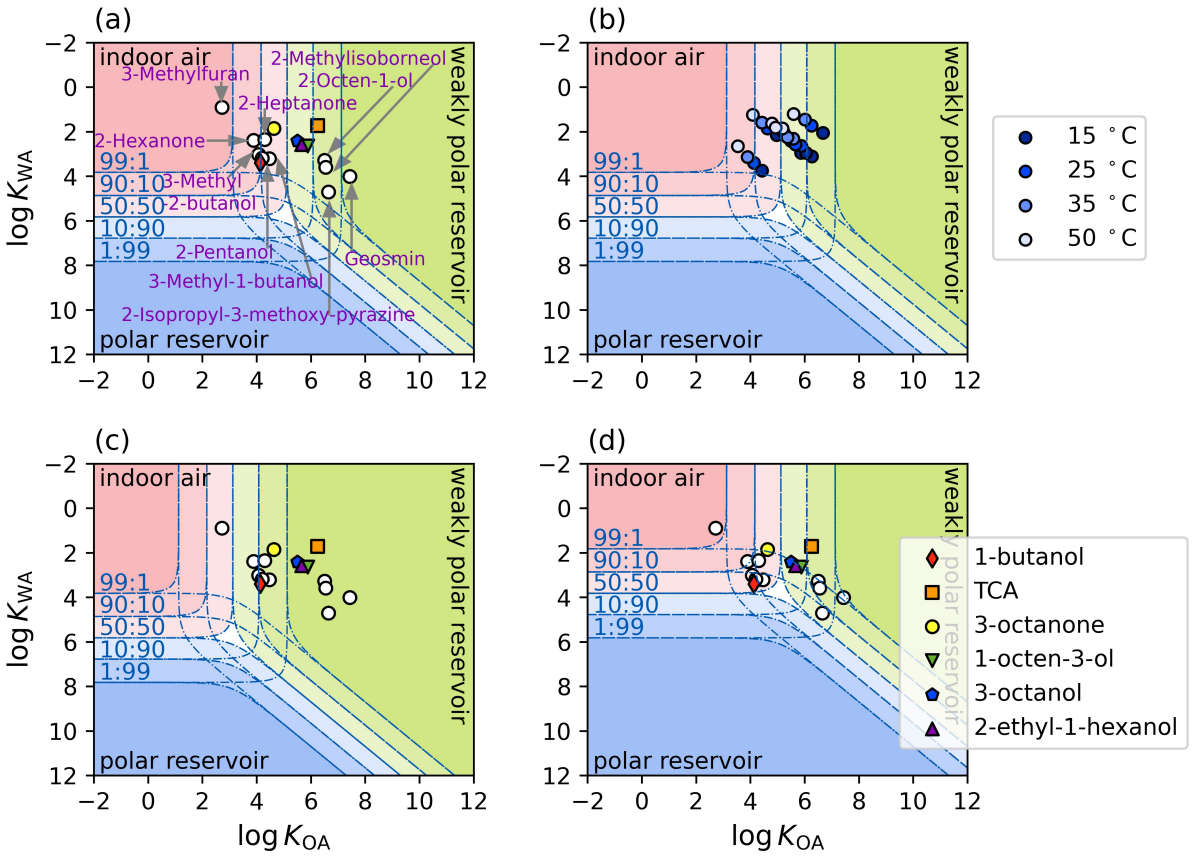

Figure 2.5: Indoor phase distribution of MVOCs. The coloured ones are target species in this work. The gray circles are other frequently detected indoor MVOCs that are not studied in this work. (a) An indoor environment with polar and weakly-polar surface reservoirs equivalent to thicknesses of 500 and 2500 nm under 25 °C; (b) Same assumption as (a) at 15, 25, 35 and 50 °C including only those investigated in this work; (c) An indoor environment with polar and weakly-polar surface reservoirs equivalent to thicknesses of 500 nm and 250 μm under 25 °C; (d) An indoor environment with polar and weakly-polar surface reservoirs equivalent to thicknesses of 50 μm and 2500 nm under 25 °C.

To better understand the phase distribution, behavior, and potential exposure pathways of MVOCs in indoor environment, we applied the 2D-partitioning space plots for our target MVOCs and other typical MVOCs that are most often detected in buildings.[50] K_{wa} and K_{oa} values used in the model have been summarized in Section A.1.4.

We made several essential assumptions following Wang *et al.*[71] to simplify the model: (i) Indoor phases are divided into three pure phases with constant temperature: gas phase, polar (e.g., water-rich) phase and weakly polar (e.g., organic-rich) phase, where water/1-octanol are used as thermodynamic surrogates for these phases. (ii) Equilibria have been fully achieved among these phases. (iii) The volume of the gas phase is assumed to be equal to the room volume. (iv) Indoor surface-area-to-volume ratio is evaluated as 3 m^{-1}, which is an average number accounting for contents.[11] (v) If the polar and weakly polar phases are uniformly distributed on all surfaces in the room, their volume can be estimated from the distributed thickness and surface-area-to-volume ratio (Section A.1.5). In reality, however, the partitioning equilibria and the distribution of the reservoirs are unlikely to be perfect in a complex chemical system; therefore, the thickness should be regarded as a representation of the total size of the reservoirs.

Figure 2.5(a) and (b) consider an indoor environment with polar and weakly-polar reservoirs equivalent to thicknesses of 500 and 2500 nm, respectively. Figure 2.5(a) shows the partitioning space of indoor MVOCs at 25 °C, while (b) shows the impact of varying indoor temperatures on target MVOCs. The thickness of indoor surface reservoirs is poorly constrained, Wang *et al.*[71] found that the thicknesses used in Figure 2.5(a) and (b) best described the observation in an experimental house. Despite some studies having reported surface weakly polar film thicknesses as tens of nanometers,[76] specific indoor environments can attain thicker organic films, e.g., kitchen stoves and surface of the couch.[15, 161, 162] Also, the thickness of dry paint has been measured at the range of tens to hundreds of micrometres.[12, 163] In Figure 2.5(c), we consider an environment with a larger weakly polar reservoir, equivalent to a film thickness of 250 μm. On the other hand, certain indoor environments can contain a significant volume of liquid water. Periodically wet indoor spaces are where visible bulk water is present. Besides visible bulk water, umbrellas on rainy days, condensation of water on cold surfaces, and invisible water undergoing sorption to fabrics, should also be taken into account the source of indoor polar phase.[164, 165] Figure 2.5(d) considers an environment with an polar reservoir a hundred times that used in (a). We consider the case in (d) an upper limit for the amount of polar phase present in an indoor environment. These scenarios serve as useful case studies to

probe the impact of various indoor environments on the partitioning of MVOCs. We recommend future studies to better characterize the size and composition of indoor surface reservoirs, such that more realistic estimations can be made.

Interpretation of the 2D-partitioning model has been described with details by Wania *et al.*[98] Briefly, species that predominantly reside in indoor air appear within the gas phase region on a 2D-partitioning plot (red area in Figure 2.5), while those predominantly present in the polar and weakly polar phases appear in the corresponding regions (blue and green areas, respectively). The further a species appears inside a region, the greater the fraction of this species in the corresponding phase. The isolines that indicate phase split ratios are also included in Figure 2.5.

The results in Figure 2.5(a) show that most MVOCs would be in the gas or weakly polar phases under the scenario presented at 25 °C. Figure 2.5(b) demonstrates that the partitioning of MVOCs investigated in this work is highly sensitive to the temperatures within the range relevant to indoor environments; i.e., MVOCs tend to partition more into the gas phase when the temperature increases. Using PROTEX (PROduction-To-EXposure) model, previous studies have shown that chemical partitioning governs human exposure pathways.[70, 103] According to their simulations, inhalation is the major exposure route for compounds with similar partitioning coefficients as MVOCs studied in this work. Other routes are also possible, such as dietary, non-dietary ingestion and dermal permeation, which are attributed to partitioning into food, human skin, and indoor surfaces. Our results are consistent with these studies, as species present in the gas phase are exposed to the occupants through inhalation, while those present in surface reservoirs can be exposed through the other pathways. The non-airborne routes of exposure have been shown to be important for semi-volatile organic compounds,[166] while there has been no focus specifically on indoor MVOCs. Figure 2.5(a) and (b) indicate that the fraction of exposure attributable to inhalation likely increases with temperature, but there can be other potential pathways of human exposure at lower temperatures, especially for MVOCs with large K_{oa} values. Meanwhile, partitioning to weakly polar reservoirs leads to a longer residence time in indoor environment, which also suggests the possibility of re-emission and exposure through inhalation at a later time if temperature rises or the indoor air is ventilated.[71]

Results from the alternative scenarios are presented in Figure 2.5(c) and (d). Figure 2.5(c) shows that more than 90% of the target MVOCs are present in the weakly polar phase with a thicker weakly polar reservoir, indicating the possibility of non-airborne routes of exposure in such environments. Figure 2.5(d) illustrates that more MVOCs are present in the polar phase with a larger polar surface reservoir. Still, the majority of MVOCs likely remain in the gas and weakly polar phases. Given that the scenario in (d) is considered an upper limit for the amount of polar phase present in an environment, our results show that the target MVOCs are unlikely to be found in the indoor aqueous phase under any conditions.

Although we are highly confident with the H values obtained in this work, K_{wa} values of some MVOCs and K_{oa} values had to be modeled (Section A.1.4). The MVOCs that are commercially unavailable, especially sulphur- and nitrogen-containing compounds and terpenoids classes would benefit from the chemical synthesis in the future. The K_{oa} values from SPARC and other models are in excellent agreement at 25 °C, but the accuracy under other temperatures are difficult to evaluate, since only SPARC offers temperature-dependent predictions. It would be better if the K_{oa} values used in this work can be confirmed with other laboratory measurements,[92] such as the generator column method[167, 168] and specialized capillary gas chromatographic retention time (GC-RT) method.[169, 170]

Overall, the 2D-partitioning space plots of MVOCs serve as the first-cut estimate for indoor environmental behaviors and preferential exposure pathways based on chemical properties. Such understanding was achieved through careful quantification of H values of MVOCs demonstrated throughout this work. In particular, the temperature dependence of H values was presented for the first time for many of the target MVOCs. This study provides a reliable experimental constraint for the H values of MVOCs, given that currently available data are both incomplete and inconsistent. The findings are timely; given the odorous and harmful nature of many MVOCs, and the fact that humans are spending most of their time indoors. The benefit of robust H data determined in this study goes beyond indoor air quality and is expected to benefit many other environmental research areas involving MVOCs.

2.5 Acknowledgement

This research was supported by the Natural Sciences and Engineering Research Council of Canada (Award Number: RGPIN-2018-03814) and the University of Alberta. The authors thank the Harynuk Group members (Ryan Dias, Trevor Johnson) for assistance in GC-FID, Jason Dibbs and the Glass Shop for assistance in glassware, Dr. Frank Wania and Sivani Baskaran for helpful discussions. SW thanks Alberta Graduate Excellence Scholarship for funding. EK thanks NSERC USRA and Lloyd and Margaret Cooley Memorial Studentship in Analytical Chemistry for funding.

2.6 Supporting Information Available in Appendix A

The Supporting Information includes the structures of MVOCs, model-based prediction of K_{ia}, flow rate and equilibration of IGS, model-based prediction of K_{wa} and K_{oa}, construction of the 2D-partitioning model, IGS results for all the MVOCs, and VPR-HS results for all the MVOCs.

References

[1] N. E. Klepeis *et al.*, "The national human activity pattern survey (NHAPS): A resource for assessing exposure to environmental pollutants," *Journal of Exposure Science & Environmental Epidemiology*, vol. 11, no. 3, pp. 231–252, 2001.

[11] A. Manuja *et al.*, "Total surface area in indoor environments," *Environmental Science: Processes & Impacts*, vol. 21, no. 8, pp. 1384–1392, 2019.

[12] L. B. Algrim, D. Pagonis, J. A. de Gouw, J. L. Jimenez, and P. J. Ziemann, "Measurements and modeling of absorptive partitioning of volatile organic compounds to painted surfaces," *Indoor Air*, vol. 30, no. 4, pp. 745–756, 2020.

[15] C. J. Weschler, "Roles of the human occupant in indoor chemistry," *Indoor Air*, vol. 26, no. 1, pp. 6–24, 2016.

[49] P. K. Misztal *et al.*, "Emission factors of microbial volatile organic compounds from environmental bacteria and fungi," *Environmental Science & Technology*, vol. 52, no. 15, pp. 8272–8282, 2018.

[50] A. Korpi, J. Järnberg, and A.-L. Pasanen, "Microbial volatile organic compounds," *Critical Reviews in Toxicology*, vol. 39, no. 2, pp. 139–193, 2009.

[70] K. Yeh, L. Li, F. Wania, and J. P. Abbatt, "Thirdhand smoke from tobacco, e-cigarettes, cannabis, methamphetamine and cocaine: Partitioning, reactive fate, and human exposure in indoor environments," *Environment International*, vol. 160, p. 107 063, 2022.

[71] C. Wang *et al.*, "Surface reservoirs dominate dynamic gas-surface partitioning of many indoor air constituents," *Science Advances*, vol. 6, no. 8, eaay8973, 2020.

[76] C. J. Weschler and W. W. Nazaroff, "Growth of organic films on indoor surfaces," *Indoor Air*, vol. 27, no. 6, pp. 1101–1112, 2017.

[86] C. J. Weschler and W. W. Nazaroff, "Semivolatile organic compounds in indoor environments," *Atmospheric Environment*, vol. 42, no. 40, pp. 9018–9040, 2008.

[90] J.-C. Lerol, J.-C. Masson, H. Renon, J.-F. Fabries, and H. Sannier, "Accurate measurement of activity coefficient at infinite dilution by inert gas stripping and gas chromatography," *Industrial & Engineering Chemistry Process Design and Development*, vol. 16, no. 1, pp. 139–144, 1977.

[92] S. Baskaran, Y. D. Lei, and F. Wania, "A database of experimentally derived and estimated octanol–air partition ratios (K_{oa})," *Journal of Physical and Chemical Reference Data*, vol. 50, no. 4, 2021.

[98] F Wania, Y. Lei, C Wang, J. Abbatt, and K.-U. Goss, "Using the chemical equilibrium partitioning space to explore factors influencing the phase distribution of compounds involved in secondary organic aerosol formation," *Atmospheric Chemistry and Physics*, vol. 15, no. 6, pp. 3395–3412, 2015.

[99] C. Wang *et al.*, "Uncertain Henry's law constants compromise equilibrium partitioning calculations of atmospheric oxidation products," *Atmospheric Chemistry and Physics*, vol. 17, no. 12, pp. 7529–7540, 2017.

[100] J. P. Abbatt and C. Wang, "The atmospheric chemistry of indoor environments," *Environmental Science: Processes & Impacts*, vol. 22, no. 1, pp. 25–48, 2020.

[103] L. Li, J. A. Arnot, and F. Wania, "How are humans exposed to organic chemicals released to indoor air?" *Environmental Science & Technology*, vol. 53, no. 19, pp. 11 276–11 284, 2019.

[108] L. Ettre, C Welter, and B Kolb, "Determination of gas-liquid partition coefficients by automatic equilibrium headspace-gas chromatography utilizing the phase ratio variation method," *Chromatographia*, vol. 35, pp. 73–84, 1993.

[112] R. Sander, "Compilation of Henry's law constants (version 4.0) for water as solvent," *Atmospheric Chemistry and Physics*, vol. 15, no. 8, pp. 4399–4981, 2015.

[115] S. Wu *et al.*, "Henry's law constants and indoor partitioning of microbial volatile organic compounds," *Environmental Science & Technology*, vol. 56, no. 11, pp. 7143–7152, 2022.

[116] M. C. Lemfack, J. Nickel, M. Dunkel, R. Preissner, and B. Piechulla, "MVOC: A database of microbial volatiles," *Nucleic Acids Research*, vol. 42, no. D1, pp. D744–D748, 2014.

[117] J. Bäck *et al.*, "Variable emissions of microbial volatile organic compounds (MVOCs) from root-associated fungi isolated from Scots pine," *Atmospheric Environment*, vol. 44, no. 30, pp. 3651–3659, 2010.

[118] G. D. Bending and S. D. Lincoln, "Inhibition of soil nitrifying bacteria communities and their activities by glucosinolate hydrolysis products," *Soil Biology and Biochemistry*, vol. 32, no. 8-9, pp. 1261–1269, 2000.

[119] K. S. Ramirez, C. L. Lauber, and N. Fierer, "Microbial consumption and production of volatile organic compounds at the soil-litter interface," *Biogeochemistry*, vol. 99, no. 1, pp. 97–107, 2010.

[120] E Kaminśki, S Stawicki, and E Wasowicz, "Volatile flavor compounds produced by molds of Aspergillus, Penicillium, and Fungi imperfecti," *Applied Microbiology*, vol. 27, no. 6, pp. 1001–1004, 1974.

[121] A Nyström, A Grimvall, C Krantz-Rüilcker, R Sävenhed, and K Åkerstrand, "Drinking water off-flavour caused by 2,4,6-trichloroanisole," *Water Science and Technology*, vol. 25, no. 2, pp. 241–249, 1992.

[122] W Lorenz, T Diederich, and M Conrad, "Practical experiences with MVOC as an indicator for microbial growth," *Proc. Indoor Air*, vol. 2002, 341e346, 2002.

[123] M. C. Lemfack, B.-O. Gohlke, S. M. T. Toguem, S. Preissner, B. Piechulla, and R. Preissner, "MVOC 2.0: A database of microbial volatiles," *Nucleic Acids Research*, vol. 46, no. D1, pp. D1261–D1265, 2018.

[124] J. A. Leech, W. C. Nelson, R. T. Burnett, S. Aaron, and M. E. Raizenne, "It's about time: A comparison of canadian and american time-activity patterns," *Journal of Exposure Science & Environmental Epidemiology*, vol. 12, no. 6, pp. 427–432, 2002.

[125] K. Kristensen *et al.*, "Sources and dynamics of semivolatile organic compounds in a single-family residence in northern California," *Indoor air*, vol. 29, no. 4, pp. 645–655, 2019.

[126] J. W. Bennett and A. A. Inamdar, "Are some fungal volatile organic compounds (VOCs) mycotoxins?" *Toxins*, vol. 7, no. 9, pp. 3785–3804, 2015.

[127] J. Cox-Ganser, "Indoor dampness and mould health effects-ongoing questions on microbial exposures and allergic versus nonallergic mechanisms," *Clinical and Experimental Allergy: Journal of the British Society for Allergy and Clinical Immunology*, vol. 45, no. 10, p. 1478, 2015.

[128] K. Engvall, C. Norrby, and D. Norbäck, "Sick building syndrome in relation to building dampness in multi-family residential buildings in Stockholm," *International Archives of Occupational and Environmental Health*, vol. 74, no. 4, pp. 270–278, 2001.

[129] J. Lorentzen, S. Juran, M. Nilsson, S. Nordin, and G Johanson, "Chloroanisoles may explain mold odor and represent a major indoor environment problem in Sweden," *Indoor Air*, vol. 26, no. 2, pp. 207–218, 2016.

[130] R. Wålinder, L. Ernstgård, D. Norbäck, G. Wieslander, and G. Johanson, "Acute effects of 1-octen-3-ol, a microbial volatile organic compound (MVOC)-an experimental study," *Toxicology Letters*, vol. 181, no. 3, pp. 141–147, 2008.

[131] A. A. Inamdar, M. M. Hossain, A. I. Bernstein, G. W. Miller, J. R. Richardson, and J. W. Bennett, "Fungal-derived semiochemical 1-octen-3-ol disrupts dopamine packaging and causes neurodegeneration," *Proceedings of the National Academy of Sciences*, vol. 110, no. 48, pp. 19 561–19 566, 2013.

[132] N. Carslaw and D. Shaw, "Secondary product creation potential (SPCP): A metric for assessing the potential impact of indoor air pollution on human health," *Environmental Science: Processes & Impacts*, vol. 21, no. 8, pp. 1313–1322, 2019.

[133] W. Nazaroff and A. Goldstein, "Indoor chemistry: Research opportunities and challenges.," *Indoor Air*, vol. 25, no. 4, pp. 357–361, 2015.

[134] R. R. Dunn, N. Fierer, J. B. Henley, J. W. Leff, and H. L. Menninger, "Home life: Factors structuring the bacterial diversity found within and between homes," *PloS One*, vol. 8, no. 5, e64133, 2013.

[135] R. I. Adams *et al.*, "Microbes and associated soluble and volatile chemicals on periodically wet household surfaces," *Microbiome*, vol. 5, no. 1, pp. 1–16, 2017.

[136] B. Sahlberg *et al.*, "Airborne molds and bacteria, microbial volatile organic compounds (MVOC), plasticizers and formaldehyde in dwellings in three north european cities in relation to sick building syndrome (SBS)," *Science of the Total Environment*, vol. 444, pp. 433–440, 2013.

[137] C. Shunthirasingham, Y. D. Lei, and F. Wania, "Evidence of bias in air-water Henry's law constants for semivolatile organic compounds measured by inert gas stripping," *Environmental Science & Technology*, vol. 41, no. 11, pp. 3807–3814, 2007.

[138] H. A. Bamford, D. L. Poster, and J. E. Baker, "Henry's law constants of polychlorinated biphenyl congeners and their variation with temperature," *Journal of Chemical & Engineering Data*, vol. 45, no. 6, pp. 1069–1074, 2000.

[139] L. Sahsuvar, P. A. Helm, L. M. Jantunen, and T. F. Bidleman, "Henry's law constants for α-, β-, and γ-hexachlorocyclohexanes (HCHs) as a function of temperature and revised estimates of gas exchange in Arctic regions," *Atmospheric Environment*, vol. 37, no. 7, pp. 983–992, 2003.

[140] F. K. Lau, M. J. Charles, and T. M. Cahill, "Evaluation of gas-stripping methods for the determination of Henry's law constants for polybrominated diphenyl ethers and polychlorinated biphenyls," *Journal of Chemical & Engineering Data*, vol. 51, no. 3, pp. 871–878, 2006.

[141] F. Fang, S. Chu, and C.-S. Hong, "Air-water Henry's law constants for PCB congeners: Experimental determination and modeling of structure-property relationship," *Analytical Chemistry*, vol. 78, no. 15, pp. 5412–5418, 2006.

[142] L. M. Jantunen and T. F. Bidleman, "Henry's law constants for hexachlorobenzene, *p, p'*-DDE and components of technical chlordane and estimates of gas exchange for Lake Ontario," *Chemosphere*, vol. 62, no. 10, pp. 1689–1696, 2006.

[143] B. Cetin, S. Ozer, A. Sofuoglu, and M. Odabasi, "Determination of Henry's law constants of organochlorine pesticides in deionized and saline water as a function of temperature," *Atmospheric Environment*, vol. 40, no. 24, pp. 4538–4546, 2006.

[144] D. Mackay, W. Y. Shiu, and R. P. Sutherland, "Determination of air-water Henry's law constants for hydrophobic pollutants," *Environmental Science & Technology*, vol. 13, no. 3, pp. 333–337, 1979.

[145] Y. D. Lei, C. Shunthirasingham, and F. Wania, "Comparison of headspace and gas-stripping techniques for measuring the air-mackiewater partitioning of normal alkanols (C4 to C10): Effect of temperature, chain length, and adsorption to the water surface," *Journal of Chemical & Engineering Data*, vol. 52, no. 1, pp. 168–179, 2007.

[146] K.-U. Goss, F. Wania, M. S. McLachlan, D. Mackay, and R. P. Schwarzenbach, "Comment on "Reevaluation of air-water exchange fluxes of PCBs in green bay and southern lake michigan"," *Environmental Science & Technology*, vol. 38, no. 9, pp. 1626–1628, 2004.

[147] C. M. Roth, K.-U. Goss, and R. P. Schwarzenbach, "Adsorption of a diverse set of organic vapors on the bulk water surface," *Journal of Colloid and Interface Science*, vol. 252, no. 1, pp. 21–30, 2002.

[148] Y. D. Lei, S. Baskaran, and F. Wania, "Measuring the octan-1-ol air partition coefficient of volatile organic chemicals with the variable phase ratio headspace technique," *Journal of Chemical & Engineering Data*, vol. 64, no. 11, pp. 4793–4800, 2019.

[149] R. Bell, "The reversible hydration of carbonyl compounds," *Advances in Physical Organic Chemistry*, vol. 4, pp. 1–29, 1966.

[150] M. H. Abraham and W. E. Acree Jr, "Prediction of gas to water partition coefficients from 273 to 373 K using predicted enthalpies and heat capacities of hydration," *Fluid Phase Equilibria*, vol. 262, no. 1-2, pp. 97–110, 2007.

[151] C. Mouchel-Vallon *et al.*, "Explicit modeling of volatile organic compounds partitioning in the atmospheric aqueous phase," *Atmospheric Chemistry and Physics*, vol. 13, no. 2, pp. 1023–1037, 2013.

[152] S. Endo, A. Pfennigsdorff, and K.-U. Goss, "Salting-out effect in aqueous NaCl solutions: Trends with size and polarity of solute molecules," *Environmental Science & Technology*, vol. 46, no. 3, pp. 1496–1503, 2012.

[153] J. B. Falabella, A. Nair, and A. S. Teja, "Henry's constants of 1-alkanols and 2-ketones in salt solutions," *Journal of Chemical & Engineering Data*, vol. 51, no. 5, pp. 1940–1945, 2006.

[154] H. S. Ip, X. H. Huang, and J. Z. Yu, "Effective Henry's law constants of glyoxal, glyoxylic acid, and glycolic acid," *Geophysical Research Letters*, vol. 36, no. 1, p. L01802, 2009.

[155] C. Wang, Y. D. Lei, S. Endo, and F. Wania, "Measuring and modeling the salting-out effect in ammonium sulfate solutions," *Environmental Science & Technology*, vol. 48, no. 22, pp. 13 238–13 245, 2014.

[156] C. Wang, Y. D. Lei, and F. Wania, "Effect of sodium sulfate, ammonium chloride, ammonium nitrate, and salt mixtures on aqueous phase partitioning of organic compounds," *Environmental Science & Technology*, vol. 50, no. 23, pp. 12 742–12 749, 2016.

[157] A. Díaz, F. Ventura, and M. T. Galceran, "Determination of odorous mixed chloro-bromoanisoles in water by solid-phase micro-extraction and gas chromatography-mass detection," *Journal of Chromatography A*, vol. 1064, no. 1, pp. 97–106, 2005.

[158] *HSDB: Hazardous Substances Data Bank, TOXicology data NET-work (TOXNET), National Library of Medicine (US)*, https://www.nlm.nih.gov/toxnet/index.html, Last access: 2021-10-29.

[159] D. D. Roberts and P. Pollien, "Analysis of aroma release during microwave heating," *Journal of Agricultural and Food Chemistry*, vol. 45, no. 11, pp. 4388–4392, 1997.

[160] C. L. Yaws, J. R. Hopper, S. D. Sheth, M. Han, and R. W. Pike, "Solubility and Henry's law constant for alcohols in water," *Waste Management*, vol. 17, no. 8, pp. 541–547, 1998.

[161] V. W. Or, M. R. Alves, M. Wade, S. Schwab, R. L. Corsi, and V. H. Grassian, "Crystal clear? Microspectroscopic imaging and physicochemical characterization of indoor depositions on window glass," *Environmental Science & Technology Letters*, vol. 5, no. 8, pp. 514–519, 2018.

[162] R. E. O'Brien *et al.*, "Emerging investigator series: Chemical and physical properties of organic mixtures on indoor surfaces during HOMEChem," *Environmental Science: Processes & Impacts*, vol. 23, no. 4, pp. 559–568, 2021.

[163] T Salthammer and F Fuhrmann, "Photocatalytic surface reactions on indoor wall paint," *Environmental Science & Technology*, vol. 41, no. 18, pp. 6573–6578, 2007.

[164] W. W. Nazaroff and C. J. Weschler, "Indoor acids and bases," *Indoor Air*, vol. 30, no. 4, pp. 559–644, 2020.

[165] J. W. Rowen and R. Blaine, "Sorption of nitrogen and water vapor on textile fibers," *Industrial & Engineering Chemistry*, vol. 39, no. 12, pp. 1659–1663, 1947.

[166] M. Pelletier, N. Bonvallot, and P. Glorennec, "Aggregating exposures & cumulating risk for semivolatile organic compounds: A review," *Environmental research*, vol. 158, pp. 649–659, 2017.

[167] F. Wania, Y. D. Lei, and T. Harner, "Estimating octanol-air partition coefficients of nonpolar semivolatile organic compounds from gas chromatographic retention times," *Analytical Chemistry*, vol. 74, no. 14, pp. 3476–3483, 2002.

[168] Y. Yao, T. Harner, J. Ma, L. Tuduri, and P. Blanchard, "Sources and occurrence of dacthal in the Canadian atmosphere," *Environmental Science & Technology*, vol. 41, no. 3, pp. 688–694, 2007.

[169] J. O. Okeme, T. F. Rodgers, J. M. Parnis, M. L. Diamond, T. F. Bidleman, and L. M. Jantunen, "Gas chromatographic estimation of vapor pressures and octanol–air partition coefficients of semivolatile organic compounds of emerging concern," *Journal of Chemical & Engineering Data*, vol. 65, no. 5, pp. 2467–2475, 2020.

[170] Q. T. Vuong, P. Q. Thang, T. Ohura, and S.-D. Choi, "Determining sub-cooled liquid vapor pressures and octanol-air partition coefficients for chlorinated and brominated polycyclic aromatic hydrocarbons based on gas chromatographic retention times: Application for gas/particle partitioning in air," *Atmospheric Environment*, vol. 229, p. 117 461, 2020.

Chapter 3

Indoor Partitioning and Potential Thirdhand Exposure to Carbonyl Flavoring Agents Added in E-cigarette and Hookah Tobacco

3.1 Chapter Overview

Flavoring agents added to the e-cigarette and hookah have increased the attractiveness of novel nicotine products. Many widely used flavorings are carbonyls, which are toxic to humans. In an indoor environment, residents can be exposed to such harmful flavorings previously emitted to the surrounding environment, through a process termed thirdhand exposure. The recent discovery of a large volume of indoor reservoirs emphasizes the importance of indoor partitioning, which is responsible for thirdhand exposure. Indoor partitioning can be expressed with partitioning coefficients, such as Henrys law solubility constant (H). However, reliable H values for many key flavorings are currently lacking. To better understand their environmental behavior, this study experimentally determined the effective Henrys law constant ($H^{cp}_{s,eff}$) using the inert gas stripping (IGS) method. Further, the influence of the hydration process for target flavorings was quantified using proton nuclear magnetic resonance (^{1}H NMR) spectroscopy. We found that hydration of α-dicarbonyls (diacetyl and 2,3-pentanedione) enhanced their $H^{cp}_{s,eff}$ from their intrinsic Henrys law constant (H^{cp}_{s}) by a factor of 3.52 and 2.88, respectively. The two-dimensional partitioning plots were employed to simulate the indoor phase distribution and evaluate the pathways of human exposure. Our findings show that the indoor partitioning of many harmful flavorings is highly sensitive to temperature and the size of indoor reservoirs, indicating that residents are likely to experience third-hand exposure.

3.2 Introduction

Electronic cigarettes (e-cigarettes) and hookah tobacco have become popular in recent years, especially among teen users.[172, 173] A large number of available flavors are the main contributors to the attractiveness of these new nicotine delivery methods, with more than 7000 flavors currently available in e-liquids, the liquid vaporized in e-cigarette products.[174–176] Recent papers reported that more than 200 chemical flavorings are used in e-liquids, and more than 100 were identified from hookah tobacco.[177, 178] According to research in the United States, up to 66% of e-cigarette users consumed flavored e-cigarettes, and 87% of hookah tobacco users consumed flavored hookah tobacco.[179] Sweet flavors, such as fruit and candy, are especially preferred by youth and young adult users.[180, 181] Flavorings not only encourage nicotine use but may also lead to abusing e-cigarettes.[182]

The widespread popularity of flavored e-cigarettes and hookah tobacco has raised public health concerns.[183–185] Users are exposed to aerosols containing irritants through the oral cavity, respiratory tract, and lungs.[186–189] A major flavoring agents class is carbonyls, a compound class recognized as toxic upon inhalation.[190] Although these flavorings have been approved as safe compounds for ingestion, they cannot be considered safe for other exposure routes.[191] Tierney *et al.* found that the concentrations of flavorings in e-liquids are high enough to pose a health risk via inhalation and needed to be considered.[190] However, little is known about the adverse health effects of flavorings when inhaled, beyond several chemicals. For instance, diacetyl (2,3-butanedione) and 2,3-pentanedione, which are commonly used for buttery or creamy flavors,[192, 193] have been shown to cause bronchiolitis obliterans (or popcorn lung disease), when workers in a popcorn factory were exposed to a high dose of aerosolized flavorings.[194, 195] Furthermore, diacetyl and 2,3-pentanedione have been observed to induce chromosomal damages.[196] Other commonly used flavorings display similar cytotoxicity. According to a safety classification in the literature,[177, 197] half of the top ten most frequently added flavorings, including vanillin, maltol, ethyl vanillin, benzyl alcohol, and benzaldehyde, have been classified as harmful chemicals. Others have been classified as irritants, such as ethyl butyrate, ethyl acetate, cis-3-hexenol, isoamyl acetate, and linalool. Therefore, further research is needed to

evaluate the potential exposure to flavoring agents.

The risk of exposure is not limited to users. Once emitted to the surrounding environment, the toxic flavoring agents can cause secondhand and thirdhand exposures. Secondhand exposures are defined as those resulting from inhalation of sidestream smoke or vapors, while thirdhand exposures are inhalation, ingestion, and dermal permeation of chemicals previously released to the surrounding environment.[83] Specifically, thirdhand chemicals are found to partition to residential surfaces or dust after smoking or vaping and maybe re-emitted to indoor air.[70] The indoor environment, where humans spend more than 90% of the time,[1, 124] represents an environment where such exposures can be magnified. In particular, a recent paper has demonstrated that an unexpectedly large volume of reservoirs of volatile and semivolatile organic compounds exist in the indoor environment, with the partitioning between air and reservoirs happening faster than the typical residence time of indoor air.[71] Meanwhile, the physical features of indoor space, such as the high surface-area-to-volume ratio and restricted ventilation, enhance the relative importance of partitioning processes as well.[11, 100] While secondhand and thirdhand smoke arising from traditional, combustive smoking have been investigated, the equivalence to new nicotine delivery methods, such as e-cigarettes and hookah tobacco, is poorly understood. Consequently, thirdhand exposure to flavorings may be causing persistent chemical exposures to humans without them being aware.

To better understand the chemical fate and potential routes of human exposure, it is essential to obtain reliable data for partitioning coefficients, which include Henry's law constants (H) and the underlying chemical reactions that affect the H values. In the aqueous phase, carbonyl compounds undergo reversible hydration to give hydrated carbonyl products (geminal diols), as shown in Figure 3.1.[149] Previous studies have shown that the magnitude of hydration, determined by K_{hyd}, dictates the effective Henry's law constant ($H^{\mathrm{cp}}_{\mathrm{s,eff}}$) of carbonyl compounds.[154]

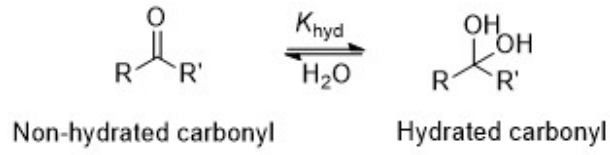

Figure 3.1: Scheme of hydration process for carbonyl.

Many frequently used flavorings have been studied previously, with their partitioning coefficients reported in the literature. However, those of certain toxic flavorings, including those introduced above, have not been reliably measured, and the temperature-dependent data is currently unavailable.[112] Furthermore, careful investigations of carbonyl hydration are rare, despite the important role of hydration after the chemicals partition into the aqueous phase. The overall objective of this study is to experimentally determine the H and K_{hyd} values of key flavoring agents in e-cigarettes and hookah tobacco. In particular, this work will be the first to report the experimentally determined H and K_{hyd} values of target key flavoring agents, as well as the temperature-dependent data relevant to indoor environments. Furthermore, a two-dimensional partitioning model was used to predict the indoor phase distribution of flavoring agents and evaluate potential human exposure pathways. The results provide insight into thirdhand exposures to e-cigarette and hookah tobacco emissions. This is greatly beneficial for people to better understand the potential health hazards caused by flavoring agents from e-cigarettes and hookah tobacco.

3.3 Theory

Chemical partitioning processes are governed by partitioning coefficients, such as the water-air (K_{wa}) and octanol-air (K_{oa}) partitioning coefficients.[100] The Henry's law constant (H) is synonymous with K_{wa}. According to Henry's law, the abundance of a chemical species dissolved in an infinitely diluted aqueous phase is proportional to its abundance in the gas phase in equilibrium. The proportional ratio is equivalent to H. In particular, the dimensionless Henry's law solubility constant ($H_{\mathrm{s}}^{\mathrm{cp}}$) has been recommended to represent K_{wa} using eq 3.1.[198] Similarly, the dimensionless octanol-air coefficient (K_{oa}) is given by eq 3.2.

$$K_{\mathrm{wa}} = H_{\mathrm{s}}^{\mathrm{cp}} = c_{\mathrm{l}}/c_{\mathrm{g}} \tag{3.1}$$

$$K_{\mathrm{oa}} = c_{\mathrm{o}}/c_{\mathrm{g}} \tag{3.2}$$

where c_{l}, c_{g} and c_{o} are the molar concentrations of a chemical species under equilibrium in the aqueous, gas, and octanol phase, respectively.

We have employed the superscript and subscript system recommended by Sander *et al.*[198] The subscription, 's', denotes Henry's law solubility (i.e., aqueous over gas phase). The superscription, 'cc', reflects that this H value is the concentration ratio (i.e., dimensionless), while 'cp' represents the ratio between concentration and partial pressure. While various expressions for the H have been used in previous studies, all the experimental H values in the current work are defined via molar concentration in the aqueous phase and partial pressure in the gas phase, reported as H_s^{cp} in units of $mol \cdot m^{-3} \cdot Pa^{-1}$ (eq 3.3), the unit conversion between H_s^{cc} and H_s^{cp} is expressed as eq 3.4:

$$H_s^{cp} = c_l / p \tag{3.3}$$

$$H_s^{cc} = H_s^{cp} \times RT \tag{3.4}$$

where c_l is the molar concentration of a chemical species in the aqueous phase in units of $mol \cdot m^{-3}$, p is the partial pressure in the gas phase in units of Pa, R is the ideal gas constant 8.314 $Pa \cdot m^3 \cdot K^{-1} \cdot mol^{-1}$, and T is the absolute temperature in K.

The temperature dependence of the solubility Henry's law constant (H_s) can be described by the van't Hoff equation:

$$d \ln H_s / d(1/T) = -\Delta_{sol} H / R \tag{3.5}$$

where $\Delta_{sol} H$ is the standard molar enthalpy of solvation ($kJ \cdot mol^{-1}$), which can be considered as a constant in a narrow range of temperature.[198] The temperature dependence and the $\Delta_{sol} H$ value depend on the various expressions of H.

When the H refers to the same species in the aqueous and gas phases, it is the intrinsic Henry's law constant (H_s^{cp}). When other equilibria occur to the species in the aqueous phase, the measured Henry's law constant is called the effective Henry's law constant ($H_{s,eff}^{cp}$), which is commonly used to evaluate the environmental fate of chemicals. There are several key factors influencing the $H_{s,eff}^{cp}$ values, such as acid-base chemistry, hydration and temperature.[198]

Hydration equilibrium constant (K_{hyd}), in the case of a carbonyl compound (Figure 3.1) can be calculated by eq 3.6:

$$K_{\text{hyd}} = c_{\text{l}}(\text{carbonyl}_{\text{hyd}})/c_{\text{l}}(\text{carbonyl}_{\text{non-hyd}}) \tag{3.6}$$

where the $c_{\text{l}}(\text{carbonyl}_{\text{hyd}})$ and $c_{\text{l}}(\text{carbonyl}_{\text{non-hyd}})$ are the concentrations of the hydrated and the non-hydrated forms of a carbonyl under equilibrium in a diluted aqueous solution. It should be noted that K_{hyd} is dimensionless and highly temperature-dependent, which also follows van't Hoff equation.

For a compound undergoing single hydration, the intrinsic Henry's law constant (H_{s}^{cp}) and the effective Henry's law constant ($H_{\text{s,eff}}^{\text{cp}}$) are related by eq 3.7:[112]

$$H_{\text{s,eff}}^{\text{cp}} = H_{\text{s}}^{\text{cp}} \times (1 + K_{\text{hyd}}) \tag{3.7}$$

3.4 Methods

3.4.1 Materials

All the chemicals were purchased from Sigma-Aldrich (CA) without further purification, commonly-used flavoring agents added in e-cigarette and hookah tobacco have been studied:[177, 178, 197, 199–202] butane-2,3-dione (diacetyl) (97%), pentane-2,3-dione (2,3-pentanedione) (97%), 3-hydroxybutan-2-one (acetoin) (≥98%), 4-methylbenzaldehyde (p-tolualdehyde) (97%), 3-methylbenzaldehyde (m-tolualdehyde) (97%), 6-methylhept-5-en-2-one (6-methyl-5-hepten-2-one) (99%), (2E)-3,7-dimethylocta-2,6-dienal (citral) (95%). These flavorings provide various tastes and aromas: diacetyl, 2,3-pentanedione and acetoin have a buttery flavor, p-tolualdehyde provides fruity flavor, while 6-methyl-5-hepten-2-one and citral give citrus flavor.[199] These flavors are particularly popular with the young generation.[180, 181] As mentioned earlier, some of these compounds are known to be toxic upon inhalation. The structures of the target compounds investigated in this work can be found in Supplementary Information (SI) Section B.1.1. Omaiye *et al.*[199] have determined the top ten frequently-added flavoring compounds in e-liquids. The H values of these compounds were not determined in this work either because they have been previously reported or because their values are not within our measurement range.[115] Instead, they will be discussed in the partitioning model later in this work with their known partitioning coefficients. The solvent and internal standard

of ^{1}H NMR samples were deuterium oxide (D_2O) (99.9 atom % D) and dimethyl sulfoxide (DMSO) (≥99.5%), respectively.

3.4.2 Inert gas-stripping (IGS) method

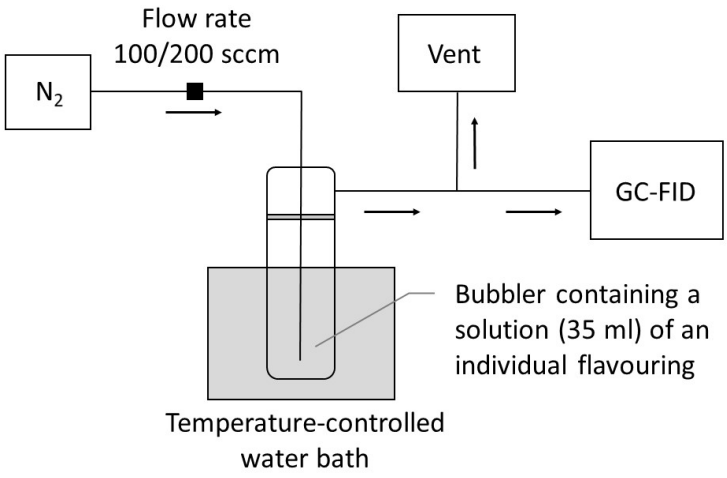

Figure 3.2: Diagram of experimental setup for the inert gas-stripping method.

The inert gas-stripping (IGS) method has been applied for the effective Henry's law constant ($H^{cp}_{s,eff}$) measurement for over 30 years.[90, 154] The bubbler-column apparatus, which we adapted from Mackay *et al.*[144] is shown schematically in Figure 3.2. Our IGS setup has been discussed with detail in our previous work (see Chapter 2) and hence will be described only briefly here.[115] The technique consists of an upper glass top and a bottom stripping column (25 cm high, 2 cm i.d.) containing the diluted solution of one chemical species (35 ml), placed in a temperature-controlled water bath - Fisher Isotemp 138 1006S Refrigerated Chiller Heated Water Bath. The upper and bottom parts were sealed by a rubber o-ring. Since Henry's law applies to the limit of infinite dilution of the solute, all solutions were prepared with the concentration of 0.001g/L, except for diacetyl and acetoin (0.01 g/L and 0.02g/L, respectively due to the small signal from the detector). The experiments were performed in triplicates at 15, 25, 35 and 50 °C to better investigate indoor-relevant temperatures. The inert gas N_2 (from liquid nitrogen boil-off) was introduced into the solution from the bottom of the stripped column and used to carry the chemical away from the aqueous phase to the gas phase with a specific flow rate controlled by a

mass flow controller. Once the equilibrium between two phases in the bubbler column has been established, the $H^{cp}_{s,eff}$ can be described by the following equation:[203]

$$\ln(C_t/C_0) = -(G/H^{cp}_{s,eff}VRT)t \tag{3.8}$$

where G is the gas flow rate ($m^3 \cdot min^{-1}$), V is the volume of the solution (m^3) in the stripping column, R is the ideal gas constant (8.314 $Pa \cdot m^3 \cdot K^{-1} \cdot mol^{-1}$), T is the system temperature (K), C_0 and C_t are solute concentrations at time 0 and t (min) in either aqueous phase or gas phase.

The calculation of $H^{cp}_{s,eff}$ value relies on the slope ($-G/H^{cp}_{s,eff}VRT$), which is yielded by the linear correlation between $\ln(C_t/C_0)$ and time t (min). All the experimental measurements were carried out for one hour to avoid the effect of evaporation on liquid volume, but with a few exceptions. Less than 2% evaporation of water was observed under 50 °C after 1 hour, which we consider negligible. Diacetyl (two hours) and citral (three hours) under 15 °C were carried out with extended length due to the slow decay of the chemical concentration signal (Section B.1.2). As will be discussed later, experiments for acetoin were performed for up to eight hours.

The solute concentration in the gas phase exiting the bubbler was monitored by a Thermo Scientific TRACE 1310 gas chromatograph (GC) with an RTX-5 capillary column (7 m, 0.32 mm i.d., 0.25 m film thickness, Restek, CA) and flame ionization detector (FID) set at 250 °C. Each sample was injected into the injection port (100 °C) by an automatic gas sampling valve and carried by He (ultra high purity 5.0, Praxair, CA), which was set as 3 $ml \cdot min^{-1}$. The optimized oven setting for diacetyl and 2,3-pentanedione was 27 °C for 1.5 min, with split (5:1 ratio) and splitless injection, respectively. For other flavorings, the oven setting was a splitless injection, with the temperature held at 50 °C for 1 min, then ramped with 125 $°C \cdot min^{-1}$ to a final temperature of 175 °C (no hold). Thus, the time interval between two samplings was 1.9 min for diacetyl and 2,3-pentanedione, and 3.5 min for other flavorings.

The IGS technique used here was optimized and validated by our previous work.[115] We have shown that the method can reliably measure the H values of volatile organic compounds in the range of 0.003 to 2.3 $mol \cdot m^{-3} \cdot Pa^{-1}$. The influences of a number of factors on H values were examined, such as bubble size, the flow

rate of N_2, and the concentration of the target compounds. In our previous work (see Chapter 2), the H values determined with our IGS method exhibited good agreement with the literature values, as well as those obtained with a variable phase ratio headspace technique, an independent method used to verify the results.[115] Following the prior work, there are several aspects that need to be considered to avoid the potential bias: (i) Diacetyl has been chosen to confirm the IGS method as a representative of flavoring agents, its H value has been measured experimentally in the literature. (ii) All the target flavorings investigated in the study - and at the temperatures of interest - have the $H^{cp}_{s,eff}$ values falling into the range in which we can achieve reliable determination. The only exception is acetoin, which can not be measured due to the absence of signal decay. (iii) Two bubbler-column setups have been employed for measurement. One produces large bubbles (diameter around 6 mm) with a flow rate of 100 sccm for citral, and another one produces small bubbles (diameter around 3 mm) with a flow rate of 200 sccm for other flavorings. A detailed description of the choice of setup can be found in Section B.1.3.

We would like to point out that the influence of salinity in indoor reservoirs on $H^{cp}_{s,eff}$ is not investigated in the current work due to a lack of data. The concentration and type of salinity in indoor reservoirs remain open questions. Previous studies have illustrated the salting out and salting in" effects on ketones similar to our target flavorings, which exemplifies the importance of the salinity effect.[155, 156, 204] Apart from that, the ionic dissociation has not been considered, the work from Tilgner *et al.*[205] has stated that the K_{hyd} of a simple ketone shows no pH dependence and none of the target compounds are acidic. Thus, the solution pH was not controlled for the experiments in this study.

3.4.3 Proton nuclear magnetic resonance (^{1}H NMR) spectroscopy

The hydration equilibrium constants (K_{hyd}) and their temperature dependence of target compounds were quantified using the proton nuclear magnetic resonance (^{1}H NMR) spectroscopy. ^{1}H NMR spectroscopy is suited for the measurements of K_{hyd} values under equilibrium, it detects the carbonyls and hydrated carbonyl products directly in the aqueous phase.[206]

Triplicate aqueous solutions of an individual target flavoring were prepared at a concentration of 10 mM in D_2O, but up to 100 mM for acetoin due to the insignificant hydrated carbonyl product peak. D_2O was used as the solvent to minimize the impact of the H_2O peak at around 4.7 ppm, which can otherwise overwhelm the NMR spectra. DMSO with a known concentration (10 mM) was added as an internal standard for chemical shift calibration and quantification. 700 μL of the mixed solution was transferred into a Norell Standard Series 5 mm NMR tube for measurement. The ^{1}H NMR data were acquired by an Agilent/Varian Inova spectrometer (400 MHz) with an AutoXDB probe and an SMS autosampler. Temperature-dependent K_{hyd} determination was achieved by adjusting the temperature of the probe to 15, 25, 35, and 50 °C and the temperature range was calibrated on the probe. Measurements for each target compound and each temperature were performed in triplicates. Peak assignment was conducted with the assistance of an online ^{1}H NMR spectra predictor.[207–210]

An NMR spinner with an NMR tube inside was put in the spectrometer for 3.5 min for locking and shimming to correct any inhomogeneities in the magnetic field before scanning the spectrum. Other parameters have been optimized prior to the ^{1}H NMR experiments: (i) A simple presat was used for water suppression, and presaturation delay was 2 s. (ii) A line broadening of 0.25 Hz was used to enhance the signal-to-noise ratio. (iii) The samples were detected with 8 scans and the total relaxation time was 5.1 s, including 0.1 s relaxation delay and 5 s acquisition. Each sample took less than 1 min. The time for the hydration process was suggested to be within 1 hour in work from Zhao *et al.*[206] All the ^{1}H NMR measurements were taken within 24 h after the preparation of samples after the hydration equilibrium has been fully established. D_2O blank and control experiments have been conducted to confirm the purity of the solvent and internal standard for the NMR samples.

The concentration of non-hydrated carbonyls and hydrated carbonyl products in the solution can be quantified by relating their peak integrations and proton numbers with those of an internal standard (DMSO), their definitions are below:[211]

$$[\text{carbonyl}] = [\text{DMSO}] \times [\text{I(carbonyl)/nH(carbonyl)}]/[\text{I(DMSO)/nH(DMSO)}] \quad (3.9)$$

where [carbonyl] and [DMSO] represent the equilibrium concentrations of the hydrated form or non-hydrated form of a target flavoring and DMSO, respectively. I is the peak integration from ^{1}H NMR spectrum, and nH is the number of protons responsible for the peak of interest. The hydration equilibrium constant (K_{hyd}) can be analyzed relating to the eq 3.6 mentioned before based on the quantified concentrations.

3.4.4 Chemical two-dimensional (2D) partitioning model

A chemical two-dimensional (2D) partitioning model has been employed to further investigate the indoor phase distribution of the flavoring agents added in e-cigarettes and hookah tobacco. This model was initially introduced to the atmospheric chemistry field to evaluate secondary organic aerosol formation in the atmosphere,[98] then was developed to be applied in the indoor environment.[71] Herein, we applied the model to simulate chemical equilibrium partitioning space plots of the flavoring compound, which is linked to the thirdhand exposure.[70] In brief, a three-phase system including gas, polar and weakly polar phases is employed as a simplified representation of the indoor environment. The model simulates the indoor phase distribution of a chemical species depending on its partitioning coefficients (K_{wa} and K_{oa}) under equilibrium. A detailed description of the model can be found in Wania *et al.*[98]

The K_{wa} and K_{oa} values used in the model have been summarized in Section B.1.4. Specifically, the input K_{wa} values of the target compounds were measured from the IGS method, K_{wa} values of other flavorings and all K_{oa} values are either from previous studies[112] or predicted by SPARC Performs Automated Reasoning in Chemistry (SPARC).[212] Briefly, SPARC is an online calculator (http://archemcalc.com/sparc-web/calc) that predicts the physical-chemical properties of chemicals based on their fundamental molecular structure.[212]

3.5 Results and discussion

3.5.1 Determination of the effective Henry's law constant ($H^{cp}_{s,eff}$) using the IGS method

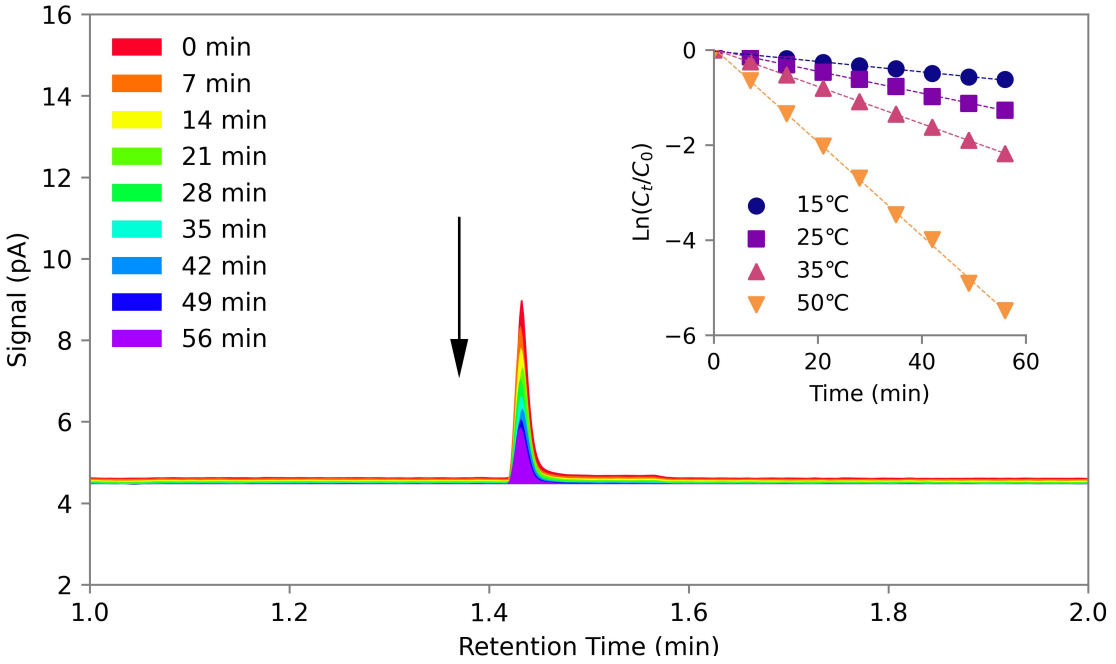

Figure 3.3: Chromatogram of 6-methyl-5-hepten-2-one at 25 °C over time during an example IGS experiment. The inset presents plots of $\ln(C_t/C_0)$ versus time at 15, 25, 35 and 50 °C.

A first-order decay of concentration in the gas phase of the bubbler was observed during the IGS experiment. An example experiment with 6-methyl-5-hepten-2-one is shown in Figure 3.3. The decrease of its signal can be seen from the disappearance of its GC peak. In the inset of Figure 4.3, the values of $\ln(C_t/C_0)$ at 15, 25, 35 and 50 °C. are plotted as a function of time. Excellent linearity was obtained between $\ln(C_t/C_0)$ and time, and the temperature dependence indicates higher $H^{cp}_{s,eff}$ values at a colder temperature according to eq 3.5. The plots of $\ln(C_t/C_0)$ versus time at 15, 25, 35 and 50 °C for all target flavorings have exhibited a similar trend and been included in Section B.1.2.

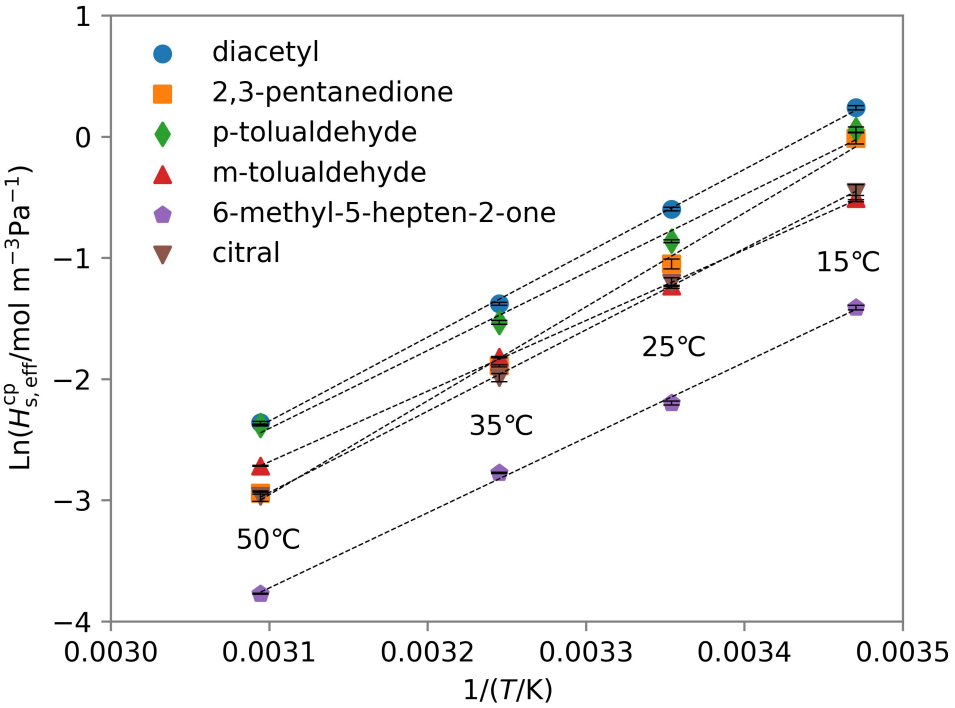

Figure 3.4: van't Hoff diagram of the flavoring compounds obtained by the IGS method between 15 °C and 50 °C. The dashed lines represent the linear regressions of the measured data.

The van't Hoff plots of the $H^{cp}_{s,eff}$values between 15 °C and 50 °C are presented in Figure 3.4, the natural logarithm of $H^{cp}_{s,eff}$ is plotted against the reciprocal of the absolute temperature between 15 °C and 50 °C. Solid markers are the average measured values from triplicates at the four temperatures, while the error bars represent the standard deviations. The plots display the decline of $H^{cp}_{s,eff}$ in units of mol·m^{-3}·Pa^{-1} as the temperature increases, the dashed lines are obtained from the linear least-squares analysis. The values of r^2 of the regression lines are all above 0.996, indicating the data reliability.

Table 3.1 lists the measured $H^{cp}_{s,eff}$ values, their temperature dependence, the literature data at 25°C, and the derived molar enthalpy of dissolution (kJ·mol^{-1}) of $H^{cp}_{s,eff}$ using eq 3.5. $H^{cp}_{s,eff}$ values at other temperatures are given in Section B.1.5. Consistency of the testing compound with literature data is especially important to verify the credibility of the IGS experimental setup. For diacetyl, there is a pronounced discrepancy among the previous studies at 25°C, up to 10 times difference,

Table 3.1: Comparison of the measured $H^{cp}_{s,eff}$ at 25°C and temperature dependence for target flavorings with literature values.

	H at 25 °C (mol·m^{-3}·Pa^{-1})		$\mathrm{d}\ln H/\mathrm{d}\ln(1/T)$ (K)		$-\Delta_{sol}H$ (kJ·mol^{-1})
	this study[b]	lit. data[d]	this study	lit. data[d]	this study
diacetyl[a]	$(5.50 \pm 0.18)\times10^{-1}$	$(3.7 - 38)\times10^{-1}$	6900	5700-6700	57
2,3-pentanedione	$(3.50 \pm 0.33)\times10^{-1}$	n.a.	7800	n.a.	65
p-tolualdehyde	$(4.22 \pm 0.13)\times10^{-1}$	$(5.2 - 7.9)\times10^{-1}$, 4.9×10^{-1}[e]	6400	7200[e]	53
m-tolualdehyde	$(2.92 \pm 0.02)\times10^{-1}$	3.3×10^{-1}, 3.2×10^{-1}[e]	5800	7200[e]	48
6-methyl-5-hepten-2-one	$(1.11 \pm 0.04)\times10^{-1}$	n.a.	6200	n.a.	52
citral	$(2.99 \pm 0.29)\times10^{-1}$	2.3×10^{-1}	6700	n.a.	56
acetoin	2.3 - 4.0[c]	5.7×10^{-1}, 9.9×10^{-1}	n.d.	n.a.	n.d.

[a]Testing compound. [b]Mean standard deviation (n=3). [c]Estimated combining the IGS method and syringe pump-GC method. [d]Previous published data summarized by Sander[112] unless otherwise noted. [e]Measurements by Ji *et al.*[213] n.d.: Not detected due to the absence of signal decay. n.a.: Not available.

which implies that more experimental constraints are required in the determination of H values. These previous studies employed three main approaches to obtaining H values, experimental measurement, a calculation based on the vapor pressure of the pure compound divided by aqueous solubility, and theoretical methods such as quantitative structure-property relationship (QSPR).[112] The $H^{cp}_{s,eff}$ value at 25 °C of diacetyl from the current study is 0.55 mol·m^{-3}·Pa^{-1}, which shows agreement with the previous data, especially with the ones from the laboratory measurements. The corresponding temperature dependence between 15 °C and 50 °C is also consistent with reported values, which range from 5700 to 6700 K. The current work is the first to report the experimentally determined $H^{cp}_{s,eff}$ values and temperature dependence for 2,3-pentanedione, 6-methyl-5-hepten-2-one and citral in the range of 15 °C to 50 °C. The results for p-tolualdehyde and m-tolualdehyde at 25 °C are much closer to the only laboratory measurements at the temperature range of 5 °C to 25 °C reported by Ji *et al.*[213] The previous data for these two chemicals summarized by Sander[112] was either based on vapor pressure and solubility or QSPR. Besides, we found that p-tolualdehyde has a slightly larger $H^{cp}_{s,eff}$ than m-tolualdehyde which may be explained by its higher solubility in water.[214]

The $H^{cp}_{s,eff}$ for acetoin could not be measured using the IGS method due to the absence of signal decay after eight hours, which indicated that $H^{cp}_{s,eff}$was larger than

the upper limit of the measurement range (2.3 mol·m^{-3}·Pa^{-1}) according to our prior study.[115] Therefore, a syringe pump-GC setup was employed to quantify the gas phase concentration in the bubbler headspace and estimate the $H^{cp}_{s,eff}$ at 25 °C (see Section B.1.6). The upper-limit estimate of acetoin's $H^{cp}_{s,eff}$ was 4.0 mol·m^{-3}·Pa^{-1}. Along with the upper capacity of the IGS method (2.3 mol·m^{-3}·Pa^{-1}) from our previous study, we managed to constrain the $H^{cp}_{s,eff}$ of acetoin to a range of 2.3 to 4.0 mol·m^{-3}·Pa^{-1}. We note that this result is inconsistent with the only two values available in the literature: 0.57 and 0.99 mol·m^{-3}·Pa^{-1}, with one of which was determined experimentally and the other by QSPR.[112] The exact reason for such discrepancy is unknown. We have also consulted with another compound, hydroxyacetone, which has a similar structure to acetoin. The $H^{cp}_{s,eff}$ value for hydroxyacetone was reported to be quite large in literature: 77 mol·m^{-3}·Pa^{-1}. Hydroxyacetone has a hydroxyl group at the alpha position from the ketone, which is very similar to the case of acetoin. It is likely that such α-hydroxy carbonyl structure serves to enhance the $H^{cp}_{s,eff}$ of the compounds. Additional measurements are required to confirm this hypothesis.

3.5.2 Determination of hydration equilibrium constants (K_{hyd}) using the ^{1}H NMR

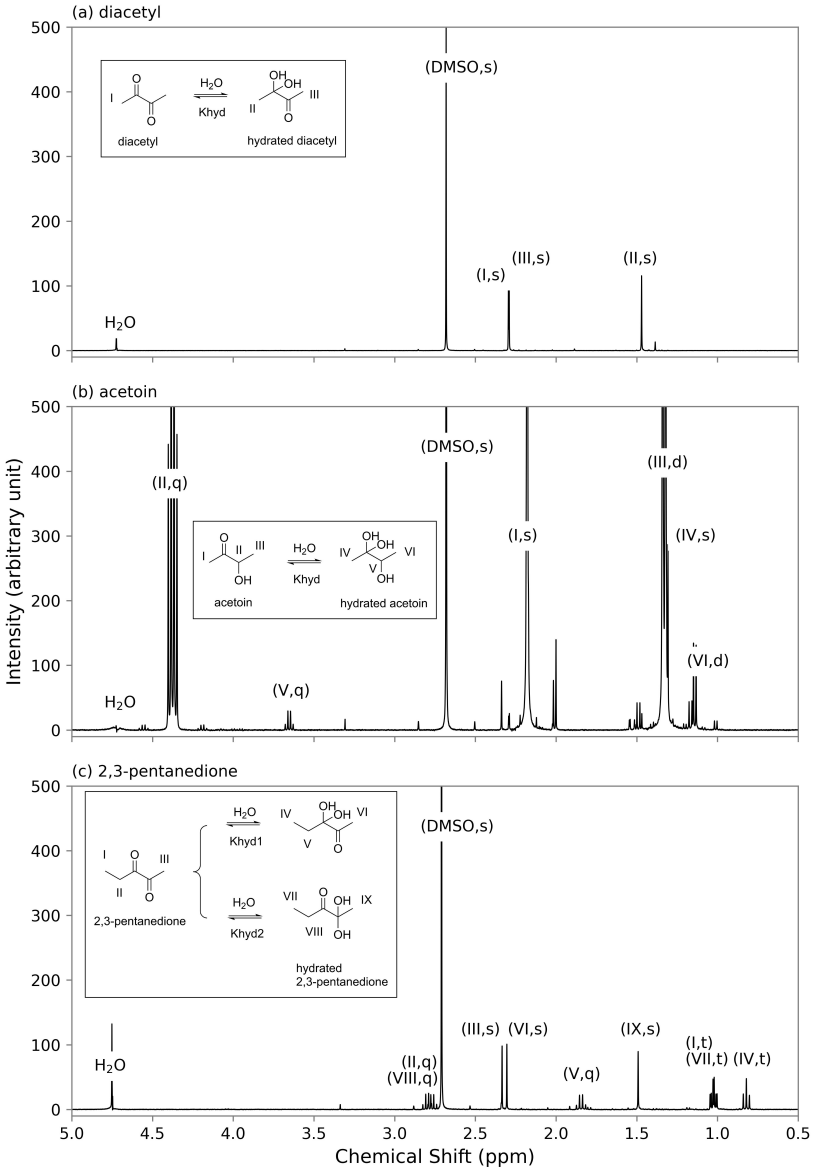

Figure 3.5: ^{1}H NMR spectra for the flavoring agents diluted in D_2O with DMSO as an internal standard at 25 °C. (a) Diacetyl; (b) Acetoin; (c) 2,3-Pentanedione. The identity of the peak (the numbers match those in the chemical structures) and splitting pattern are shown in the brackets. Schematics of the hydration processes of acetoin, diacetyl and 2,3-pentanedione are included in the subwindows.

The ^{1}H NMR spectra of diacetyl, acetoin, and 2,3-pentandione are shown in Figure 3.5. The singlet peak of the internal standard, DMSO, appears at 2.71 ppm. A H_2O peak is observed at 4.75 ppm despite the use of D_2O as the solvent, likely due to a H_2O impurity present in D_2O and DMSO. Multiple peaks from carbonyl and hydrated carbonyl were detected in the ^{1}H NMR spectrum. We have performed peak assignment to as many peaks as possible, as labeled in brackets according to their chemical shift and splitting pattern in Figure 3.5. However, for larger carbonyl compounds, including p-tolualdehyde, m-tolualdehyde, 6-methyl-5-hepten-2-one and citral, the NMR spectra become increasingly complex, and an explicit peak assignment is infeasible under the influence of background noise, impure chemicals and peak overlapping; more information can be found in Section B.1.7. For the purpose of determining K_{hyd}, not all but only one peak is required from each compound. As such, one peak each from the carbonyl and different hydrated carbonyl was selected to calculate the respective concentrations based on eq 3.9. The K_{hyd} values for p-tolualdehyde, m-tolualdehyde, 6-methyl-5-hepten-2-one and citral cannot be determined in the aqueous phase with our method due to the absence of the hydrated product peak even at low temperature (15 °C) or with high scans (128 scans). We thus conclude that they have small K_{hyd} values that cannot be detected in our current method.

The hydration processes of acetoin, diacetyl and 2,3-pentanedione are given in Figure 3.5, while p-tolualdehyde, m-tolualdehyde, 6-methyl-5-hepten-2-one and citral undergo a similar process (Figure B.4). Generally, the carbonyl group (C=O) is hydrated to produce a geminal diol, which has two hydroxyl functional groups (-OH) bound to the same carbon atom. Diacetyl and 2,3-pentanedione both have two carbonyls. Diacetyl exhibits only one hydrated product due to its symmetrical chemical structure, whereras 2,3-pentanedione has two hydrated products with two different K_{hyd} values. Particularly, the calculation of 2,3-pentanedione H_{s}^{cp} should be conducted by eq 3.7, where K_{hyd} equals the sum of K_{hyd_1} and K_{hyd_2}. Two observations need to be addressed according to ^{1}H NMR results, (i) no hydrated product peak was found for p-tolualdehyde, m-tolualdehyde, 6-methyl-5-hepten-2-one and citral. This shows consistency with the predicted K_{hyd} from SPARC at 25 °C (Table B.5). The efficiency of the addition reaction in the hydration process depends on how electrophilic the C=O carbon atom is. The attached alkyl groups are electron-donating

and are able to suppress the partial positive charge of the carbon, making it less electrophilic. This can explain why carbonyls with longer chains and larger molecular structures are less reactive to water. (ii) Diacetyl and 2,3-pentanedione underwent single hydration, as evidenced by the absence of NMR peaks attributable to products of double hydration. It is likely that the formation of the first geminal diol impedes the formation of a second one due to the electron-donating nature of hydroxyl groups. Similarly, the electron-donating nature of a hydroxy group likely explains the small K_{hyd} observed for acetoin.

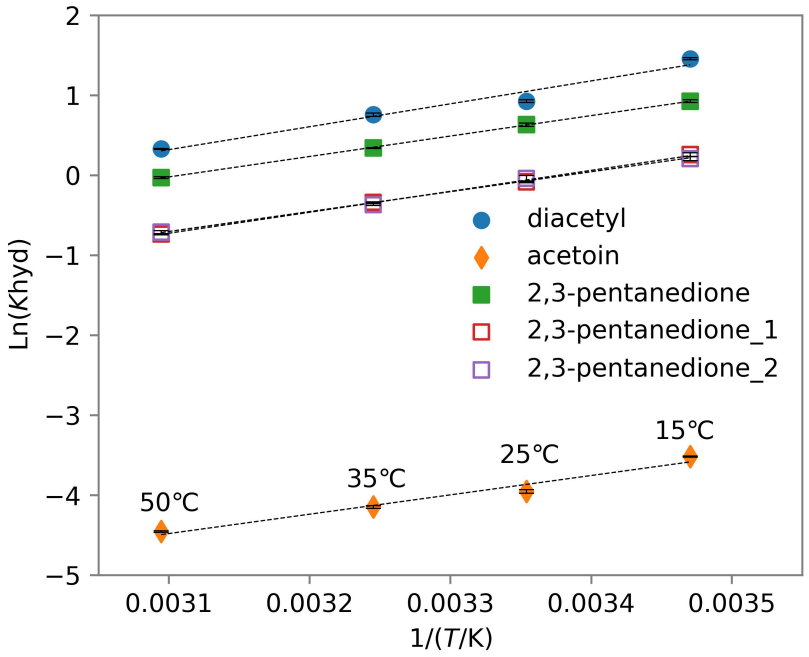

Figure 3.6: Plots of $\ln(K_{\mathrm{hyd}})$ versus T^{-1} for the flavoring compounds obtained by ^{1}H NMR between 15 °C and 50 °C. The dashed lines represent the linear regressions of the measured data.

The temperature dependence of K_{hyd} follows the van't Hoff equation as shown in Figure 3.6. The markers are the average measured data points for diacetyl, acetoin and 2,3-pentanedione, while error bars are standard deviations from triplicates at certain temperatures: 15, 25, 35 and 50 °C. As mentioned before, K_{hyd} of 2,3-pentanedione is obtained by summing its K_{hyd_1} and K_{hyd_2} values. Figure 3.6 also includes linear correlations for van't Hoff plots, which exhibit good linearity, with r^2 values being 0.983, 0.985 and 1.00 for diacetyl, acetoin and 2,3-pentanedione, respec-

tively.

Table 3.2: Comparison of hydration equilibrium constants (K_{hyd}) values at 25 and temperature dependence for target flavorings measured by ^{1}H NMR with literature data.

	K_{hyd} at 25		$d\ln K_{hyd}/d\ln(1/T)$
	this study[b]	lit. data	this study
diacetyl[a]	2.52 ± 0.10	$(2.4 \pm 33)\times10^{-1}$[205]	2800
acetoin	$(1.92 \pm 0.10)\times10^{-2}$	n.a.	2400
2,3-pentanedione	1.88 ± 0.09	1.7[215]	2600
2,3-pentanedione_K_{hyd_1}	$(9.20 \pm 0.25)\times10^{-1}$	n.a.	2600
2,3-pentanedione_K_{hyd_2}	$(9.60 \pm 0.83)\times10^{-1}$	n.a.	2500
p-tolualdehyde	n.d.	n.a.	n.d.
m-tolualdehyde	n.d.	n.a.	n.d.
6-methyl-5-hepten-2-one	n.d.	n.a.	n.d.
citral	n.d.	n.a.	n.d.

[a]Testing compound. [b]Mean standard deviation (n=3). n.d.: Not detected due to the absence of the hydrated product peak. n.a.: Not available.

The measured K_{hyd} values at 25 °C and their temperature dependence for diacetyl, acetoin and 2,3-pentanedione from ^{1}H NMR are tabulated in Table 3.2 to be compared with previous literature data. The K_{hyd} values for diacetyl at 25 °C have been reported, and thus it was used as a testing chemical to confirm the ^{1}H NMR analysis. The measured K_{hyd} of diacetyl at 25 °C is 2.52, which agrees with the recommended value of 2.00 from review papers.[205, 216] Additionally, the K_{hyd} (K_{hyd_1}+K_{hyd_2}) of 2,3-pentanedione at 25°C is consistent with a literature data obtained by the stopped-flow measurement.[215] This study is the first to report the measured K_{hyd} of acetoin and the temperature dependence of K_{hyd} of all of these carbonyl compounds (see Table B.6). It is necessary to account for the hydration contribution to the measurement of $H^{cp}_{s,eff}$, especially for the target flavorings that are known to undergo significant hydration, such as diacetyl and 2,3-pentanedione.

3.5.3 Comparison between the intrinsic and effective Henry's law constants (H_s^{cp} and $H_{s,eff}^{cp}$)

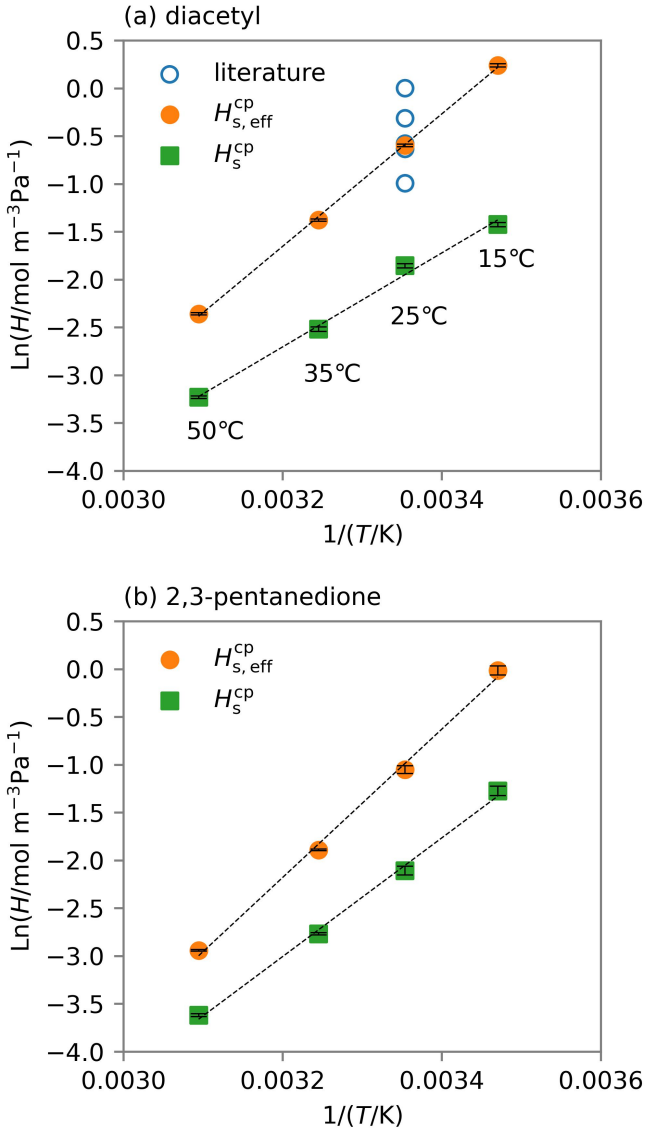

Figure 3.7: van't Hoff diagram for the $H_{s,eff}^{cp}$ and H_s^{cp} of (a) diacetyl and (b) 2,3-pentanedione between 15 °C and 50 °C. The dashed lines represent the linear regressions of the data. The literature points at 25 °C are the ones from measurements summarized by Sander.[112]

Figure 3.7 shows the $H^{cp}_{s,eff}$ and H^{cp}_{s} as a function of 1/T for (a) diacetyl and (b) 2,3-pentanedione between 15 °C and 50 °C. The solid markers represent the average measured $H^{cp}_{s,eff}$ values and calculated H^{cp}_{s} values at 15, 25, 35 and 50 °C of all triplicates. The H^{cp}_{s} values are obtained via eq 3.7 using the $H^{cp}_{s,eff}$ values measured by IGS and K_{hyd} values from ^{1}H NMR. Diacetyl and 2,3-pentanedione were determined to have H^{cp}_{s} with values of $(1.56 \pm 0.08)\times10^{-1}$ and $(1.22 \pm 0.13)\times10^{-1}$ mol·m^{-3}·Pa^{-1}, respectively, at 25 °C. The H^{cp}_{s} values at other temperatures are given in Table B.6. The $H^{cp}_{s,eff}$ values of diacetyl and 2,3-pentanedione are enhanced by three times in the presence of hydration. A stronger temperature dependence was observed for $H^{cp}_{s,eff}$ than H^{cp}_{s}, indicating a greater hydration effect on $H^{cp}_{s,eff}$ at lower temperatures. The van't Hoff plots of H^{cp}_{s} yielded the dissolution enthalpy to be -41 and -52 kJ·mol^{-1} for diacetyl and 2,3-pentanedione, respectively. The error bar around the linear regression line (the dashed line) of H^{cp}_{s} data is derived by propagating the standard deviations of $H^{cp}_{s,eff}$ and K_{hyd} data. The values of r^2 for the regression lines of H^{cp}_{s} values are (a) 0.997 and (b) 0.998, respectively. Acetoin, due to its smaller K_{hyd}, has little difference in its $H^{cp}_{s,eff}$ and H^{cp}_{s} (approximately 2%). As discussed before, p-tolualdehyde, m-tolualdehyde, 6-methyl-5-hepten-2-one, and citral were evaluated to have small K_{hyd} values, and the difference caused by hydration reaction should be negligible; therefore, they were excluded from the Figure 3.7.

Figure 3.7(a) included the published measurements of diacetyl for a better comparison. A few previous studies experimentally measured the H of diacetyl at 25 °C, reporting the values in the range of 0.37 to 1 mol·m^{-3}·Pa^{-1}, while only two of them provided the temperature dependence values, which are 5700 and 6700 K, respectively.[112] Our measured $H^{cp}_{s,eff}$ falls into the range of the literature data. Previous literature had inconsistency in their reporting of $H^{cp}_{s,eff}$ for diacetyl, most of the previous studies provided the $H^{cp}_{s,eff}$ results without any consideration for the hydration processes during laboratory measurements.[159, 217–219]. Few other studies suggested that the hydration process does not affect the $H^{cp}_{s,eff}$ measurements of diacetyl, and concluded that $H^{cp}_{s,eff}$ value is approximately equal to the H^{cp}_{s} value.[203, 220] However, our ^{1}H NMR analysis clearly shows that hydration, instead, plays a major role in governing the $H^{cp}_{s,eff}$ of these two compounds.

Table 3.3: Ratio of $H^{cp}_{s,eff}$ to H^{cp}_{s} and difference between log $K_{wa,eff}$ and log K_{wa} at 25 °C for target flavorings and representative carbonyls.

	$H^{cp}_{s,eff}/H^{cp}_{s}$ [b]	Difference between log $K_{wa,eff}$ and log K_{wa} [c]
diacetyl[a]	3.52	0.55
2,3-pentanedione	2.88	0.46
acetoin	1.02	0.01
p-tolualdehyde	∼1.00	0.00
m-tolualdehyde	∼1.00	0.00
6-methyl-5-hepten-2-one	∼1.00	0.00
citral	∼1.00	0.00
glyoxal	2.21×10^{5}[d]	5.34
formaldehyde	2.00×10^{3}[e]	3.30
acetaldehyde	2.20[e]	0.34
propionaldehyde	1.85[e]	0.27

[a]Testing compound. [b]From this study unless otherwise noted. [c]Calculated from $H^{cp}_{s,eff}$ and H^{cp}_{s} accordingly (see Table B.7). [d]Reported by Ip *et al.*[154] [e]Based on eq 3.7 and previous published data recommended by Tilgner *et al.*[205] n.d.: Not detected due to the absence of the hydrated product peak.

To better understand the relationship between $H^{cp}_{s,eff}$ and H^{cp}_{s} under the influence of the hydration process for carbonyls, Table 3.3 summarizes the ratio of $H^{cp}_{s,eff}$ to H^{cp}_{s} and the difference between log $K_{wa,eff}$ and log K_{wa} accordingly at 25 °C for target flavorings and those of other representative carbonyls previously reported by the literature. The actual values of K_{hyd}, $H^{cp}_{s,eff}$, H^{cp}_{s}, log $K_{wa,eff}$ and log K_{wa} are listed in Section B.1.8. For diacetyl and 2,3-pentanedione, hydration enhanced $H^{cp}_{s,eff}$ by a factor of approximately three compared to their H^{cp}_{s}. For the other target flavorings investigated in this study, the hydration processes have no pronounced effect on $H^{cp}_{s,eff}$. The enhancement of $H^{cp}_{s,eff}$ has been shown for other carbonyl compounds in the literature. Glyoxal is an example with extremely large $H^{cp}_{s,eff}$ due to the large 1st and 2nd K_{hyd} values, resulting in a ratio of 2.21×10^{5} between $H^{cp}_{s,eff}$ and H^{cp}_{s},[154] which implies that the hydration should be considered as a dominant factor in chemical

partitioning for compounds with large K_{hyd} values. A structure-reactivity relationship on K_{hyd} is evidenced by a comparison between formaldehyde, acetaldehyde and propionaldehyde. In particular, formaldehyde is an important indoor volatile organic compound steadily emitted from building materials and furnishings,[100] its $H^{\mathrm{cp}}_{\mathrm{s,eff}}$ and $H^{\mathrm{cp}}_{\mathrm{s}}$ differ by three orders of magnitude. As shown on Table 3.3, the longer the carbon chain of a carbonyl compound, the smaller the K_{hyd}, corresponding to a smaller difference between $H^{\mathrm{cp}}_{\mathrm{s,eff}}$ and $H^{\mathrm{cp}}_{\mathrm{s}}$. Similar to the explanation of NMR observation that large target flavorings have small K_{hyd} values, the attached alkyl groups suppress the nucleophilic addition reaction and make the large carbonyls less reactive to water. When it comes to α-dicarbonyls (diacetyl and 2,3-pentanedione), the nucleophilic attack is more likely to happen. The electron-withdrawing nature of C=O double bond decreases the electron density of the adjacent carbonyl carbon, thus making it more electrophilic with a more positive partial charge. Therefore, diacetyl and 2,3-pentanedione have relatively large K_{hyd} which in turn affects the $H^{\mathrm{cp}}_{\mathrm{s,eff}}$ and chemical environmental fate.

3.5.4 Chemical 2D-Partitioning space plots and implications to indoor air

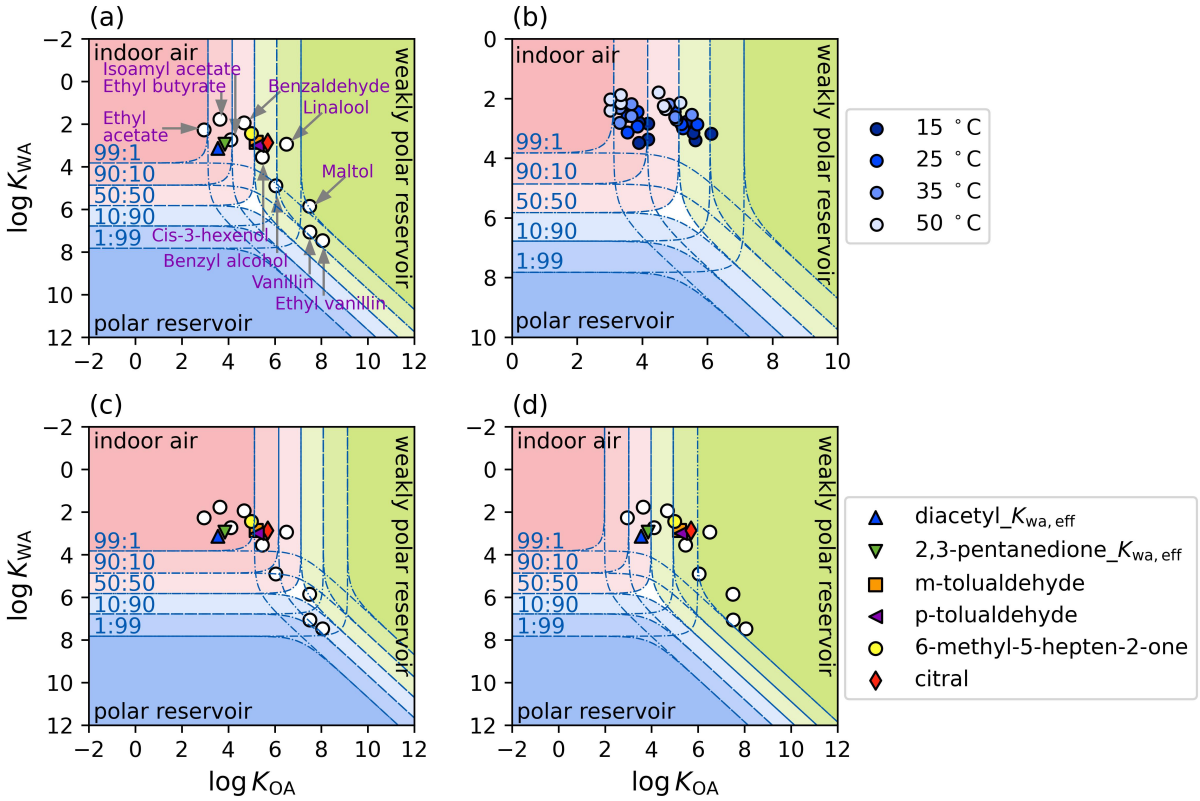

Figure 3.8: Indoor phase distribution of flavoring agents in e-cigarettes and hookah tobacco. The colored markers are the target compounds in this work, the white markers are the top ten most frequently added flavoring ingredients.[199] (a) An indoor environment with polar and weakly-polar surface reservoirs equivalent to thicknesses of 500 and 2500 nm under 25 °C. (b) Same assumption as (a) at 15, 25, 35, and 50 °C including target compounds studied in this work; (c) An indoor environment with polar and weakly-polar surface reservoirs equivalent to thicknesses of 500 and 25 nm under 25 °C; (d) An indoor environment with polar and weakly-polar surface reservoirs equivalent to thicknesses of 500 nm and 35 μm under 25 °C.

The detailed description of a Chemical 2D-Partitioning Plot can be found in previous studies.[71, 98] Briefly, compounds are distributed over three indoor phases represented by different colors based on their partitioning coefficients. The K_{wa} and K_{oa} values used in the model have been tabulated in Section B.1.4. The blue lines between phases indicate the ratios between them. For example, the 50:50 line leads to equal distribution of a chemical in two phases. Figure 3.8(a) presents the partition-

ing prediction of flavorings in an indoor environment with polar and weakly-polar surface reservoirs equivalent to thicknesses of 500 and 2500 nm under 25 °C. Figure 3.8(b) investigates other temperatures related to the indoor environment under the same scenario. The thicknesses of indoor reservoirs used in Figure 3.8(a) and (b) best match the real-time measurement in an indoor environment stated by Wang *et al.*[71] and was employed as the base case scenario in our previous publication.[115] Although the polar and weakly-polar reservoirs are represented by water and 1-octanol in the model; in daily life, the polar and weakly-polar reservoirs are considered as water-rich and organic-rich phases, respectively. For instance, the water surface in a sink and the water absorbed in clothes are both indoor water-rich reservoirs.[221] Meanwhile, the organic film on kitchen surfaces after cooking and the paint layer of walls can be organic-rich reservoirs indoors.[12, 162] From a microscopic perspective, the surface organic films with the thickness up to tens of nanometers are formed from molecule accumulation over months, and the composition of semi-volatile compounds can be uniform over weeks.[76, 77] In Figure 3.8(c), an indoor environment with polar and weakly-polar surface reservoirs equivalent to thicknesses of 500 and 25 nm under 25 °C is applied to simulate the partitioning of flavoring into surface organic films at room temperature after the system reaches equilibrium. The timescale of equilibrium establishment relies on the gas-surface interactions.[72] In general, the molecular diffusion to surface organic films happens fast in seconds, while partitioning into materials, such as paint layers, can be on the order of hours.[12, 78] Figure 3.8(d) is an example of an indoor environment with a thicker weakly-polar reservoir (35 μm) under 25 °C, to better illustrate the potential partitioning to building materials. In reality, however, indoor partitioning can be complicated and affected by diverse factors. The polar indoor reservoir is likely more complex and dynamic than what is represented by an ideal aqueous solution in this model. The model simulates fully-established partitioning equilibria; however, the actual equilibria may not be fully established or can be compound-specific. All the following multiphase partitioning discussions are described without considering the chemical removal of the target compounds. In a realistic indoor environment, certain compounds can be removed via chemical reactions. For instance, the ozonolysis reactions of alkenes can occur rapidly. For flavorings that contain unsaturated structures (e.g., citral in this study),

their actual exposure risk can be lower than what our mode suggests due to removal by ozonolysis.[100] The chemical 2D-partitioning space plots should be regarded as a valuable conceptual implications to view the indoor partitioning of flavoring agents.

In addition to ones that were investigated in the current work, we have also added the top ten most frequently used flavorings to Figure 3.8(a), (c) and (d).[199] The results in Figure 3.8(a) clearly demonstrate that frequently detected flavoring agents added in e-liquids predominantly reside in the indoor gas phase and weakly polar reservoir at 25 °C. Interestingly, some flavoring agents are located right between the gas phase and the weakly polar reservoir, which may result perturbation of phase partitioning due to its sensitivity to various conditions, such as temperature and amount of reservoirs. According to PROduction-To-Exposure (PROTEX) model, which simulates human exposure based on partitioning coefficients (K_{wa} and K_{oa}), the estimated routes of human exposure for both adults and children are consistent with our phase distribution in Figure 3.8.[103] In brief, humans are exposed to the flavorings mainly distributed in the gas phase via inhalation, while the major route of exposure to flavorings residing in the weakly-polar phase is dermal permeation. Correspondingly, the flavorings located in the boundary between the gas phase and weakly-polar phase can be exposed to humans via both routes. Figure 3.8(b) presents that the indoor partitioning of flavorings is sensitive to temperature in the range of 15 °C to 50 °C. As the room temperature increases, the flavorings are likely to partition into the gas phase more. Accordingly, inhalation becomes more likely to be the dominant path of human exposure. Meanwhile, partitioning to weakly-polar reservoirs represents a longer residence time indoors, which suggests the re-emission of compounds at higher temperatures or during ventilation.[71] Thirdhand exposure can likely be caused following these phenomena.[70, 83]

Figure 3.8(c) and (d) investigate indoor partitioning of flavorings under different thicknesses of reservoirs and conclude that the indoor partitioning depends on the amount of reservoirs at 25 °C. In an indoor environment with less weakly-polar reservoirs, the compounds are more partitioning to the gas phase and polar phase as shown in Figure 3.8(c). By contrast, a larger amount of weakly-polar reservoir leads to more fraction of chemicals distributed in organic-rich phases in Figure 3.8(d). Similar to the discussions of Figure 8(a) and (b) before, the pathways of human exposure are closely

associated with phase distribution in Figure 8(c) and (d) as well. It should be noted that indoor partitioning is also time-dependent. When considering not only surface films but also permeable surface materials,[72] the indoor partitioning of flavorings is closer to Figure 3.8(d) after a long time. In this case, routes other than inhalation may become the main pathways of indoor exposure, such as dermal permeation and non-dietary ingestion.[103] So far, the thickness of indoor surface reservoirs has not been well defined and rarely measured.[72] More experimental constraints are needed for the reliable prediction of indoor partitioning in the future.

In the previous section, we have discussed the impact of hydration on $H^{cp}_{s,eff}$. Here, we evaluated the magnitude to which hydration can affect indoor partitioning. Given that the chemical 2D partitioning plot is in the log scale, we have added the difference of log $K_{wa,eff}$ and log K_{wa} to Table 3.3. Despite that hydration of diacetyl and 2,3-pentanedione enhances their H^{cp}_{s} by an approximate factor of three, it does not significantly affect their indoor partitioning (See Figure B.5). For the other top ten most used flavorings, based on the prediction from SPARC, the K_{hyd} values are in the range of 0.002 - 0.033 (see Table B.3), which suggests that the effect of the hydration reaction on indoor partitioning is also negligible. By contrast, the carbonyls with large K_{hyd} values exhibit a significant difference between log $K_{wa,eff}$ and log K_{wa} in Table 3.3. The difference can be up to five for glyoxal and three for formaldehyde when applied in the chemical 2D-partitioning space plots, which results in a shift in chemical phase distribution on the vertical axis, between indoor air and a polar surface reservoir. For example, indoor formaldehyde is more likely to reside in polar reservoirs instead of the air. This serves as a reminder that $H^{cp}_{s,eff}$ should be explicitly used while presenting the chemical partitioning in the atmosphere and indoor environment, especially for the compounds with large K_{hyd} values, such as glyoxal and formaldehyde; otherwise the model results might be inaccurate and biased. Also, note that the models based on chemical structures often provide the predicted H^{cp}_{s} rather than the $H^{cp}_{s,eff}$.

3.6 Conclusions

This work explores the indoor partitioning of harmful flavoring agents added to e-cigarette and hookah tobacco and further evaluates the pathways of human thirdhand exposure in indoor environments. The recent discovery of a large amount of indoor reservoirs highlights the significant impact of partitioning coefficients on indoor phase distribution,[71] prompting studies of the indoor environment that focus on more than just the air. With the assistance of the IGS method and ^{1}H NMR, we performed the measurement of $H^{cp}_{s,eff}$ and K_{hyd} for widely used flavoring agents that are carbonyls at temperatures relative to the indoor environment. Such fundamental data is critical in determining the chemical environmental fate of toxic flavorings.

This study is the first to report the experimentally measured $H^{cp}_{s,eff}$ and temperature dependence for a number of key flavorings. Using the newly obtained $H^{cp}_{s,eff}$, the 2D partitioning space plots have been applied to predict their indoor phase distribution. This thermodynamic information derived in this paper is the primary input data required by the partitioning model and humane exposure model.[71, 103, 222] We concluded from the 2D partitioning space plots that indoor partitioning for target flavorings is highly sensitive to the temperature and the volume of indoor reservoirs. This observation has significant implications to thirdhand exposure from e-cigarette vaping, a process that is poorly understood. Given that most of the flavorings reside in the middle of the gas and weakly-polar phases on the 2D partitioning plot, a rise of temperature, an air exchange, and a change in the reservoir size can lead to their re-emission from surface reservoirs, leading to prolonged exposure to residents.

The K_{hyd} values and the temperature dependence for the most of target flavorings are presented for the first time to better understand their effect on $H^{cp}_{s,eff}$ measurements. While the impact of hydration on the $H^{cp}_{s,eff}$ of carbonyl compounds are widely recognized, systematic investigations of K_{hyd} are rare. Our study represents one of the most careful evaluations of K_{hyd} and temperature dependence for carbonyl compounds of environmental interest. Our results concur with existing literature, showing that K_{hyd} is closely related to the reactivity of the carbonyl carbon. α-Dicarbonyl compounds (e.g., diacetyl and 2,3-pentanedione) undergo hydration to a substantial degree, with their $H^{cp}_{s,eff}$ enhanced by approximately a factor of three from their

H_s^{cp}. The enhancement was shown to be larger at lower temperatures. Meanwhile, hydration of larger flavoring carbonyl compounds investigated in this work, such as p-tolualdehyde, m-tolualdehyde, 6-methyl-5-hepten-2-one, and citral, was observed to be negligible. This was shown by the fact that the hydration product peaks were not detected with the ^{1}H NMR technique employed. Other methods with higher sensitivity must be carried out in the future, should one need to determine such K_{hyd} values. With regard to indoor partitioning, however, we found that the hydration of diacetyl and 2,3-pentanedione will unlikely affect the phase distribution of these compounds in the indoor environment. Hydration will affect the partitioning of compounds with much larger K_{hyd} values, such as glyoxal and formaldehyde.

Currently, a significant inconsistency is seen in the literature-reported H values of many environmentally relevant organic compounds.[112] Careful determination of H values, their temperature dependence, and the underlying chemistry that affects $H_{s,eff}^{cp}$ are timely and necessary for the understanding of the environmental behavior of these compounds. While the current work focused on the implications to indoor air quality and thirdhand exposures, the H values determined in this study will assist many other research fields, given the ubiquitous nature of air-water partitioning. For instance, hookah tobacco contains a pot of water through which the flavorings will be introduced. H values will serve to determine the exposure of flavorings to hookah users. The flavoring agents investigated in this work are also widely used as additives in food, beverage, and personal care products.[223, 224] H values will be key parameters to understand the flavors and smells of such products, as well as exposure to consumers.

3.7 Acknowledgements

This research was supported by the Natural Sciences and Engineering Research Council of Canada (Award Number: RGPIN-2018-03814) and the University of Alberta. The authors thank Ryan McKay, Mark Miskolzie, Nupur Dabral and Nuclear Magnetic Resonance Facility for the help with ^{1}H NMR, Jason Dibbs and the Glass Shop for assistance in glassware, Dr. Chen Wang (SUSTech) for assistance in 2D partitioning model. EK thanks NSERC USRA and Lloyd and Margaret Cooley Memorial

Studentship in Analytical Chemistry for funding.

3.8 Supporting Information Available in Appendix B

The Supporting Information includes the structures of flavoring compounds, plots of $\ln(C_t/C_0)$ versus time for all target flavorings, choice of setups with different purging bubble size, log K_{wa} and log K_{oa} values used in 2D partitioning plots, summary of the measured $H^{cp}_{s,eff}$, the syringe pump-GC setup, summary of the measured K_{hyd} and the H^{cp}_{s}, comparison between the $H^{cp}_{s,eff}$ and the H^{cp}_{s}.

References

[1] N. E. Klepeis *et al.*, "The national human activity pattern survey (NHAPS): A resource for assessing exposure to environmental pollutants," *Journal of Exposure Science & Environmental Epidemiology*, vol. 11, no. 3, pp. 231–252, 2001.

[11] A. Manuja *et al.*, "Total surface area in indoor environments," *Environmental Science: Processes & Impacts*, vol. 21, no. 8, pp. 1384–1392, 2019.

[12] L. B. Algrim, D. Pagonis, J. A. de Gouw, J. L. Jimenez, and P. J. Ziemann, "Measurements and modeling of absorptive partitioning of volatile organic compounds to painted surfaces," *Indoor Air*, vol. 30, no. 4, pp. 745–756, 2020.

[70] K. Yeh, L. Li, F. Wania, and J. P. Abbatt, "Thirdhand smoke from tobacco, e-cigarettes, cannabis, methamphetamine and cocaine: Partitioning, reactive fate, and human exposure in indoor environments," *Environment International*, vol. 160, p. 107 063, 2022.

[71] C. Wang *et al.*, "Surface reservoirs dominate dynamic gas-surface partitioning of many indoor air constituents," *Science Advances*, vol. 6, no. 8, eaay8973, 2020.

[72] J. P. Abbatt, G. C. Morrison, V. H. Grassian, M. Shiraiwa, C. J. Weschler, and P. J. Ziemann, "How should we define an indoor surface?" *Indoor air*, vol. 32, no. 1, e12955, 2022.

[76] C. J. Weschler and W. W. Nazaroff, "Growth of organic films on indoor surfaces," *Indoor Air*, vol. 27, no. 6, pp. 1101–1112, 2017.

[77] C. Y. Lim and J. P. Abbatt, "Chemical composition, spatial homogeneity, and growth of indoor surface films," *Environmental Science & Technology*, vol. 54, no. 22, pp. 14 372–14 379, 2020.

[78] Y. Fang *et al.*, "A molecular picture of surface interactions of organic compounds on prevalent indoor surfaces: Limonene adsorption on SiO_2," *Chemical Science*, vol. 10, no. 10, pp. 2906–2914, 2019.

[83] G. E. Matt *et al.*, "Thirdhand tobacco smoke: Emerging evidence and arguments for a multidisciplinary research agenda," *Environmental Health Perspectives*, vol. 119, no. 9, pp. 1218–1226, 2011.

[90] J.-C. Lerol, J.-C. Masson, H. Renon, J.-F. Fabries, and H. Sannier, "Accurate measurement of activity coefficient at infinite dilution by inert gas stripping and gas chromatography," *Industrial & Engineering Chemistry Process Design and Development*, vol. 16, no. 1, pp. 139–144, 1977.

[98] F Wania, Y. Lei, C Wang, J. Abbatt, and K.-U. Goss, "Using the chemical equilibrium partitioning space to explore factors influencing the phase distribution of compounds involved in secondary organic aerosol formation," *Atmospheric Chemistry and Physics*, vol. 15, no. 6, pp. 3395–3412, 2015.

[100] J. P. Abbatt and C. Wang, "The atmospheric chemistry of indoor environments," *Environmental Science: Processes & Impacts*, vol. 22, no. 1, pp. 25–48, 2020.

[103] L. Li, J. A. Arnot, and F. Wania, "How are humans exposed to organic chemicals released to indoor air?" *Environmental Science & Technology*, vol. 53, no. 19, pp. 11 276–11 284, 2019.

[112] R. Sander, "Compilation of Henry's law constants (version 4.0) for water as solvent," *Atmospheric Chemistry and Physics*, vol. 15, no. 8, pp. 4399–4981, 2015.

[115] S. Wu *et al.*, "Henry's law constants and indoor partitioning of microbial volatile organic compounds," *Environmental Science & Technology*, vol. 56, no. 11, pp. 7143–7152, 2022.

[124] J. A. Leech, W. C. Nelson, R. T. Burnett, S. Aaron, and M. E. Raizenne, "It's about time: A comparison of canadian and american time-activity patterns," *Journal of Exposure Science & Environmental Epidemiology*, vol. 12, no. 6, pp. 427–432, 2002.

[144] D. Mackay, W. Y. Shiu, and R. P. Sutherland, "Determination of air-water Henry's law constants for hydrophobic pollutants," *Environmental Science & Technology*, vol. 13, no. 3, pp. 333–337, 1979.

[149] R. Bell, "The reversible hydration of carbonyl compounds," *Advances in Physical Organic Chemistry*, vol. 4, pp. 1–29, 1966.

[154] H. S. Ip, X. H. Huang, and J. Z. Yu, "Effective Henry's law constants of glyoxal, glyoxylic acid, and glycolic acid," *Geophysical Research Letters*, vol. 36, no. 1, p. L01802, 2009.

[155] C. Wang, Y. D. Lei, S. Endo, and F. Wania, "Measuring and modeling the salting-out effect in ammonium sulfate solutions," *Environmental Science & Technology*, vol. 48, no. 22, pp. 13 238–13 245, 2014.

[156] C. Wang, Y. D. Lei, and F. Wania, "Effect of sodium sulfate, ammonium chloride, ammonium nitrate, and salt mixtures on aqueous phase partitioning of organic compounds," *Environmental Science & Technology*, vol. 50, no. 23, pp. 12 742–12 749, 2016.

[159] D. D. Roberts and P. Pollien, "Analysis of aroma release during microwave heating," *Journal of Agricultural and Food Chemistry*, vol. 45, no. 11, pp. 4388–4392, 1997.

[162] R. E. O'Brien *et al.*, "Emerging investigator series: Chemical and physical properties of organic mixtures on indoor surfaces during HOMEChem," *Environmental Science: Processes & Impacts*, vol. 23, no. 4, pp. 559–568, 2021.

[171] S. Wu, E. Kim, D. Vethanayagam, and R. Zhao, "Indoor partitioning and potential thirdhand exposure to carbonyl flavoring agents added in e-cigarettes and hookah tobacco," *Environmental Science: Processes & Impacts*, vol. 24, no. 12, pp. 2294–2309, 2022.

[172] D. Hammond *et al.*, "Trends in e-cigarette brands, devices and the nicotine profile of products used by youth in England, Canada and the USA: 2017–2019," *Tobacco Control*, 2021.

[173] R. Jebai *et al.*, "Temporal trends in tobacco product use among US middle and high school students: National youth tobacco survey, 2011-2020," *Public Health Reports*, p. 00 333 549 221 103 812, 2022.

[174] S. S. Soneji, K. E. Knutzen, and A. C. Villanti, "Use of flavored e-cigarettes among adolescents, young adults, and older adults: Findings from the population assessment for tobacco and health study," *Public Health Reports*, vol. 134, no. 3, pp. 282–292, 2019.

[175] S.-H. Zhu *et al.*, "Four hundred and sixty brands of e-cigarettes and counting: Implications for product regulation," *Tobacco Control*, vol. 23, no. suppl 3, pp. iii3–iii9, 2014.

[176] G. Kong, M. E. Morean, D. A. Cavallo, D. R. Camenga, and S. Krishnan-Sarin, "Reasons for electronic cigarette experimentation and discontinuation among adolescents and young adults," *Nicotine & Tobacco Research*, vol. 17, no. 7, pp. 847–854, 2015.

[177] E. J. Krüsemann, A. Havermans, J. L. Pennings, K. De Graaf, S. Boesveldt, and R. Talhout, "Comprehensive overview of common e-liquid ingredients and how they can be used to predict an e-liquid's flavour category," *Tobacco Control*, vol. 30, no. 2, pp. 185–191, 2021.

[178] M. A. Farag, M. M. Elmassry, and S. H. El-Ahmady, "The characterization of flavored hookahs aroma profile and in response to heating as analyzed via headspace solid-phase microextraction (SPME) and chemometrics," *Scientific Reports*, vol. 8, no. 1, pp. 1–12, 2018.

[179] V. L. Owens, T. Ha, and J. N. Soulakova, "Widespread use of flavored e-cigarettes and hookah tobacco in the United States," *Preventive Medicine Reports*, vol. 14, p. 100 854, 2019.

[180] N. I. Goldenson, A. M. Leventhal, K. A. Simpson, and J. L. Barrington-Trimis, "A review of the use and appeal of flavored electronic cigarettes," *Current Addiction Reports*, vol. 6, pp. 98–113, 2019.

[181] L. M. Schneller, M. Bansal-Travers, M. L. Goniewicz, S. McIntosh, D. Ossip, and R. J. O'Connor, "Use of flavored e-cigarettes and the type of e-cigarette devices used among adults and youth in the US—Results from wave 3 of the population assessment of tobacco and health study (2015-2016)," *International Journal of Environmental Research and Public Health*, vol. 16, no. 16, p. 2991, 2019.

[182] J. Audrain-McGovern, A. A. Strasser, and E. P. Wileyto, "The impact of flavoring on the rewarding and reinforcing value of e-cigarettes with nicotine among young adult smokers," *Drug and Alcohol Dependence*, vol. 166, pp. 263–267, 2016.

[183] V. H. Murthy, "E-cigarette use among youth and young adults: A major public health concern," *JAMA Pediatrics*, vol. 171, no. 3, pp. 209–210, 2017.

[184] C. O. Cobb, A. Shihadeh, M. F. Weaver, and T. Eissenberg, "Waterpipe tobacco smoking and cigarette smoking: A direct comparison of toxicant exposure and subjective effects," *Nicotine & Tobacco Research*, vol. 13, no. 2, pp. 78–87, 2011.

[185] C. Lau, R. Zhao, and D. Vethanayagam, "Chemistry review of vaping products and respiratory injury," *Spectrum*, no. 6, 2020.

[186] J. L. Barrington-Trimis, J. M. Samet, and R. McConnell, "Flavorings in electronic cigarettes: An unrecognized respiratory health hazard?" *Jama*, vol. 312, no. 23, pp. 2493–2494, 2014.

[187] I. K. Sundar, F. Javed, G. E. Romanos, and I. Rahman, "E-cigarettes and flavorings induce inflammatory and pro-senescence responses in oral epithelial cells and periodontal fibroblasts," *Oncotarget*, vol. 7, no. 47, p. 77 196, 2016.

[188] G. Kaur, T. Muthumalage, and I. Rahman, "Mechanisms of toxicity and biomarkers of flavoring and flavor enhancing chemicals in emerging tobacco and non-tobacco products," *Toxicology Letters*, vol. 288, pp. 143–155, 2018.

[189] T. Eissenberg and A. Shihadeh, "Waterpipe tobacco and cigarette smoking: Direct comparison of toxicant exposure," *American Journal of Preventive Medicine*, vol. 37, no. 6, pp. 518–523, 2009.

[190] P. A. Tierney, C. D. Karpinski, J. E. Brown, W. Luo, and J. F. Pankow, "Flavour chemicals in electronic cigarette fluids," *Tobacco Control*, vol. 25, no. e1, e10–e15, 2016.

[191] K. E. Farsalinos, K. A. Kistler, G. Gillman, and V. Voudris, "Evaluation of electronic cigarette liquids and aerosol for the presence of selected inhalation toxins," *Nicotine & Tobacco Research*, vol. 17, no. 2, pp. 168–174, 2015.

[192] M Yamaguchi, J Ishida, Z. Xuan, A Nakamura, and T Yoshitake, "Determination of glyoxal, methylglyoxal, diacethyl, and 2,3-pentanedione in fermented foods by high-performance liquid chromatography with fluorescence detection," *Journal of Liquid Chromatography & Related Technologies*, vol. 17, no. 1, pp. 203–211, 1994.

[193] R. Marsili, "Monitoring bacterial metabolites in cultured buttermilk by high performance liquid chromatography and headspace gas chromatography," *Journal of Chromatographic Science*, vol. 19, no. 9, pp. 451–456, 1981.

[194] J. M. Mathews, S. L. Watson, R. W. Snyder, J. P. Burgess, and D. L. Morgan, "Reaction of the butter flavorant diacetyl (2,3-butanedione) with n-α-acetylarginine: A model for epitope formation with pulmonary proteins in the etiology of obliterative bronchiolitis," *Journal of Agricultural and Food Chemistry*, vol. 58, no. 24, pp. 12 761–12 768, 2010.

[195] K. Kreiss, A. Gomaa, G. Kullman, K. Fedan, E. J. Simoes, and P. L. Enright, "Clinical bronchiolitis obliterans in workers at a microwave-popcorn plant," *New England Journal of Medicine*, vol. 347, no. 5, pp. 330–338, 2002.

[196] S. Barhdadi *et al.*, "Identification of flavouring substances of genotoxic concern present in e-cigarette refills," *Food and Chemical Toxicology*, vol. 147, p. 111 864, 2021.

[197] M. Hua, E. E. Omaiye, W. Luo, K. J. McWhirter, J. F. Pankow, and P. Talbot, "Identification of cytotoxic flavor chemicals in top-selling electronic cigarette refill fluids," *Scientific Reports*, vol. 9, no. 1, p. 2782, 2019.

[198] R. Sander, W. E. Acree, A. De Visscher, S. E. Schwartz, and T. J. Wallington, "Henry's law constants (IUPAC Recommendations 2021)," *Pure and Applied Chemistry*, vol. 94, no. 1, pp. 71–85, 2022.

[199] E. E. Omaiye, K. J. McWhirter, W. Luo, P. A. Tierney, J. F. Pankow, and P. Talbot, "High concentrations of flavor chemicals are present in electronic cigarette refill fluids," *Scientific Reports*, vol. 9, no. 1, p. 2468, 2019.

[200] J. Schubert, F. D. Müller, R. Schmidt, A. Luch, and T. G. Schulz, "Waterpipe smoke: Source of toxic and carcinogenic VOCs, phenols and heavy metals?" *Archives of Toxicology*, vol. 89, no. 11, pp. 2129–2139, 2015.

[201] J. Schubert, A. Luch, and T. G. Schulz, "Waterpipe smoking: Analysis of the aroma profile of flavored waterpipe tobaccos," *Talanta*, vol. 115, pp. 665–674, 2013.

[202] A. Khlystov and V. Samburova, "Flavoring compounds dominate toxic aldehyde production during e-cigarette vaping," *Environmental Science & Technology*, vol. 50, no. 23, pp. 13 080–13 085, 2016.

[203] E. A. Betterton, "The partitioning of ketones between the gas and aqueous phases," *Atmospheric Environment. Part A. General Topics*, vol. 25, no. 8, pp. 1473–1477, 1991.

[204] C. J. Kampf *et al.*, "Effective Henry's law partitioning and the salting constant of glyoxal in aerosols containing sulfate," *Environmental Science & Technology*, vol. 47, no. 9, pp. 4236–4244, 2013.

[205] A. Tilgner *et al.*, "Acidity and the multiphase chemistry of atmospheric aqueous particles and clouds," *Atmospheric Chemistry and Physics*, vol. 21, no. 17, pp. 13 483–13 536, 2021.

[206] R Zhao, A. Lee, R Soong, A. Simpson, and J. Abbatt, "Formation of aqueous-phase α-hydroxyhydroperoxides (α-HHP): Potential atmospheric impacts," *Atmospheric Chemistry and Physics*, vol. 13, no. 12, pp. 5857–5872, 2013.

[207] A. M. Castillo, L. Patiny, and J. Wist, "Fast and accurate algorithm for the simulation of NMR spectra of large spin systems," *Journal of Magnetic Resonance*, vol. 209, no. 2, pp. 123–130, 2011.

[208] D. Banfi and L. Patiny, "Www. nmrdb. org: Resurrecting and processing NMR spectra on-line," *Chimia*, vol. 62, no. 4, pp. 280–280, 2008.

[209] J. Aires-de Sousa, M. C. Hemmer, and J. Gasteiger, "Prediction of ^{1}H NMR chemical shifts using neural networks," *Analytical Chemistry*, vol. 74, no. 1, pp. 80–90, 2002.

[210] Y. Binev and J. Aires-de Sousa, "Structure-based predictions of ^{1}H NMR chemical shifts using feed-forward neural networks," *Journal of Chemical Information and Computer Sciences*, vol. 44, no. 3, pp. 940–945, 2004.

[211] T. Wallace, "Quantitative analysis of a mixture by NMR spectroscopy," *Journal of Chemical Education*, vol. 61, no. 12, p. 1074, 1984.

[212] S. H. Hilal, S. N. Ayyampalayam, and L. A. Carreira, "Air-liquid partition coefficient for a diverse set of organic compounds: Henry's law constant in water and hexadecane," *Environmental Science & Technology*, vol. 42, no. 24, pp. 9231–9236, 2008.

[213] C. Ji, S. E. Day, S. A. Ortega, and G. W. Beall, "Henry's law constants of some aromatic aldehydes and ketones measured by an internal standard method," *Journal of Chemical & Engineering Data*, vol. 53, no. 5, pp. 1093–1097, 2008.

[214] I. V. Tetko *et al.*, "Virtual computational chemistry laboratory–design and description," *Journal of Computer-aided Molecular Design*, vol. 19, no. 6, pp. 453–463, 2005.

[215] H.-J. Buschmann, H.-H. Füldner, and W. Knoche, "The reversible hydration of carbonyl compounds in aqueous solution. Part I, the keto/gem-diol equilibrium," *Berichte der Bunsengesellschaft für physikalische Chemie*, vol. 84, no. 1, pp. 41–44, 1980.

[216] J.-F. Doussin and A. Monod, "Structure–activity relationship for the estimation of OH-oxidation rate constants of carbonyl compounds in the aqueous phase," *Atmospheric Chemistry and Physics*, vol. 13, no. 23, pp. 11 625–11 641, 2013.

[217] M. Marin, I. Baek, and A. J. Taylor, "Volatile release from aqueous solutions under dynamic headspace dilution conditions," *Journal of Agricultural and Food Chemistry*, vol. 47, no. 11, pp. 4750–4755, 1999.

[218] E. J. Straver and T. W. de Loos, "Determination of Henry's law constants and activity coefficients at infinite dilution of flavor compounds in water at 298 k with a gas-chromatographic method," *Journal of Chemical & Engineering Data*, vol. 50, no. 4, pp. 1171–1176, 2005.

[219] J. R. Snider and G. Dawson, "Tropospheric light alcohols, carbonyls, and acetonitrile: Concentrations in the southwestern United States and Henry's law data," *Journal of Geophysical Research: Atmospheres*, vol. 90, no. D2, pp. 3797–3805, 1985.

[220] R. S. Strekowski and C. George, "Measurement of Henry's law constants for acetone, 2-butanone, 2,3-butanedione, and isobutyraldehyde using a horizontal flow reactor," *Journal of Chemical & Engineering Data*, vol. 50, no. 3, pp. 804–810, 2005.

[221] J. Yu, F. Wania, and J. P. Abbatt, "A new approach to characterizing the partitioning of volatile organic compounds to cotton fabric," *Environmental Science & Technology*, vol. 56, no. 6, pp. 3365–3374, 2022.

[222] L. Li, J. A. Arnot, and F. Wania, "Towards a systematic understanding of the dynamic fate of polychlorinated biphenyls in indoor, urban and rural environments," *Environment international*, vol. 117, pp. 57–68, 2018.

[223] C Gupta, D Prakash, and S Gupta, "A biotechnological approach to microbial based perfumes and flavours," *J. Microbiol. Exp*, vol. 2, 2015.

[224] H. Maarse, *Volatile compounds in foods and beverages*. Routledge, 2017.

Chapter 4

Acetal Formation of Flavoring Agents with Propylene Glycol in E-cigarettes: Impacts on Indoor Partitioning and Thirdhand Exposure

Reprinted with permission from: S. Wu, E. Kim, and R. Zhao, "Acetal formation of flavoring agents with propylene glycol in e-cigarettes: Impacts on indoor partitioning and thirdhand exposure," *Environmental Science & Technology*, vol. 57, no. 50, pp. 21 284–21 294, 2023.

4.1 Chapter Overview

The widespread use of flavored e-cigarettes has led to a significant rise in teenage nicotine use. In e-liquids, the flavor carbonyls can form acetals with unknown chemical and toxicological properties. These acetals can cause adverse health effects on both smokers and non-smokers through thirdhand exposure. This study aims to explore the impacts of these acetals formed in e-cigarettes on indoor partitioning and thirdhand exposure. Specifically, the acetalization reactions of commonly-used flavor carbonyls in laboratory-made e-liquids were monitored using proton nuclear magnetic resonance (^{1}H NMR) spectroscopy. EAS-E Suite and Poly-Parameter Linear Free Energy Relationships (ppLFERs) were employed to estimate the partitioning coefficients for species. Further, a chemical two-dimensional (2D) partitioning model was applied to visualize the indoor equilibrium partitioning and estimate the distribution of flavor carbonyls and their acetals in the gas phase, aerosol phase, and surface reservoirs. Our results demonstrate that a substantial fraction of carbonyls were converted into acetals in e-liquids, and their chemical partitioning was significantly influenced. This study shows that acetalization is a determinant factor in the exposure and toxicology of harmful carbonyl flavorings, with its impact extending to both direct exposure to smokers and involuntary exposure to non-smokers.

4.2 Introduction

E-cigarettes, also referred to as electronic cigarettes or vapes, have gained significant popularity in recent years, especially among teenagers.[226, 227] One of the key factors contributing to their widespread use is the availability of a wide range of flavors.[180, 228] These devices operate by heating an e-liquid or vape juice solution, consisting of nicotine and flavoring agents dissolved in a mixture of propylene glycol (PG) and vegetable glycerin (VG), which produces inhalable aerosols.[229] A recent study revealed that a significant proportion of both adults and youth who use e-cigarettes have a preference for flavored options. Among adults, 64.6% reported using flavored e-cigarettes, while among youth, this percentage was even higher at 79.3%.[181] Additionally, the 2022 National Youth Tobacco Survey conducted in the United States provided insights into the current usage of e-cigarettes among students. The survey reported that 14.1% of high school students, equivalent to 2.14 million individuals, and 3.3% of middle school students, or 380,000 individuals, are currently using e-cigarettes. Notably, the majority of these users opt for flavored e-cigarettes, with fruit flavors being the most commonly chosen, followed by candy, desserts, or other sweet flavors.[230] This trend highlights the strong influence of flavors in attracting and retaining e-cigarette users, especially among the younger population. The appeal of different flavors plays a significant role in making the vaping experience more appealing and enjoyable for individuals.[176]

The widespread popularity of flavored e-cigarettes has raised concerns regarding their potential health risks, as the inhalation of flavorings may cause harm to users.[188, 196] Previous studies have identified over 200 different flavoring chemicals from more than 100 e-liquids, and at least 65 individual flavorings have been reported as toxic to body systems, including the respiratory tract, cardiovascular system, skeleton, and skin.[177, 231] Carbonyls, including ketones and aldehydes, are a common class of flavorings added to e-liquids to produce sweet and fruity flavors.[190] However, it is important to note that carbonyl compounds have been found to be toxic, with some of them carcinogenic, such as formaldehyde and acetaldehyde.[232] Furthermore, certain carbonyl chemicals can act as lung irritants, leading to respiratory problems among users.[233, 234] A notable example is the occurrence of bronchiolitis

obliterans, also known as "popcorn lung disease", among workers exposed to diacetyl and 2,3-pentanedione in a microwave popcorn factory. This disease developed as a result of their high levels of exposure to these chemicals.[195, 196]

A widely neglected fact is that the flavor carbonyls can react with e-liquid solvents (e.g., PG) and form stable acetals with chemical and toxicological properties that differ from either the flavorings or the solvents.[235, 236] Carbonyl PG acetals have been observed in both e-liquids and aerosols, suggesting that they remain stable during storage and persist upon inhalation by e-cigarette users.[191, 199, 237] Furthermore, a study has indicated that more than 30% of commercially available e-liquids contain detectable levels of acetal products.[238] Given the abundance of PG in e-liquids, the acetal form can become a major form (>40%) of certain carbonyl species.[236] However, acetal products are typically not listed as ingredients in e-liquids because they are formed as byproducts after the manufacturing process. In addition, these acetals have a similar but less pronounced odor than the original flavorings, which can make their presence difficult to notice.[239] Recent studies have demonstrated that carbonyl PG acetals can be cytotoxic and irritating, potentially leading to damage in the respiratory and cardiovascular systems.[240, 241] Therefore, further research is necessary to examine the formation of carbonyl acetals in e-liquids and the associated risk of human exposure.

Indoor consumption of flavored e-cigarettes poses a risk of involuntary exposure for non-smokers through various exposure routes, such as inhalation, ingestion, and dermal permeation.[70] Once emitted to the indoor environment, the harmful flavoring agents and acetals formed in e-liquids can cause secondhand and thirdhand exposures, defined as cumulative involuntary exposure to pollutants during or after the vaping events.[83] Specifically, thirdhand exposure is caused by the residual pollutants that remain in indoor environments where vaping has occurred at some earlier point in time, making their exposure risks persistent. Pollutants can remain on surfaces, in dust, or be re-emitted into indoor air. In particular, a recent study discovered rapid and substantial partitioning of indoor volatile organic compounds, which indicates the presence of a large volume of indoor reservoirs.[71] The presence of such reservoirs implies the importance of thirdhand exposure to volatile flavorings.

Chemical partitioning, including that occurring indoors, is primarily governed

by partitioning coefficients, such as the water-air partitioning coefficient (K_{wa}) and octanol-air partitioning coefficient (K_{oa}). K_{wa} and K_{oa} describe the distribution of species between two phases under equilibrium, as can be expressed by eq 4.1 and eq 4.2, respectively. The term c in the equations are equilibrium concentrations of the species in the corresponding phase. Partitioning coefficients can be used to describe phase distribution for species and govern the pathways of exposure to residents.[103, 115, 171] Moreover, the bioaccumulation potential of chemicals is frequently assessed using the K_{wa} and K_{oa} values as well.[242, 243] Studies have shown that the threshold values for determining bioaccumulation potential can vary depending on the type of organism.[244] For air-breathing organisms, chemicals with log K_{ow} values greater than 2 and log K_{oa} values greater than 5 are considered potentially bioaccumulative, indicating a long-lasting chemical risk associated with these compounds.[87] For a more comprehensive evaluation, particularly during vaping events, the partitioning coefficient between PG aerosol and air (K_{pa}, eq 4.3) can also be considered in addition to K_{wa} and K_{oa} values. This is crucial because the precise composition of the phases significantly influences the partitioning coefficients, further affecting the phase distribution.

$$K_{\mathrm{wa}} = c_{\mathrm{w}}/c_{\mathrm{a}} \tag{4.1}$$

$$K_{\mathrm{oa}} = c_{\mathrm{o}}/c_{\mathrm{a}} \tag{4.2}$$

$$K_{\mathrm{pa}} = c_{\mathrm{p}}/c_{\mathrm{a}} \tag{4.3}$$

Flavor acetal formation in e-liquids has received limited research attention, despite the significant impact it can have on the environmental implications of flavoring agents in e-cigarettes. The primary objective of this study is to advance our understanding of the poorly understood thirdhand exposure associated with e-cigarettes. For this, we aim to establish that acetalization between carbonyl flavorings and PG in e-liquids can be a determining factor. This study is the first to investigate how acetalization affects the partitioning and bioaccumulation of flavorings. The specific goals include the experimental determination of acetal formation in laboratory-made e-liquids and

the evaluation of partitioning coefficients for flavor carbonyls and their PG acetals. Acetalization of a few subclasses has been examined, including aldehyde, ketone, and α-diketone to investigate differences in their reactivities. Furthermore, the effect of acetal formation on indoor phase distribution and exposure routes to flavorings in e-cigarettes have been discussed. The findings of this study provide valuable insights into the potential health hazards of flavoring agents and their adducts formed in e-liquids, particularly with regard to indoor air quality, involuntary exposure, and environmental public health.

4.3 Methods

4.3.1 Materials

All the chemicals were purchased from Sigma-Aldrich (CA) without further purification: propylene glycol (PG), butane-2,3-dione (diacetyl) (97%), pentane-2,3-dione (2,3-pentanedione) (97%), 3-hydroxybutan-2-one(acetoin) (≥98%), 4-methylbenzaldehyde (*p*-tolualdehyde) (97%), 6-methylhept-5-en-2-one (6-methyl-5-hepten-2-one) (99%) and 3,7-dimethyl-2,6-octadienal (citral; geranial and neral mixture) (95%). This study investigated commonly-used flavor carbonyls, including acetoin, diacetyl, and 2,3-pentanedione, known for their ability to impart buttery and sweet notes, as well as p-tolualdehyde, 6-methyl-5-hepten-2-one, and citral, which contribute to fruity and citrus flavors.[177, 197, 199, 237] Our selection was influenced by their prevalence in e-liquids, with acetoin, diacetyl, and 2,3-pentendione, in particular, demonstrating notably higher frequencies of occurrence, as supported by the analysis of over 200 refill fluids and aerosol from over 50 popular flavored e-cigarettes.[197, 245] The structures of the target flavor carbonyls are provided in Supplementary Information (SI) Section C.1.1. The two deuterium solvents and internal standard for ^{1}H NMR samples were chloroform-d ($CDCl_3$) (99.9 atom % D), deuterium oxide (D_2O) (99.9 atom % D) and dimethyl sulfoxide (DMSO) (≥ 99.5%), respectively.

4.3.2 Proton Nuclear Magnetic Resonance (^{1}H NMR) Spectroscopy

Liquid-phase chemical reactions between flavoring agents and PG were monitored using ^{1}H NMR. This technique, which has been utilized in previous studies, enables the direct detection of individual flavor carbonyls and their PG acetals.[235, 236] Triplicate solutions of each target flavor carbonyl were prepared at a concentration of 20 mg/mL in PG to simulate commercial e-liquids.[190] The solutions were continuously stirred at room temperature in sealed clear glass vials, opened only for chemical analysis at specific time intervals (see results). Reactions were monitored for up to 28 days to observe acetal formation. Prior to measurement, aliquots of the samples were diluted in a deuterated solvent, with the carbonyl concentration at 10 mM. DMSO (1 mM) was added as an internal standard for chemical shift calibration and quantification. Specifically, for acetoin and α-diketones (diacetyl and 2,3-pentanedione), samples were diluted in D_2O to differentiate PG acetal products and prevent peak overlap. For other flavor carbonyls, measurements were performed with $CDCl_3$ due to the low acetal solubility in D_2O. $CDCl_3$ is also an aprotic solvent that does not react with carbonyls. All the samples were measured within one hour of dilution. Blank experiments were conducted to monitor PG without flavorings to ensure no peaks emerged over time. The fraction of PG acetal formation (F_{acetal}) can be calculated using the following equation based on the quantified concentrations:

$$F_{\text{acetal}}(\%) = \frac{[\text{acetal}]}{[\text{total}]} = \frac{[\text{acetal}]}{[\text{acetal}] + [\text{carbonyl}]} \tag{4.4}$$

where [total], [acetal] and [carbonyl] represent the concentrations (in units of mM) of the total compounds in the sample, PG acetal and flavor carbonyl, respectively. It should be noted that flavor carbonyl concentration consists of the hydration form and non-hydration form for α-diketones when the ^{1}H NMR solvent is D_2O, where the hydration process happens (see Section C.1.3).[171] According to previous literature, the results indicate that acetals remain stable in physiological aqueous solutions over time, with half-lives exceeding 36 hours.[236] Thus, we assumed that acetals did not decompose in D_2O as long as the ^{1}H NMR measurement was taken within an hour of dilution. Another necessary assumption made here is that acetal, hydrated carbonyl,

and non-hydrated carbonyl comprise the majority of the total concentration, while the amount of other byproducts (if any) is negligible.

4.3.3 Prediction for PG-Air Partitioning Coefficient (K_{pa})

To better understand the distribution of flavoring agents between air and e-cigarette smoke, it is necessary to consider the e-liquid aerosol phase, as it determines the release of carbonyls and their acetals into the indoor environment. The PG-air partitioning coefficient (K_{pa}) values were estimated using EAS-E Suite and Poly-Parameter Linear Free Energy Relationships (ppLFERs).[95, 246] In particular, the Quantitative Structure Property Relationships (QSPRs) developed by Iterative Fragment Selection (IFS) method were applied to predict Abraham Linear Solvation Energy Relationship (LSER) solute descriptors for the target flavor carbonyls and the system parameters for PG, along with their respective standard errors from EAS-E Suite.[247, 248] The log K_{pa} values can be determined using the outputs from EAS-E Suite through the following ppLFERs equation:[249]

$$\log K_{\mathrm{pa}} = \mathrm{c} + \mathrm{sS} + \mathrm{aA} + \mathrm{bB} + \mathrm{vV} + \mathrm{lL} \tag{4.5}$$

where the capital letters refer to the solute descriptors, including S (dipolarity/polarizability parameter), A (hydrogen-bond acidity), B (hydrogen-bond basicity), V (McGowan molar volume in units of 0.01 cm^3/mol), and L (logarithmic hexadecane-air partitioning coefficient at 25 °C). The small letters refer to the system parameters derived from a multiple linear regression with known partitioning coefficients of reference compounds. Each term in eq 4.5 describes the particulate energetic contribution from one type of intermolecular interaction. For example, c is the pp-LFER fitting constant, sS donates the energetic contribution from interactions related to the polarity of the molecule, aA and bB represent the energetic contribution of H-bonding interactions, vV, and lL express the energetic contribution for cavity formation and dispersion interactions. The predicted solute descriptors and system parameters are listed in Section C.1.2 (see Table C.1 and Table C.2). The calculated log K_{pa} values with propagated errors for flavor carbonyls and their PG acetals are summarized in Table C.3.

Assuming the equilibrium between the PG aerosol phase and gas phase has been established, the fraction of a chemical residing in the PG aerosol phase (F_{p}) can be estimated in a given volume of air (eq 4.6):

$$F_{\mathrm{p}} = R_{\mathrm{pa}}/(1 + R_{\mathrm{pa}}) \tag{4.6}$$

where R_{pa} is the dimensionless ratio of the equilibrium amount of a compound in the PG aerosol and gas phases, respectively, and is calculated by eq 4.7:[250]

$$R_{\mathrm{pa}} = 10^{-6} \times K_{\mathrm{pa}} \times C_{\mathrm{p}}/D_{\mathrm{p}} \tag{4.7}$$

where 10^{-6} is a conversion factor, C_{p} represents the concentration of PG aerosol vaporized in units of g m^{-3}, D_{p} is the density of PG (1.04 g cm^{-3}) and K_{pa} refers to the PG-air partitioning coefficient.

4.3.4 Indoor Phase Distribution Calculation - During and After Vaping Events

Our study first focuses on simulating chemical partitioning during a vaping event by considering four equilibrium indoor phases: e-liquid aerosol, indoor air, and both polar (e.g., water-rich) and weakly polar (e.g., organic-rich) reservoirs. We assume the e-liquid aerosol consists of pure PG, with continuous vaping emission and particle evaporation leading to a stable concentration of liquid PG aerosol. To further analyze the chemical partitioning post-vaping event, especially after the indoor dissipation of e-liquid aerosol, we employed a two-dimensional (2D) chemical partitioning model. This approach, previously utilized for studying the fate of various chemicals in atmospheric and indoor environments, assumes compounds reach equilibrium among gas phase, polar, and weakly polar reservoirs.[98, 100] Consistent with earlier studies, water and 1-octanol serve as thermodynamic surrogates for polar and weakly-polar reservoirs, respectively. The equilibrium fractions of a chemical in each phase are determined using the volume of each phase and their respective partitioning coefficients. A thorough explanation of these calculations is provided in Section C.1.4, and further model details are available in previous literature.[71, 115] It's important to note that our calculations and model simplify the complexity of chemical partitioning and

phase composition by omitting chemical reactions and removal processes. Despite these omissions, our work offers insightful estimations on the influence of PG acetals on the partitioning of flavor carbonyls during and after vaping events.

4.4 Results and discussion

4.4.1 Determination of the Flavor Carbonyl PG Acetal Formation using ^{1}H NMR

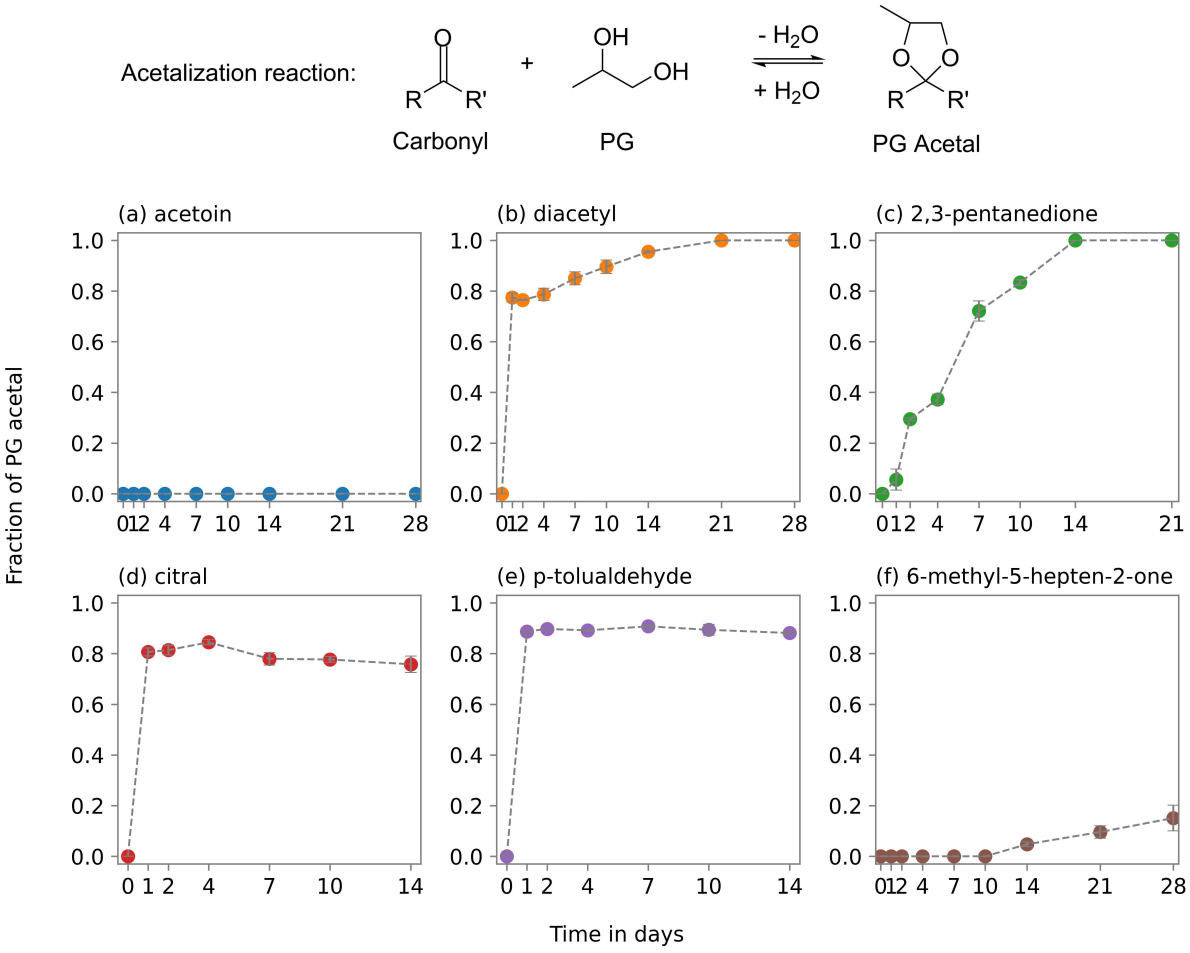

Figure 4.1: Top: General reaction scheme illustrating the acetalization process between carbonyl compounds and PG. Bottom: Fraction of flavor carbonyl converted to PG acetal over time. (a) Acetoin; (b) diacetyl; (c) 2,3-pentanedione; (d) citral; (e) *p*-tolualdehyde; (f) 6-methyl-5-hepten-2-one. Error bars represent the standard deviation observed in triplicated experiments. For citral PG acetals, the cis and trans isomers were combined and presented in this figure.

To evaluate the conversion of flavor carbonyls to PG acetals, the liquid-phase chemical reactions were monitored using ^{1}H NMR, the examples of spectra are provided in Section C.1.3. Generally, flavor carbonyls undergo acetalization in PG, leading to the formation of acetals (see Figure 1). α-Diketones, due to their two carbonyl groups, exhibit a variety of PG acetal products, which will be further explored. Figure 4.1 shows the time-dependent fractions of PG acetals with error bars indicating standard deviations from triplicate measurements. More details can be found in Table C.4 and Table C.5. For most of the target flavorings, the reactions between flavorings and PG occurred rapidly after mixing, with the product fractions increasing over time until reaching equilibrium. The consistency of the testing chemical with literature data is important to verify the accuracy of analysis; the conversion of citral to its PG acetal reached equilibrium within the first day at 81%, which is in good agreement with the previously reported value of 88%.[236] The reaction of *p*-tolualdehyde also reached stability within the first day at 89%, and these fractions remained constant over two weeks. The dominance of acetalization for these aldehydes may arise from the fact that the thermodynamic preference for the formation of five-membered ring structures in the acetals.

The reaction rates and equilibration times varied among different flavor carbonyls. In particular, the ketone species, including acetoin and 6-methyl-5-hepten-2-one, exhibited lower acetalization compared to other compounds. Acetoin did not undergo any conversion over four weeks, as confirmed by the absence of an NMR peak for PG acetal (refer to Figure C.3). The reaction effectiveness depends on the electrophilicity of the carbon atom in the carbonyl group (C=O). Ketones are generally known to be less reactive toward nucleophilic addition reactions. The lower reactivity of acetoin can be attributed to the electron-donating effects of its alkyl and hydroxyl groups, which reduce the electrophilicity of the carbon atom in the carbonyl group. This unique molecular characteristic was observed in a previous study, where acetoin did not form a geminal diol in the aqueous phase.[171] The formation of the PG acetal of 6-methyl-5-hepten-2-one was slow, with only a 15% fraction observed after four weeks, and the acetal signal was still increasing. In addition to the reasons mentioned earlier for acetoin, the bulky structure of the 6-methyl-5-hepten-2-one molecule may contribute to steric hindrance, further slowing down the reaction.

The α-diketones, diacetyl and 2,3-pentanedione, showed essentially complete conversion to PG acetals. This is attributed to the electron-withdrawing nature of the adjacent carbonyl group (C=O), which decreases the electron density of the carbon atom and benefits the nucleophilic attack. Diacetyl rapidly formed 77% of the PG acetal on day one, reaching 100% after three weeks and remaining stable. 2,3-Pentanedione exhibited a similar trend, with steady conversion to 100% after two weeks. It is important to note that the conversion of a reaction under equilibrium cannot theoretically reach 100%. However, in this study, the conversion was considered complete based on the absence of the original carbonyl peak. Overall, the stability of the carbonyl PG acetals after reaching equilibrium demonstrates their potential as stable flavoring agents in e-liquids. In terms of reactivity with PG, α-diketones (2,3-butanedione and 2,3-pentanedione) showed the highest reactivity, followed by aldehydes (citral and *p*-tolualdehyde), and then ketones (acetoin and 6-methyl-5-hepten-2-one).

4.4.2 A Detailed Investigation into α-Diketone PG Acetal Formation

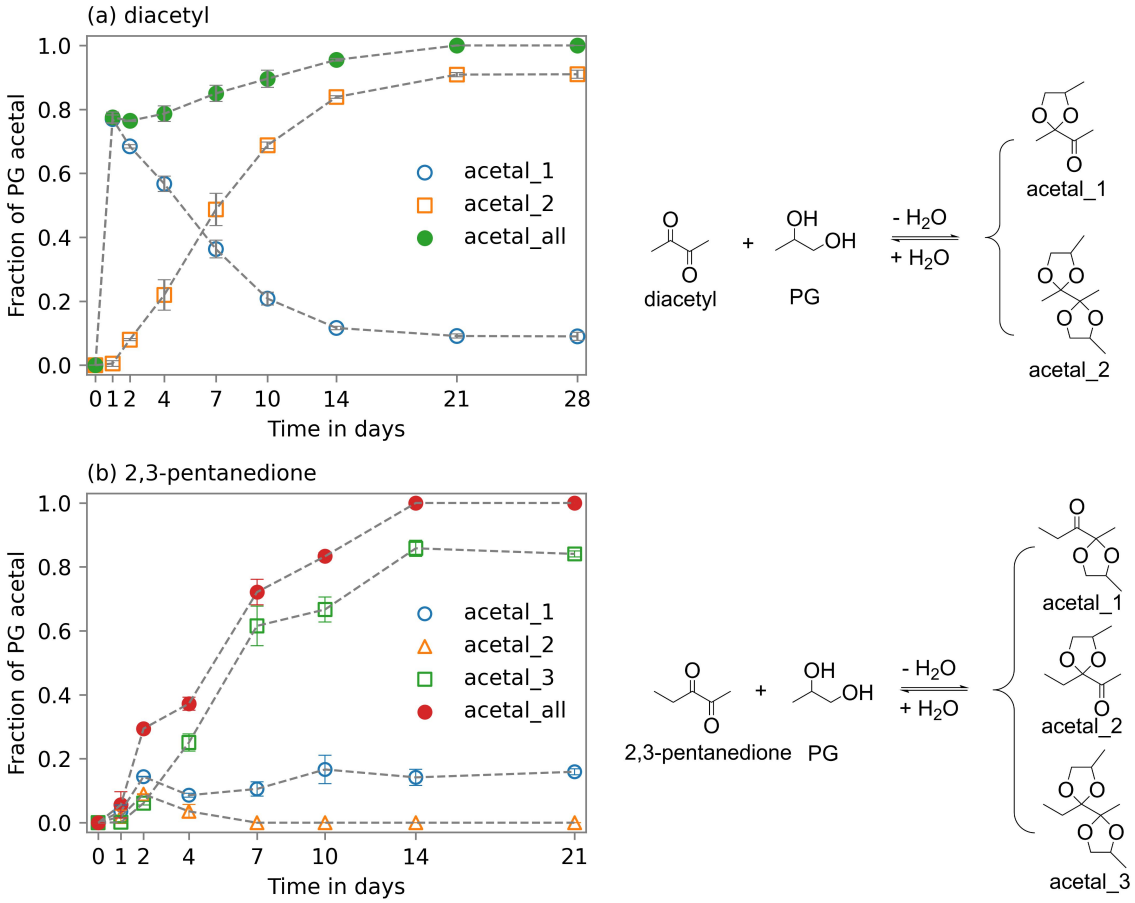

Figure 4.2: The fraction of PG acetal in a mixture of PG with 20 mg/g individual carbonyl as a function of time and the formation reactions for (a) diacetyl and (b) 2,3-pentanedione. The error bars indicate the standard deviations from triplicates.

Figure 4.2 shows the fractions of different α-diketone PG acetals as a function of time. Generally, the flavor compounds with one carbonyl group (C=O) can undergo acetalization reaction with PG and yield an acetal with two ether groups (R-O-R'), such as citral, *p*-tolualdehyde, and 6-methyl-5-hepten-2-one (Figure C.3). Being small α-diketone compounds, diacetyl and 2,3-pentanedione both have two carbonyl groups, leading to multiple equilibria in the PG due to single-acetalization and double-acetalization. In the case of diacetyl, it forms a single-acetalization product (acetal_1) and a double-acetalization product (acetal_2) due to its symmetrical chemical structure. On the other hand, 2,3-pentanedione forms two single-acetalization products

(acetal_1 and acetal_2) and one double-acetalization product (acetal_3). The formation reactions for these acetals are illustrated in Figure 4.2 as well. The reaction between diacetyl and PG was rapid, resulting in a single-acetalization product reaching 77% on the first day. Over time, the fraction of the single-acetalization product decreased to 9% after three weeks when the reaction reached equilibrium. In contrast, the double-acetalization product increased from 1% on the first day to 91% at equilibrium. For 2,3-pentanedione, a similar trend was observed. Initially, the reaction produced single-acetalization products, which gradually converted to double-acetalization products. The double-acetalization product became the predominant product after the fourth day. A summary of the fractions of different PG acetals for α-diketones can be found in Table C.5. These findings suggest that by the time e-liquids are consumed by smokers, the equilibria for α-diketones and other carbonyl flavorings are likely fully established. It should be noted that the experiments were conducted with continuous stirring, which may result in higher observed formation rates compared to real storage conditions of e-liquids. The acetalization reactions in commercial e-liquids can be influenced by various factors, including the complex mixture of ingredients, such as nicotine.[235]

As mentioned previously, the fraction calculation only included known compounds such as acetals and carbonyls (eq 4.4). However, as shown in Section C.1.3, there were always unknown and unassigned peaks observed on ^{1}H NMR spectra. An additional experiment was conducted to determine the nature of unknown peaks observed in the ^{1}H NMR spectra. This experiment involved using laboratory-made e-liquids with a ten times higher concentration of flavorings. The results showed that the unknown peaks were not proportional to the monitored products, indicating that they were not derived from the original carbonyls and were likely contaminants.

4.4.3 Partitioning of Carbonyl Flavorings in PG Aerosol from Vaping E-cigarette

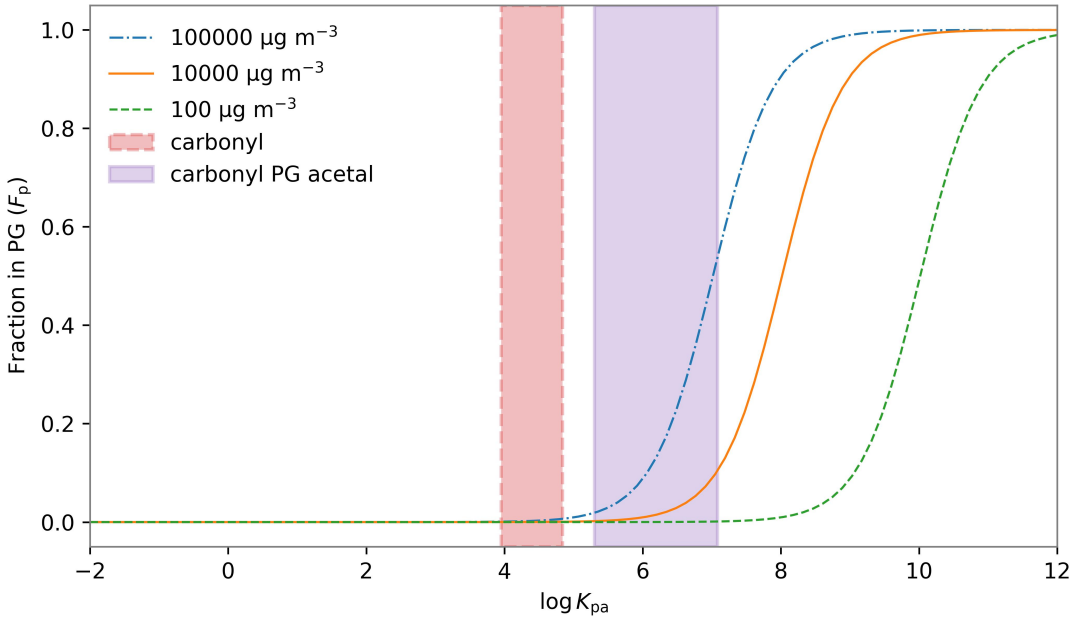

Figure 4.3: PG-air equilibria of carbonyls and their acetals. The calculated fraction in PG aerosol (F_p) under three selected concentrations for PG aerosol as a function of log K_{pa}. The shaded regions with solid and dashed lines display the range of log K_{pa} values for the carbonyls and their PG acetals. For diacetyl and 2,3-pentanedione, only the double-acetalization products were considered.

As the first step, we investigated the partitioning behavior of carbonyl flavorings and their acetalization products between air and PG aerosol at steady-state concentrations, recognizing that air and PG aerosol can exhibit distinct dynamics within the indoor environment. The purpose was to understand how these chemicals behave in a mixture of air and PG, which determines their subsequent chemical partitioning and exposure pathways indoors. Figure 4.3 shows the relationship between the fraction in PG aerosol (F_p) and the log K_{pa} under three different concentrations of PG aerosol, represented by different line types. Three values were chosen as the representatives for PG aerosol concentrations under various conditions. The 100 μg m^{-3} was selected as a typical value in an indoor space with a volume of about 40 m^3, while 10,000 μg m^{-3} represents an indoor environment with a relatively high PG aerosol concentra-

tion, e.g., e-cigarette vaping convention.[251–253] The concentration of 100,000 μg m^{-3} was selected as a typical PG concentration for mainstream vapor inhaled by users and the resulting lung concentrations.[254]

The shaded regions with solid and dashed lines in Figure 3 represent the range of log K_{pa} values for the carbonyls (3.95 to 4.84) and their PG acetals (5.30 to 7.08), as listed in Table C.3. The F_p for the carbonyls is essentially negligible under all three concentrations of PG aerosol, even at 100,000 μg m^{-3}. On the other hand, the F_p values for the PG acetals depend heavily on the concentration of PG aerosol, with higher F_p values reached under higher aerosol concentrations. Compounds with larger log K_{pa} values tend to partition more in the PG aerosol phase according to eq 4.6. In mainstream e-cigarette smoke, certain acetals may be evenly distributed between the air and PG aerosol. However, for PG aerosol concentrations relevant to the indoor environment, even at a concentration of 10,000 μg m^{-3}, only up to 10% of a carbonyl PG acetal with log K_{pa} value of 7 resides in the aerosol phase. These findings suggest that although PG acetals exhibit a greater tendency to be retained in the aerosol phase, the majority will likely evaporate in the gas phase indoors. While the dry deposition of PG aerosol on surfaces can significantly contribute to the accumulation of e-cigarette emissions, [255] our findings suggest that both carbonyls and their acetalization products are likely to partition into the indoor air upon their release during vaping. This is followed by a gas-to-surface partitioning process. In effect, these compounds may further transition into various indoor reservoirs, from which they can be re-emitted into the air, leading to sustained chemical exposure in humans.[70, 71]

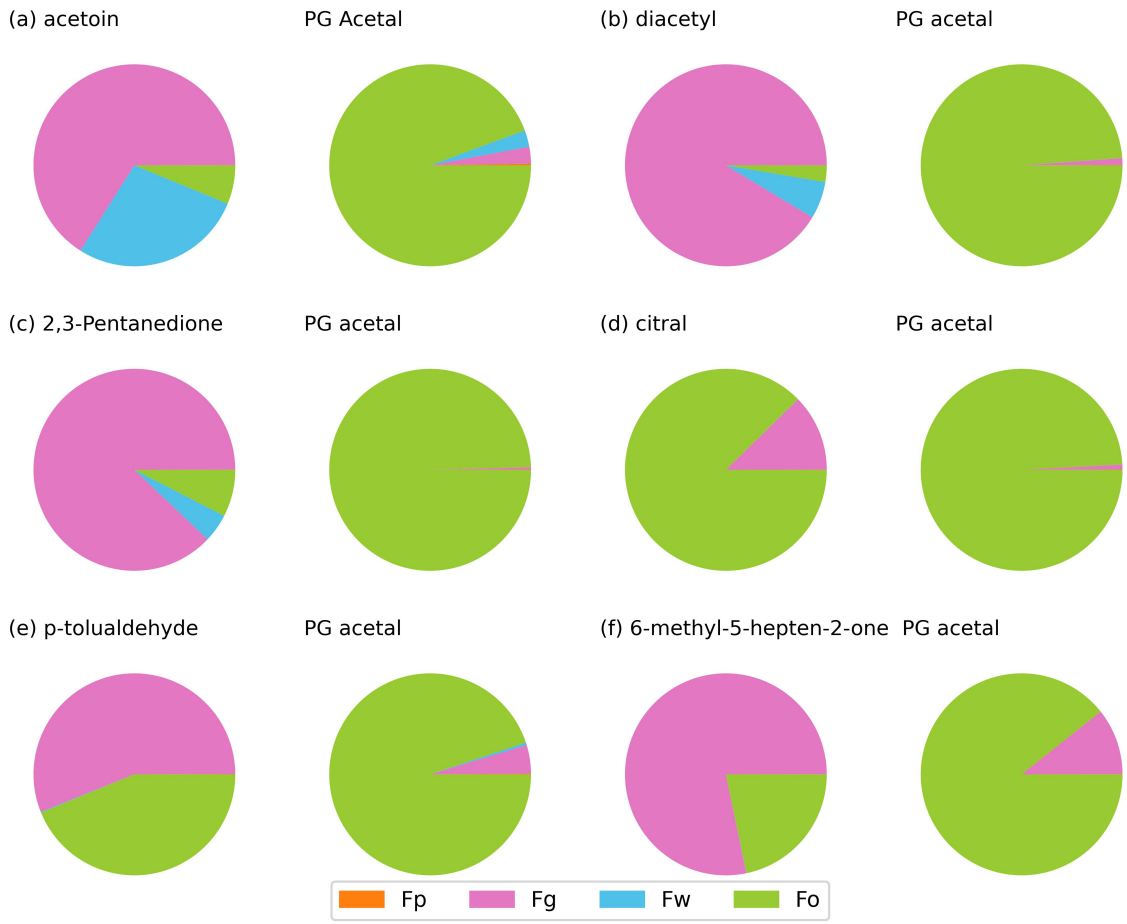

Figure 4.4: The equilibrium fractions for the target flavor carbonyls and their PG acetals in an indoor system consisting of e-liquid aerosol, indoor air, polar reservoir, and weakly-polar reservoir (F_p, F_g, F_w, and F_o): (a) acetoin; (b) diacetyl; (c) 2,3-pentanedione; (d) citral; (e) *p*-tolualdehyde; (f) 6-methyl-5-hepten-2-one. For diacetyl and 2,3-pentanedione, only the double-acetalization PG acetals were considered.

To provide a more detailed analysis of the impact of PG aerosol on the indoor partitioning for flavor carbonyls, Figure 4.4 presents the equilibrium fractions for the flavor carbonyls and their PG acetals in an indoor system consisting of e-liquid aerosol, indoor air, polar reservoir and weakly-polar reservoir (F_p, F_g, F_w, and F_o), assuming a concentration of 10,000 μg m^{-3} for the e-liquid aerosol. This value was considered representative of the upper-band scenario for the indoor PG aerosol concentration. The F_p values for all the target flavorings and their PG acetals suggest that the impact of e-liquid aerosol on indoor phase distribution is minimal when compared to other phases. Specifically, for target flavor carbonyls in this scenario, less than 0.04% are distributed in PG aerosol, while for PG acetals, less than 0.25% (see Table C.6

for more details). In addition, the flavor PG acetals formed in e-liquids have larger F_{o} values than the original flavorings, indicating that they readily partition into the organic phase indoors, while the majority of carbonyls have large fractions in the gas phase. Studies in real indoor rooms have shown that after using e-cigarettes, the average concentration of PG aerosol is around 200 μg m^{-3}, resulting in almost 0% partitioning of flavor carbonyls and their PG acetals into PG aerosol.[252, 253] The results from this section show that the fractions of carbonyl flavorings and their PG acetals in PG aerosol are likely negligible in any indoor environments, assuming that partitioning equilibria have been reached. On the other hand, their fractions in the other three phases are variable. Based on this observation, it is reasonable to consider the indoor partitioning of flavorings as a three-phase system, both during and after vaping events. This system can be visualized and evaluated by considering gas, polar, and weakly-polar reservoirs, without taking into account the PG aerosol phase. This approach allows for a simplified representation of the distribution and behavior of flavor carbonyls and their PG acetals within indoor environments. It's important to note that, in the case of compounds with higher aerosol fractions (e.g., compounds with larger K_{pa}) or environments with elevated aerosol concentrations, maintaining a four-phase system is crucial for ensuring more accurate predictions and comprehensive results.

4.4.4 Chemical 2D-Partitioning Space Plots and Implications to Indoor Air

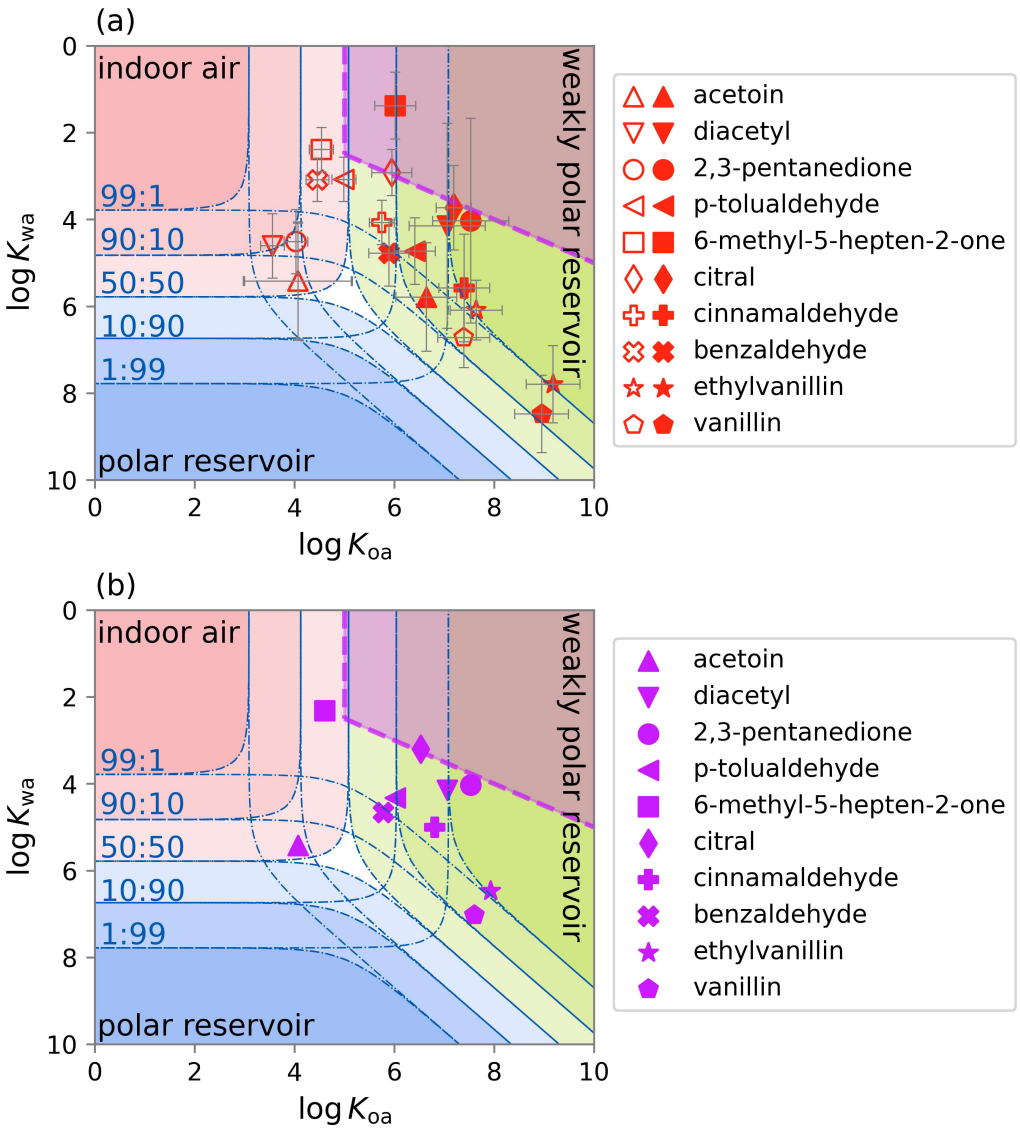

Figure 4.5: Indoor phase distribution for the flavor carbonyls and their PG acetals in an indoor environment with polar and weakly-polar surface reservoirs equivalent to thicknesses of 500 and 2500 nm under 25 °C. (a) The hollow markers are for the carbonyl forms while the solid markers are for the PG acetal forms. The error bars represent the prediction uncertainties. (b) The markers present the overall indoor partitioning by combining the carbonyl and acetal fractions. For diacetyl and 2,3-pentanedione, only the double-acetalization products were considered. The dashed line indicates bioaccumulation thresholds, i.e., log $K_{oa} > 5$ and log $K_{ow} > 2$.

Figure 4.5 presents the chemical 2D partitioning plots showing the distribution of flavor carbonyls and their PG acetals among different phases. Beyond our target compounds, the plots also encompass other frequently utilized flavor carbonyls such as cinnamaldehyde, benzaldehyde, ethylvanillin, and vanillin. These compounds have reported PG acetal conversion rates of 92%, 95%, 50%, and 40%, respectively.[236] Each phase within the plots is denoted by a distinct color, with darker shades signifying higher fractions of compounds in that phase. The compounds are depicted as markers on the plot, placed according to their K_{wa} and K_{oa} values (refer to Table C.3 and Table C.7). The isolines within the plots indicate the phase split ratios, showing the distribution of compounds between phases. It's important to note that the thickness of indoor surface reservoirs, which play a crucial role in the partitioning processes, remains poorly defined since it has been rarely measured.[72] The thickness values used in this study (500 and 2500 nm for polar and weakly-polar reservoirs) provided the best fit to actual experimental measurements in an indoor environment, and as such, were used in our previous studies as the benchmark values for a typical indoor environment.[71] In actual indoor settings, the polar and weakly-polar reservoirs are commonly referred to as water-rich and organic-rich phases, respectively. For instance, indoor water-rich reservoirs may include the water surface in a sink and water absorbed in fabrics, whereas the organic-rich reservoirs may consist of the organic film on kitchen stoves, the surface of couches, and the paint layer on walls.[12, 15, 162, 164, 221] The previously reported bioaccumulative threshold region ($\log K_{\mathrm{oa}} > 5$ and $\log K_{\mathrm{ow}} > 2$) is also highlighted in Figure 4.5, as the partitioning coefficients play a crucial role in assessing the bioaccumulation potential of chemicals in air-breathing organisms.[87, 256]

Figure 4.5(a) visualizes the phase distribution for the flavor carbonyls and their PG acetals in an indoor environment with polar and weakly-polar surface reservoirs at 25 °C. As can be seen from the simulation, the majority of the target flavor carbonyls reside in the air at 25 °C. Interestingly, some of them are located right between the gas phase and the weakly-polar reservoir, which may result in the perturbation of phase distribution since indoor partitioning is highly sensitive to temperature and the size of reservoirs.[115, 171] In contrast, most of the carbonyl PG acetals are distributed in the weakly-polar reservoirs at 25 °C. The indoor phase distribution of chemical species

is closely connected to the pathways of human exposure. Specifically, occupants are exposed to chemicals in the air through inhalation, while chemicals residing in indoor reservoirs can lead to exposure through dermal permeation and non-dietary ingestion. Previous studies have emphasized the important role that surfaces play in thirdhand exposure, enabling various pathways of thirdhand exposure.[70, 257] This raises particular concern regarding the involuntary exposure of infants and children, who are vulnerable to non-dietary ingestion routes due to their frequent contact with indoor surfaces and hand-to-mouth activities.[83, 103] Regarding bioaccumulation, most flavor carbonyls are situated outside the bioaccumulative threshold region, indicating a reduced likelihood for bioaccumulation and enhanced ease of elimination from the body.[87] Contrarily, the acetal forms of various compounds exhibit log K_{oa} values exceeding 5, coupled with relatively lower K_{wa} values. This places them nearer to the bioaccumulative threshold region, suggesting a higher potential for bioaccumulation and consequent adverse health effects. A case in point is the compound 6-methyl-5-hepten-2-one, which has transitioned into this region, signifying that its acetal form demonstrates entirely divergent behavior concerning exposure and bioaccumulation. For certain other carbonyls, the bioaccumulative characteristics of their PG acetals remain unaffected by acetalization, further complicating and adding unpredictability to the toxicological properties of flavorings. After entering the human body, carbonyl acetals can undergo complex processes, including potential hydrolysis. Notably, Erythropel et al. reported a 36-hour half-life for carbonyl acetals in physiological aqueous solutions,[236] indicating that they do not instantaneously decompose and have the opportunity to partition into non-aqueous environments (e.g., lipids) during this time.

Given that the flavor carbonyls reach acetalization equilibria at variable degrees, Figure 4.5(b) illustrates the combined effect of flavor carbonyls and their PG acetals on the indoor phase distribution, specifically highlighting the impact of acetal formation on the partitioning of flavor carbonyls. By considering both the carbonyl and acetal fractions, the overall indoor partitioning of flavor compounds is evaluated. It is observed that flavor carbonyl with a greater conversion to PG acetal shifts towards the right on the horizontal axis in Figure 4.5(b). This shift indicates that the flavoring compounds have a higher propensity to partition into the weakly-polar reservoir overall, suggesting that the primary exposure route may not be inhalation. This ef-

fect is particularly significant for α-diketones, which are mostly converted to acetals. Similarly, the combined impact of the carbonyl form and the acetal form on bioaccumulation leads to their positioning closer to the bioaccumulative threshold region. Specifically, citral was found to be relocated within the bioaccumulative threshold region due to its high conversion to the PG acetal form.

Our results provide a valuable conceptual framework to view the impact of carbonyl acetal formation on indoor partitioning. However, there are important factors in real-life settings that need to be considered. Firstly, the equilibria observed in e-liquids may not fully represent the behavior of flavorings and their acetals in the complex indoor environment, where additional chemical reactions and interactions can occur. For instance, PG acetals have the potential to undergo hydrolysis in polar phases and decomposition in weakly-polar reservoirs.[258] Further investigation is necessary to examine the carryover rates of acetals to vapor and their stability in both the gas phase and indoor reservoirs. This is crucial for achieving a comprehensive understanding of their impact on partitioning behavior. Additionally, indoor temperature can significantly influence the partitioning coefficients, as demonstrated in our previous studies where higher indoor temperatures promoted partitioning into the gas phase and vice versa.[115, 171] Furthermore, while we relied on predicted partitioning coefficients due to limited experimental data, the consistency of these predictions with available experimental data for K_{wa} supports their reliability.[171] Moreover, it is necessary to explore the potential formation of acetals from flavor carbonyls reacting with glycerin (VG), another common component in e-liquids, to assess its impact on indoor air quality and human exposure.[229, 236, 259]

4.4.5 Environmental Implications

This study investigates the chemical properties and environmental impact of flavoring carbonyls in e-cigarettes, specifically focusing on their acetalization products in e-liquids. The intention is to illuminate the potential implications associated with indoor partitioning, thirdhand exposure, and bioaccumulation. The research brings attention to the frequently disregarded occurrence of acetal formation between flavor carbonyls and propylene glycol (PG) during the stages of shipping and storage. By employing a chemical 2D partitioning model, the study not only visualizes indoor

distributions but also assesses the exposure pathways influenced by acetal formation. The findings emphasize the potential for thirdhand exposure, with chemicals from indoor reservoirs re-entering the air and creating risks of involuntary exposure. Additionally, it is discovered that newly formed acetals exhibit unpredictable toxicological properties, and certain ones demonstrate a higher potential for bioaccumulation, prompting specific concerns for individuals working in e-cigarette production facilities. Overall, this research offers vital insights into the effects of flavor additives in e-cigarettes on indoor air quality and public health.

4.5 Acknowledgements

This research was supported by the Natural Sciences and Engineering Research Council of Canada (Award Number: RGPIN-2018-03814) and the University of Alberta. The authors thank Ryan McKay, Mark Miskolzie, Nupur Dabral and Nuclear Magnetic Resonance Facility for the help with ^{1}H NMR, Dr. Chen Wang (SUSTech) for assistance in 2D partitioning model, and Dr. Frank Wania for the helpful discussions. S.W. thanks the Chemistry Alumni International Graduate Scholarship for funding. E.K. thanks the NSERC USRA and the Lloyd and Margaret Cooley Memorial Studentship in Analytical Chemistry for funding. The TOC art was created using BioRender.com with a license obtained.

4.6 Supporting Information Available in Appendix C

The Supporting Information includes the structures of the flavor carbonyls, predicted partitioning coefficients, carbonyl acetal formation, indoor partitioning in PG aerosol, and calculation of the overall K_{wa} and K_{oa} values.

References

[12] L. B. Algrim, D. Pagonis, J. A. de Gouw, J. L. Jimenez, and P. J. Ziemann, "Measurements and modeling of absorptive partitioning of volatile organic compounds to painted surfaces," *Indoor Air*, vol. 30, no. 4, pp. 745–756, 2020.

[15] C. J. Weschler, "Roles of the human occupant in indoor chemistry," *Indoor Air*, vol. 26, no. 1, pp. 6–24, 2016.

[70] K. Yeh, L. Li, F. Wania, and J. P. Abbatt, "Thirdhand smoke from tobacco, e-cigarettes, cannabis, methamphetamine and cocaine: Partitioning, reactive fate, and human exposure in indoor environments," *Environment International*, vol. 160, p. 107 063, 2022.

[71] C. Wang *et al.*, "Surface reservoirs dominate dynamic gas-surface partitioning of many indoor air constituents," *Science Advances*, vol. 6, no. 8, eaay8973, 2020.

[72] J. P. Abbatt, G. C. Morrison, V. H. Grassian, M. Shiraiwa, C. J. Weschler, and P. J. Ziemann, "How should we define an indoor surface?" *Indoor air*, vol. 32, no. 1, e12955, 2022.

[83] G. E. Matt *et al.*, "Thirdhand tobacco smoke: Emerging evidence and arguments for a multidisciplinary research agenda," *Environmental Health Perspectives*, vol. 119, no. 9, pp. 1218–1226, 2011.

[87] F. A. Gobas, B. C. Kelly, and J. A. Arnot, "Quantitative structure activity relationships for predicting the bioaccumulation of pops in terrestrial foodwebs," *QSAR & Combinatorial Science*, vol. 22, no. 3, pp. 329–336, 2003.

[95] S. Endo and K.-U. Goss, "Applications of polyparameter linear free energy relationships in environmental chemistry," *Environmental Science & Technology*, vol. 48, no. 21, pp. 12 477–12 491, 2014.

[98] F Wania, Y. Lei, C Wang, J. Abbatt, and K.-U. Goss, "Using the chemical equilibrium partitioning space to explore factors influencing the phase distribution of compounds involved in secondary organic aerosol formation," *Atmospheric Chemistry and Physics*, vol. 15, no. 6, pp. 3395–3412, 2015.

[100] J. P. Abbatt and C. Wang, "The atmospheric chemistry of indoor environments," *Environmental Science: Processes & Impacts*, vol. 22, no. 1, pp. 25–48, 2020.

[103] L. Li, J. A. Arnot, and F. Wania, "How are humans exposed to organic chemicals released to indoor air?" *Environmental Science & Technology*, vol. 53, no. 19, pp. 11 276–11 284, 2019.

[115] S. Wu *et al.*, "Henry's law constants and indoor partitioning of microbial volatile organic compounds," *Environmental Science & Technology*, vol. 56, no. 11, pp. 7143–7152, 2022.

[162] R. E. O'Brien *et al.*, "Emerging investigator series: Chemical and physical properties of organic mixtures on indoor surfaces during HOMEChem," *Environmental Science: Processes & Impacts*, vol. 23, no. 4, pp. 559–568, 2021.

[164] W. W. Nazaroff and C. J. Weschler, "Indoor acids and bases," *Indoor Air*, vol. 30, no. 4, pp. 559–644, 2020.

[171] S. Wu, E. Kim, D. Vethanayagam, and R. Zhao, "Indoor partitioning and potential thirdhand exposure to carbonyl flavoring agents added in e-cigarettes and hookah tobacco," *Environmental Science: Processes & Impacts*, vol. 24, no. 12, pp. 2294–2309, 2022.

[176] G. Kong, M. E. Morean, D. A. Cavallo, D. R. Camenga, and S. Krishnan-Sarin, "Reasons for electronic cigarette experimentation and discontinuation among adolescents and young adults," *Nicotine & Tobacco Research*, vol. 17, no. 7, pp. 847–854, 2015.

[177] E. J. Krüsemann, A. Havermans, J. L. Pennings, K. De Graaf, S. Boesveldt, and R. Talhout, "Comprehensive overview of common e-liquid ingredients and how they can be used to predict an e-liquid's flavour category," *Tobacco Control*, vol. 30, no. 2, pp. 185–191, 2021.

[180] N. I. Goldenson, A. M. Leventhal, K. A. Simpson, and J. L. Barrington-Trimis, "A review of the use and appeal of flavored electronic cigarettes," *Current Addiction Reports*, vol. 6, pp. 98–113, 2019.

[181] L. M. Schneller, M. Bansal-Travers, M. L. Goniewicz, S. McIntosh, D. Ossip, and R. J. O'Connor, "Use of flavored e-cigarettes and the type of e-cigarette devices used among adults and youth in the US—Results from wave 3 of the population assessment of tobacco and health study (2015-2016)," *International Journal of Environmental Research and Public Health*, vol. 16, no. 16, p. 2991, 2019.

[188] G. Kaur, T. Muthumalage, and I. Rahman, "Mechanisms of toxicity and biomarkers of flavoring and flavor enhancing chemicals in emerging tobacco and non-tobacco products," *Toxicology Letters*, vol. 288, pp. 143–155, 2018.

[190] P. A. Tierney, C. D. Karpinski, J. E. Brown, W. Luo, and J. F. Pankow, "Flavour chemicals in electronic cigarette fluids," *Tobacco Control*, vol. 25, no. e1, e10–e15, 2016.

[191] K. E. Farsalinos, K. A. Kistler, G. Gillman, and V. Voudris, "Evaluation of electronic cigarette liquids and aerosol for the presence of selected inhalation toxins," *Nicotine & Tobacco Research*, vol. 17, no. 2, pp. 168–174, 2015.

[195] K. Kreiss, A. Gomaa, G. Kullman, K. Fedan, E. J. Simoes, and P. L. Enright, "Clinical bronchiolitis obliterans in workers at a microwave-popcorn plant," *New England Journal of Medicine*, vol. 347, no. 5, pp. 330–338, 2002.

[196] S. Barhdadi *et al.*, "Identification of flavouring substances of genotoxic concern present in e-cigarette refills," *Food and Chemical Toxicology*, vol. 147, p. 111 864, 2021.

[197] M. Hua, E. E. Omaiye, W. Luo, K. J. McWhirter, J. F. Pankow, and P. Talbot, "Identification of cytotoxic flavor chemicals in top-selling electronic cigarette refill fluids," *Scientific Reports*, vol. 9, no. 1, p. 2782, 2019.

[199] E. E. Omaiye, K. J. McWhirter, W. Luo, P. A. Tierney, J. F. Pankow, and P. Talbot, "High concentrations of flavor chemicals are present in electronic cigarette refill fluids," *Scientific Reports*, vol. 9, no. 1, p. 2468, 2019.

[221] J. Yu, F. Wania, and J. P. Abbatt, "A new approach to characterizing the partitioning of volatile organic compounds to cotton fabric," *Environmental Science & Technology*, vol. 56, no. 6, pp. 3365–3374, 2022.

[225] S. Wu, E. Kim, and R. Zhao, "Acetal formation of flavoring agents with propylene glycol in e-cigarettes: Impacts on indoor partitioning and thirdhand exposure," *Environmental Science & Technology*, vol. 57, no. 50, pp. 21 284–21 294, 2023.

[226] S. Sapru, M. Vardhan, Q. Li, Y. Guo, X. Li, and D. Saxena, "E-cigarettes use in the United States: Reasons for use, perceptions, and effects on health," *BMC Public Health*, vol. 20, no. 1, pp. 1–10, 2020.

[227] F. Measham, K. O'Brien, and G. Turnbull, ""Skittles & Red Bull is my favourite flavour": E-cigarettes, smoking, vaping and the changing landscape of nicotine consumption amongst British teenagers-implications for the normalisation debate," *Drugs: Education, Prevention and Policy*, vol. 23, no. 3, pp. 224–237, 2016.

[228] A. M. Leventhal, R. Miech, J. Barrington-Trimis, L. D. Johnston, P. M. O'Malley, and M. E. Patrick, "Flavors of e-cigarettes used by youths in the United States," *Jama*, vol. 322, no. 21, pp. 2132–2134, 2019.

[229] R. Grana, N. Benowitz, and S. A. Glantz, "E-cigarettes: A scientific review," *Circulation*, vol. 129, no. 19, pp. 1972–1986, 2014.

[230] M. Cooper, "Notes from the field: E-cigarette use among middle and high school students—United States, 2022," *MMWR. Morbidity and Mortality Weekly Report*, vol. 71, 2022.

[231] A. B. Stefaniak, R. F. LeBouf, A. C. Ranpara, and S. S. Leonard, "Toxicology of flavoring- and cannabis-containing e-liquids used in electronic delivery systems," *Pharmacology & Therapeutics*, vol. 224, p. 107 838, 2021.

[232] M. L. Goniewicz *et al.*, "Levels of selected carcinogens and toxicants in vapour from electronic cigarettes," *Tobacco Control*, vol. 23, no. 2, pp. 133–139, 2014.

[233] C. Hutzler, M. Paschke, S. Kruschinski, F. Henkler, J. Hahn, and A. Luch, "Chemical hazards present in liquids and vapors of electronic cigarettes," *Archives of Toxicology*, vol. 88, pp. 1295–1308, 2014.

[234] S. Salam, N. A. Saliba, A. Shihadeh, T. Eissenberg, and A. El-Hellani, "Flavor-toxicant correlation in e-cigarettes: A meta-analysis," *Chemical Research in Toxicology*, vol. 33, no. 12, pp. 2932–2938, 2020.

[235] P. J. Kerber and D. H. Peyton, "Kinetics of aldehyde flavorant-acetal formation in e-liquids with different e-cigarette solvents and common additives studied by ^{1}H NMR spectroscopy," *Chemical Research in Toxicology*, vol. 35, no. 8, pp. 1410–1417, 2022.

[236] H. C. Erythropel *et al.*, "Formation of flavorant–propylene glycol adducts with novel toxicological properties in chemically unstable e-cigarette liquids," *Nicotine & Tobacco Research*, vol. 21, no. 9, pp. 1248–1258, 2019.

[237] R. Z. Behar, W. Luo, K. J. McWhirter, J. F. Pankow, and P. Talbot, "Analytical and toxicological evaluation of flavor chemicals in electronic cigarette refill fluids," *Scientific Reports*, vol. 8, no. 1, p. 8288, 2018.

[238] G. Gschwend, C. Jenkins, A. Jones, C. Kelso, and J. Morgan, "A wide range of flavoring-carrier fluid adducts form in e-cigarette liquids," *Chemical Research in Toxicology*, vol. 36, no. 1, pp. 14–22, 2023.

[239] H. Surburg and J. Panten, *Common fragrance and flavor materials: preparation, properties and uses*. John Wiley & Sons, 2016.

[240] J.-C. Noël, D. Rainer, R. Gstir, M. Rainer, and G. Bonn, "Quantification of selected aroma compounds in e-cigarette products and toxicity evaluation in HUVEC/Tert2 cells," *Biomedical Chromatography*, vol. 34, no. 3, e4761, 2020.

[241] S. V. Jabba, A. N. Diaz, H. C. Erythropel, J. B. Zimmerman, and S.-E. Jordt, "Chemical adducts of reactive flavor aldehydes formed in e-cigarette liquids are cytotoxic and inhibit mitochondrial function in respiratory epithelial cells," *Nicotine and Tobacco Research*, vol. 22, no. Supplement_1, S25–S34, 2020.

[242] D. Mackay, "Correlation of bioconcentration factors," *Environmental Science & Technology*, vol. 16, no. 5, pp. 274–278, 1982.

[243] C. T. Chiou, V. H. Freed, D. W. Schmedding, and R. L. Kohnert, "Partition coefficient and bioaccumulation of selected organic chemicals," *Environmental Science & Technology*, vol. 11, no. 5, pp. 475–478, 1977.

[244] B. C. Kelly, M. G. Ikonomou, J. D. Blair, A. E. Morin, and F. A. Gobas, "Food web specific biomagnification of persistent organic pollutants," *Science*, vol. 317, no. 5835, pp. 236–239, 2007.

[245] J. G. Allen *et al.*, "Flavoring chemicals in e-cigarettes: Diacetyl, 2,3-pentanedione, and acetoin in a sample of 51 products, including fruit-, candy-, and cocktail-flavored e-cigarettes," *Environmental Health Perspectives*, vol. 124, no. 6, pp. 733–739, 2016.

[246] *US EPA. [2012]. Estimation Programs Interface Suite™ for Microsoft® Windows, v 4.11 or insert version used]. United States Environmental Protection Agency, Washington, DC, USA*. http://www.eas-e-suite.com, Last access: 2023-05-29.

[247] T. N. Brown, "QSPRs for predicting equilibrium partitioning in solvent-air systems from the chemical structures of solutes and solvents," *Journal of Solution Chemistry*, vol. 51, no. 9, pp. 1101–1132, 2022.

[248] J. C. McGowan, "The estimation of solubility parameters and related properties of liquids," *Journal of Chemical Technology and Biotechnology. Chemical Technology*, vol. 34, no. 1, pp. 38–42, 1984.

[249] K.-U. Goss, "Predicting the equilibrium partitioning of organic compounds using just one linear solvation energy relationship (LSER)," *Fluid Phase Equilibria*, vol. 233, no. 1, pp. 19–22, 2005.

[250] J. H. Seinfeld and S. N. Pandis, *Atmospheric chemistry and physics: from air pollution to climate change*. John Wiley & Sons, 2016.

[251] R. Chen *et al.*, "Assessment of indoor air quality at an electronic cigarette (Vaping) convention," *Journal of Exposure Science & Environmental Epidemiology*, vol. 28, no. 6, pp. 522–529, 2018.

[252] G. O'Connell, S. Colard, X. Cahours, and J. D. Pritchard, "An assessment of indoor air quality before, during and after unrestricted use of e-cigarettes in a small room," *International Journal of Environmental Research and Public Health*, vol. 12, no. 5, pp. 4889–4907, 2015.

[253] W. Schober *et al.*, "Use of electronic cigarettes (e-cigarettes) impairs indoor air quality and increases feno levels of e-cigarette consumers," *International Journal of Hygiene and Environmental Health*, vol. 217, no. 6, pp. 628–637, 2014.

[254] O. Geiss, I. Bianchi, F. Barahona, and J. Barrero-Moreno, "Characterisation of mainstream and passive vapours emitted by selected electronic cigarettes," *International Journal of Hygiene and Environmental Health*, vol. 218, no. 1, pp. 169–180, 2015.

[255] S. F. Schick *et al.*, "Thirdhand cigarette smoke in an experimental chamber: Evidence of surface deposition of nicotine, nitrosamines and polycyclic aromatic hydrocarbons and de novo formation of NNK," *Tobacco Control*, vol. 23, no. 2, pp. 152–159, 2014.

[256] F. Wania, Y. D. Lei, S. Baskaran, and A. Sangion, "Identifying organic chemicals not subject to bioaccumulation in air-breathing organisms using predicted partitioning and biotransformation properties," *Integrated Environmental Assessment and Management*, vol. 18, no. 5, pp. 1297–1312, 2022.

[257] L. Li, L. Hughes, and J. A. Arnot, "Addressing uncertainty in mouthing-mediated ingestion of chemicals on indoor surfaces, objects, and dust," *Environment International*, vol. 146, p. 106 266, 2021.

[258] B. Liu and S. Thayumanavan, "Substituent effects on the pH sensitivity of acetals and ketals and their correlation with encapsulation stability in polymeric nanogels," *Journal of the American Chemical Society*, vol. 139, no. 6, pp. 2306–2317, 2017.

[259] C. J. Mussinan and M. J. Morello, *Flavor analysis: Developments in isolation and characterization*. ACS Publications, 1998.

Chapter 5

Conclusions and Future Work

Contributions: The conclusion was written by Shuang Wu with review and feedback by Dr. Ran Zhao.

5.1 Thesis Summary

This thesis investigates the chemical partitioning and potential human exposure to indoor organic pollutants, with a particular focus on VOCs emitted from microbial sources and e-cigarette emissions. The primary objectives of this thesis are, firstly, to determine the equilibrium partitioning of VOCs using laboratory methods. Secondly, to predict their phase distributions under various scenarios in indoor environments using advanced modeling techniques. Finally, to assess the pathways of human exposure, including thirdhand exposure to e-cigarette emissions, to better understand their impacts on indoor air quality and human health.

In Chapter 2, the study experimentally determined the H values and their temperature dependence for key indoor MVOCs using the IGS method and the VPR-HS technique, combined with GC-FID. The 2D partitioning space plots were utilized to visualize the indoor phase distributions and preferential exposure pathways based on chemical properties. The findings indicate that MVOCs are likely distributed between the gas phase and weakly polar (e.g., organic-rich) reservoirs indoors. Temperature and the volume of reservoirs significantly affect indoor partitioning. Overall, the results provide a more comprehensive understanding of MVOCs in indoor environments, marking the first study to offer reliable experimental constraints for the H values of MVOCs.

Building on the insights from this study, the next chapter explores a different but related aspect of indoor chemical partitioning. Chapter 3 explored thirdhand exposure to toxic flavoring agents in e-cigarettes and hookah tobacco. Utilizing the IGS method and ^{1}H NMR, this study is the first to report the experimentally measured H_{eff} and K_{hyd} for widely used flavoring carbonyls and their temperature dependence. The observations showed that α-dicarbonyl compounds (e.g., diacetyl and 2,3-pentanedione) undergo significant hydration, resulting in their H_{eff} being enhanced by approximately a factor of three compared to their H. This enhancement was found to be larger at lower temperatures. The 2D partitioning space plots, with the measured H_{eff} as input, concluded that most flavorings reside between the gas phase and weakly polar phases. Changes in temperature, air exchange rates, and reservoir sizes can lead to the re-emission of these compounds from surface reservoirs, resulting in prolonged

thirdhand exposure for residents without their awareness.

To further understand the environmental behavior of e-cigarette emissions, the following chapter delves into the acetalization reactions in e-liquids between flavor carbonyls and the solvent (PG). Chapter 4 examines how acetalization products affect indoor chemical partitioning, thirdhand exposure, and bioaccumulation for flavoring carbonyls. Specifically, aqueous reactions were monitored using ^{1}H NMR, and partitioning coefficients were predicted using ppLFERs model. Employing a chemical 2D partitioning model, the indoor phase distribution of flavor carbonyls and their acetals was presented across the gas phase, aerosol phase, and surface reservoirs. The study discovered that a substantial fraction of carbonyls were converted into acetals in e-liquids. These newly formed acetals exhibit chemical and toxicological properties distinct from those of their carbonyl forms, with a few of acetals demonstrating a higher potential for bioaccumulation. This impact extends to both direct exposure for smokers and involuntary exposure for nonsmokers.

5.2 Proposed Future Studies

Despite the rapidly increasing advancements in indoor air quality, there are still gaps in knowledge of indoor chemical partitioning. Looking ahead, the field presents several challenges and opportunities for further study.

5.2.1 Determination of Partitioning Coefficients between Air and Specific Materials

Indoor environments consist of a variety of materials, yet information on the composition of surfaces and reservoirs is often unavailable. To better understand the indoor partitioning process, it is essential to characterize the properties of materials within indoor environments, where chemicals can partition. While previous studies have investigated the partitioning properties of several materials, such as paint, cotton, and pillow filling, little is known about representative indoor materials like carpet and leather.[12, 260, 261] Additionally, it is important to investigate the amount of

chemicals partitioning into these materials and the timescale of equilibration, which determine the lifetime of chemicals indoors and the related health impacts on human exposure. Research on indoor partitioning typically focuses on the K_{wa} and K_{oa} to simplify complex indoor environments. Consequently, assessments of partitioning coefficients between air and more representative materials indoors are lacking.

A fundamental investigation of the material-air partitioning coefficients of key VOCs in indoor environments should be conducted in the future. A GC-MS method will be developed to experimentally determine these coefficients. This method involves using a filter holder with an individual material serving as the filter. Gas-phase compounds with a constant concentration will pass through the filter driven by zero air at a constant flow rate until the filter is saturated, enabling the calculation of the partitioning coefficient and the rate of uptake. The gas-phase concentration will be monitored over time by the GC-MS. After the filter material is saturated, passing zero air at a constant flow rate through the filter will provide information on the amount of compound absorbed and the rate of release. Specifically, measurements of the cotton-air partitioning coefficient will be conducted to validate the experimental setup by comparing the results with those of previous studies.[221, 262]

This study aims to provide critical insights into the interaction of VOCs with common surface materials in indoor environments. It will generate data on the equilibria and the timescales of interactions between air and indoor materials.

5.2.2 Salinity Determination of Indoor Surface Reservoirs

The presence of inorganic salts in indoor environments is influenced by various sources, such as outdoor air intrusion, indoor activities like cooking and cleaning, and building materials. For example, building ventilation can bring outdoor sea salt and road salt during winter indoors.[263, 264] Sodium chloride (table salt) used in cooking can become aerosolized.[265] Ultrasonic humidifiers convert dissolved solute in the water into particulate matter, which can be deposited on indoor surfaces.[266] Cleaning products containing salts, such as sodium bicarbonate (baking soda) and sodium hypochlorite (bleach), release these salts during use. Building materials and furnishings also contribute, with gypsum boards containing calcium sulfate adding to the

salt content in indoor air.[267]

Previous studies have demonstrated that the salinity of the aqueous phase impacts Henry's law constant of VOCs, showing a salting out effect, where the solubility of a gas decreases with increasing salinity.[155] This effect can be described by the Sechenov equation:[112]

$$log(\frac{H_0^{\mathrm{bp}}}{H^{\mathrm{bp}}}) = K_{\mathrm{s}} \times b(\mathrm{salt}) \tag{5.1}$$

where H_0^{bp} is the H value in pure water, H^{bp} is the H value in the salt solution, K_{s} is the molality-based Sechenov constant, and b(salt) is the molality of the salt.

Despite these findings, there remains a substantial gap in understanding the salinity levels of indoor reservoirs. This gap is critical, as the presence of inorganic salts can significantly influence the indoor partitioning behavior of VOCs, especially in environments with high chemical concentrations. Addressing this gap will help better understand and predict the behavior of VOCs in indoor environments, ultimately contributing to improved indoor air quality and occupant health.

A future study can be conducted to determine the salinity of indoor reservoirs and investigate its impact on the chemical partitioning of indoor VOCs. Briefly, the salinity measurements will be conducted using ion chromatography by collecting samples from diverse indoor surfaces, such as windows, countertops, and floors. The IGS method connected with GC-FID will be employed to measure H values for selected VOCs under various salinity conditions and generate the Sechenov constant. A 2D chemical partitioning model will be used to simulate indoor VOC phase distribution, incorporating measured salinity data and H values. Model predictions will be compared with and without salinity effects to quantify the impact on indoor partitioning.

This study will provide a quantitative understanding of how salinity affects H values for common indoor VOCs. Improved models for predicting indoor VOC partitioning that account for surface salinity effects will offer insights into the potential health and comfort implications of salinity-induced changes in indoor air chemistry. The findings can also be applied to environmentally relevant aqueous phases in outdoor atmospheres, such as seawater, cloud droplets, and aerosols.

5.2.3 Development of a Dynamic Multiphase Partitioning Model

Current predictive partitioning models have proven valuable for visualizing the phase distribution of indoor organic pollutants and assessing human exposure. These models typically rely on a simplified framework that includes a limited number of partitioning volumes, such as air, polar surface reservoirs (e.g., water), and weakly polar reservoirs (e.g., 1-octanol).[71] However, this simplified approach does not fully capture the complexity of chemical interactions within indoor environments. Although recent advancements have integrated more complex factors such as temperature and aerosols, a significant gap remains in understanding the specific interactions between materials and air for indoor VOCs.[115, 225]

Indoor environments consist of a variety of materials, such as wood, concrete, carpets, and clothing, each with distinct chemical properties. The partitioning behavior of VOCs varies across these materials, as the partitioning coefficient between air and different materials differs. However, most predictive models do not account for the wide range of materials and their impact on partitioning behavior. There is a clear need to develop more comprehensive models that better simulate the diverse conditions of real indoor environments.

A future study can be conducted to address the limitations of existing partitioning models by developing a more detailed multiphase model that incorporates a broader range of indoor surfaces and materials. A crucial enhancement to this model will be the inclusion of parameters that describe the timescale of equilibration. Many indoor materials, such as wall and paint, require significant time to reach equilibrium with VOCs, while others, like certain surface coatings, equilibrate more rapidly.[72] Therefore, the model will incorporate dynamic factors to simulate not only the final equilibrium states but also the temporal aspects of partitioning. Specifically, the model will be modified to include experimentally determined partitioning coefficients between air and specific materials to predict the equilibrium phase distribution, as well as rate constants for the partitioning process to enable the simulation of time-dependent behavior. Details of these measurements can be found in section 5.3.1. Additionally, key materials influencing chemical partitioning and VOC exposure will

be identified based on simulation results and sensitivity analysis.

The development of a more comprehensive multiphase model that includes both equilibrium and kinetic parameters will provide a more realistic representation of chemical partitioning in indoor environments. By considering a wider range of materials and their dynamic behavior, this research will enhance our understanding of how different conditions affect chemical behavior and exposure over time. Incorporating the timescale of equilibration will make the model more applicable to real-world scenarios, ultimately leading to better strategies for managing indoor air quality and reducing exposure risks.

References

[12] L. B. Algrim, D. Pagonis, J. A. de Gouw, J. L. Jimenez, and P. J. Ziemann, "Measurements and modeling of absorptive partitioning of volatile organic compounds to painted surfaces," *Indoor Air*, vol. 30, no. 4, pp. 745–756, 2020.

[71] C. Wang *et al.*, "Surface reservoirs dominate dynamic gas-surface partitioning of many indoor air constituents," *Science Advances*, vol. 6, no. 8, eaay8973, 2020.

[72] J. P. Abbatt, G. C. Morrison, V. H. Grassian, M. Shiraiwa, C. J. Weschler, and P. J. Ziemann, "How should we define an indoor surface?" *Indoor air*, vol. 32, no. 1, e12955, 2022.

[112] R. Sander, "Compilation of Henry's law constants (version 4.0) for water as solvent," *Atmospheric Chemistry and Physics*, vol. 15, no. 8, pp. 4399–4981, 2015.

[115] S. Wu *et al.*, "Henry's law constants and indoor partitioning of microbial volatile organic compounds," *Environmental Science & Technology*, vol. 56, no. 11, pp. 7143–7152, 2022.

[155] C. Wang, Y. D. Lei, S. Endo, and F. Wania, "Measuring and modeling the salting-out effect in ammonium sulfate solutions," *Environmental Science & Technology*, vol. 48, no. 22, pp. 13 238–13 245, 2014.

[221] J. Yu, F. Wania, and J. P. Abbatt, "A new approach to characterizing the partitioning of volatile organic compounds to cotton fabric," *Environmental Science & Technology*, vol. 56, no. 6, pp. 3365–3374, 2022.

[225] S. Wu, E. Kim, and R. Zhao, "Acetal formation of flavoring agents with propylene glycol in e-cigarettes: Impacts on indoor partitioning and thirdhand exposure," *Environmental Science & Technology*, vol. 57, no. 50, pp. 21 284–21 294, 2023.

[260] C. M. Eichler *et al.*, "Cloth–air partitioning of neutral per-and polyfluoroalkyl substances (PFAS) in North Carolina homes during the indoor PFAS assessment (IPA) campaign," *Environmental Science & Technology*, vol. 57, no. 40, pp. 15 173–15 183, 2023.

[261] G. E. Matt, E. Hoh, P. J. Quintana, J. M. Zakarian, and J. Arceo, "Cotton pillows: A novel field method for assessment of thirdhand smoke pollution," *Environmental Research*, vol. 168, pp. 206–210, 2019.

[262] X. Zhou, X. Dong, R. Ma, X. Wang, and F. Wang, "Characterizing the partitioning behavior of formaldehyde, benzene and toluene on indoor fabrics: Effects of temperature and humidity," *Journal of Hazardous Materials*, vol. 416, p. 125 827, 2021.

[263] V. Chithra and S. S. Nagendra, "Chemical and morphological characteristics of indoor and outdoor particulate matter in an urban environment," *Atmospheric Environment*, vol. 77, pp. 579–587, 2013.

[264] K. R. Kolesar, C. N. Mattson, P. K. Peterson, N. W. May, R. K. Prendergast, and K. A. Pratt, "Increases in wintertime $PM_{2.5}$ sodium and chloride linked to snowfall and road salt application," *Atmospheric Environment*, vol. 177, pp. 195–202, 2018.

[265] M. A. Torkmahalleh, S. Gorjinezhad, H. S. Unluevcek, and P. K. Hopke, "Review of factors impacting emission/concentration of cooking generated particulate matter," *Science of the Total Environment*, vol. 586, pp. 1046–1056, 2017.

[266] C. J. Lau, M. Loebel Roson, K. M. Klimchuk, T. Gautam, B. Zhao, and R. Zhao, "Particulate matter emitted from ultrasonic humidifiers—chemical composition and implication to indoor air," *Indoor Air*, vol. 31, no. 3, pp. 769–782, 2021.

[267] F Thevenet, O Debono, M Rizk, F Caron, M Verriele, and N Locoge, "VOC uptakes on gypsum boards: Sorption performances and impact on indoor air quality," *Building and Environment*, vol. 137, pp. 138–146, 2018.

Bibliography

[1] N. E. Klepeis *et al.*, "The national human activity pattern survey (NHAPS): A resource for assessing exposure to environmental pollutants," *Journal of Exposure Science & Environmental Epidemiology*, vol. 11, no. 3, pp. 231–252, 2001.

[2] A. Cincinelli and T. Martellini, "Indoor air quality and health," *International Journal of Environmental Research and Public Health*, vol. 14, no. 11, p. 1286, 2017.

[3] C. A. Redlich, J. Sparer, and M. R. Cullen, "Sick-building syndrome," *The Lancet*, vol. 349, no. 9057, pp. 1013–1016, 1997.

[4] T. Wainman, J. Zhang, C. J. Weschler, and P. J. Lioy, "Ozone and limonene in indoor air: A source of submicron particle exposure.," *Environmental Health Perspectives*, vol. 108, no. 12, pp. 1139–1145, 2000.

[5] A. P. Jones, "Indoor air quality and health," *Atmospheric Environment*, vol. 33, no. 28, pp. 4535–4564, 1999.

[6] C. Weschler, "Chemistry in indoor environments: 20 years of research," *Indoor Air*, vol. 21, no. 3, pp. 205–218, 2011.

[7] G. Morrison, *Interfacial chemistry in indoor environments*, 2008.

[8] I. Turiel, C. Hollowell, R. Miksch, J. Rudy, R. Young, and M. Coye, "The effects of reduced ventilation on indoor air quality in an office building," *Atmospheric Environment (1967)*, vol. 17, no. 1, pp. 51–64, 1983.

[9] D. M. Murray and D. E. Burmaster, "Residential air exchange rates in the United States: Empirical and estimated parametric distributions by season and climatic region," *Risk Analysis*, vol. 15, no. 4, pp. 459–465, 1995.

[10] A. K. Persily, "Field measurement of ventilation rates," *Indoor Air*, vol. 26, no. 1, pp. 97–111, 2016.

[11] A. Manuja *et al.*, "Total surface area in indoor environments," *Environmental Science: Processes & Impacts*, vol. 21, no. 8, pp. 1384–1392, 2019.

[12] L. B. Algrim, D. Pagonis, J. A. de Gouw, J. L. Jimenez, and P. J. Ziemann, "Measurements and modeling of absorptive partitioning of volatile organic compounds to painted surfaces," *Indoor Air*, vol. 30, no. 4, pp. 745–756, 2020.

[13] M. Blocquet *et al.*, "Impact of the spectral and spatial properties of natural light on indoor gas-phase chemistry: Experimental and modeling study," *Indoor Air*, vol. 28, no. 3, pp. 426–440, 2018.

[14] C. J. Young, S. Zhou, J. A. Siegel, and T. F. Kahan, "Illuminating the dark side of indoor oxidants," *Environmental Science: Processes & Impacts*, vol. 21, no. 8, pp. 1229–1239, 2019.

[15] C. J. Weschler, "Roles of the human occupant in indoor chemistry," *Indoor Air*, vol. 26, no. 1, pp. 6–24, 2016.

[16] L. S. Pandrangi and G. C. Morrison, "Ozone interactions with human hair: Ozone uptake rates and product formation," *Atmospheric Environment*, vol. 42, no. 20, pp. 5079–5089, 2008.

[17] K. L. Abdullahi, J. M. Delgado-Saborit, and R. M. Harrison, "Emissions and indoor concentrations of particulate matter and its specific chemical components from cooking: A review," *Atmospheric Environment*, vol. 71, pp. 260–294, 2013.

[18] T. Li *et al.*, "Household concentrations and personal exposure of $PM_{2.5}$ among urban residents using different cooking fuels," *Science of the Total Environment*, vol. 548, pp. 6–12, 2016.

[19] E. K. Soule, S. F. Maloney, T. R. Spindle, A. K. Rudy, M. M. Hiler, and C. O. Cobb, "Electronic cigarette use and indoor air quality in a natural setting," *Tobacco Control*, vol. 26, no. 1, pp. 109–112, 2017.

[20] G. Drago *et al.*, "Relationship between domestic smoking and metals and rare earth elements concentration in indoor $PM_{2.5}$," *Environmental Research*, vol. 165, pp. 71–80, 2018.

[21] T.-C. Lin, G. Krishnaswamy, and D. S. Chi, "Incense smoke: Clinical, structural and molecular effects on airway disease," *Clinical and Molecular Allergy*, vol. 6, pp. 1–9, 2008.

[22] W. Ji and B. Zhao, "Contribution of outdoor-originating particles, indoor-emitted particles and indoor secondary organic aerosol (SOA) to residential indoor $PM_{2.5}$ concentration: A model-based estimation," *Building and Environment*, vol. 90, pp. 196–205, 2015.

[23] I. Rivas *et al.*, "Outdoor infiltration and indoor contribution of UFP and BC, OC, secondary inorganic ions and metals in $PM_{2.5}$ in schools," *Atmospheric Environment*, vol. 106, pp. 129–138, 2015.

[24] Y. Liang, D. Sengupta, M. J. Campmier, D. M. Lunderberg, J. S. Apte, and A. H. Goldstein, "Wildfire smoke impacts on indoor air quality assessed using crowdsourced data in California," *Proceedings of the National Academy of Sciences*, vol. 118, no. 36, e2106478118, 2021.

[25] A. Persily and L. de Jonge, "Carbon dioxide generation rates for building occupants," *Indoor Air*, vol. 27, no. 5, pp. 868–879, 2017.

[26] A. Klosterköther, R. Kurtenbach, P. Wiesen, and J. Kleffmann, "Determination of the emission indices for NO, NO_2, HONO, HCHO, CO, and particles emitted from candles," *Indoor Air*, vol. 31, no. 1, pp. 116–127, 2021.

[27] Z. Peng and J. L. Jimenez, "Exhaled CO_2 as a COVID-19 infection risk proxy for different indoor environments and activities," *Environmental Science & Technology Letters*, vol. 8, no. 5, pp. 392–397, 2021.

[28] W. M. Alberts, "Indoor air pollution: NO, NO_2, CO, and CO_2," *Journal of Allergy and Clinical Immunology*, vol. 94, no. 2, pp. 289–295, 1994.

[29] W. W. Nazaroff and C. J. Weschler, "Indoor ozone: Concentrations and influencing factors," *Indoor Air*, vol. 32, no. 1, e12942, 2022.

[30] M. Maroni, B. Seifert, and T. Lindvall, *Indoor air quality: a comprehensive reference book*. Elsevier, 1995.

[31] S. K. Brown, M. R. Sim, M. J. Abramson, and C. N. Gray, "Concentrations of volatile organic compounds in indoor air-A review," *Indoor Air*, vol. 4, no. 2, pp. 123–134, 1994.

[32] J. L. Adgate *et al.*, "Outdoor, indoor, and personal exposure to VOCs in children," *Environmental Health Perspectives*, vol. 112, no. 14, pp. 1386–1392, 2004.

[33] C.-C. Lin and R. Corsi, "Texanol® ester alcohol emissions from latex paints: Temporal variations and multi-component recoveries," *Atmospheric Environment*, vol. 41, no. 15, pp. 3225–3234, 2007.

[34] T. Salthammer, S. Mentese, and R. Marutzky, "Formaldehyde in the indoor environment," *Chemical Reviews*, vol. 110, no. 4, pp. 2536–2572, 2010.

[35] C. Yu and D. Crump, "A review of the emission of VOCs from polymeric materials used in buildings," *Building and Environment*, vol. 33, no. 6, pp. 357–374, 1998.

[36] J.-Y. Chin *et al.*, "Levels and sources of volatile organic compounds in homes of children with asthma," *Indoor Air*, vol. 24, no. 4, pp. 403–415, 2014.

[37] M. Odabasi, "Halogenated volatile organic compounds from the use of chlorine-bleach-containing household products," *Environmental Science & Technology*, vol. 42, no. 5, pp. 1445–1451, 2008.

[38] D. A. Olson and R. L. Corsi, "In-home formation and emissions of trihalomethanes: The role of residential dishwashers," *Journal of Exposure Science & Environmental Epidemiology*, vol. 14, no. 2, pp. 109–119, 2004.

[39] J. Wong, N Carslaw, R Zhao, S Zhou, and J. Abbatt, "Observations and impacts of bleach washing on indoor chlorine chemistry," *Indoor Air*, vol. 27, no. 6, pp. 1082–1090, 2017.

[40] W. W. Nazaroff and C. J. Weschler, "Cleaning products and air fresheners: Exposure to primary and secondary air pollutants," *Atmospheric Environment*, vol. 38, no. 18, pp. 2841–2865, 2004.

[41] C. Arata *et al.*, "Volatile organic compound emissions during HOMEChem," *Indoor Air*, vol. 31, no. 6, pp. 2099–2117, 2021.

[42] R. J. Shaughnessy, T. McDaniels, and C. J. Weschler, "Indoor chemistry: Ozone and volatile organic compounds found in tobacco smoke," *Environmental Science & Technology*, vol. 35, no. 13, pp. 2758–2764, 2001.

[43] G. Pandit, P. Srivastava, and A. M. Rao, "Monitoring of indoor volatile organic compounds and polycyclic aromatic hydrocarbons arising from kerosene cooking fuel," *Science of the Total Environment*, vol. 279, no. 1-3, pp. 159–165, 2001.

[44] Q. Liu and J. P. Abbatt, "Liquid crystal display screens as a source for indoor volatile organic compounds," *Proceedings of the National Academy of Sciences*, vol. 118, no. 23, e2105067118, 2021.

[45] B. G. Ooi, D. Dutta, K. Kazipeta, and N. S. Chong, "Influence of the e-cigarette emission profile by the ratio of glycerol to propylene glycol in e-liquid composition," *ACS Omega*, vol. 4, no. 8, pp. 13 338–13 348, 2019.

[46] Y. Huang, S. S. H. Ho, K. F. Ho, S. C. Lee, J. Z. Yu, and P. K. Louie, "Characteristics and health impacts of VOCs and carbonyls associated with residential cooking activities in Hong Kong," *Journal of Hazardous Materials*, vol. 186, no. 1, pp. 344–351, 2011.

[47] R. Hyšpler, Š. Crhová, J. Gasparič, Z. Zadák, M. Čížková, and V. Balasová, "Determination of isoprene in human expired breath using solid-phase microextraction and gas chromatography–mass spectrometry," *Journal of Chromatography B: Biomedical Sciences and Applications*, vol. 739, no. 1, pp. 183–190, 2000.

[48] S Liu *et al.*, "Contribution of human-related sources to indoor volatile organic compounds in a university classroom," *Indoor Air*, vol. 26, no. 6, pp. 925–938, 2016.

[49] P. K. Misztal *et al.*, "Emission factors of microbial volatile organic compounds from environmental bacteria and fungi," *Environmental Science & Technology*, vol. 52, no. 15, pp. 8272–8282, 2018.

[50] A. Korpi, J. Järnberg, and A.-L. Pasanen, "Microbial volatile organic compounds," *Critical Reviews in Toxicology*, vol. 39, no. 2, pp. 139–193, 2009.

[51] A. Y. Davis, Q. Zhang, J. P. Wong, R. J. Weber, and M. S. Black, "Characterization of volatile organic compound emissions from consumer level material extrusion 3D printers," *Building and Environment*, vol. 160, p. 106 209, 2019.

[52] H. Schwartz-Narbonne, B. Du, and J. A. Siegel, "Volatile organic compound and particulate matter emissions from an ultrasonic essential oil diffuser," *Indoor Air*, vol. 31, no. 6, pp. 1982–1992, 2021.

[53] D. A. Missia, E. Demetriou, N Michael, E. Tolis, and J. G. Bartzis, "Indoor exposure from building materials: A field study," *Atmospheric Environment*, vol. 44, no. 35, pp. 4388–4395, 2010.

[54] C. H. Halios, V. D. Assimakopoulos, C. G. Helmis, and H. A. Flocas, "Investigating cigarette-smoke indoor pollution in a controlled environment," *Science of the Total Environment*, vol. 337, no. 1-3, pp. 183–190, 2005.

[55] F. Klein, U. Baltensperger, A. S. Prévôt, and I. El Haddad, "Quantification of the impact of cooking processes on indoor concentrations of volatile organic species and primary and secondary organic aerosols," *Indoor Air*, vol. 29, no. 6, pp. 926–942, 2019.

[56] L. Wallace *et al.*, "The Los Angeles TEAM Study: Personal exposures, indoor-outdoor air concentrations, and breath concentrations of 25 volatile organic compounds.," *Journal of Exposure Analysis and Environmental Epidemiology*, vol. 1, no. 2, pp. 157–192, 1991.

[57] R. Wiglusz, E. Sitko, G. Nikel, I. Jarnuszkiewicz, and B. Igielska, "The effect of temperature on the emission of formaldehyde and volatile organic compounds (VOCs) from laminate flooring—case study," *Building and Environment*, vol. 37, no. 1, pp. 41–44, 2002.

[58] C. J. Weschler, "Ozone's impact on public health: Contributions from indoor exposures to ozone and products of ozone-initiated chemistry," *Environmental Health Perspectives*, vol. 114, no. 10, pp. 1489–1496, 2006.

[59] C.-Y. Lu, J.-M. Lin, Y.-Y. Chen, and Y.-C. Chen, "Building-related symptoms among office employees associated with indoor carbon dioxide and total volatile organic compounds," *International Journal of Environmental Research and Public Health*, vol. 12, no. 6, pp. 5833–5845, 2015.

[60] A. J. Li, V. K. Pal, and K. Kannan, "A review of environmental occurrence, toxicity, biotransformation and biomonitoring of volatile organic compounds," *Environmental Chemistry and Ecotoxicology*, vol. 3, pp. 91–116, 2021.

[61] L Mølhave *et al.*, "Total volatile organic compounds (TVOC) in indoor air quality investigations," *Indoor Air*, vol. 7, no. 4, pp. 225–240, 1997.

[62] T. Vera, F Villanueva, L Wimmerová, and E. Tolis, "An overview of methodologies for the determination of volatile organic compounds in indoor air," *Applied Spectroscopy Reviews*, vol. 57, no. 8, pp. 625–674, 2022.

[63] C. P. Weisel, S. Alimokhtari, and P. F. Sanders, "Indoor air VOC concentrations in suburban and rural New Jersey," *Environmental Science & Technology*, vol. 42, no. 22, pp. 8231–8238, 2008.

[64] B. Son, P. Breysse, and W. Yang, "Volatile organic compounds concentrations in residential indoor and outdoor and its personal exposure in Korea," *Environment International*, vol. 29, no. 1, pp. 79–85, 2003.

[65] D. K. Farmer *et al.*, "Overview of HOMEChem: House observations of microbial and environmental chemistry," *Environmental Science: Processes & Impacts*, vol. 21, no. 8, pp. 1280–1300, 2019.

[66] Y. Liu *et al.*, "Characterizing sources and emissions of volatile organic compounds in a northern California residence using space-and time-resolved measurements," *Indoor Air*, vol. 29, no. 4, pp. 630–644, 2019.

[67] C. Veenaas, M. Ripszam, and P. Haglund, "Analysis of volatile organic compounds in indoor environments using thermal desorption with comprehensive two-dimensional gas chromatography and high-resolution time-of-flight mass spectrometry," *Journal of Separation Science*, vol. 43, no. 8, pp. 1489–1498, 2020.

[68] J. P. Sá, M. C. M. Alvim-Ferraz, F. G. Martins, and S. I. Sousa, "Application of the low-cost sensing technology for indoor air quality monitoring: A review," *Environmental Technology & Innovation*, vol. 28, p. 102 551, 2022.

[69] S. Yang, X. Yang, and D. Licina, "Emissions of volatile organic compounds from interior materials of vehicles," *Building and Environment*, vol. 170, p. 106 599, 2020.

[70] K. Yeh, L. Li, F. Wania, and J. P. Abbatt, "Thirdhand smoke from tobacco, e-cigarettes, cannabis, methamphetamine and cocaine: Partitioning, reactive fate, and human exposure in indoor environments," *Environment International*, vol. 160, p. 107 063, 2022.

[71] C. Wang *et al.*, "Surface reservoirs dominate dynamic gas-surface partitioning of many indoor air constituents," *Science Advances*, vol. 6, no. 8, eaay8973, 2020.

[72] J. P. Abbatt, G. C. Morrison, V. H. Grassian, M. Shiraiwa, C. J. Weschler, and P. J. Ziemann, "How should we define an indoor surface?" *Indoor air*, vol. 32, no. 1, e12955, 2022.

[73] A Saini, J. Okeme, J Mark Parnis, R. McQueen, and M. Diamond, "From air to clothing: Characterizing the accumulation of semi-volatile organic compounds to fabrics in indoor environments," *Indoor Air*, vol. 27, no. 3, pp. 631–641, 2017.

[74] D. Won, R. L. Corsi, and M. Rynes, "New indoor carpet as an adsorptive reservoir for volatile organic compounds," *Environmental Science & Technology*, vol. 34, no. 19, pp. 4193–4198, 2000.

[75] Q.-T. Liu, R. Chen, B. E. McCarry, M. L. Diamond, and B. Bahavar, "Characterization of polar organic compounds in the organic film on indoor and outdoor glass windows," *Environmental Science & Technology*, vol. 37, no. 11, pp. 2340–2349, 2003.

[76] C. J. Weschler and W. W. Nazaroff, "Growth of organic films on indoor surfaces," *Indoor Air*, vol. 27, no. 6, pp. 1101–1112, 2017.

[77] C. Y. Lim and J. P. Abbatt, "Chemical composition, spatial homogeneity, and growth of indoor surface films," *Environmental Science & Technology*, vol. 54, no. 22, pp. 14 372–14 379, 2020.

[78] Y. Fang *et al.*, "A molecular picture of surface interactions of organic compounds on prevalent indoor surfaces: Limonene adsorption on SiO_2," *Chemical Science*, vol. 10, no. 10, pp. 2906–2914, 2019.

[79] C. Liu, B. Kolarik, L. Gunnarsen, and Y. Zhang, "C-depth method to determine diffusion coefficient and partition coefficient of PCB in building materials," *Environmental Science & Technology*, vol. 49, no. 20, pp. 12 112–12 119, 2015.

[80] G. Löfroth, C. Stensman, and M. Brandhorst-Satzkorn, "Indoor sources of mutagenic aerosol particulate matter: Smoking, cooking and incense burning," *Mutation Research/Genetic Toxicology*, vol. 261, no. 1, pp. 21–28, 1991.

[81] A. Matsunaga and P. J. Ziemann, "Gas-wall partitioning of organic compounds in a Teflon film chamber and potential effects on reaction product and aerosol yield measurements," *Aerosol Science and Technology*, vol. 44, no. 10, pp. 881–892, 2010.

[82] P. F. DeCarlo, A. M. Avery, and M. S. Waring, "Thirdhand smoke uptake to aerosol particles in the indoor environment," *Science Advances*, vol. 4, no. 5, eaap8368, 2018.

[83] G. E. Matt *et al.*, "Thirdhand tobacco smoke: Emerging evidence and arguments for a multidisciplinary research agenda," *Environmental Health Perspectives*, vol. 119, no. 9, pp. 1218–1226, 2011.

[84] G. Meng, Z. Nie, Y. Feng, X. Wu, Y. Yin, and Y. Wang, "Typical halogenated persistent organic pollutants in indoor dust and the associations with childhood asthma in Shanghai, China," *Environmental Pollution*, vol. 211, pp. 389–398, 2016.

[85] S. Baskaran and F. Wania, "Applications of the octanol-air partitioning ratio: A critical review," *Environmental Science: Atmospheres*, vol. 3, no. 7, pp. 1045–1065, 2023.

[86] C. J. Weschler and W. W. Nazaroff, "Semivolatile organic compounds in indoor environments," *Atmospheric Environment*, vol. 42, no. 40, pp. 9018–9040, 2008.

[87] F. A. Gobas, B. C. Kelly, and J. A. Arnot, "Quantitative structure activity relationships for predicting the bioaccumulation of pops in terrestrial foodwebs," *QSAR & Combinatorial Science*, vol. 22, no. 3, pp. 329–336, 2003.

[88] C. B. Castells, P. W. Carr, D. I. Eikens, D. Bush, and C. A. Eckert, "Comparative study of semitheoretical models for predicting infinite dilution activity coefficients of alkanes in organic solvents," *Industrial & Engineering Chemistry Research*, vol. 38, no. 10, pp. 4104–4109, 1999.

[89] T. Harner and D. Mackay, "Measurement of octanol-air partition coefficients for chlorobenzenes, PCBs, and DDT," *Environmental Science & Technology*, vol. 29, no. 6, pp. 1599–1606, 1995.

[90] J.-C. Lerol, J.-C. Masson, H. Renon, J.-F. Fabries, and H. Sannier, "Accurate measurement of activity coefficient at infinite dilution by inert gas stripping and gas chromatography," *Industrial & Engineering Chemistry Process Design and Development*, vol. 16, no. 1, pp. 139–144, 1977.

[91] X. Zhang *et al.*, "A method to estimate the octanol-air partition coefficient of semivolatile organic compounds," *Analytical Chemistry*, vol. 71, no. 17, pp. 3834–3838, 1999.

[92] S. Baskaran, Y. D. Lei, and F. Wania, "A database of experimentally derived and estimated octanol–air partition ratios (K_{oa})," *Journal of Physical and Chemical Reference Data*, vol. 50, no. 4, 2021.

[93] M. Zhu, H. Su, Y. Bao, J. Li, and G. Su, "Experimental determination of octanol-water partition coefficient (K_{ow}) of 39 liquid crystal monomers (LCMs) by use of the shake-flask method," *Chemosphere*, vol. 287, p. 132 407, 2022.

[94] B. McDuffie, "Estimation of octanol/water partition coefficients for organic pollutants using reverse-phase HPLC," *Chemosphere*, vol. 10, no. 1, pp. 73–83, 1981.

[95] S. Endo and K.-U. Goss, "Applications of polyparameter linear free energy relationships in environmental chemistry," *Environmental Science & Technology*, vol. 48, no. 21, pp. 12 477–12 491, 2014.

[96] T. N. Brown, "Empirical regressions between system parameters and solute descriptors of polyparameter linear free energy relationships (PPLFERs) for predicting solvent-air partitioning," *Fluid Phase Equilibria*, vol. 540, p. 113 035, 2021.

[97] T. N. Brown, A. Sangion, and J. A. Arnot, "Identifying uncertainty in physical–chemical property estimation with IFSQSAR," *Journal of Cheminformatics*, vol. 16, no. 1, p. 65, 2024.

[98] F Wania, Y. Lei, C Wang, J. Abbatt, and K.-U. Goss, "Using the chemical equilibrium partitioning space to explore factors influencing the phase distribution of compounds involved in secondary organic aerosol formation," *Atmospheric Chemistry and Physics*, vol. 15, no. 6, pp. 3395–3412, 2015.

[99] C. Wang *et al.*, "Uncertain Henry's law constants compromise equilibrium partitioning calculations of atmospheric oxidation products," *Atmospheric Chemistry and Physics*, vol. 17, no. 12, pp. 7529–7540, 2017.

[100] J. P. Abbatt and C. Wang, "The atmospheric chemistry of indoor environments," *Environmental Science: Processes & Impacts*, vol. 22, no. 1, pp. 25–48, 2020.

[101] X. Zhang, J. A. Arnot, and F. Wania, "Model for screening-level assessment of near-field human exposure to neutral organic chemicals released indoors," *Environmental Science & Technology*, vol. 48, no. 20, pp. 12 312–12 319, 2014.

[102] A. Askari, F. Wania, and A. W. Chan, "Modeling the fate and involuntary exposure to tetrahydrocannabinol emitted from indoor cannabis smoking," *Environmental Science: Atmospheres*, vol. 3, no. 4, pp. 760–772, 2023.

[103] L. Li, J. A. Arnot, and F. Wania, "How are humans exposed to organic chemicals released to indoor air?" *Environmental Science & Technology*, vol. 53, no. 19, pp. 11 276–11 284, 2019.

[104] W. Henry, "Experiments on the quantity of gases absorbed by water, at different temperatures, and under different pressures," in *Abstracts of the Papers Printed in the Philosophical Transactions of the Royal Society of London*, The Royal Society London, 1832, pp. 103–104.

[105] E. Atlas, R. Foster, and C. Giam, "Air-sea exchange of high-molecular weight organic pollutants: Laboratory studies," *Environmental Science & Technology*, vol. 16, no. 5, pp. 283–286, 1982.

[106] R. Sander, "Modeling atmospheric chemistry: Interactions between gas-phase species and liquid cloud/aerosol particles," *Surveys in Geophysics*, vol. 20, pp. 1–31, 1999.

[107] R. Weiss, "Carbon dioxide in water and seawater: The solubility of a non-ideal gas," *Marine chemistry*, vol. 2, no. 3, pp. 203–215, 1974.

[108] L. Ettre, C Welter, and B Kolb, "Determination of gas-liquid partition coefficients by automatic equilibrium headspace-gas chromatography utilizing the phase ratio variation method," *Chromatographia*, vol. 35, pp. 73–84, 1993.

[109] A. C. Soria, S. Rodríguez-Sánchez, J. Sanz, and I. Martínez-Castro, "Gas chromatographic analysis of food bioactive oligosaccharides," *Food Oligosaccharides: Production, Analysis and Bioactivity*, pp. 370–398, 2014.

[110] K. Badjagbo, S. Sauvé, and S. Moore, "Real-time continuous monitoring methods for airborne VOCs," *TrAC Trends in Analytical Chemistry*, vol. 26, no. 9, pp. 931–940, 2007.

[111] W. Winiwarter *et al.*, "Henry's law and the behavior of weak acids and bases in fog and cloud," *Journal of Atmospheric Chemistry*, vol. 19, pp. 173–188, 1994.

[112] R. Sander, "Compilation of Henry's law constants (version 4.0) for water as solvent," *Atmospheric Chemistry and Physics*, vol. 15, no. 8, pp. 4399–4981, 2015.

[113] M. Rivlin, U. Eliav, and G. Navon, "NMR studies of the equilibria and reaction rates in aqueous solutions of formaldehyde," *The Journal of Physical Chemistry B*, vol. 119, no. 12, pp. 4479–4487, 2015.

[114] K. Zia, T. Siddiqui, S. Ali, I. Farooq, M. S. Zafar, and Z. Khurshid, "Nuclear magnetic resonance spectroscopy for medical and dental applications: A comprehensive review," *European journal of dentistry*, vol. 13, no. 01, pp. 124–128, 2019.

[115] S. Wu *et al.*, "Henry's law constants and indoor partitioning of microbial volatile organic compounds," *Environmental Science & Technology*, vol. 56, no. 11, pp. 7143–7152, 2022.

[116] M. C. Lemfack, J. Nickel, M. Dunkel, R. Preissner, and B. Piechulla, "MVOC: A database of microbial volatiles," *Nucleic Acids Research*, vol. 42, no. D1, pp. D744–D748, 2014.

[117] J. Bäck *et al.*, "Variable emissions of microbial volatile organic compounds (MVOCs) from root-associated fungi isolated from Scots pine," *Atmospheric Environment*, vol. 44, no. 30, pp. 3651–3659, 2010.

[118] G. D. Bending and S. D. Lincoln, "Inhibition of soil nitrifying bacteria communities and their activities by glucosinolate hydrolysis products," *Soil Biology and Biochemistry*, vol. 32, no. 8-9, pp. 1261–1269, 2000.

[119] K. S. Ramirez, C. L. Lauber, and N. Fierer, "Microbial consumption and production of volatile organic compounds at the soil-litter interface," *Biogeochemistry*, vol. 99, no. 1, pp. 97–107, 2010.

[120] E Kaminśki, S Stawicki, and E Wasowicz, "Volatile flavor compounds produced by molds of Aspergillus, Penicillium, and Fungi imperfecti," *Applied Microbiology*, vol. 27, no. 6, pp. 1001–1004, 1974.

[121] A Nyström, A Grimvall, C Krantz-Rüilcker, R Sävenhed, and K Åkerstrand, "Drinking water off-flavour caused by 2,4,6-trichloroanisole," *Water Science and Technology*, vol. 25, no. 2, pp. 241–249, 1992.

[122] W Lorenz, T Diederich, and M Conrad, "Practical experiences with MVOC as an indicator for microbial growth," *Proc. Indoor Air*, vol. 2002, 341e346, 2002.

[123] M. C. Lemfack, B.-O. Gohlke, S. M. T. Toguem, S. Preissner, B. Piechulla, and R. Preissner, "MVOC 2.0: A database of microbial volatiles," *Nucleic Acids Research*, vol. 46, no. D1, pp. D1261–D1265, 2018.

[124] J. A. Leech, W. C. Nelson, R. T. Burnett, S. Aaron, and M. E. Raizenne, "It's about time: A comparison of canadian and american time-activity patterns," *Journal of Exposure Science & Environmental Epidemiology*, vol. 12, no. 6, pp. 427–432, 2002.

[125] K. Kristensen *et al.*, "Sources and dynamics of semivolatile organic compounds in a single-family residence in northern California," *Indoor air*, vol. 29, no. 4, pp. 645–655, 2019.

[126] J. W. Bennett and A. A. Inamdar, "Are some fungal volatile organic compounds (VOCs) mycotoxins?" *Toxins*, vol. 7, no. 9, pp. 3785–3804, 2015.

[127] J. Cox-Ganser, "Indoor dampness and mould health effects-ongoing questions on microbial exposures and allergic versus nonallergic mechanisms," *Clinical and Experimental Allergy: Journal of the British Society for Allergy and Clinical Immunology*, vol. 45, no. 10, p. 1478, 2015.

[128] K. Engvall, C. Norrby, and D. Norbäck, "Sick building syndrome in relation to building dampness in multi-family residential buildings in Stockholm," *International Archives of Occupational and Environmental Health*, vol. 74, no. 4, pp. 270–278, 2001.

[129] J. Lorentzen, S. Juran, M. Nilsson, S. Nordin, and G Johanson, "Chloroanisoles may explain mold odor and represent a major indoor environment problem in Sweden," *Indoor Air*, vol. 26, no. 2, pp. 207–218, 2016.

[130] R. Wålinder, L. Ernstgård, D. Norbäck, G. Wieslander, and G. Johanson, "Acute effects of 1-octen-3-ol, a microbial volatile organic compound (MVOC)-an experimental study," *Toxicology Letters*, vol. 181, no. 3, pp. 141–147, 2008.

[131] A. A. Inamdar, M. M. Hossain, A. I. Bernstein, G. W. Miller, J. R. Richardson, and J. W. Bennett, "Fungal-derived semiochemical 1-octen-3-ol disrupts dopamine packaging and causes neurodegeneration," *Proceedings of the National Academy of Sciences*, vol. 110, no. 48, pp. 19 561–19 566, 2013.

[132] N. Carslaw and D. Shaw, "Secondary product creation potential (SPCP): A metric for assessing the potential impact of indoor air pollution on human health," *Environmental Science: Processes & Impacts*, vol. 21, no. 8, pp. 1313–1322, 2019.

[133] W. Nazaroff and A. Goldstein, "Indoor chemistry: Research opportunities and challenges.," *Indoor Air*, vol. 25, no. 4, pp. 357–361, 2015.

[134] R. R. Dunn, N. Fierer, J. B. Henley, J. W. Leff, and H. L. Menninger, "Home life: Factors structuring the bacterial diversity found within and between homes," *PloS One*, vol. 8, no. 5, e64133, 2013.

[135] R. I. Adams *et al.*, "Microbes and associated soluble and volatile chemicals on periodically wet household surfaces," *Microbiome*, vol. 5, no. 1, pp. 1–16, 2017.

[136] B. Sahlberg *et al.*, "Airborne molds and bacteria, microbial volatile organic compounds (MVOC), plasticizers and formaldehyde in dwellings in three north european cities in relation to sick building syndrome (SBS)," *Science of the Total Environment*, vol. 444, pp. 433–440, 2013.

[137] C. Shunthirasingham, Y. D. Lei, and F. Wania, "Evidence of bias in air-water Henry's law constants for semivolatile organic compounds measured by inert gas stripping," *Environmental Science & Technology*, vol. 41, no. 11, pp. 3807–3814, 2007.

[138] H. A. Bamford, D. L. Poster, and J. E. Baker, "Henry's law constants of polychlorinated biphenyl congeners and their variation with temperature," *Journal of Chemical & Engineering Data*, vol. 45, no. 6, pp. 1069–1074, 2000.

[139] L. Sahsuvar, P. A. Helm, L. M. Jantunen, and T. F. Bidleman, "Henry's law constants for α-, β-, and γ-hexachlorocyclohexanes (HCHs) as a function of temperature and revised estimates of gas exchange in Arctic regions," *Atmospheric Environment*, vol. 37, no. 7, pp. 983–992, 2003.

[140] F. K. Lau, M. J. Charles, and T. M. Cahill, "Evaluation of gas-stripping methods for the determination of Henry's law constants for polybrominated diphenyl ethers and polychlorinated biphenyls," *Journal of Chemical & Engineering Data*, vol. 51, no. 3, pp. 871–878, 2006.

[141] F. Fang, S. Chu, and C.-S. Hong, "Air-water Henry's law constants for PCB congeners: Experimental determination and modeling of structure-property relationship," *Analytical Chemistry*, vol. 78, no. 15, pp. 5412–5418, 2006.

[142] L. M. Jantunen and T. F. Bidleman, "Henry's law constants for hexachlorobenzene, *p, p'*-DDE and components of technical chlordane and estimates of gas exchange for Lake Ontario," *Chemosphere*, vol. 62, no. 10, pp. 1689–1696, 2006.

[143] B. Cetin, S. Ozer, A. Sofuoglu, and M. Odabasi, "Determination of Henry's law constants of organochlorine pesticides in deionized and saline water as a function of temperature," *Atmospheric Environment*, vol. 40, no. 24, pp. 4538–4546, 2006.

[144] D. Mackay, W. Y. Shiu, and R. P. Sutherland, "Determination of air-water Henry's law constants for hydrophobic pollutants," *Environmental Science & Technology*, vol. 13, no. 3, pp. 333–337, 1979.

[145] Y. D. Lei, C. Shunthirasingham, and F. Wania, "Comparison of headspace and gas-stripping techniques for measuring the air-mackiewater partitition-ing of normal alkanols (C4 to C10): Effect of temperature, chain length, and adsorption to the water surface," *Journal of Chemical & Engineering Data*, vol. 52, no. 1, pp. 168–179, 2007.

[146] K.-U. Goss, F. Wania, M. S. McLachlan, D. Mackay, and R. P. Schwarzenbach, "Comment on "Reevaluation of air-water exchange fluxes of PCBs in green bay and southern lake michigan"," *Environmental Science & Technology*, vol. 38, no. 9, pp. 1626–1628, 2004.

[147] C. M. Roth, K.-U. Goss, and R. P. Schwarzenbach, "Adsorption of a diverse set of organic vapors on the bulk water surface," *Journal of Colloid and Interface Science*, vol. 252, no. 1, pp. 21–30, 2002.

[148] Y. D. Lei, S. Baskaran, and F. Wania, "Measuring the octan-1-ol air partition coefficient of volatile organic chemicals with the variable phase ratio headspace technique," *Journal of Chemical & Engineering Data*, vol. 64, no. 11, pp. 4793–4800, 2019.

[149] R. Bell, "The reversible hydration of carbonyl compounds," *Advances in Physical Organic Chemistry*, vol. 4, pp. 1–29, 1966.

[150] M. H. Abraham and W. E. Acree Jr, "Prediction of gas to water partition coefficients from 273 to 373 K using predicted enthalpies and heat capacities of hydration," *Fluid Phase Equilibria*, vol. 262, no. 1-2, pp. 97–110, 2007.

[151] C. Mouchel-Vallon *et al.*, "Explicit modeling of volatile organic compounds partitioning in the atmospheric aqueous phase," *Atmospheric Chemistry and Physics*, vol. 13, no. 2, pp. 1023–1037, 2013.

[152] S. Endo, A. Pfennigsdorff, and K.-U. Goss, "Salting-out effect in aqueous NaCl solutions: Trends with size and polarity of solute molecules," *Environmental Science & Technology*, vol. 46, no. 3, pp. 1496–1503, 2012.

[153] J. B. Falabella, A. Nair, and A. S. Teja, "Henry's constants of 1-alkanols and 2-ketones in salt solutions," *Journal of Chemical & Engineering Data*, vol. 51, no. 5, pp. 1940–1945, 2006.

[154] H. S. Ip, X. H. Huang, and J. Z. Yu, "Effective Henry's law constants of glyoxal, glyoxylic acid, and glycolic acid," *Geophysical Research Letters*, vol. 36, no. 1, p. L01802, 2009.

[155] C. Wang, Y. D. Lei, S. Endo, and F. Wania, "Measuring and modeling the salting-out effect in ammonium sulfate solutions," *Environmental Science & Technology*, vol. 48, no. 22, pp. 13 238–13 245, 2014.

[156] C. Wang, Y. D. Lei, and F. Wania, "Effect of sodium sulfate, ammonium chloride, ammonium nitrate, and salt mixtures on aqueous phase partitioning of organic compounds," *Environmental Science & Technology*, vol. 50, no. 23, pp. 12 742–12 749, 2016.

[157] A. Díaz, F. Ventura, and M. T. Galceran, "Determination of odorous mixed chloro-bromoanisoles in water by solid-phase micro-extraction and gas chromatography-mass detection," *Journal of Chromatography A*, vol. 1064, no. 1, pp. 97–106, 2005.

[158] *HSDB: Hazardous Substances Data Bank, TOXicology data NET-work (TOXNET), National Library of Medicine (US)*, https://www.nlm.nih.gov/toxnet/index.html, Last access: 2021-10-29.

[159] D. D. Roberts and P. Pollien, "Analysis of aroma release during microwave heating," *Journal of Agricultural and Food Chemistry*, vol. 45, no. 11, pp. 4388–4392, 1997.

[160] C. L. Yaws, J. R. Hopper, S. D. Sheth, M. Han, and R. W. Pike, "Solubility and Henry's law constant for alcohols in water," *Waste Management*, vol. 17, no. 8, pp. 541–547, 1998.

[161] V. W. Or, M. R. Alves, M. Wade, S. Schwab, R. L. Corsi, and V. H. Grassian, "Crystal clear? Microspectroscopic imaging and physicochemical characterization of indoor depositions on window glass," *Environmental Science & Technology Letters*, vol. 5, no. 8, pp. 514–519, 2018.

[162] R. E. O'Brien *et al.*, "Emerging investigator series: Chemical and physical properties of organic mixtures on indoor surfaces during HOMEChem," *Environmental Science: Processes & Impacts*, vol. 23, no. 4, pp. 559–568, 2021.

[163] T Salthammer and F Fuhrmann, "Photocatalytic surface reactions on indoor wall paint," *Environmental Science & Technology*, vol. 41, no. 18, pp. 6573–6578, 2007.

[164] W. W. Nazaroff and C. J. Weschler, "Indoor acids and bases," *Indoor Air*, vol. 30, no. 4, pp. 559–644, 2020.

[165] J. W. Rowen and R. Blaine, "Sorption of nitrogen and water vapor on textile fibers," *Industrial & Engineering Chemistry*, vol. 39, no. 12, pp. 1659–1663, 1947.

[166] M. Pelletier, N. Bonvallot, and P. Glorennec, "Aggregating exposures & cumulating risk for semivolatile organic compounds: A review," *Environmental research*, vol. 158, pp. 649–659, 2017.

[167] F. Wania, Y. D. Lei, and T. Harner, "Estimating octanol-air partition coefficients of nonpolar semivolatile organic compounds from gas chromatographic retention times," *Analytical Chemistry*, vol. 74, no. 14, pp. 3476–3483, 2002.

[168] Y. Yao, T. Harner, J. Ma, L. Tuduri, and P. Blanchard, "Sources and occurrence of dacthal in the Canadian atmosphere," *Environmental Science & Technology*, vol. 41, no. 3, pp. 688–694, 2007.

[169] J. O. Okeme, T. F. Rodgers, J. M. Parnis, M. L. Diamond, T. F. Bidleman, and L. M. Jantunen, "Gas chromatographic estimation of vapor pressures and octanol–air partition coefficients of semivolatile organic compounds of emerging concern," *Journal of Chemical & Engineering Data*, vol. 65, no. 5, pp. 2467–2475, 2020.

[170] Q. T. Vuong, P. Q. Thang, T. Ohura, and S.-D. Choi, "Determining sub-cooled liquid vapor pressures and octanol-air partition coefficients for chlorinated and brominated polycyclic aromatic hydrocarbons based on gas chromatographic retention times: Application for gas/particle partitioning in air," *Atmospheric Environment*, vol. 229, p. 117 461, 2020.

[171] S. Wu, E. Kim, D. Vethanayagam, and R. Zhao, "Indoor partitioning and potential thirdhand exposure to carbonyl flavoring agents added in e-cigarettes and hookah tobacco," *Environmental Science: Processes & Impacts*, vol. 24, no. 12, pp. 2294–2309, 2022.

[172] D. Hammond *et al.*, "Trends in e-cigarette brands, devices and the nicotine profile of products used by youth in England, Canada and the USA: 2017–2019," *Tobacco Control*, 2021.

[173] R. Jebai *et al.*, "Temporal trends in tobacco product use among US middle and high school students: National youth tobacco survey, 2011-2020," *Public Health Reports*, p. 00 333 549 221 103 812, 2022.

[174] S. S. Soneji, K. E. Knutzen, and A. C. Villanti, "Use of flavored e-cigarettes among adolescents, young adults, and older adults: Findings from the population assessment for tobacco and health study," *Public Health Reports*, vol. 134, no. 3, pp. 282–292, 2019.

[175] S.-H. Zhu *et al.*, "Four hundred and sixty brands of e-cigarettes and counting: Implications for product regulation," *Tobacco Control*, vol. 23, no. suppl 3, pp. iii3–iii9, 2014.

[176] G. Kong, M. E. Morean, D. A. Cavallo, D. R. Camenga, and S. Krishnan-Sarin, "Reasons for electronic cigarette experimentation and discontinuation among adolescents and young adults," *Nicotine & Tobacco Research*, vol. 17, no. 7, pp. 847–854, 2015.

[177] E. J. Krüsemann, A. Havermans, J. L. Pennings, K. De Graaf, S. Boesveldt, and R. Talhout, "Comprehensive overview of common e-liquid ingredients and how they can be used to predict an e-liquid's flavour category," *Tobacco Control*, vol. 30, no. 2, pp. 185–191, 2021.

[178] M. A. Farag, M. M. Elmassry, and S. H. El-Ahmady, "The characterization of flavored hookahs aroma profile and in response to heating as analyzed via headspace solid-phase microextraction (SPME) and chemometrics," *Scientific Reports*, vol. 8, no. 1, pp. 1–12, 2018.

[179] V. L. Owens, T. Ha, and J. N. Soulakova, "Widespread use of flavored e-cigarettes and hookah tobacco in the United States," *Preventive Medicine Reports*, vol. 14, p. 100 854, 2019.

[180] N. I. Goldenson, A. M. Leventhal, K. A. Simpson, and J. L. Barrington-Trimis, "A review of the use and appeal of flavored electronic cigarettes," *Current Addiction Reports*, vol. 6, pp. 98–113, 2019.

[181] L. M. Schneller, M. Bansal-Travers, M. L. Goniewicz, S. McIntosh, D. Ossip, and R. J. O'Connor, "Use of flavored e-cigarettes and the type of e-cigarette devices used among adults and youth in the US—Results from wave 3 of the population assessment of tobacco and health study (2015-2016)," *International Journal of Environmental Research and Public Health*, vol. 16, no. 16, p. 2991, 2019.

[182] J. Audrain-McGovern, A. A. Strasser, and E. P. Wileyto, "The impact of flavoring on the rewarding and reinforcing value of e-cigarettes with nicotine among young adult smokers," *Drug and Alcohol Dependence*, vol. 166, pp. 263–267, 2016.

[183] V. H. Murthy, "E-cigarette use among youth and young adults: A major public health concern," *JAMA Pediatrics*, vol. 171, no. 3, pp. 209–210, 2017.

[184] C. O. Cobb, A. Shihadeh, M. F. Weaver, and T. Eissenberg, "Waterpipe tobacco smoking and cigarette smoking: A direct comparison of toxicant exposure and subjective effects," *Nicotine & Tobacco Research*, vol. 13, no. 2, pp. 78–87, 2011.

[185] C. Lau, R. Zhao, and D. Vethanayagam, "Chemistry review of vaping products and respiratory injury," *Spectrum*, no. 6, 2020.

[186] J. L. Barrington-Trimis, J. M. Samet, and R. McConnell, "Flavorings in electronic cigarettes: An unrecognized respiratory health hazard?" *Jama*, vol. 312, no. 23, pp. 2493–2494, 2014.

[187] I. K. Sundar, F. Javed, G. E. Romanos, and I. Rahman, "E-cigarettes and flavorings induce inflammatory and pro-senescence responses in oral epithelial cells and periodontal fibroblasts," *Oncotarget*, vol. 7, no. 47, p. 77 196, 2016.

[188] G. Kaur, T. Muthumalage, and I. Rahman, "Mechanisms of toxicity and biomarkers of flavoring and flavor enhancing chemicals in emerging tobacco and non-tobacco products," *Toxicology Letters*, vol. 288, pp. 143–155, 2018.

[189] T. Eissenberg and A. Shihadeh, "Waterpipe tobacco and cigarette smoking: Direct comparison of toxicant exposure," *American Journal of Preventive Medicine*, vol. 37, no. 6, pp. 518–523, 2009.

[190] P. A. Tierney, C. D. Karpinski, J. E. Brown, W. Luo, and J. F. Pankow, "Flavour chemicals in electronic cigarette fluids," *Tobacco Control*, vol. 25, no. e1, e10–e15, 2016.

[191] K. E. Farsalinos, K. A. Kistler, G. Gillman, and V. Voudris, "Evaluation of electronic cigarette liquids and aerosol for the presence of selected inhalation toxins," *Nicotine & Tobacco Research*, vol. 17, no. 2, pp. 168–174, 2015.

[192] M Yamaguchi, J Ishida, Z. Xuan, A Nakamura, and T Yoshitake, "Determination of glyoxal, methylglyoxal, diacethyl, and 2,3-pentanedione in fermented foods by high-performance liquid chromatography with fluorescence detection," *Journal of Liquid Chromatography & Related Technologies*, vol. 17, no. 1, pp. 203–211, 1994.

[193] R. Marsili, "Monitoring bacterial metabolites in cultured buttermilk by high performance liquid chromatography and headspace gas chromatography," *Journal of Chromatographic Science*, vol. 19, no. 9, pp. 451–456, 1981.

[194] J. M. Mathews, S. L. Watson, R. W. Snyder, J. P. Burgess, and D. L. Morgan, "Reaction of the butter flavorant diacetyl (2,3-butanedione) with n-α-acetylarginine: A model for epitope formation with pulmonary proteins in the etiology of obliterative bronchiolitis," *Journal of Agricultural and Food Chemistry*, vol. 58, no. 24, pp. 12 761–12 768, 2010.

[195] K. Kreiss, A. Gomaa, G. Kullman, K. Fedan, E. J. Simoes, and P. L. Enright, "Clinical bronchiolitis obliterans in workers at a microwave-popcorn plant," *New England Journal of Medicine*, vol. 347, no. 5, pp. 330–338, 2002.

[196] S. Barhdadi *et al.*, "Identification of flavouring substances of genotoxic concern present in e-cigarette refills," *Food and Chemical Toxicology*, vol. 147, p. 111 864, 2021.

[197] M. Hua, E. E. Omaiye, W. Luo, K. J. McWhirter, J. F. Pankow, and P. Talbot, "Identification of cytotoxic flavor chemicals in top-selling electronic cigarette refill fluids," *Scientific Reports*, vol. 9, no. 1, p. 2782, 2019.

[198] R. Sander, W. E. Acree, A. De Visscher, S. E. Schwartz, and T. J. Wallington, "Henry's law constants (IUPAC Recommendations 2021)," *Pure and Applied Chemistry*, vol. 94, no. 1, pp. 71–85, 2022.

[199] E. E. Omaiye, K. J. McWhirter, W. Luo, P. A. Tierney, J. F. Pankow, and P. Talbot, "High concentrations of flavor chemicals are present in electronic cigarette refill fluids," *Scientific Reports*, vol. 9, no. 1, p. 2468, 2019.

[200] J. Schubert, F. D. Müller, R. Schmidt, A. Luch, and T. G. Schulz, "Waterpipe smoke: Source of toxic and carcinogenic VOCs, phenols and heavy metals?" *Archives of Toxicology*, vol. 89, no. 11, pp. 2129–2139, 2015.

[201] J. Schubert, A. Luch, and T. G. Schulz, "Waterpipe smoking: Analysis of the aroma profile of flavored waterpipe tobaccos," *Talanta*, vol. 115, pp. 665–674, 2013.

[202] A. Khlystov and V. Samburova, "Flavoring compounds dominate toxic aldehyde production during e-cigarette vaping," *Environmental Science & Technology*, vol. 50, no. 23, pp. 13 080–13 085, 2016.

[203] E. A. Betterton, "The partitioning of ketones between the gas and aqueous phases," *Atmospheric Environment. Part A. General Topics*, vol. 25, no. 8, pp. 1473–1477, 1991.

[204] C. J. Kampf *et al.*, "Effective Henry's law partitioning and the salting constant of glyoxal in aerosols containing sulfate," *Environmental Science & Technology*, vol. 47, no. 9, pp. 4236–4244, 2013.

[205] A. Tilgner *et al.*, "Acidity and the multiphase chemistry of atmospheric aqueous particles and clouds," *Atmospheric Chemistry and Physics*, vol. 21, no. 17, pp. 13 483–13 536, 2021.

[206] R Zhao, A. Lee, R Soong, A. Simpson, and J. Abbatt, "Formation of aqueous-phase α-hydroxyhydroperoxides (α-HHP): Potential atmospheric impacts," *Atmospheric Chemistry and Physics*, vol. 13, no. 12, pp. 5857–5872, 2013.

[207] A. M. Castillo, L. Patiny, and J. Wist, "Fast and accurate algorithm for the simulation of NMR spectra of large spin systems," *Journal of Magnetic Resonance*, vol. 209, no. 2, pp. 123–130, 2011.

[208] D. Banfi and L. Patiny, "Www. nmrdb. org: Resurrecting and processing NMR spectra on-line," *Chimia*, vol. 62, no. 4, pp. 280–280, 2008.

[209] J. Aires-de Sousa, M. C. Hemmer, and J. Gasteiger, "Prediction of ^{1}H NMR chemical shifts using neural networks," *Analytical Chemistry*, vol. 74, no. 1, pp. 80–90, 2002.

[210] Y. Binev and J. Aires-de Sousa, "Structure-based predictions of ^{1}H NMR chemical shifts using feed-forward neural networks," *Journal of Chemical Information and Computer Sciences*, vol. 44, no. 3, pp. 940–945, 2004.

[211] T. Wallace, "Quantitative analysis of a mixture by NMR spectroscopy," *Journal of Chemical Education*, vol. 61, no. 12, p. 1074, 1984.

[212] S. H. Hilal, S. N. Ayyampalayam, and L. A. Carreira, "Air-liquid partition coefficient for a diverse set of organic compounds: Henry's law constant in water and hexadecane," *Environmental Science & Technology*, vol. 42, no. 24, pp. 9231–9236, 2008.

[213] C. Ji, S. E. Day, S. A. Ortega, and G. W. Beall, "Henry's law constants of some aromatic aldehydes and ketones measured by an internal standard method," *Journal of Chemical & Engineering Data*, vol. 53, no. 5, pp. 1093–1097, 2008.

[214] I. V. Tetko *et al.*, "Virtual computational chemistry laboratory–design and description," *Journal of Computer-aided Molecular Design*, vol. 19, no. 6, pp. 453–463, 2005.

[215] H.-J. Buschmann, H.-H. Füldner, and W. Knoche, "The reversible hydration of carbonyl compounds in aqueous solution. Part I, the keto/gem-diol equilibrium," *Berichte der Bunsengesellschaft für physikalische Chemie*, vol. 84, no. 1, pp. 41–44, 1980.

[216] J.-F. Doussin and A. Monod, "Structure–activity relationship for the estimation of OH-oxidation rate constants of carbonyl compounds in the aqueous phase," *Atmospheric Chemistry and Physics*, vol. 13, no. 23, pp. 11 625–11 641, 2013.

[217] M. Marin, I. Baek, and A. J. Taylor, "Volatile release from aqueous solutions under dynamic headspace dilution conditions," *Journal of Agricultural and Food Chemistry*, vol. 47, no. 11, pp. 4750–4755, 1999.

[218] E. J. Straver and T. W. de Loos, "Determination of Henry's law constants and activity coefficients at infinite dilution of flavor compounds in water at 298 k with a gas-chromatographic method," *Journal of Chemical & Engineering Data*, vol. 50, no. 4, pp. 1171–1176, 2005.

[219] J. R. Snider and G. Dawson, "Tropospheric light alcohols, carbonyls, and acetonitrile: Concentrations in the southwestern United States and Henry's law data," *Journal of Geophysical Research: Atmospheres*, vol. 90, no. D2, pp. 3797–3805, 1985.

[220] R. S. Strekowski and C. George, "Measurement of Henry's law constants for acetone, 2-butanone, 2,3-butanedione, and isobutyraldehyde using a horizontal flow reactor," *Journal of Chemical & Engineering Data*, vol. 50, no. 3, pp. 804–810, 2005.

[221] J. Yu, F. Wania, and J. P. Abbatt, "A new approach to characterizing the partitioning of volatile organic compounds to cotton fabric," *Environmental Science & Technology*, vol. 56, no. 6, pp. 3365–3374, 2022.

[222] L. Li, J. A. Arnot, and F. Wania, "Towards a systematic understanding of the dynamic fate of polychlorinated biphenyls in indoor, urban and rural environments," *Environment international*, vol. 117, pp. 57–68, 2018.

[223] C Gupta, D Prakash, and S Gupta, "A biotechnological approach to microbial based perfumes and flavours," *J. Microbiol. Exp*, vol. 2, 2015.

[224] H. Maarse, *Volatile compounds in foods and beverages*. Routledge, 2017.

[225] S. Wu, E. Kim, and R. Zhao, "Acetal formation of flavoring agents with propylene glycol in e-cigarettes: Impacts on indoor partitioning and thirdhand exposure," *Environmental Science & Technology*, vol. 57, no. 50, pp. 21 284–21 294, 2023.

[226] S. Sapru, M. Vardhan, Q. Li, Y. Guo, X. Li, and D. Saxena, "E-cigarettes use in the United States: Reasons for use, perceptions, and effects on health," *BMC Public Health*, vol. 20, no. 1, pp. 1–10, 2020.

[227] F. Measham, K. O'Brien, and G. Turnbull, ""Skittles & Red Bull is my favourite flavour": E-cigarettes, smoking, vaping and the changing landscape of nicotine consumption amongst British teenagers-implications for the normalisation debate," *Drugs: Education, Prevention and Policy*, vol. 23, no. 3, pp. 224–237, 2016.

[228] A. M. Leventhal, R. Miech, J. Barrington-Trimis, L. D. Johnston, P. M. O'Malley, and M. E. Patrick, "Flavors of e-cigarettes used by youths in the United States," *Jama*, vol. 322, no. 21, pp. 2132–2134, 2019.

[229] R. Grana, N. Benowitz, and S. A. Glantz, "E-cigarettes: A scientific review," *Circulation*, vol. 129, no. 19, pp. 1972–1986, 2014.

[230] M. Cooper, "Notes from the field: E-cigarette use among middle and high school students—United States, 2022," *MMWR. Morbidity and Mortality Weekly Report*, vol. 71, 2022.

[231] A. B. Stefaniak, R. F. LeBouf, A. C. Ranpara, and S. S. Leonard, "Toxicology of flavoring- and cannabis-containing e-liquids used in electronic delivery systems," *Pharmacology & Therapeutics*, vol. 224, p. 107 838, 2021.

[232] M. L. Goniewicz *et al.*, "Levels of selected carcinogens and toxicants in vapour from electronic cigarettes," *Tobacco Control*, vol. 23, no. 2, pp. 133–139, 2014.

[233] C. Hutzler, M. Paschke, S. Kruschinski, F. Henkler, J. Hahn, and A. Luch, "Chemical hazards present in liquids and vapors of electronic cigarettes," *Archives of Toxicology*, vol. 88, pp. 1295–1308, 2014.

[234] S. Salam, N. A. Saliba, A. Shihadeh, T. Eissenberg, and A. El-Hellani, "Flavor-toxicant correlation in e-cigarettes: A meta-analysis," *Chemical Research in Toxicology*, vol. 33, no. 12, pp. 2932–2938, 2020.

[235] P. J. Kerber and D. H. Peyton, "Kinetics of aldehyde flavorant-acetal formation in e-liquids with different e-cigarette solvents and common additives studied by ^{1}H NMR spectroscopy," *Chemical Research in Toxicology*, vol. 35, no. 8, pp. 1410–1417, 2022.

[236] H. C. Erythropel *et al.*, "Formation of flavorant–propylene glycol adducts with novel toxicological properties in chemically unstable e-cigarette liquids," *Nicotine & Tobacco Research*, vol. 21, no. 9, pp. 1248–1258, 2019.

[237] R. Z. Behar, W. Luo, K. J. McWhirter, J. F. Pankow, and P. Talbot, "Analytical and toxicological evaluation of flavor chemicals in electronic cigarette refill fluids," *Scientific Reports*, vol. 8, no. 1, p. 8288, 2018.

[238] G. Gschwend, C. Jenkins, A. Jones, C. Kelso, and J. Morgan, "A wide range of flavoring-carrier fluid adducts form in e-cigarette liquids," *Chemical Research in Toxicology*, vol. 36, no. 1, pp. 14–22, 2023.

[239] H. Surburg and J. Panten, *Common fragrance and flavor materials: preparation, properties and uses*. John Wiley & Sons, 2016.

[240] J.-C. Noël, D. Rainer, R. Gstir, M. Rainer, and G. Bonn, "Quantification of selected aroma compounds in e-cigarette products and toxicity evaluation in HUVEC/Tert2 cells," *Biomedical Chromatography*, vol. 34, no. 3, e4761, 2020.

[241] S. V. Jabba, A. N. Diaz, H. C. Erythropel, J. B. Zimmerman, and S.-E. Jordt, "Chemical adducts of reactive flavor aldehydes formed in e-cigarette liquids are cytotoxic and inhibit mitochondrial function in respiratory epithelial cells," *Nicotine and Tobacco Research*, vol. 22, no. Supplement_1, S25–S34, 2020.

[242] D. Mackay, "Correlation of bioconcentration factors," *Environmental Science & Technology*, vol. 16, no. 5, pp. 274–278, 1982.

[243] C. T. Chiou, V. H. Freed, D. W. Schmedding, and R. L. Kohnert, "Partition coefficient and bioaccumulation of selected organic chemicals," *Environmental Science & Technology*, vol. 11, no. 5, pp. 475–478, 1977.

[244] B. C. Kelly, M. G. Ikonomou, J. D. Blair, A. E. Morin, and F. A. Gobas, "Food web specific biomagnification of persistent organic pollutants," *Science*, vol. 317, no. 5835, pp. 236–239, 2007.

[245] J. G. Allen *et al.*, "Flavoring chemicals in e-cigarettes: Diacetyl, 2,3-pentanedione, and acetoin in a sample of 51 products, including fruit-, candy-, and cocktail-flavored e-cigarettes," *Environmental Health Perspectives*, vol. 124, no. 6, pp. 733–739, 2016.

[246] *US EPA. [2012]. Estimation Programs Interface Suite™ for Microsoft® Windows, v 4.11 or insert version used]. United States Environmental Protection Agency, Washington, DC, USA.* http://www.eas-e-suite.com, Last access: 2023-05-29.

[247] T. N. Brown, "QSPRs for predicting equilibrium partitioning in solvent-air systems from the chemical structures of solutes and solvents," *Journal of Solution Chemistry*, vol. 51, no. 9, pp. 1101–1132, 2022.

[248] J. C. McGowan, "The estimation of solubility parameters and related properties of liquids," *Journal of Chemical Technology and Biotechnology. Chemical Technology*, vol. 34, no. 1, pp. 38–42, 1984.

[249] K.-U. Goss, "Predicting the equilibrium partitioning of organic compounds using just one linear solvation energy relationship (LSER)," *Fluid Phase Equilibria*, vol. 233, no. 1, pp. 19–22, 2005.

[250] J. H. Seinfeld and S. N. Pandis, *Atmospheric chemistry and physics: from air pollution to climate change*. John Wiley & Sons, 2016.

[251] R. Chen *et al.*, "Assessment of indoor air quality at an electronic cigarette (Vaping) convention," *Journal of Exposure Science & Environmental Epidemiology*, vol. 28, no. 6, pp. 522–529, 2018.

[252] G. O'Connell, S. Colard, X. Cahours, and J. D. Pritchard, "An assessment of indoor air quality before, during and after unrestricted use of e-cigarettes in a small room," *International Journal of Environmental Research and Public Health*, vol. 12, no. 5, pp. 4889–4907, 2015.

[253] W. Schober *et al.*, "Use of electronic cigarettes (e-cigarettes) impairs indoor air quality and increases feno levels of e-cigarette consumers," *International Journal of Hygiene and Environmental Health*, vol. 217, no. 6, pp. 628–637, 2014.

[254] O. Geiss, I. Bianchi, F. Barahona, and J. Barrero-Moreno, "Characterisation of mainstream and passive vapours emitted by selected electronic cigarettes," *International Journal of Hygiene and Environmental Health*, vol. 218, no. 1, pp. 169–180, 2015.

[255] S. F. Schick *et al.*, "Thirdhand cigarette smoke in an experimental chamber: Evidence of surface deposition of nicotine, nitrosamines and polycyclic aromatic hydrocarbons and de novo formation of NNK," *Tobacco Control*, vol. 23, no. 2, pp. 152–159, 2014.

[256] F. Wania, Y. D. Lei, S. Baskaran, and A. Sangion, "Identifying organic chemicals not subject to bioaccumulation in air-breathing organisms using predicted partitioning and biotransformation properties," *Integrated Environmental Assessment and Management*, vol. 18, no. 5, pp. 1297–1312, 2022.

[257] L. Li, L. Hughes, and J. A. Arnot, "Addressing uncertainty in mouthing-mediated ingestion of chemicals on indoor surfaces, objects, and dust," *Environment International*, vol. 146, p. 106 266, 2021.

[258] B. Liu and S. Thayumanavan, "Substituent effects on the pH sensitivity of acetals and ketals and their correlation with encapsulation stability in polymeric nanogels," *Journal of the American Chemical Society*, vol. 139, no. 6, pp. 2306–2317, 2017.

[259] C. J. Mussinan and M. J. Morello, *Flavor analysis: Developments in isolation and characterization*. ACS Publications, 1998.

[260] C. M. Eichler *et al.*, "Cloth–air partitioning of neutral per-and polyfluoroalkyl substances (PFAS) in North Carolina homes during the indoor PFAS assessment (IPA) campaign," *Environmental Science & Technology*, vol. 57, no. 40, pp. 15 173–15 183, 2023.

[261] G. E. Matt, E. Hoh, P. J. Quintana, J. M. Zakarian, and J. Arceo, "Cotton pillows: A novel field method for assessment of thirdhand smoke pollution," *Environmental Research*, vol. 168, pp. 206–210, 2019.

[262] X. Zhou, X. Dong, R. Ma, X. Wang, and F. Wang, "Characterizing the partitioning behavior of formaldehyde, benzene and toluene on indoor fabrics: Effects of temperature and humidity," *Journal of Hazardous Materials*, vol. 416, p. 125 827, 2021.

[263] V. Chithra and S. S. Nagendra, "Chemical and morphological characteristics of indoor and outdoor particulate matter in an urban environment," *Atmospheric Environment*, vol. 77, pp. 579–587, 2013.

[264] K. R. Kolesar, C. N. Mattson, P. K. Peterson, N. W. May, R. K. Prendergast, and K. A. Pratt, "Increases in wintertime $PM_{2.5}$ sodium and chloride linked to snowfall and road salt application," *Atmospheric Environment*, vol. 177, pp. 195–202, 2018.

[265] M. A. Torkmahalleh, S. Gorjinezhad, H. S. Unluevcek, and P. K. Hopke, "Review of factors impacting emission/concentration of cooking generated particulate matter," *Science of the Total Environment*, vol. 586, pp. 1046–1056, 2017.

[266] C. J. Lau, M. Loebel Roson, K. M. Klimchuk, T. Gautam, B. Zhao, and R. Zhao, "Particulate matter emitted from ultrasonic humidifiers—chemical composition and implication to indoor air," *Indoor Air*, vol. 31, no. 3, pp. 769–782, 2021.

[267] F Thevenet, O Debono, M Rizk, F Caron, M Verriele, and N Locoge, "VOC uptakes on gypsum boards: Sorption performances and impact on indoor air quality," *Building and Environment*, vol. 137, pp. 138–146, 2018.

[268] Ulrich, N., Endo, S., Brown, T.N., Watanabe, N., Bronner, G., Abraham, M.H., Goss, K.-U., *UFZ-LSER database v 3.2 [Internet], Leipzig, Germany, Helmholtz Centre for Environmental Research-UFZ*, http://www.ufz.de/lserd, Last access: 2022-08-26, 2017.

[269] C. M. Roth, K.-U. Goss, and R. P. Schwarzenbach, "Sorption of diverse organic vapors to snow," *Environmental Science & Technology*, vol. 38, no. 15, pp. 4078–4084, 2004.

[270] C. Shunthirasingham, X. Cao, Y. D. Lei, and F. Wania, "Large bubbles reduce the surface sorption artifact of the inert gas stripping method," *Journal of Chemical & Engineering Data*, vol. 58, no. 3, pp. 792–797, 2013.

[271] M. H. Abraham, J. Le, W. E. Acree Jr, P. W. Carr, and A. J. Dallas, "The solubility of gases and vapours in dry octan-1-ol at 298 K," *Chemosphere*, vol. 44, no. 4, pp. 855–863, 2001.

[272] W. M. Meylan and P. H. Howard, "Estimating octanol-air partition coefficients with octanol-water partition coefficients and Henry's law constants," *Chemosphere*, vol. 61, no. 5, pp. 640–644, 2005.

[273] US EPA, *Estimation Programs Interface Suite™ for Microsoft® Windows, v 4.11. United States Environmental Protection Agency, Washington, DC, USA.* 2021.

Appendix A: Chapter 2

A.1 Supplementary information for Chapter 2

A.1.1 Structures of MVOCs

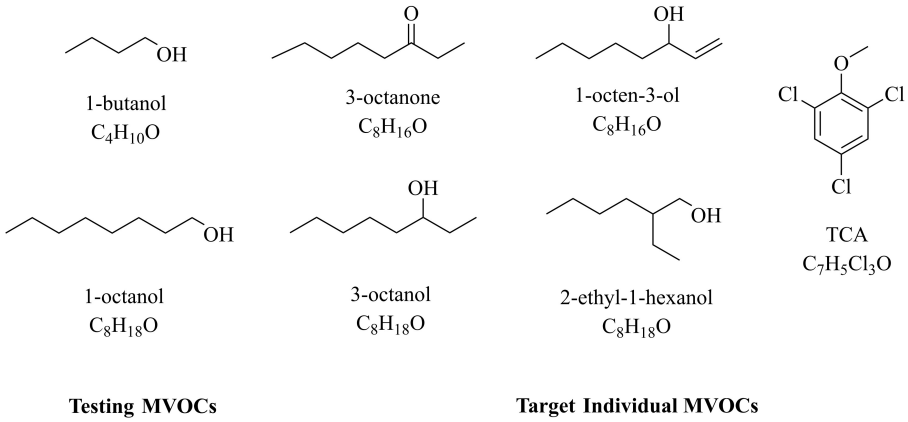

Figure A.1: Structures of the testing compounds and target MVOCs.

A.1.2 Model-Based Prediction of K_{ia}

The K_{ia} [m = (mol· m^{-2})/(mol· m^{-3})] values are estimated by an online UFZ-LSER database[268] since no available experimental derived K_{ia} values from previous literature exist. K_{ia} values are predicted from a poly-parameter linear free-energy relationship (pp-LFERs)[147] at 15 °C:

$$\log(K_{\mathrm{ia}}/\mathrm{m}) = 0.635 \cdot \log\mathrm{L16} + 5.11 \cdot \mathrm{B} + 3.60 \cdot \mathrm{A} - 8.47 \tag{A.1}$$

where L16 is the heaxadecane/air partition coefficient, and A and B are measures of a solute's hydrogen bonding acidity and basicity.

The enthalpy of adsorption to the water interface $\Delta_{\mathrm{ads}}H$ was estimated by eq A.2[269], then the K_{ia} values can be adjusted to experimental temperatures using the

van't Hoff relationship (eq A.3).

$$\Delta_{\text{ads}}H(\text{J/mol}) = (-5.52 \cdot \ln K_{\text{ia}}(15^{\circ}\text{C}) - 107) \cdot 1000 \tag{A.2}$$

$$\ln(K_{\text{ia}}(T_2)/K_{\text{ia}}(T_1)) = (\Delta_{\text{ads}}H/R) \cdot (1/T_1 - 1/T_2) \tag{A.3}$$

According to the Lei *et al.*,[145] three factors contribute to the surface adsorption artifacts and deviations in H values. The first one is the adsorption coefficient K_{ia} in units of m, expressed as the ratio between the concentration on the bubble surface and inside the bubble.[147] Second is the bubble surface-area-to-volume ratio 3/r $((4\pi r^2)/(4/3\pi r^3)$, where r is the radius of a spherical bubble. The third factor is the fraction of surface-bound chemicals transferred to the gas phase upon bubble bursting. This fraction has a range of 0 to 1.

Generally speaking, small bubbles facilitate the water-air mass transfer, which ensures the establishment of equilibrium. A previous study has suggested 0.001 m as a K_{ia} threshold when applying the IGS method with small bubbles.[137] It states that the small bubbles with a high surface-area-to-volume ratio are prone to the surface adsorption artifacts if the target compound has a large K_{ia}, leading to more substances adsorbed on the bubble surface. Also, this interfacial sorption is pronounced at lower temperatures due to larger K_{ia} values at a lower temperature. Another study also noticed the discrepancies in results measured by the IGS methods between different studies and suggested that an IGS setup with large bubbles (diameter around 5.5 mm) is suitable for MVOCs with large K_{ia} (below 0.02 m).[270] The larger bubbles have a smaller surface-area-to-volume ratio, reducing the chemical adsorbed fraction to the bubble surface. These investigations demonstrated that the use of larger bubbles in the IGS method reduces the surface adsorption artifacts.

During the initial test of the experiments, we started with a bubbler setup which produced bubbles with 1.5 mm diameter. The bubble size was roughly estimated by photographing the bubbler setup alongside a ruler and averaging the diameters of ten arbitrarily chosen bubbles. A significant deviation (up to a factor of 5) was noticed between the 1-octanol result and the literature value at 25°C from Shunthirasingham *et al.*[270], who also considered the effect of bubble surface and employed

larger bubbles in their IGS setup (Figure A.2). This difference was consistent with previous work showing that the impact of the bubble surface was enhanced when small bubbles were used, especially for the chemicals with large K_{ia} values.[137] We designed two upper parts of the IGS setup for MVOCs with different K_{ia} values following this observation. One with a fritted gas dispenser produces small bubbles (with an estimated average diameter of 3 mm) for compounds with small K_{ia} values (below 0.001m). Another one with only one perforation produces large bubbles (with an estimated average diameter of around 6 mm) for compounds with large K_{ia} values (0.001 m to 0.02 m). The improvement of the measurements promoted by the experimental device optimization is shown in Figure A.2. For 1-butanol with a small K_{ia} value, the optimization brings the H result closer to the literature value to a certain extent, narrowing the gap from 15% to 5%. In comparison, the optimized device helped the 1-octanol reduce the error caused by the large K_{ia} value and the H value after optimization only shows a 15% difference from the previous literature.

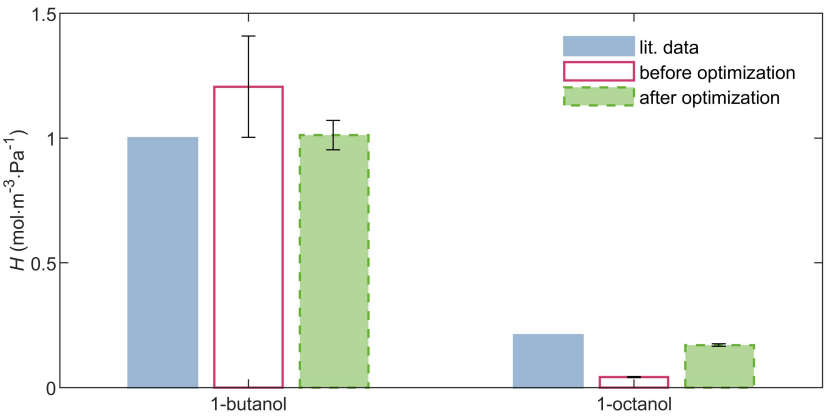

Figure A.2: Measured H values of testing chemicals before and after optimization of the IGS setup at 25°C. The literature data is from Shunthirasingham *et al.*[137] Before optimization, bubble size of 1.5 mm was used. After optimization, bubble sizes of 3 and 6 mm were used for 1-butanol and 1-octanol, respectively.

Table A.1 presents the UFZ-LSER-predicted K_{ia} values of MVOCs at 15 °C and the choice of the bubble size accordingly. Please note that there is no available model-predicted K_{ia} value for 1-octen-3-ol, we assumed it has a large K_{ia} value due to its similar structure to 3-octanol. The large difference between the results obtained by the two setups also confirmed the K_{ia} value of 1-octen-3-ol at least larger than 0.001

m at 15 °C.

Table A.1: K_{ia} values of the target MVOCs and accordingly setup choice.

	K_{ia}/m at 15 °C	purging bubble size[b]
1-butanol[a]	0.0009	small
1-octanol[a]	0.0178	large
TCA	0.0002	small
3-octanone	0.0007	small
1-octen-3-ol	-	large
3-octanol	0.0200	large
2-ethyl-1-hexanol	0.0135	large

[a]Testing compounds. [b]Small bubbles are $\sim$ 3 mm in diameter, large bubbles are $\sim$ 6 mm in diameter.

A.1.3 Flow Rate and Equilibration of IGS

H values measured by the IGS method under 15, 25, 35 and 50°C with different flow rates are presented in Table A.2. Different flow rates were applied for the two testing chemicals (1-octanol and 1-butanol) to determine the appropriate flow rate. The flow rates of 100 and 200 sccm were chosen to test the equilibration of 1-butanol. H values exhibit excellent agreement between these two flow rates at all four temperatures. These observations confirm that equilibrium has been fully achieved for 1-butanol with 200 sccm. Similarly, comparing H values obtained at 50 and 100 sccm for 1-octanol, we determined that 100 sccm is the optimal flow rate. Given that 1-butanol and 1-octanol are used as representatives for compounds with large and small K_{ia} values, respectively, we have decided to use 200 sccm for compounds with large K_{ia} and 100 sccm for those with small K_{ia} values. The only exception were 3-octanone and TCA. We had to use slow flow rates at 35 and 50 °C due to the volatility of 3-octanone; For the toxic TCA, we used a slower flow rate to ensure that no gas enters the indoor air.

Table A.2: H values determined by the IGS method at different temperatures T and gas flow rates G.

Compound	T/°C	G/sccm	H/mol·m^{-3}·Pa^{-1}
1-butanol[a]	15	100	2.47 ± 0.24
	15	200	2.33 ± 0.39
	25	100	1.18 ± 0.03
	25	200	1.01 ± 0.06
	35	100	$(5.33 \pm 0.25)\times10^{-1}$
	35	200	$(5.25 \pm 0.20)\times10^{-1}$
	50	100	$(1.70 \pm 0.10)\times10^{-1}$
	50	200	$(1.66 \pm 0.01)\times10^{-1}$
1-octanol[a]	15	50	$(3.02 \pm 0.16)\times10^{-1}$
	15	100	$(3.65 \pm 0.41)\times10^{-1}$
	25	50	$(1.74 \pm 0.19)\times10^{-1}$
	25	100	$(1.70 \pm 0.05)\times10^{-1}$
	35	50	$(8.52 \pm 3.29)\times10^{-2}$
	35	100	$(7.86 \pm 0.14)\times10^{-2}$
	50	50	$(2.69 \pm 0.04)\times10^{-2}$
	50	100	$(2.61 \pm 0.00)\times10^{-2}$
TCA	15	50	$(4.67 \pm 0.06)\times10^{-2}$
	25	50	$(2.13 \pm 0.02)\times10^{-2}$
	35	50	$(1.11 \pm 0.02)\times10^{-2}$
	50	50	$(5.89 \pm 0.03)\times10^{-3}$
3-octanone	15	200	$(5.86 \pm 0.21)\times10^{-2}$
	25	200	$(2.88 \pm 0.12)\times10^{-3}$
	35	100	$(1.52 \pm 0.02)\times10^{-4}$
	50	50	$(6.49 \pm 0.09)\times10^{-4}$
1-octen-3-ol	15	100	$(5.30 \pm 0.44)\times10^{-1}$
	25	100	$(1.74 \pm 0.05)\times10^{-1}$
	35	100	$(8.12 \pm 0.23)\times10^{-2}$
	50	100	$(2.63 \pm 0.01)\times10^{-2}$
3-octanol	15	200	$(3.71 \pm 0.38)\times10^{-1}$
	25	200	$(1.04 \pm 0.02)\times10^{-1}$
	35	200	$(4.16 \pm 0.05)\times10^{-2}$
	50	200	$(1.58 \pm 0.03)\times10^{-2}$
2-ethyl-1-hexanol	15	100	$(3.66 \pm 0.32)\times10^{-1}$
	25	100	$(1.51 \pm 0.04)\times10^{-1}$
	35	100	$(7.01 \pm 0.20)\times10^{-2}$
	50	100	$(2.40 \pm 0.08)\times10^{-2}$

[a]Testing compounds.

A.1.4 Model-Based Prediction of K_{wa} and K_{oa}

The 2D-partitioning space plots were applied for target MVOCs using the K_{wa} values determined by this work and K_{oa} values obtained using the modelling approach. For the other typical MVOCs, the model was applied with either existing H values in the literature or model-predicted values. Some of these MVOCs have been studied thoroughly and their K_{wa} values were adapted from the literature directly. A few other chemicals are either commercially unavailable or extremely expensive; therefore, their K_{wa} values have been simulated with SPARC.

We used the modelling approach to obtain K_{oa} values because there is no experimental data available in the literature except 1-butanol.[271] The difference in K_{oa} values predicted with three different models at 25 °C is insignificant for the MVOCs studied in this paper (Table A.3). The online prediction calculator SPARC Performs Automated Reasoning in Chemistry (http://www.archemcalc.com) uses computational algorithms based on fundamental chemical structure theory to estimate a wide variety of reactivity parameters.[212] The online UFZ-LSER database[268] derives K_{oa} values from poly-parameter linear free-energy relationships (ppLFERs).[95] The KOAWIN model[272] included in EPI Suite[273] obtains the K_{oa} values based on the thermodynamic triangle calculation using either experimental or estimated values of K_{wa} and K_{ow}: $K_{oa} = K_{wa} \cdot K_{ow}$. The K_{oa} temperature-dependent prediction is only available in SPARC.

Table A.4 and Table A.5 list the log K_{wa} and log K_{oa} values used in the 2D-partitioning chemical space plots.

Table A.3: log K_{oa} predictions from SPARC, ppLFERs and EPI Suite at 25 °C.

Compounds	SPARC	ppLFERs	EPI Suite
1-butanol[a]	4.13	4.15	4.32
3-octanol	5.50	5.64	5.63
TCA	6.25	5.82	6.38
1-octen-3-ol	5.88	-	5.62
3-octanone	4.63	4.60	4.49
2-ethyl-1-hexanol	5.66	5.86	5.70

[a]Testing compound.

Table A.4: log K_{wa} and log K_{oa} values for target MVOCs.

	15 °C		25 °C		35 °C		50 °C	
Compounds	log K_{wa}	log K_{oa}	log K_{wa}	log K_{oa}	log K_{wa}	log K_{oa}	log K_{wa}	log K_{oa}
1-butanol[a]	3.75	4.43	3.40	4.13	3.13	3.89	2.65	3.54
3-octanol	2.95	5.87	2.41	5.5	2.03	5.22	1.63	4.79
TCA	2.05	6.67	1.72	6.25	1.45	6.01	1.20	5.59
1-octen-3-ol	3.10	6.27	2.64	5.88	2.32	5.58	1.85	5.18
3-octanone	2.15	4.97	1.85	4.63	1.59	4.43	1.24	4.09
2-ethyl-1-hexanol	2.94	6.05	2.57	5.66	2.25	5.37	1.81	4.93

[a]Testing compound.

Table A.5: log K_{wa} and log K_{oa} values for other indoor MVOCs.

Compounds	log K_{wa}[a]	log K_{oa}
3-methyl-1-butanol	3.21	4.47
3-methyl-2-butanol	3.02	4.07
2-pentanol	3.19	4.20
2-octen-1-ol	3.28*	6.50
3-methylfuran	0.90*	2.72
2-hexanone	2.39	3.89
2-heptanone	2.35	4.30
2-methylisoborneol	3.59*	6.55
2-isopropyl-3-methoxy-pyrazine	4.71*	6.65
geosmin	4.01*	7.43

[a]The average of previous published data summarized by Sander[112] unless otherwise noted.
*Predicted data from SPARC.

A.1.5 Construction of the 2D-Partitioning Model

In the two-dimensional chemical partitioning model, the fractions of a species residing in the gas phase, polar reservoir, and weakly polar reservoir (F_g, F_w and F_o) can be calculated by the following equations from Wang *et al.*[71] The model assumes the indoor surface-to-volume ratio *(S/V)* to be 3 m^{-1} as commonly used.[11]

$$F_g = 1/(1 + K_{oa} V_O / V_A + K_{wa} V_W / V_A) \quad (A.4)$$

$$F_w = 1/(1 + K_{wa} V_W / V_A + K_{oa}/K_{wa} V_O / V_W) \quad (A.5)$$

$$F_o = 1/(1 + K_{oa} V_O / V_A + K_{wa}/K_{oa} V_W / V_O) \quad (A.6)$$

where V_A, V_W and V_O, in units of m^3, are the volumes of indoor air, polar reservoir and weakly polar reservoir.

In fact, the gas phase is the dominant part of the indoor environment. We thus assumed that the gas phase volume is equal to the volume indoor. We also assumed the polar and weakly polar reservoirs are uniformly distributed on the indoor surface

with a certain thickness (X_{W} and X_{O} in units of m); their volumes can be derived by thickness and S/V value:

$$V_{\mathrm{W}}/V_{\mathrm{A}} = X_{\mathrm{W}}S/V \tag{A.7}$$

$$V_{\mathrm{O}}/V_{\mathrm{A}} = X_{\mathrm{O}}S/V \tag{A.8}$$

$$V_{\mathrm{W}}/V_{\mathrm{O}} = X_{\mathrm{W}}/X_{\mathrm{O}} \tag{A.9}$$

The 2D-partitioning plot is constructed and visualized with a custom-written Python script.

A.1.6 IGS Results for all MVOCs

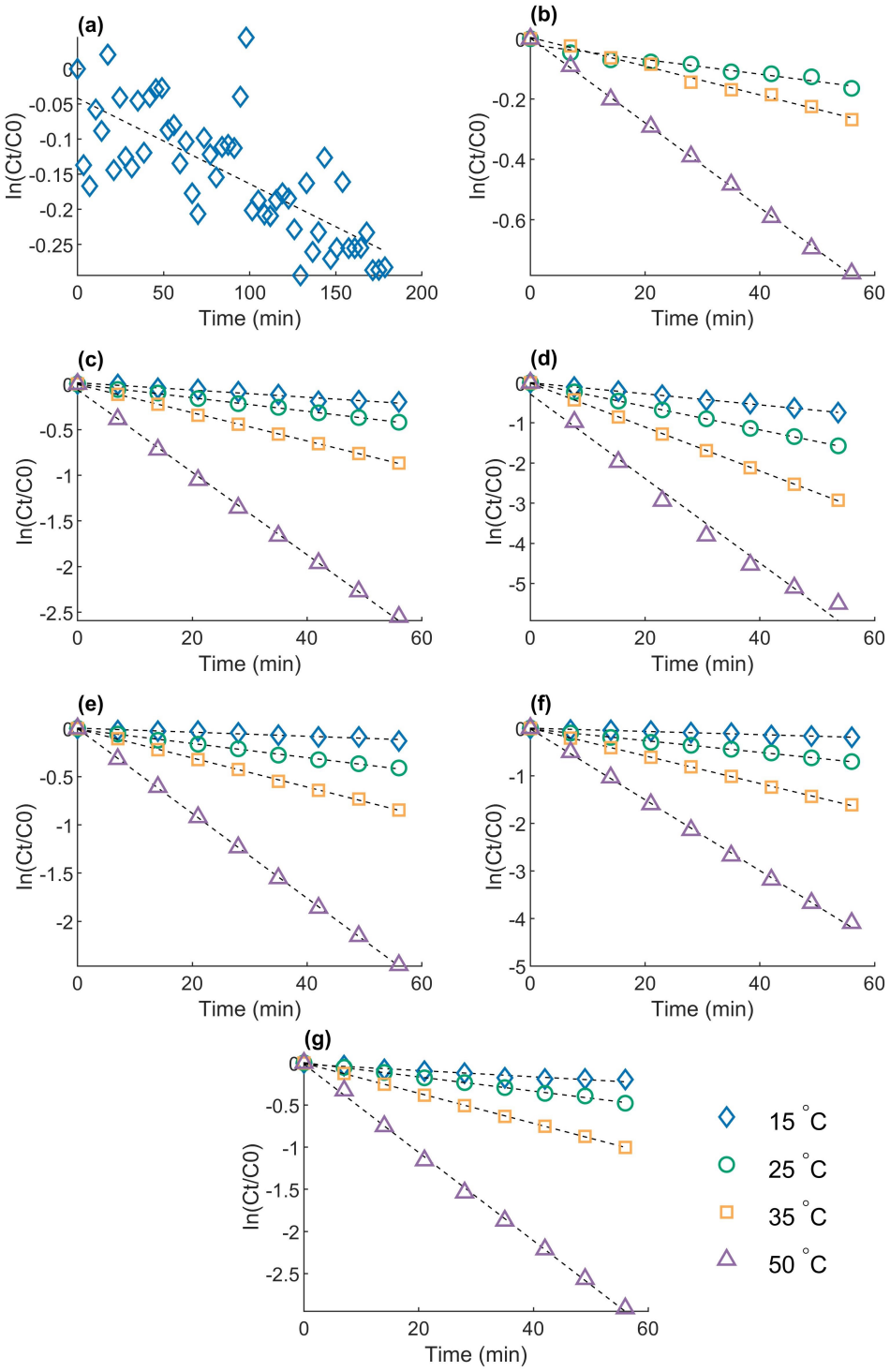

Figure A.3: First-order decay plots of $\ln(C_t/C_0)$ *vs.* time at 15, 25, 35 and 50 °C for all MVOCs. (a) 1-butanol at 15 °C; (b) 1-butanol at 25, 35 and 50 °C; (c) 1-octanol; (d) TCA; (e) 1-octen-3-ol; (f) 3-octanol; (g) 2-ethyl-1-hexanol.

A.1.7 VPR-HS Results for all MVOCs

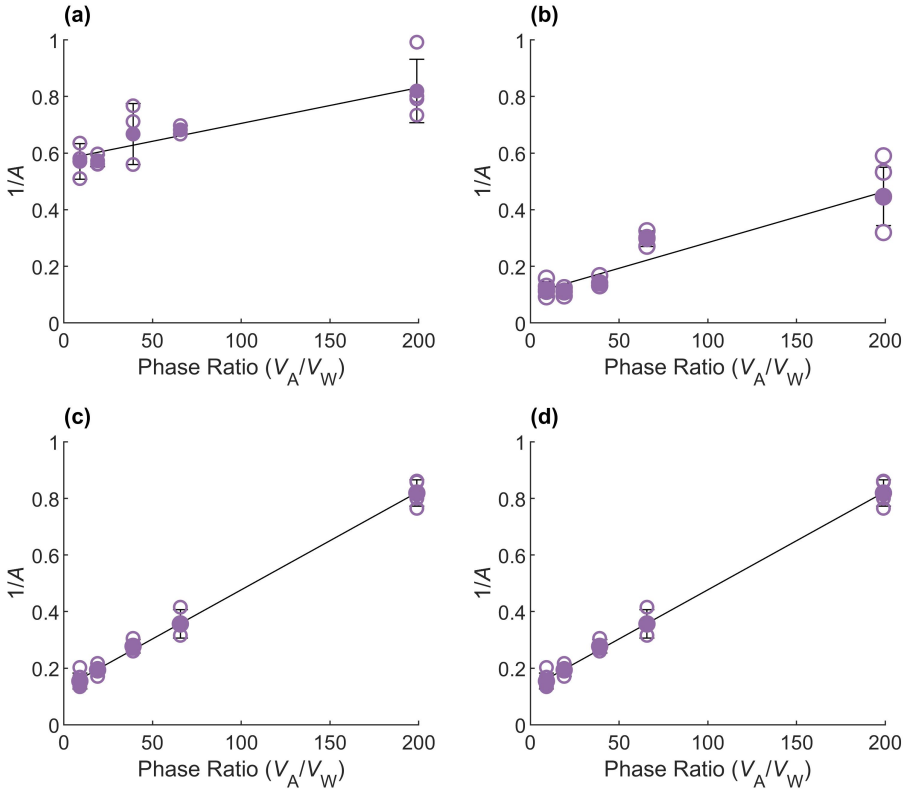

Figure A.4: Linear relationships between the reciprocal chemical concentration (peak area, A) in the gas phase over phase ratio (V_A/V_W). (a) 1-octanol at 25 °C; (b) 1-octanol at 50 °C; (c) TCA at 25 °C; (d) TCA at 50 °C. The solid markers are the averages of all the replicates performed at a certain phase ratio, while the hollow markers represent the results of each individual measurement. The error bar around the regression line is derived by propagating the standard deviations of the slope and intercept from the regression analysis.

Table A.6: Slopes, Intercepts, and Correlation Coefficient (r^2) of the Linear Regression of Reciprocal Peak Area $1/A$ over phase ratio (V_A/V_W) and H values for 1-octenol, 1-octen-3-ol and TCA.

Compound	T/°C	Slope	Intercept	r^2	H/mol·m^{-3}·Pa^{-1}
1-octanol[a]	25	1.26×10^{-3}	5.82×10^{-1}	0.919	$(1.86 \pm 0.32)\times10^{-1}$
	50	1.81×10^{-3}	1.02×10^{-1}	0.909	$(2.10 \pm 0.76)\times10^{-2}$
1-octen-3-ol	25	5.30×10^{-4}	2.23×10^{-1}	0.937	$(1.65 \pm 0.26)\times10^{-1}$
	50	5.81×10^{-4}	4.11×10^{-2}	0.982	$(2.63 \pm 0.35)\times10^{-2}$
TCA	25	3.47×10^{-3}	1.33×10^{-1}	0.999	$(1.55 \pm 0.06)\times10^{-2}$
	50	4.20×10^{-3}	5.26×10^{-2}	0.997	$(4.66 \pm 1.20)\times10^{-3}$

[a]Testing compound.

Appendix B: Chapter 3

B.1 Supplementary information for Chapter 3

B.1.1 Structures of flavoring compounds

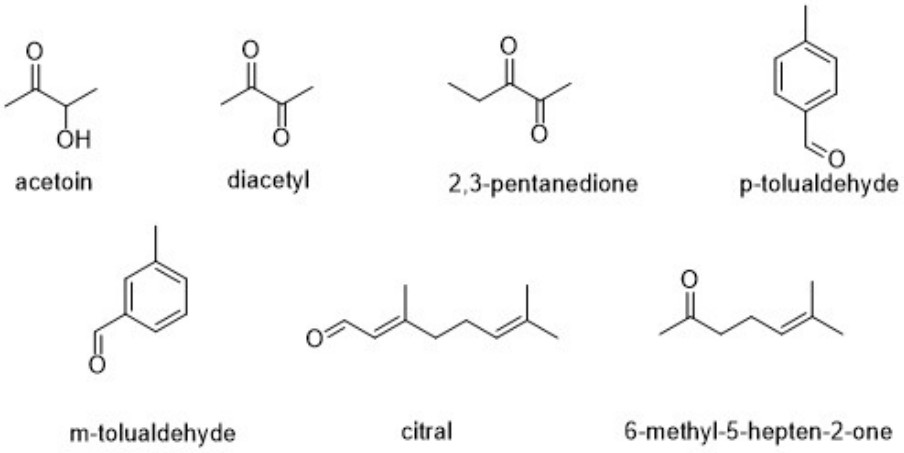

Figure B.1: Structures of the flavoring compounds.

B.1.2 Plots of $\ln(C_t/C_0)$ versus time for all target flavorings

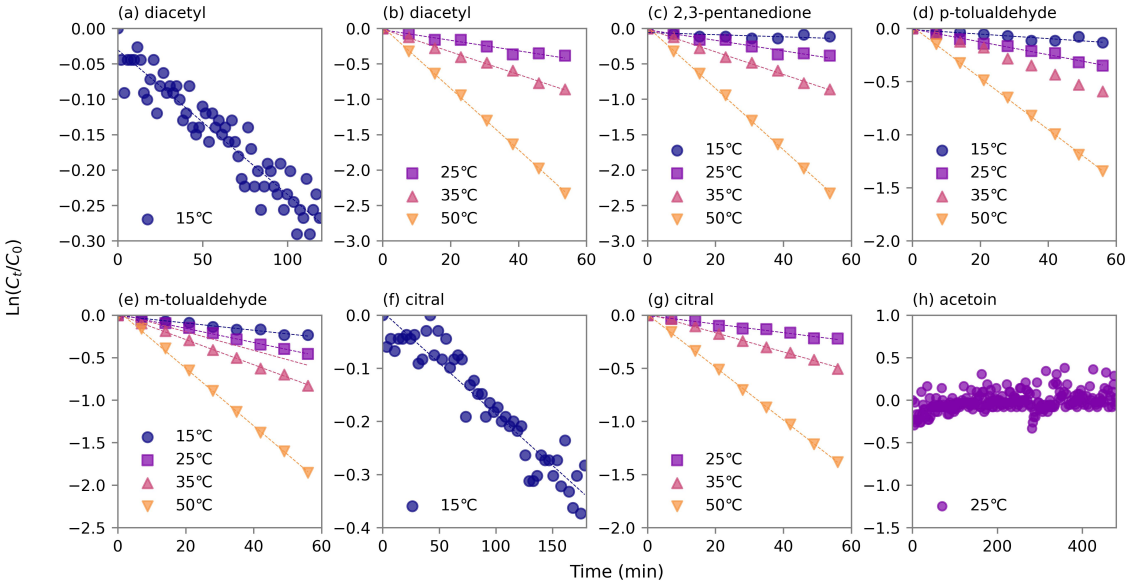

Figure B.2: Plots of $\ln(C_t/C_0)$ versus time at 15, 25, 35 and 50 °C for all target flavorings. (a) Diacetyl at 15 °C; (b) Diacetyl at 25, 35 and 50 °C; (c) 2,3-Pentanedione; (d) p-Tolualdehyde; (e) m-Tolualdehyde; (f) Citral at 15 °C; (g) Citral at 25, 35 and 50 °C; (h) Acetoin at 25 °C.

B.1.3 Choice of setups with different purging bubble sizes

Previous studies have demonstrated that the adsorption of the target molecule to the bubble surface can cause bias in the IGS method, and 0.001 m has been suggested as an interface-air adsorption coefficient (K_{ia}) threshold when applying the small bubbles.[137] Briefly, K_{ia}, in the unit of m, is expressed as the partitioning coefficient between the water-air interface (on the bubble surface) and the gas phase (inside the bubble).[147] Following this conclusion, another paper recommended large bubbles (diameter around 5.5 mm) be applied for chemicals with large K_{ia} (below 0.02 m).[270]

Table B.1: K_{ia} values, difference percentage of the measured $H^{cp}_{s,eff}$ between two setups and accordingly setup choice for target flavorings.

	Log K_{ia} at 15 °C[268]	$H^{cp}_{s,eff}$ difference at 25 °C (%)	Bubble size[b]
diacetyl[a]	-3.89	n.d.	small
2,3-pentanedione	n.a.	1.14%	small
p-tolualdehyde	-3.41	n.d.	small
m-tolualdehyde	-3.44	n.d.	small
6-methyl-5-hepten-2-one	n.a.	7.79%	small
citral	-2.31	n.d.	large

[a]Testing compound. [b]Small bubbles are ∼3 mm in diameter with flow rate 100 sccm, large bubbles are ∼6 mm in diameter with flow rate 200 sccm. n.d.: Not detected due to the known K_{ia} value. n.a.: Not available.

Two bubbler-column setups have been used according to the K_{ia} values of the target compounds, see Table C.1. One setup produces small bubbles (diameter around 3 mm) with a flow rate of 100 sccm for diacetyl, p-tolualdehyde and m-tolualdehyde, which have small K_{ia} values. Another one with a single-perforation on the glass head, produces large bubbles (diameter around 6 mm) for citral with large K_{ia} values. The K_{ia} values were predicted by an online UFZ-LSER database based on a poly-parameter linear free-energy relationship (pp-LFERs).[147, 268] Please note that there are no available model-predicted K_{ia} values for 2,3-pentanedione and 6-methyl-5-hepten-2-one, we decided to use small bubbles because of the differences between the results obtained by the two setups were less than 10% at 25 °C.

B.1.4 Log K_{wa} and log K_{oa} values used in 2D partitioning plots

Table B.2: Log K_{wa} and log K_{oa} values used in 2D partitioning plots for target flavourings.

	15 °C		25 °C		35 °C		50 °C	
	log K_{wa}	log K_{oa}	log K_{wa}	log K_{oa}	log K_{wa}	log K_{oa}	log K_{wa}	log K_{oa}
diacetyl[a]	3.48	3.90	3.13	3.55	2.81	3.31	2.40	3.02
2,3-pentanedione	3.37	4.18	2.94	3.85	2.59	3.67	2.15	3.34
p-tolualdehyde	3.40	5.63	3.00	5.25	2.71	5.05	2.35	4.71
m-tolualdehyde	3.16	5.57	2.86	5.20	2.62	5.01	2.25	4.66
6-methyl-5-hepten-2-one	2.77	5.38	2.44	4.99	2.20	4.82	1.79	4.50
citral	3.18	6.12	2.87	5.69	2.55	5.52	2.14	5.17

[a]Testing compound.

Table B.3: Log K_{wa} and log K_{oa} values used in 2D partitioning plots for other frequently added flavourings in e-cigarettes at 25 °C.

	log K_{wa}[a]	log K_{oa}[b]	K_{hyd}[b]
vanillin	7.07	7.5	0.002
ethyl butyrate	1.77	3.64	0.018
ethyl acetate	2.27	2.95	0.033
maltol	5.85[b]	7.49	n.a.
ethyl vanillin	7.47	8.05	0.002
cis-3-hexenol	3.55[b]	5.46	n.a.
isoamyl acetate	2.73	4.11	0.027
linalool	2.94	6.50	n.a.
benzyl alcohol	4.90	6.04	n.a.
benzaldehyde	1.94	4.68	0.011

[a]The average of previous published data summarized by Sander unless otherwise noted.[112]
[b]Predicted data from SPARC.[212] n.a.: Not available.

B.1.5 Summary of the measured effective Henry's law constant ($H^{cp}_{s,eff}$)

Table B.4: Summary of the measured $H^{cp}_{s,eff}$ for target flavorings at different temperatures with two bubbler setups.

	Temperature(°C)	$H^{cp}_{s,eff}$(mol·m^{-3}·Pa^{-1})	Bubble size[b]
diacetyl[a]	15	1.27 ± 0.05	small
	25	(5.50 ± 0.18)×10^{-1}	small
	35	(2.52 ± 0.07)×10^{-1}	small
	50	(9.44 ± 0.25)×10^{-2}	small
2,3-pentanedione	15	(9.86 ± 1.06)×10^{-1}	small
	25	(3.50 ± 0.33)×10^{-1}	small
	25	(3.54 ± 0.46)×10^{-1}	large
	35	(1.51 ± 0.03)×10^{-1}	small
	50	(5.28 ± 0.10)×10^{-2}	small
p-tolualdehyde	15	1.06 ± 0.05	small
	25	(4.22 ± 0.13)×10^{-1}	small
	35	(2.16 ± 0.07)×10^{-1}	small
	50	(9.24 ± 0.10)×10^{-2}	small
m-tolualdehyde	15	(6.00 ± 0.37)×10^{-1}	small
	25	(2.92 ± 0.02)×10^{-1}	small
	35	(1.62 ± 0.02)×10^{-1}	small
	50	(6.61± 0.08)×10^{-2}	small
6-methyl-5-hepten-2-one	15	(2.44 ± 0.10)×10^{-1}	small
	25	(1.11 ± 0.04)×10^{-1}	small
	25	(1.20 ± 0.06)×10^{-1}	large
	35	(6.24 ± 0.07)×10^{-2}	small
	50	(2.30 ± 0.02)×10^{-2}	small
citral	15	(6.33 ± 0.91)×10^{-1}	large
	25	(2.99 ± 0.29)×10^{-1}	large
	35	(1.37 ± 0.11)×10^{-1}	large
	50	(5.15 ± 0.51)×10^{-2}	large

[a]Testing compound. [b]Small bubbles are ∼3 mm in diameter with flow rate 100 sccm, large bubbles are ∼6 mm in diameter with flow rate 200 sccm.

B.1.6 Syringe pump-GC setup for acetoin

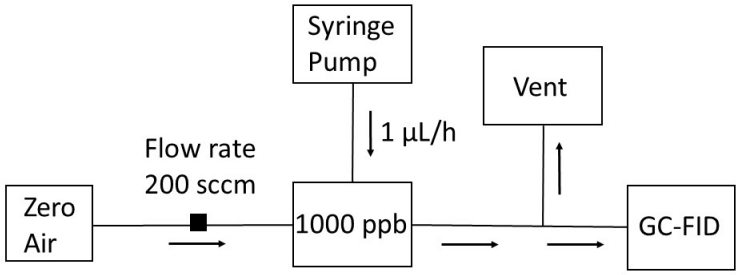

Figure B.3: Schematic of syringe pump-GC setup.

Given that our IGS setup was unable to determine the $H^{\mathrm{cp}}_{\mathrm{s,eff}}$ of acetoin, we have attempted to determine it by taking the ratio between its aqueous- and gas-phase concentrations at equilibrium, according to eq 1 introduced in the main article:

$$K_{\mathrm{wa}} = c_{\mathrm{l}}/c_{\mathrm{g}} \tag{B.1}$$

where c_{l} is the known concentration of acetoin in the aqueous solution inside the bubbler. c_{g} is the gas-phase concentration of acetoin at equilibrium. To determine c_{g}, we have utilized a syringe pump-GC setup (Figure C.3) to calibrate the GC-FID signal of acetoin. Briefly, a known amount of acetoin was diluted in methanol and placed in a 100 μL gas-tight syringe (Hamilton, USA). The syringe pump injected the solution into the glass container at a rate of 1 μL/h, and the liquid was assumed to be fully volatilized with a stream of zero air (200 sccm) flowing through the container. The sample was injected into GC-FID via the gas-sampling valve automatically, and the acetoin signal was monitored over eight hours. As a result, a signal (0.075 pA*min) was obtained with a 1000 ppb gas concentration in the glass container, which was translated into a calibration factor of our GC-FID for acetoin. In the IGS setup, the 0.02 g/L acetoin solution gave a stable signal (0.038 pA*min) after eight hours in both bubblers with different bubble sizes. Therefore, the estimated $H^{\mathrm{cp}}_{\mathrm{s,eff}}$ for acetoin at 25 °C is 4.0 mol·m^{-3}·Pa^{-1}. Considering potential wall loss of acetoin (glass and tube) and the fact that the chemical may not be fully volatilized, the value of 4.0 mol·m^{-3}·Pa^{-1} should be considered an upper limit.

B.1.7 Summary of the hydration equilibrium constant (K_{hyd}) and the intrinsic Henry's law constant ($H_{\mathrm{s}}^{\mathrm{cp}}$)

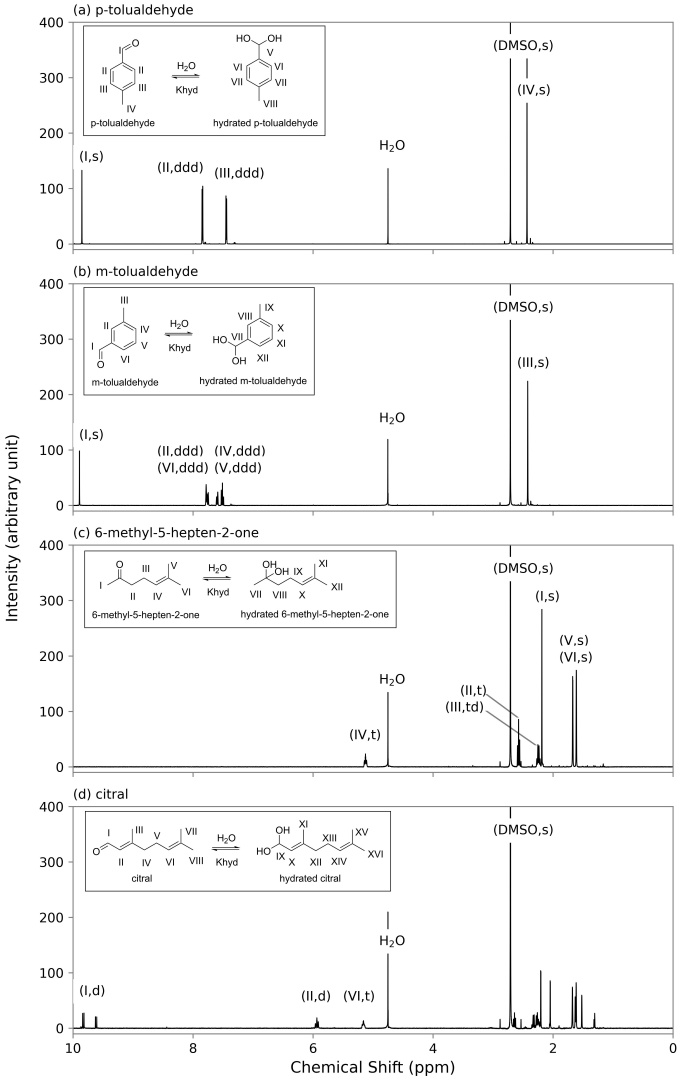

Figure B.4: ^{1}H NMR spectra for the flavoring agents diluted in D_2O with DMSO as an internal standard at 25 °C. (a) p-Tolualdehyde; (b) m-Tolualdehyde; (c) 6-Methyl-5-hepten-2-one; (d) Citral. The identity of the peak (the numbers match those in the chemical structures) and splitting pattern are shown in the brackets. Schematics of the hydration processes are included.

In order to determine K_{hyd}, quantifications for one peak from carbonyl and another from hydrated carbonyl are needed according to eq 6. Figure C.4 presents the spectra for p-tolualdehyde, m-tolualdehyde, 6-methyl-5-hepten-2-one and citral, with the peak assignments displayed in brackets, including chemical shift and the splitting

pattern. The H_2O singlet peak shows up at around 4.75 ppm, while the DMSO singlet peak is observed at around 2.71 ppm. However, hydrated peaks have not been identified in their spectra. In Figure C.4(a), the peaks for non-hydrated p-tolualdehyde are shown in the spectrum. The singlet peak V for hydrated p-tolualdehyde didn't appear at around 6.11 ppm as predicted; other peaks such as (VI, ddd), (VII, ddd) and (VIII, s), that are supposed to show up at around 7.26 ppm, 7.25 ppm and 2.23 ppm, respectively, might be overlapping with peak III and IV. For the hydrated m-tolualdehyde in Figure C.4(b), the singlet peak labeled as VII is predicted to be at approximately 6.13 ppm, and likewise, a singlet peak IX to be around 2.29 ppm; however, there were no peaks observed at these chemial shifts. The other four protons (VIIII, X, XI, and XII) on the benzene ring with the ddd multiplicity are predicted to appear between 7 to 7.4ppm. These peaks were not observed either. Though, they might be overlapping with m-tolualdehyde peaks. In Figure C.4(c), the hydrated 6-methyl-5-hepten-2-one peaks labeled as VII and IX are predicted to be at around 1.21ppm and 2.04 ppm with multiplicity s and td, respectively. Based on our observation, there is no peak identified under the influence of noise. The hydrated peaks triplet VIII and singlet peaks IX and XI have chemical shifts between 1.56 to 1.57ppm, which are likely overlapping with peaks V and VI due to the tiny signal. As a result of the geometric stereoisomersthere for citral, there are two groups of doublet peaks from the peak I at 9.81 ppm and 9.78 ppm in Figure C.4(d). Besides the labeled citral peaks, other citral peaks are challenging to identify due to the peak overlapping, especially between 1.5 to 2.5 ppm and the impurity of the citral (95% purity, a mixture of cis- and trans-citral). Such as (III, s), (IV, t), (V, td), (VII, s) and (VIII, s). Similarly, it is hard to identify hydrated peaks (XI, d), (XII, t), (XIII, td), (XV, s), and (XVI, s) that show up between 1.5 to 2.5 ppm. By contrast, hydrated citral peaks, including doublet IX, doublet X and triplet XIV are predicted to be at 5.12 to 5.28 ppm, but there is no peak observed.

Table B.5: Comparison of the measured K_{hyd} values with the predicted values for target flavorings.

	K_{hyd} at 25°C	
	NMR	SPARC[212]
diacetyl[a]	2.52 ± 0.10	2.047
acetoin	$(1.92 \pm 0.10) \times 10^{-2}$	0.099
2,3-pentanedione	1.88 ± 0.09	1.164
2,3-pentanedione_K_{hyd_1}	$(9.20 \pm 0.25) \times 10^{-1}$	0.543
2,3-pentanedione_K_{hyd_2}	$(9.60 \pm 0.83) \times 10^{-1}$	0.621
p-tolualdehyde	n.d.	0.004
m-tolualdehyde	n.d.	0.007
6-methyl-5-hepten-2-one	n.d.	0.014
citral	n.d.	0.003

[a]Testing compound. n.d.: Not detected due to the absence of the hydrated product peak.

Table B.6: Summary of the K_{hyd} and $H_{\mathrm{s}}^{\mathrm{cp}}$ at different temperatures for diacetyl, acetoin and 2,3-pentanedione.

	Temperature(°C)	K_{hyd}	$H_{\mathrm{s}}^{\mathrm{cp}}$(mol·m^{-3}·Pa^{-1})
diacetyl[a]	15	4.29 ± 0.14	(2.40 ± 0.13)×10^{-1}
	25	2.50 ± 0.10	(1.56 ± 0.08)×10^{-1}
	35	2.13 ± 0.10	(8.05 ± 0.45)×10^{-2}
	50	1.39 ± 0.02	(3.95 ± 0.12)×10^{-2}
acetoin	15	(2.97 ± 0.05)×10^{-2}	n.d.
	25	(1.92 ± 0.10)×10^{-2}	n.d.
	35	(1.58 ± 0.06)×10^{-2}	n.d.
	50	(1.16 ± 0.02)×10^{-2}	n.d.
2,3-pentanedione	15	2.52 ± 0.10	(2.80 ± 0.32)×10^{-1}
	25	1.88 ± 0.09	(1.22 ± 0.13)×10^{-1}
	35	1.40 ± 0.02	(6.28 ± 0.16)×10^{-2}
	50	(9.69 ± 0.25)×10^{-1}	(2.68 ± 0.09)×10^{-2}
2,3-pentanedione_K_{hyd_1}	15	1.29 ± 0.07	n.a.
	25	(9.20 ± 0.25)×10^{-1}	n.a.
	35	(7.13 ± 0.08)×10^{-1}	n.a.
	50	(4.78 ± 0.09)×10^{-1}	n.a.
2,3-pentanedione_K_{hyd_2}	15	1.23 ± 0.07	n.a.
	25	(9.60 ± 0.83)×10^{-1}	n.a.
	35	(6.92 ± 0.18)×10^{-1}	n.a.
	50	(4.91 ± 0.23)×10^{-1}	n.a.

[a]Testing compound. n.d.: Not detected due to the absence of signal decay in $H_{\mathrm{s,eff}}^{\mathrm{cp}}$ measurement. n.a.: Not available.

B.1.8 Comparison between the effective Henry's law constant ($H^{cp}_{s,eff}$) and the intrinsic Henry's law constant (H^{cp}_{s})

Table B.7: K_{hyd}, $H^{cp}_{s,eff}$, H^{cp}_{s}, log $K_{wa,eff}$ and log K_{wa} values at 25°C for target flavorings and representative carbonyls.

	K_{hyd}[b]	$H^{cp}_{s,eff}$[b]	H^{cp}_{s}[c]	log K^{d}_{wa}	log $K_{wa,eff}$[d]
diacetyl[a]	2.52	0.55	0.16	2.59	3.13
2,3-pentanedione	1.88	0.35	0.12	2.48	2.94
acetoin	0.02	0.57[e]	0.56	3.14	3.15
p-tolualdehyde	n.d.	0.42	0.42	3.02	3.02
m-tolualdehyde	n.d.	0.29	0.29	2.86	2.86
6-methyl-5-hepten-2-one	n.d.	0.11	0.11	2.44	2.44
citral	n.d.	0.30	0.30	2.87	2.87
glyoxal	1st hydration: 207[f] 2nd hydration: 20000[f]	4135.21[g]	0.02[g]	1.67	7.01
formaldehyde	2000[f]	47.17[e]	0.02	1.77	5.07
acetaldehyde	1.20[f]	0.14[e]	0.06	2.20	2.55
propionaldehyde	0.85[f]	0.11[e]	0.06	2.19	2.45

[a]Testing compound. [b]From this study unless otherwise noted. [c]Calculated using eq 7. [d]Converted from H values accordingly. [e]The average of previously measured data summarized by Sander.[112] [f]Previous published data recommended by Tilgner *et al.*[205] [g]Reported by Ip *et al.*[154] n.d.: Not detected due to the absence of the hydrated product peak.

To better show the difference in partitioning for target compounds using $H^{cp}_{s,eff}$ ($K_{wa,eff}$) and H^{cp}_{s} (K_{wa}), points using H^{cp}_{s} (K_{wa}) values have been included in Figure C.5. The difference is observable, but it does not affect the overall partitioning significantly.

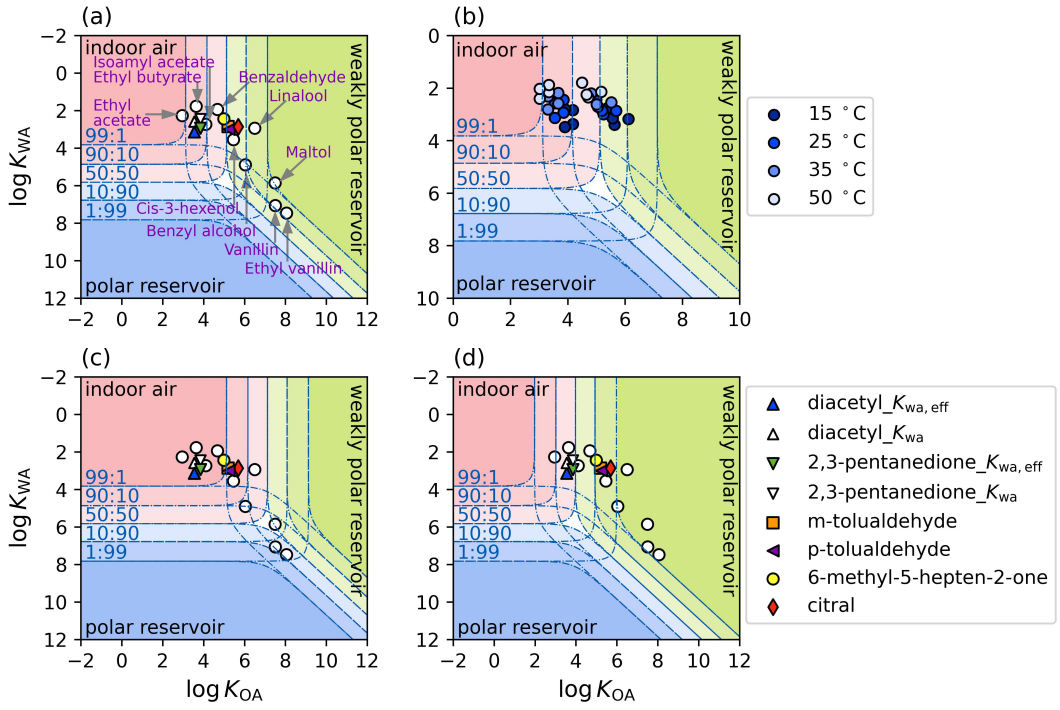

Figure B.5: Indoor phase distribution of flavoring agents in e-cigarettes and hookah tobacco. The colored markers are the target compounds in this work, the white dots are the top ten most frequently added flavoring ingredients.[199] (a) An indoor environment with polar and weakly-polar surface reservoirs equivalent to thicknesses of 500 and 2500 nm under 25 °C. (b) Same assumption as (a) at 15, 25, 35, and 50 °C including target compounds studied in this work; (c) An indoor environment with polar and weakly-polar surface reservoirs equivalent to thicknesses of 500 and 25 nm under 25 °C; (d) An indoor environment with polar and weakly-polar surface reservoirs equivalent to thicknesses of 500 nm and 35 μm under 25 °C.

Appendix C: Chapter 4

C.1 Supplementary information for Chapter 4

C.1.1 Structures of the Flavor Carbonyls

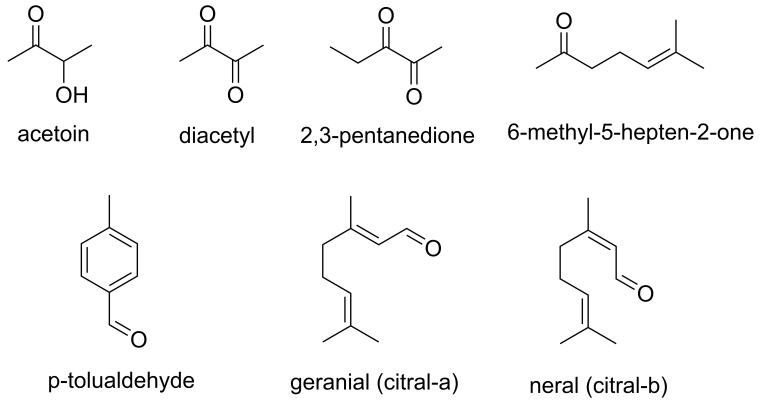

Figure C.1: Structures of the flavor carbonyls.

C.1.2 Summary of the Predicted Partitioning Coefficients (K_{wa}, K_{oa} and K_{pa})

Table C.1: Predicted system parameters and respective standard errors for PG via EAS-E Suite.[246]

	c	s	a	b	l	v
PG	-0.337±0.075	1.173±0.389	4.64±0.797	1.44±0.29	0.705±0.042	0.097±0.195

Table C.2: Predicted LSER solute descriptors and respective standard errors for target flavor carbonyls and their PG acetals via EAS-E Suite.[246]

		S	A	B	L	V[a]
acetoin	carbonyl	0.96±0.30	0.156±0.246	0.82±0.14	2.69±0.74	0.747
	PG acetal	0.80±0.13	0.320±0.125	0.85±0.23	5.04±0.43	1.162
diacetyl[b]	carbonyl	1.05±0.13	0±0.032	0.70±0.14	2.81±0.21	0.704
	PG acetal	0.88±0.45	0±0.032	0.75±0.44	6.79±0.74	1.535
2,3-pentanedione[b]	carbonyl	1.04±0.13	0±0.032	0.71±0.14	3.31±0.21	0.844
	PG acetal	0.88±0.45	0±0.032	0.75±0.44	7.29±0.74	1.676
citral	carbonyl	0.73±0.13	0±0.032	0.48±0.08	4.91±0.21	1.306
	PG acetal	0.63±0.30	0±0.032	0.93±0.14	6.80±0.21	1.863
p-tolualdehyde	carbonyl	1.01±0.13	0±0.032	0.39±0.08	4.73±0.21	1.014
	PG acetal	0.82±0.13	0±0.032	0.92±0.14	5.93±0.43	1.430
6-methyl-5-hepten-2-one	carbonyl	0.66±0.13	0±0.032	0.54±0.08	4.21±0.21	1.208
	PG acetal	0.48±0.13	0±0.032	0.46±0.14	6.04±0.43	1.624

[a]The error was not provided by EAS-E-Suite. [b]For diacetyl and 2,3-pentanedione, only the double-acetalization PG acetals were considered.

Table C.3: Predicted log K_{wa}, log K_{oa}, and log K_{pa} values and respective standard errors for flavoring carbonyls and PG acetals.

	log K_{wa}[b]		log K_{oa}[b]		log K_{pa}[c]	
	carbonyl	PG acetal	carbonyl	PG acetal	carbonyl	PG acetal
acetoin	5.42±1.35	5.79±1.25	4.07±1.08	6.64±0.61	4.66±1.41	6.98±0.94
diacetyl[a]	4.61±0.74	4.15±2.36	3.56±0.24	7.06±0.76	3.95±0.58	6.71±1.17
2,3-pentanedione[a]	4.51±0.74	4.03±2.36	4.03±0.24	7.53±0.76	4.32±0.59	7.08±1.06
citral	2.92±0.53	3.73±0.97	5.95±0.40	7.19±0.35	4.80±0.52	6.72±0.73
p-tolualdehyde	3.08±0.51	4.73±0.77	4.99±0.24	6.41±0.41	4.84±0.56	6.27±0.69
6-methyl-5-hepten-2-one	2.39±0.51	1.38±0.77	4.54±0.24	6.02±0.41	4.30±0.49	5.30±0.62
cinnamaldehyde	4.07±0.51	5.58±1.24	5.75±0.25	7.40±0.51	-	-
benzaldehyde	3.09±0.50	4.78±0.76	4.46±0.23	5.89±0.40	-	-
ethylvanillin	6.09±0.69	7.80±0.89	7.64±0.52	9.18±0.54	-	-
vanillin	6.72±0.69	8.48±0.89	7.39±0.52	8.95±0.54	-	-

[a]For diacetyl and 2,3-pentanedione, only the double-acetalization PG acetals were considered.
[b]The values were predicted directly by EAS-E-Suite.[246] [c]The K_{pa} values with propagated errors were estimated using the data from Table C.1 and Table C.2 in ppLEFERs equation (eq 5).[95]

C.1.3 Summary of the Carbonyl Acetal Formation in PG

The ^{1}H NMR experiments were carried out by an Agilent VNMRS 700 MHz spectrometer equipped with a cryo-cooled probe and an Agilent 7620 automatic sample handling system. A 4-minute locking and shimming time corrected magnetic field inhomogeneities prior to scanning. Solvent suppression with multiple sites was employed to suppress large PG peaks. All samples were measured with 8 scans, and the total relaxation time was 5.1 s, including a 0.1 s relaxation delay and 5 s acquisition. An online ^{1}H NMR spectra predictor (https://www.nmrdb.org/new_predictor/) assisted in peak assignment.[207–210] The concentration of individual carbonyl and PG acetal in the solution can be quantified by the following formula:[211]

$$[\text{chemical}] = [\text{DMSO}] \times [\text{I(chemical)/nH(chemical)}]/[\text{I(DMSO)/nH(DMSO)}] \quad \text{(C.1)}$$

where [chemical] and [DMSO] represent the concentrations (in units of mg/ml) of the target chemical and DMSO, respectively. I is the peak integration and nH is the number of protons responsible for the peak of interest. Citral and citral PG acetal were quantified as a combination of cis- and trans-isomers (geranial and neral).

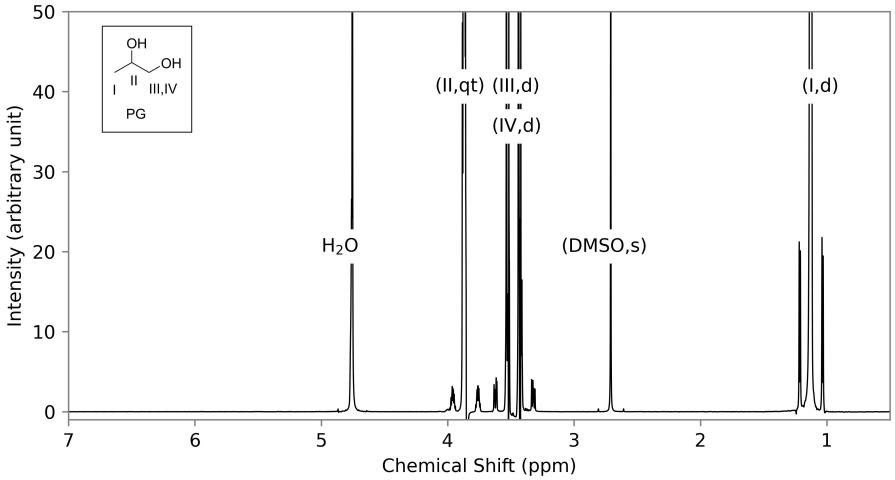

Figure C.2: ^{1}H NMR spectrum for PG at day 28 with multiple sites solvent suppression. The identity of the peak (the numbers match those in the chemical structures) and splitting pattern are shown in the brackets.

Blank experiments were conducted to monitor PG without any flavorings, ensuring no peaks from PG itself over time. Figure C.2 presents the PG ^{1}H NMR spectrum at

day 28 with peak assignments included. To suppress the huge PG peaks and avoid influencing other peaks, solvent suppression with multiple sites was applied for all the samples, as indicated by (II, qt), (III, d), (IV, d), and (I, d) in the spectrum. The internal standard DMSO appears as a singlet peak at $\delta = 2.71$ ppm, and the residual H_2O peak is observed at $\delta = 4.75$ ppm, possibly due to the H_2O impurity present in D_2O and DMSO. Overall, the observation confirmed that no product formed from PG during the reaction monitoring experiments for flavorings.

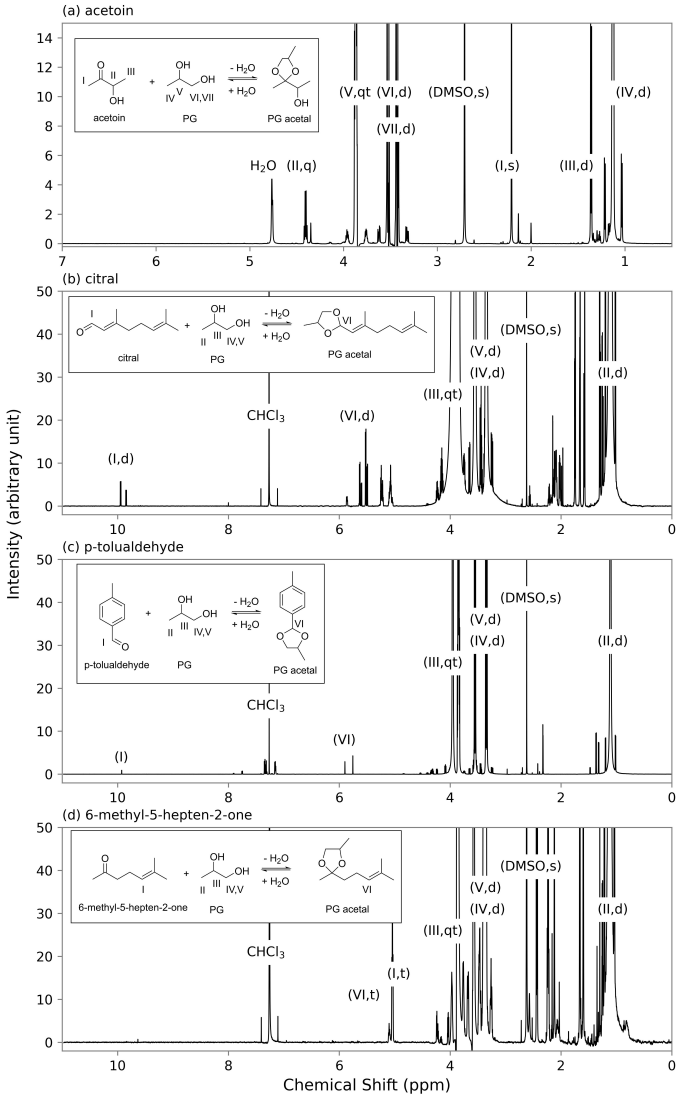

Figure C.3: ^{1}H NMR spectra for the flavor carbonyls PG acetal formation: (a) acetoin at day 21; (b) citral at day 4; (c) *p*-tolualdehyde at day 2 ; (d) 6-methyl-5-hepten-2-one at day 28.

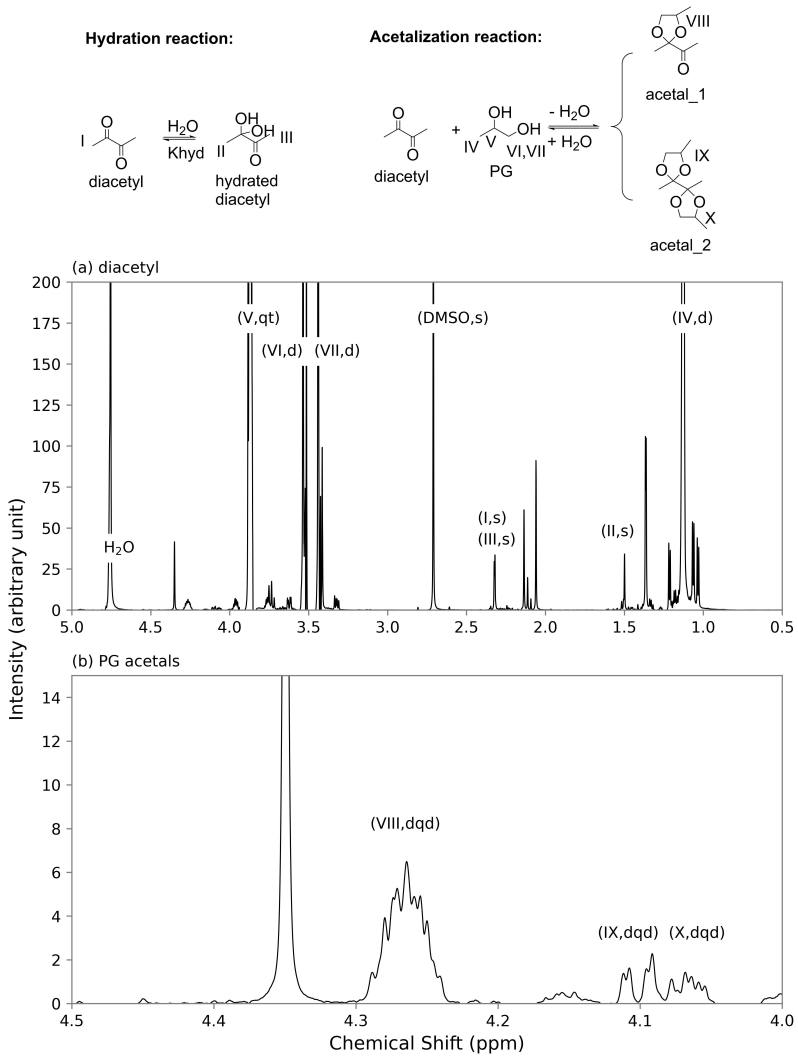

Figure C.4: Top: schematics of the hydration and acetalization reactions for diacetyl. Bottom: (a) ^{1}H NMR spectrum for the diacetyl PG acetal formation at day 4; (b) ^{1}H NMR spectrum for the diacetyl acetalization products.

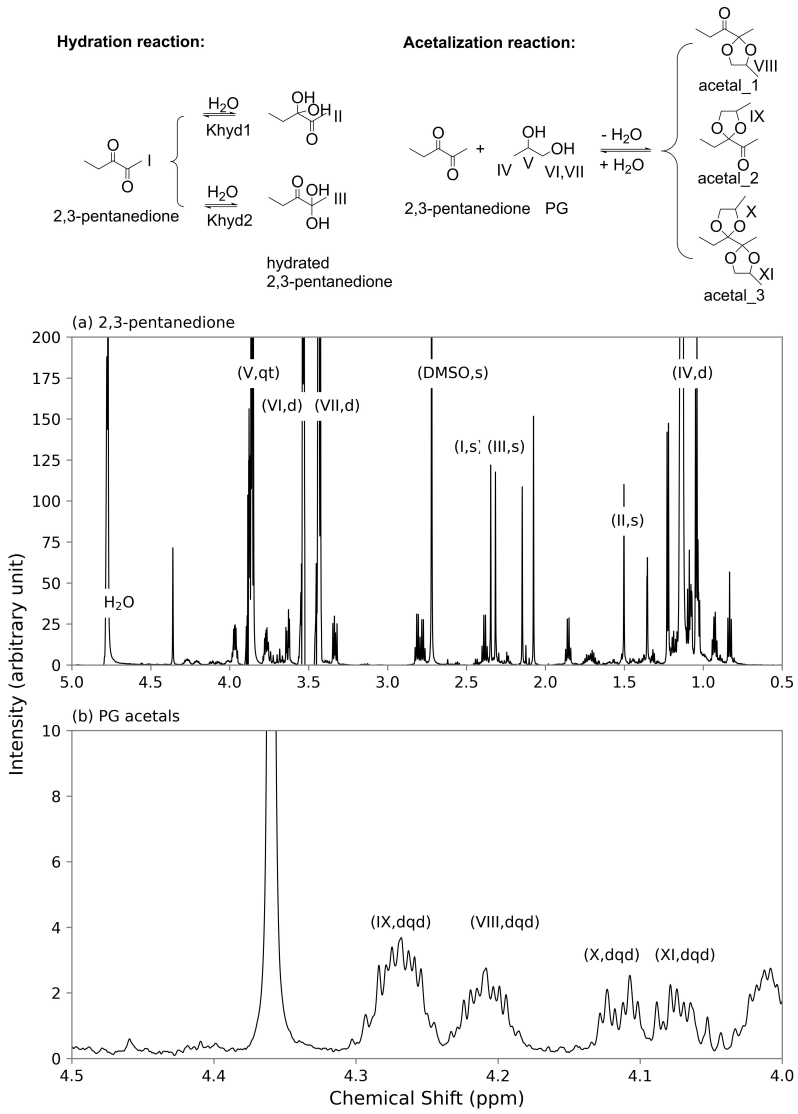

Figure C.5: Top: schematics of the hydration and acetalization reactions for 2,3-pentanedione. Bottom: (a) ^{1}H NMR spectrum for the 2,3-pentanedione PG acetal formation at day 4; (b) ^{1}H NMR spectrum for the 2,3-pentanedione acetalization products.

Figure C.3, Figure C.4, and Figure C.5 show example spectra for the formation of flavor carbonyl PG acetal with DMSO as an internal standard. The identity of the peak (the numbers match those in the chemical structures) and splitting pattern are shown in the brackets. To monitor acetal conversion over time in laboratory-made e-liquids, it is only necessary to quantify one peak from each compound, as per eq C.1. As stated in the method, citral and citral PG acetal were quantified as a combination of cis- and trans-isomers. In addition, both cis- and trans- PG acetals exhibit two

diastereomers, which can be distinguished by the presence of doublet peaks at δ = 5.6 - 5.8 ppm (Figure C.3(b)). Similarly, the NMR spectra demonstrate that the two diastereomers for 6-methyl-5-hepten-2-one PG acetals can also be detected, with peaks at δ = 5.8 - 6.0 ppm(Figure C.3(c)). Quantifying peaks for α-diketones is challenging due to the small size of the acetal products, as well as the influence of hydration processes and difficulties in accurately assigning peaks due to background noise, impure chemicals, and peak overlapping (see Figure C.4 and Figure C.5).

Table C.4: Summary of the flavor carbonyl PG acetal fraction over time.

	acetoin	diacetyl	2,3-pentanedione	citral	*p*-tolualdehyde	6-methyl-5-hepten-2-one
day1	0.00±0.00%	77.49±1.69%	5.59±4.12%	80.64±1.56%	88.74±0.36%	0.00±0.00%
day2	0.00±0.00%	76.43±0.19%	29.43±0.50%	81.39±1.91%	89.72±0.11%	0.00±0.00%
day4	0.00±0.00%	78.66±2.41%	37.23±2.04%	84.48±0.99%	89.20±0.31%	0.00±0.00%
day7	0.00±0.00%	85.01±2.55%	72.12±3.99%	77.96±2.46%	90.76±0.70%	0.00±0.00%
day10	0.00±0.00%	89.59±2.67%	83.34±1.16%	77.67±1.14%	89.39±2.13%	0.00±0.00%
day14	0.00±0.00%	95.50±0.41%	100.00±0.00%	75.79±3.23%	88.13±0.58%	4.76±0.91%
day21	0.00±0.00%	100.00±0.00%	100.00±0.00%	-	-	9.59±2.48%
day28	0.00±0.00%	100.00±0.00%	-	-	-	15.10±5.09%

Table C.5: Summary of the flavor α-diketone PG acetal fraction over time.

	diacetyl		2,3-pentanedione		
	conversion1	conversion2	conversion1	conversion2	conversion3
day1	76.97±1.30%	0.51±0.89%	3.53±2.03%	1.94±1.94%	0.12±0.20%
day2	68.44±0.52%	7.98±0.34%	14.39±0.09%	8.92±0.15%	6.12±0.55%
day4	56.71±2.41%	21.96±4.77%	8.59±0.61%	3.56±2.14%	25.08±2.69%
day7	36.31±2.77%	48.70±5.06%	10.57±2.22%	0.00±0.00%	61.56±6.20%
day10	20.81±1.97%	68.78±1.04%	16.65±4.41%	0.00±0.00%	66.69±3.90%
day14	11.64±0.54%	83.86±0.42%	14.18±2.51%	0.00±0.00%	85.82±2.51%
day21	9.12±0.64%	90.88±0.64%	15.93±0.91%	0.00±0.00%	84.07±0.91%
day28	9.01±1.28%	90.99±1.28%	-	-	-

C.1.4 Indoor Partitioning for the Flavor Carbonyls and their PG Acetals in PG Aerosol

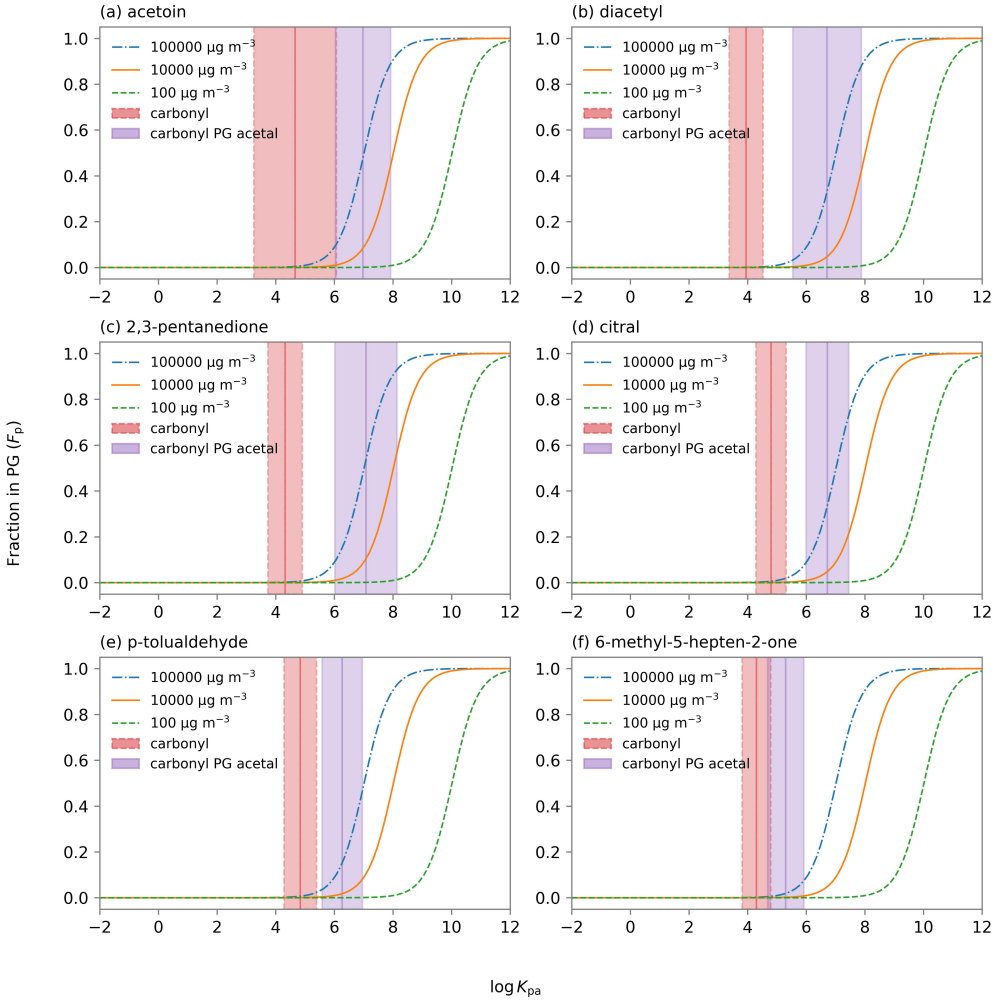

Figure C.6: The calculated fraction of each carbonyl and its acetal in PG aerosol under three selected aerosol concentrations as a function of log K_{pa}. The figure also shows the estimated log K_{pa} values with propagated errors: (a) acetoin; (b) diacetyl; (c) 2,3-pentanedione; (d) citral; (e) *p*-tolualdehyde; (f) 6-methyl-5-hepten-2-one. For diacetyl and 2,3-pentanedione, only the double-acetalization PG acetals were considered.

The equilibrium fractions of a chemical in e-liquid aerosol, indoor air, polar reservoir and weakly-polar reservoir (F_{p}, F_{g}, F_{w} and F_{o}) can be estimated using the volume of each phase and partitioning coefficients between phases:

$$F_{\mathrm{p}} = 1/(1+1/(K_{\mathrm{pa}}\times V_{\mathrm{p}}/V_{\mathrm{g}})+K_{\mathrm{wa}}/K_{\mathrm{pa}}\times(V_{\mathrm{w}}/V_{\mathrm{g}})/(V_{\mathrm{p}}/V_{\mathrm{g}})+K_{\mathrm{oa}}/K_{\mathrm{pa}}\times(V_{\mathrm{o}}/V_{\mathrm{g}})\times(V_{\mathrm{p}}/V_{\mathrm{g}})) \tag{C.2}$$

$$F_{\mathrm{g}} = 1/(1 + (K_{\mathrm{oa}} \times V_{\mathrm{o}}/V_{\mathrm{g}}) + K_{\mathrm{wa}} \times (V_{\mathrm{w}}/V_{\mathrm{g}}) + K_{\mathrm{pa}} \times (V_{\mathrm{p}}/V_{\mathrm{g}})) \tag{C.3}$$

$$F_{\mathrm{w}} = 1/(1 + 1/(K_{\mathrm{wa}} \times V_{\mathrm{w}}/V_{\mathrm{g}}) + K_{\mathrm{oa}}/K_{\mathrm{wa}} \times (V_{\mathrm{o}}/V_{\mathrm{w}}) + K_{\mathrm{pa}}/K_{\mathrm{wa}} \times (V_{\mathrm{p}}/V_{\mathrm{g}}) \times (V_{\mathrm{w}}/V_{\mathrm{g}})) \tag{C.4}$$

$$F_{\mathrm{o}} = 1/(1 + 1/(K_{\mathrm{oa}} \times V_{\mathrm{o}}/V_{\mathrm{g}}) + K_{\mathrm{wa}}/K_{\mathrm{oa}} \times (V_{\mathrm{w}}/V_{\mathrm{o}}) + K_{\mathrm{pa}}/K_{\mathrm{oa}} \times (V_{\mathrm{p}}/V_{\mathrm{g}}) \times (V_{\mathrm{o}}/V_{\mathrm{g}})) \tag{C.5}$$

where K_{pa} (in units of m^3 air per m^3 PG), K_{wa} (in units of m^3 air per m^3 water) and K_{oa} (in units of m^3 air per m^3 octanol) are PG-air, water-air and octanol-air partitioning coefficients at 25 °C, respectively. V_{p}, V_{g}, V_{w} and V_{o} (in units of m^3) are the volumes of the e-liquid aerosol, indoor air, polar reservoir and weakly-polar reservoir, respectively. Similar to the prediction of K_{pa}, the K_{wa} and K_{oa} for the target flavor carbonyls and their PG acetals were predicted directly via EAS-E Suite relying on QSPRs and ppLFERs.[96, 246, 247] The K_{wa} and K_{oa} values with prediction uncertainties have been tabulated in Table C.3.

Several essential assumptions were made to simplify the calculation of volumes. These assumptions are as follows: (i) The volume of indoor air (V_{g}) is approximately equal to the volume of the room (V, in units of m^3). (ii) The volume ratio between the e-liquid aerosol and the indoor air can be estimated by the concentration of PG aerosol vaporized (C_{p}, in units of g m^{-3}) and the density of PG (D_{p}, 1.04 g cm^{-3}). This estimation is calculated using eq C.6, where 10^{-6} is a conversion factor. (iii) Assuming that the reservoir is evenly distributed throughout the surfaces of the room, the volume of the polar and weakly-polar reservoirs can be expressed in terms of surface area to volume ratio (S/V, in units of m^{-1}) and thicknesses of reservoirs (X_{W} and X_{o}, in units of m) as shown in eq C.7 and eq C.8. In this work, a representative S/V value of 3.2 m^{-1} was selected for a room including its contents.[11] The volume

ratios between the reservoir and the indoor air can be associated with the X_{w} and X_{o} values of 500 and 2500 nm, respectively, which were found to best describe real-time measurements in an experimental indoor environment.[71] The volume estimations in a real indoor environment may be subject to fluctuations due to variations in e-liquid volume, room size, and the non-uniform distribution of indoor reservoirs.

$$V_{\mathrm{p}}/V_{\mathrm{g}} = V_{\mathrm{p}}/V = C_{\mathrm{p}}/D_{\mathrm{p}} \times 10^{-6} \tag{C.6}$$

$$V_{\mathrm{w}}/V_{\mathrm{g}} = V_{\mathrm{w}}/V = X_{\mathrm{w}} \times S/V \tag{C.7}$$

$$V_{\mathrm{o}}/V_{\mathrm{g}} = V_{\mathrm{o}}/V = X_{\mathrm{o}} \times S/V \tag{C.8}$$

Table C.6: The equilibrium fractions for the target flavor carbonyls and their PG acetals in an indoor system consisting of e-liquid aerosol, indoor air, polar reservoir, and weakly-polar reservoir (F_{p}, F_{g}, F_{w}, and F_{o}).

		F_{p}	F_{g}	F_{o}	F_{w}
acetoin	carbonyl	0.03%	65.99%	6.20%	27.77%
	PG acetal	0.25%	2.70%	94.38%	2.67%
diacetyl[a]	carbonyl	0.01%	91.38%	2.65%	5.96%
	PG acetal	0.05%	1.08%	98.85%	0.02%
2,3-pentanedione[a]	carbonyl	0.02%	87.90%	7.53%	4.55%
	PG acetal	0.04%	0.37%	99.58%	0.01%
citral	carbonyl	0.01%	12.30%	87.68%	0.02%
	PG acetal	0.04%	0.80%	99.15%	0.01%
p-tolualdehyde	carbonyl	0.04%	56.04%	43.81%	0.11%
	PG acetal	0.08%	4.62%	94.91%	0.40%
6-methyl-5-hepten-2-one	carbonyl	0.02%	78.25%	21.71%	0.03%
	PG acetal	0.02%	10.66%	89.32%	0.00%

[a]For diacetyl and 2,3-pentanedione, only the double-acetalization products were considered.

C.1.5 Calculation of the Overall K_{wa} and K_{oa} Values with Carbonyl and its PG Acetal Forms Combined

To better reflect the actual indoor phase distribution for flavorings in e-cigarettes and how acetal formation affects indoor partitioning, we assumed that each carbonyl and its PG acetal reached equilibrium in the same triphasic indoor system (air, polar and weakly-polar reservoirs), and derived the representative K_{wa} and K_{oa} values based on the partitioning coefficients for the carbonyl ($K_{\mathrm{wa_1}}$, $K_{\mathrm{oa_1}}$) and its PG acetal ($K_{\mathrm{wa_2}}$, $K_{\mathrm{oa_2}}$), the fraction of PG acetal formation (F_{acetal}), and the volume ratios between the reservoirs and the indoor air ($V_{\mathrm{o}}/V_{\mathrm{g}}$, $V_{\mathrm{w}}/V_{\mathrm{g}}$):

$$K_{\mathrm{wa}} = \frac{K_{\mathrm{wa_1}} + K_{\mathrm{wa_2}} \times \frac{F_{\mathrm{acetal}}}{1-F_{\mathrm{acetal}}} \times \left(1 + K_{\mathrm{oa_1}} \times \frac{V_{\mathrm{o}}}{V_{\mathrm{g}}} + K_{\mathrm{wa_1}} \times \frac{V_{\mathrm{w}}}{V_{\mathrm{g}}}\right) \Big/ \left(1 + K_{\mathrm{oa_2}} \times \frac{V_{\mathrm{o}}}{V_{\mathrm{g}}} + K_{\mathrm{wa_2}} \times \frac{V_{\mathrm{w}}}{V_{\mathrm{g}}}\right)}{1 + \frac{F_{\mathrm{acetal}}}{1-F_{\mathrm{acetal}}} \times \left(1 + K_{\mathrm{oa_1}} \times \frac{V_{\mathrm{o}}}{V_{\mathrm{g}}} + K_{\mathrm{wa_1}} \times \frac{V_{\mathrm{w}}}{V_{\mathrm{g}}}\right) \Big/ \left(1 + K_{\mathrm{oa_2}} \times \frac{V_{\mathrm{o}}}{V_{\mathrm{g}}} + K_{\mathrm{wa_2}} \times \frac{V_{\mathrm{w}}}{V_{\mathrm{g}}}\right)} \tag{C.9}$$

$$K_{\mathrm{oa}} = \frac{K_{\mathrm{oa_1}} + K_{\mathrm{oa_2}} \times \frac{F_{\mathrm{acetal}}}{1-F_{\mathrm{acetal}}} \times \left(1 + K_{\mathrm{oa_1}} \times \frac{V_{\mathrm{o}}}{V_{\mathrm{g}}} + K_{\mathrm{wa_1}} \times \frac{V_{\mathrm{w}}}{V_{\mathrm{g}}}\right) \Big/ \left(1 + K_{\mathrm{oa_2}} \times \frac{V_{\mathrm{o}}}{V_{\mathrm{g}}} + K_{\mathrm{wa_2}} \times \frac{V_{\mathrm{w}}}{V_{\mathrm{g}}}\right)}{1 + \frac{F_{\mathrm{acetal}}}{1-F_{\mathrm{acetal}}} \times \left(1 + K_{\mathrm{oa_1}} \times \frac{V_{\mathrm{o}}}{V_{\mathrm{g}}} + K_{\mathrm{wa_1}} \times \frac{V_{\mathrm{w}}}{V_{\mathrm{g}}}\right) \Big/ \left(1 + K_{\mathrm{oa_2}} \times \frac{V_{\mathrm{o}}}{V_{\mathrm{g}}} + K_{\mathrm{wa_2}} \times \frac{V_{\mathrm{w}}}{V_{\mathrm{g}}}\right)} \tag{C.10}$$

Table C.7: Calculated representative log K_{wa} and log K_{oa} values at 25 °C for individual flavoring carbonyl and its PG acetal.

	log K_{wa}	log K_{oa}
acetoin	5.420	4.070
diacetyl[a]	4.150	7.060
2,3-pentanedione[a]	4.030	7.530
citral	3.204	6.527
p-tolualdehyde	4.325	6.015
6-methyl-5-hepten-2-one	2.381	4.768
cinnamaldehyde	4.998	6.808
benzaldehyde	4.665	5.777
ethylvanillin	6.472	7.929
vanillin	7.021	7.601

[a]For diacetyl and 2,3-pentanedione, only the double-acetalization products were considered.